- Supporting Information -

A [2]Rotaxane-Based Circularly Polarized Luminescence Switch

Arthur H. G. David, Raquel Casares, Juan M. Cuerva,* Araceli G. Campaña, Victor Blanco*

Departamento de Química Orgánica, Facultad de Ciencias, Unidad de Excelencia de Química Aplicada a Biomedicina y Medioambiente (UEQ), Universidad de Granada (UGR), Avda. Fuente Nueva S/N, 18071 Granada, Spain.

*E-mail: jmcuerva@ugr.es; victorblancos@ugr.es

Table of Contents

1. Experimental Section

1.1. General Methods

Unless otherwise noted, commercially available reagents, solvents and anhydrous solvents were used as purchased without further purification. Anhydrous THF was freshly distilled over Na/benzophenone. Tris[(1-benzyl-1H-1,2,3-triazol-4-yl)methyl]amine (TBTA),[S1] $Pd(dba)_2$,[S2] Boc-L-phenylalanine,[S3] compounds **S1**,[S4] **S3**,[S5] **S8**,[S6] **6**[S7] and **10**[S8] were prepared according to literature procedures. TLC plates were purchased from Sigma-Aldrich (silica gel matrix, with fluorescent indicator 254 nm) and were stained with potassium permanganate (1% w/v in water), cerium molybdate stain (Hanessian's stain) or phosphomolybdic acid (5% ethanol solution), or observed under UV light. Flash column chromatography was performed with Silica gel 60 (230-400 mesh, Scharlab, Spain). Silica gel G preparative TLC plates (20×20cm, 500 micron), were purchased from ANALTECH. Gel permeation chromatography was performed with Biobeads® SX−1 resin beads. ^{1}H and ^{13}C NMR spectra were recorded at room temperature on a Varian Inova Unity (300 MHz), Varian Direct Drive (500 MHz), Bruker Avance III HD NanoBay (400 MHz) or Bruker Avance Neo (400 MHz or 500 MHz) spectrometers at a constant temperature of 298 K. Chemical shifts are given in ppm and referenced to the signal of the residual protiated solvent (^{1}H: δ = 7.26 for $CDCl_3$, δ = 2.05 for acetone-d_6 and δ = 2.55 for DMSO-d_6 at room temperature) or the ^{13}C signal of the solvents (^{13}C: δ = 77.16 for $CDCl_3$ and δ = 39.52 for DMSO-d_6) or to the signal of the residual TMS (^{1}H: δ = 0.00). Coupling constant (J) values are given in Hz. Abbreviations indicating multiplicity were used as follow: m = multiplet, p = quintet, q = quartet, t = triplet, d = doublet, s = singlet, br = broad. Signals were assigned by means of 2D NMR spectroscopy (COSY, HSQC, HMBC). Electrospray (ESI) HRMS spectra were recorded on a Waters Xevo G2-XS QTOF or a Waters LCT Premier XE spectrometer. Electronic impact (EI) HRMS spectra were recorded on a Bruker Maxis II spectrometer. IR spectra were recorded with a Perkin-Elmer Spectrum Two FTIR ATR spectrometer. Optical rotations were recorded on a Perkin-Elmer 341 polarimeter.

1.2. Synthesis Overview

1.2.1. Synthesis of macrocycle 8

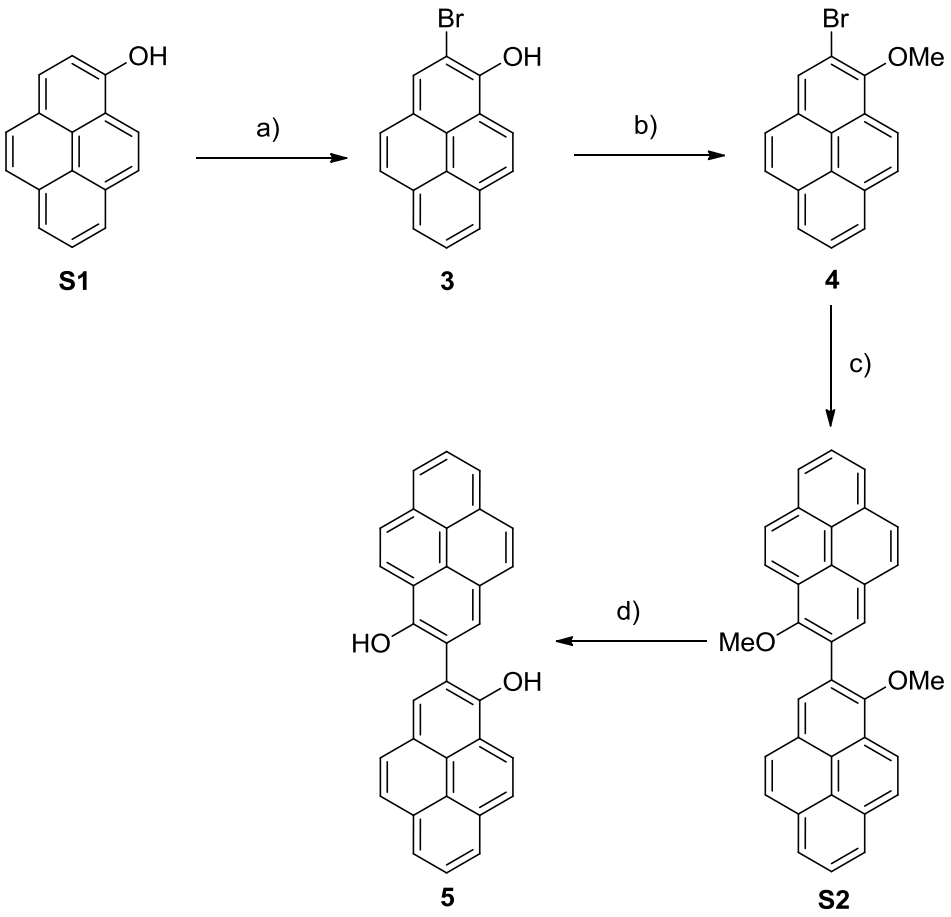

Scheme S1. Synthesis of compound **5**. Reagents and conditions: a) Br_2, $^tBuNH_2$, toluene, −78 ºC to r.t., 6 h, 67%; b) MeI, K_2CO_3, acetone, 0 ºC to reflux, 18 h, 83%; c) ^tBuLi, $Pd(dba)_2$, XPhos, toluene, r.t., 20 h, 79%; d) $BF_3{\cdot}SMe_2$, CH_2Cl_2, r.t., 6 h, 26%.

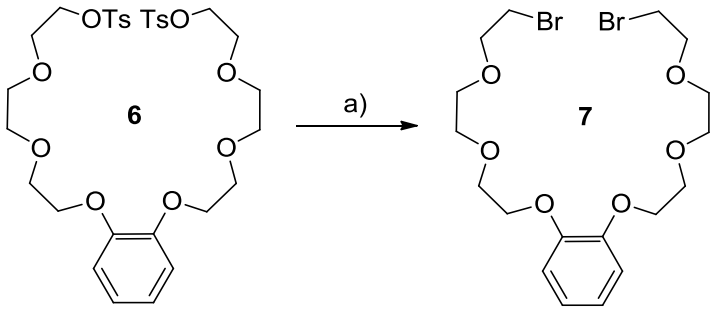

Scheme S2. Synthesis of compound **7**. Reagents and conditions: a) LiBr, acetone, reflux, O/N, 92%.

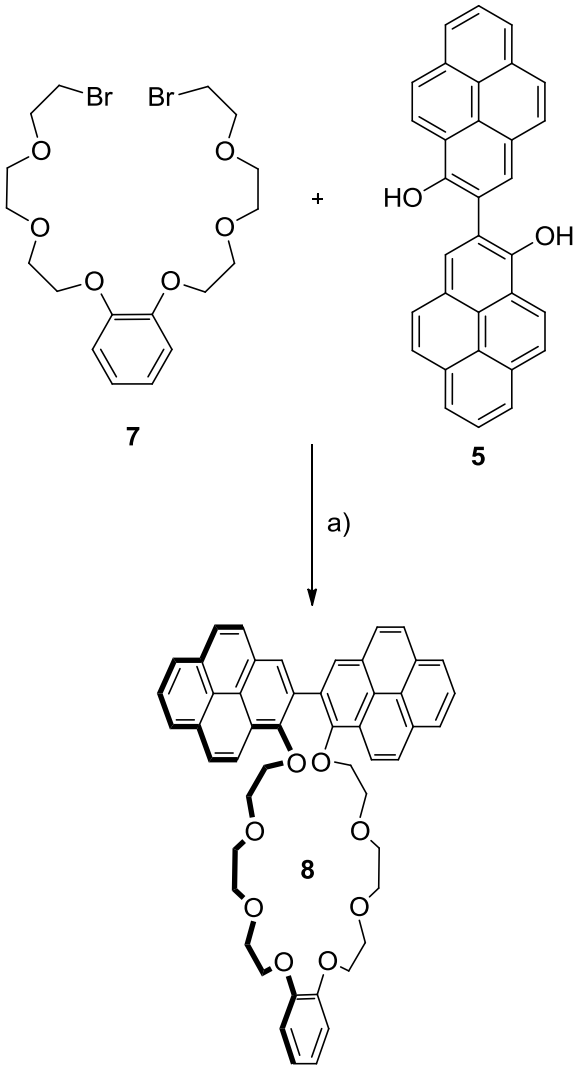

Scheme S3. Synthesis of macrocycle **8**. Reagents and conditions: a) ^{t}BuOK, KPF_6, $^{n}Bu_4NI$, 0.6 mM, dioxane, r.t. to reflux, 24 h, 34%.

1.2.2. Synthesis of stopper 12

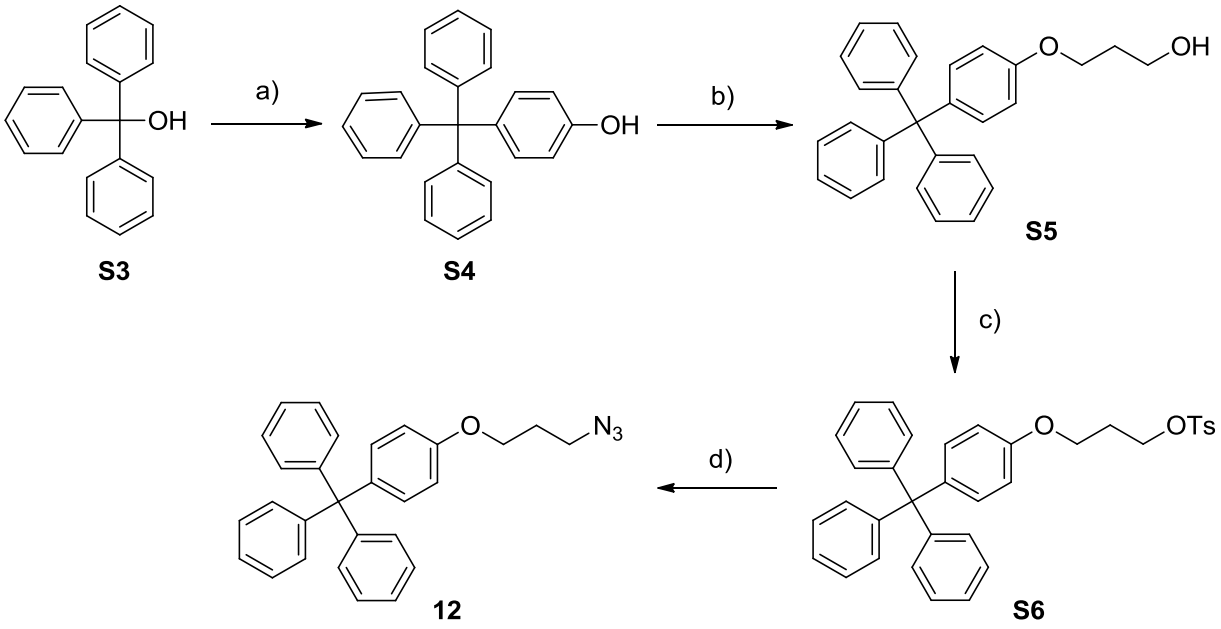

Scheme S4: Synthesis of stopper **12**. Reagents and conditions: a) Phenol, $HCl_{(aq.)}$ (37%), 160 ºC, 6 h, 60%; b) K_2CO_3, 3-Bromo-1-propanol, acetone, reflux, 24 h, 98%; c) TsCl, Et_3N, $DMAP_{(cat)}$, CH_2Cl_2, r.t., O/N, 87%; d) NaN_3, DMF, 70 ºC, 15 h, 73%.

1.2.3. Synthesis of axles (*R*)/(*S*)-11-$H^+ \cdot PF_6^-$

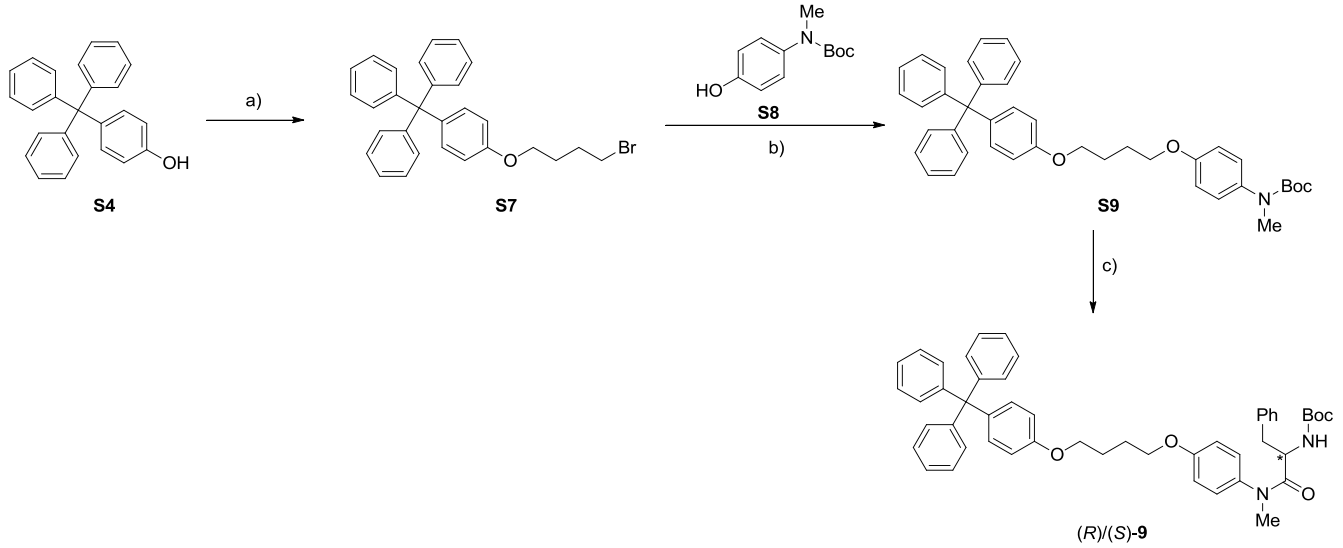

Scheme S5: Synthesis of compounds (*R*)/(*S*)-**9**. Reagents and conditions: a) 1,4-Dibromobutane, K_2CO_3, CH_3CN, 75 ºC, O/N, 54%; b) **S8**, Cs_2CO_3, DMF, 70 ºC, O/N, 59%; c) 1. CF_3CO_2H, CH_2Cl_2, r.t., 4 h; 2. Boc-D-phenylalanine (or Boc-L-phenylalanine), HOBt, EDCI, DIPEA, CH_2Cl_2, 0 ºC to r.t., 19 h, 60% (for (*R*)-**9**) and 66% (for (*S*)-**9**).

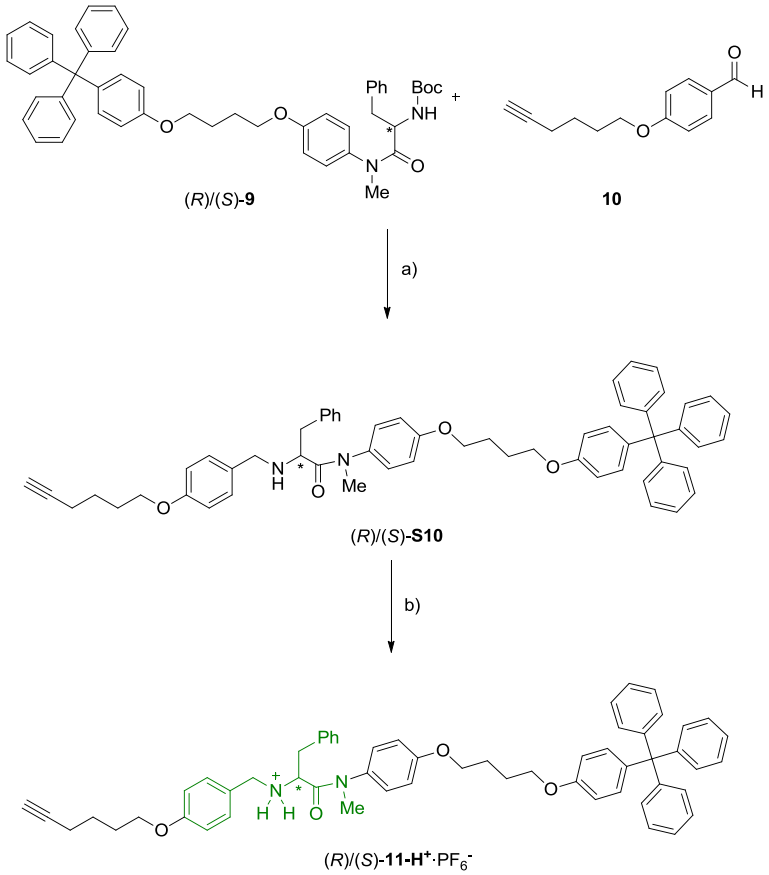

Scheme S6: Synthesis of axles (*R*)/(*S*)-**11**-$H^+ \cdot PF_6^-$. Reagents and conditions: a) 1. CF_3CO_2H, CH_2Cl_2, r.t., 4 h; 2. **10**, Et_3N, MeOH, r.t., 24 h; 3. $NaBH_4$, THF/MeOH, r.t., 18 h, 32% (for (*R*)-**S10**) and 34% (for (*S*)-**S10**); b) 1. HCl (1.0 M in Et_2O), CH_2Cl_2, r.t., 8 h; 2. KPF_6, CH_2Cl_2/acetone/H_2O, r.t., 16 h, 98% (for (*R*)-**11**-$H^+ \cdot PF_6^-$) and 91% (for (*S*)-**11**-$H^+ \cdot PF_6^-$).

1.2.4. Synthesis of threads (*R*)/(*S*)-2-$H^+ \cdot 2PF_6^-$

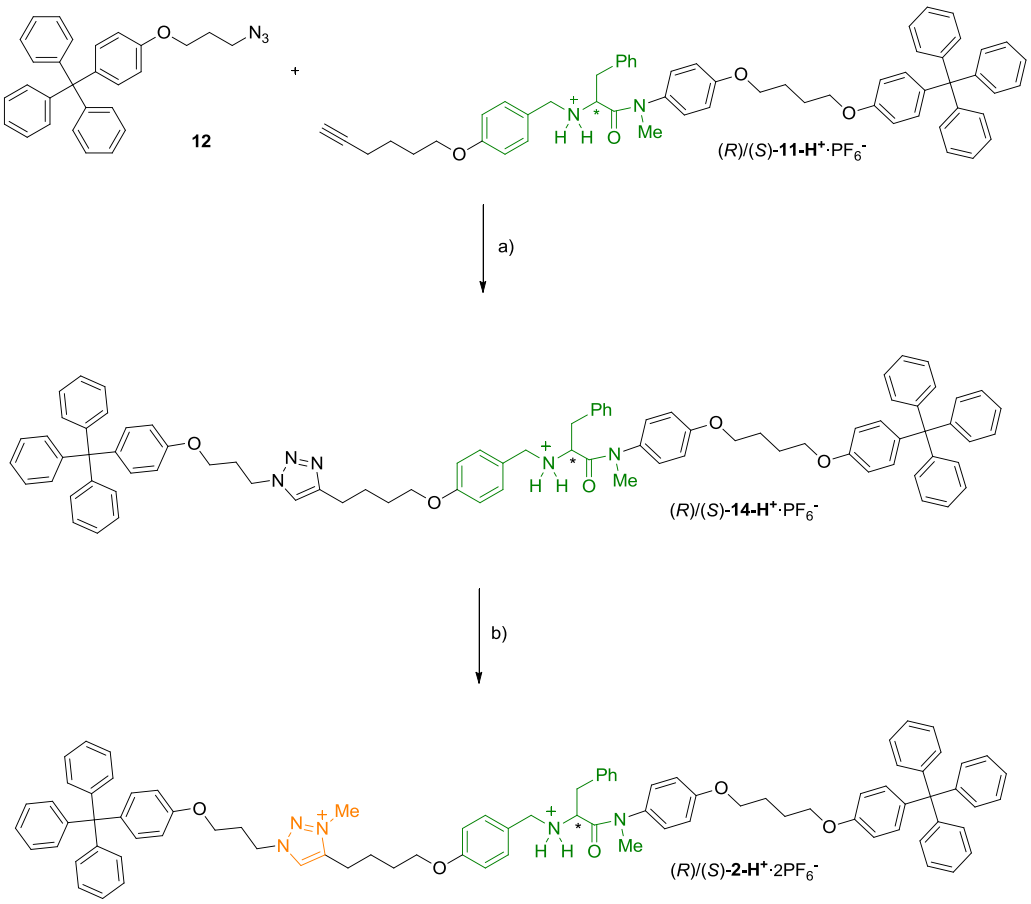

Scheme S7: Synthesis of threads (*R*)/(*S*)-**2**-$\mathbf{H}^+ \cdot 2PF_6^-$. Reagents and conditions: a) $Cu(CH_3CN)_4PF_6$, TBTA, CH_2Cl_2, r.t., 48 h, 95% (for (*R*)-**14**-$\mathbf{H}^+ \cdot PF_6^-$) and 59% (for (*S*)-**14**-$\mathbf{H}^+ \cdot PF_6^-$); b) 1. MeI, r.t., 4 d; 2. KPF_6, CH_2Cl_2/acetone/H_2O, r.t., 18 h, 58% (for (*R*)-**2**-$\mathbf{H}^+ \cdot 2PF_6^-$) and 98% (for (*S*)-**2**-$\mathbf{H}^+ \cdot 2PF_6^-$).

1.2.5. Synthesis of rotaxanes (*R*)/(*S*)-1-$H^+ \cdot 2PF_6^-$

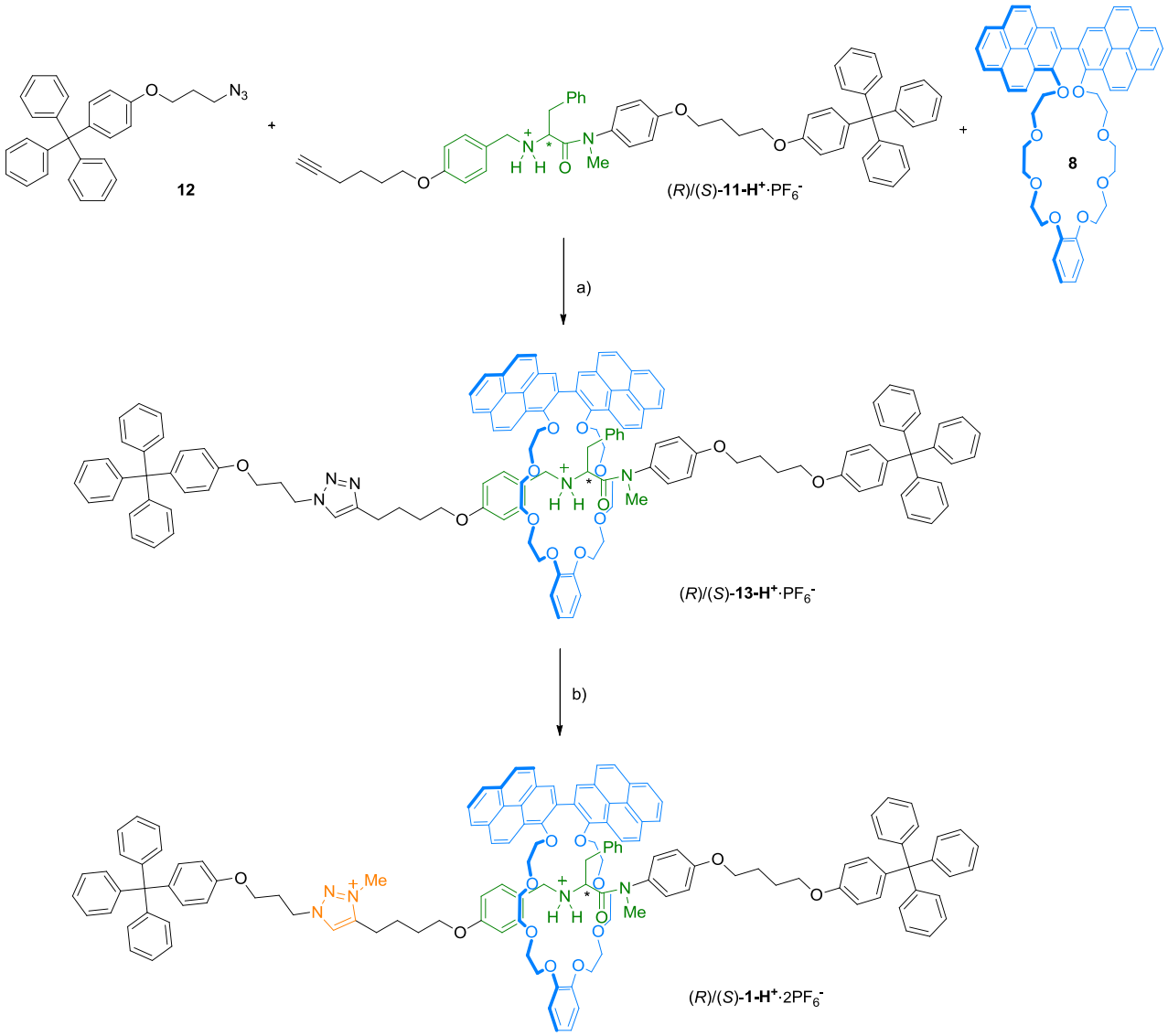

Scheme S8: Synthesis of rotaxanes (*R*)/(*S*)-**1**-$\mathbf{H}^+ \cdot 2PF_6^-$: Reagents and conditions: a) $Cu(CH_3CN)_4PF_6$, TBTA, CH_2Cl_2, r.t., 3 d, 35% (for (*R*)-**13**-$\mathbf{H}^+ \cdot PF_6^-$) and 19% (for (*S*)-**13**-$\mathbf{H}^+ \cdot PF_6^-$); b) 1. MeI, r.t., 4 d; 2. KPF_6, CH_2Cl_2/acetone/H_2O, r.t., 5 h, 68% (for (*R*)-**1**-$\mathbf{H}^+ \cdot 2PF_6^-$) and 55% (for (*S*)-**1**-$\mathbf{H}^+ \cdot 2PF_6^-$).

1.2.6. Switching of rotaxanes (*R*)/(*S*)-1

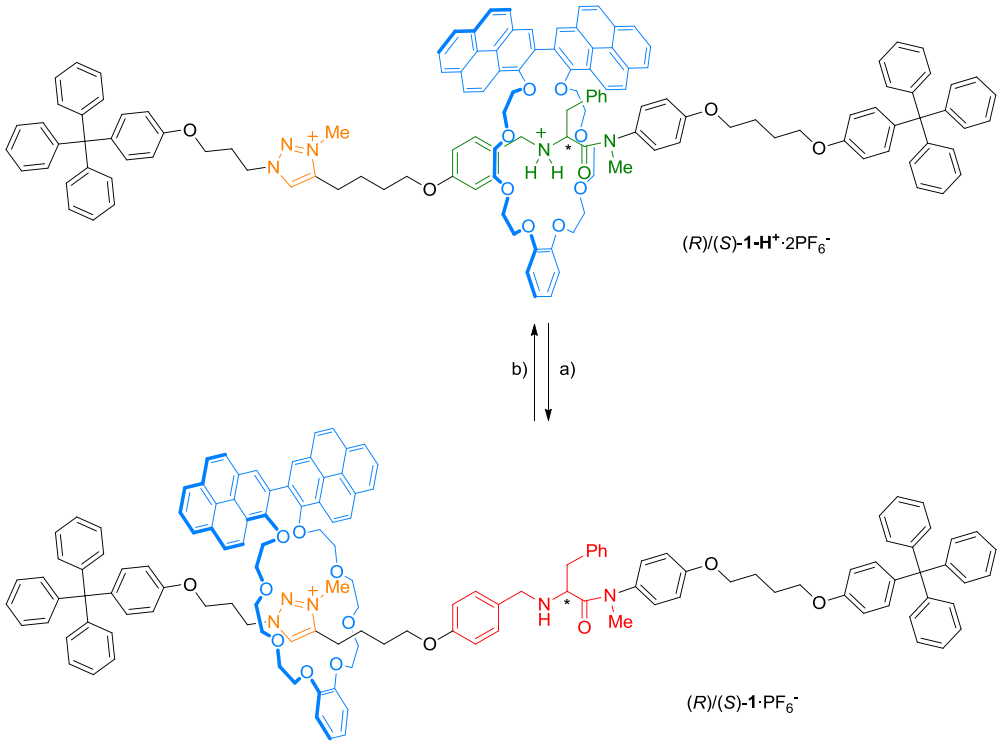

Scheme S9: Switching of rotaxanes (R)/(S)-**1**: Reagents and conditions: a) K_2CO_3, $CHCl_3$, r.t., 1 min; b) CF_3CO_2H, $CHCl_3$, r.t., 1 min.

1.3. Synthetic procedures and characterization details

Compound 3:

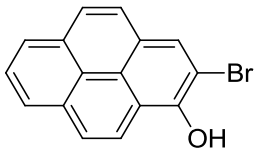

Compound **3** was prepared according to Koreeda's procedure:[S4] To a degassed solution of $^{t}BuNH_2$ (1.50 mL, 14.5 mmol) in anhydrous toluene (20 mL) at −30 ºC was added rapidly Br_2 (400 μL, 7.95 mmol). The solution was stirred for 30 min at −30 ºC and cooled to −78 ºC. In another round-bottom flask, a solution of **S1** (1.58 g, 7.23 mmol) and $^{t}BuNH_2$ (0.750 mL, 7.23 mmol) in anhydrous toluene (150 mL) was stirred for 20 min at −78 ºC. The bromine solution was then added to the pyrene solution. The resulting mixture was stirred for 30 min at −78 ºC and then warmed up slowly to room temperature over 6 h. To this mixture was added EtOAc (200 mL). The organic layer was washed with H_2O (2 × 200 mL) and brine (200 mL). The organic layer was dried over anhydrous Na_2SO_4 and the solvent was evaporated under vacuum. The crude material was purified by column chromatography (SiO_2, CH_2Cl_2/hexane 40:60) to afford **3** (1.45 g, 67%) as a yellow solid.

^{1}H NMR (300 MHz, acetone-d_6) δ = 8.87 (s, 1H), 8.47 (d, J = 9.3 Hz, 1H), 8.44 (s, 1H), 8.25 – 8.15 (m, 3H), 8.05 (d, J = 7.6 Hz, 1H), 8.02 (m, 2H). Spectral data agree with those previously reported. [S4]

Compound 4:

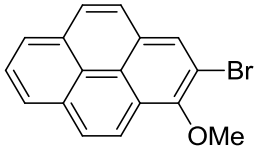

Under inert atmosphere, to a solution of **3** (744 mg, 2.50 mmol) in anhydrous acetone (50 mL), at 0 ºC, were added K_2CO_3 (1.70 g, 12.5 mmol) and iodomethane (315 μL, 5.00 mmol). The solution was stirred for 30 min at 0 ºC and then, refluxed for 18 h. The solvent was removed under reduced pressure and the solid was dissolved in a mixture of CH_2Cl_2/H_2O (1:1, 150 mL). Layers were separated and the aqueous one was extracted with CH_2Cl_2 (75 mL). The combined organic layers were dried over anhydrous Na_2SO_4 and the solvent was evaporated under vacuum. The crude material was purified by column chromatography (SiO_2, CH_2Cl_2/hexane 20:80) to give **4** (650 mg, 83%) as a yellow solid.

^{1}H NMR (500 MHz, $CDCl_3$): δ = 8.32 – 8.27 (m, 2H), 8.13 (m, 2H), 8.07 (d, J = 9.1 Hz, 1H), 8.01 – 7.93 (m, 2H), 7.84 (d, J = 9.0 Hz, 1H), 4.14 (s, 3H). ^{13}C NMR (126 MHz, $CDCl_3$): δ = 150.89, 130.97, 130.95, 129.12, 128.52, 128.45, 127.55, 126.46, 126.05, 125.57, 125.55, 125.45, 125.07, 124.60, 121.21, 115.17, 62.42. IR (neat): ν = 3046, 2934, 1588, 1480, 1421, 1254, 1107, 1003, 840, 826, 783, 737. HR-MS (EI$^+$): *m/z*: 310.0007 $[M]^+$ (calcd for $C_{17}H_{11}OBr$: 309.9993).

Compound S2:

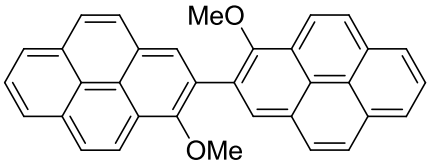

Caution! *The ^{t}BuLi solution in pentane is a pyrophoric liquid as ^{t}BuLi catches fire spontaneously if exposed to air. Although we did not experience any problem, this reagent should be handled with care under inert atmosphere and adequate safety measures should be taken during the synthesis. Moreover, the reaction should not be scaled up.*

Compound **S2** was prepared by adapting the methodology developed by Feringa and co-workers:[S9] **4** (602 mg, 1.94 mmol), $Pd(dba)_2$ (333 mg, 0.581 mmol) and XPhos (553 mg, 1.16 mmol) were dissolved in degassed anhydrous toluene (20 mL). To this solution was added ^{t}BuLi (1.6 M in pentane, 1.80 mL, 2.90 mmol) over 2 h using a syringe pump at room temperature. The solution was further stirred for 18 h at room temperature. The mixture was concentrated and the crude was purified by column chromatography (SiO_2, CH_2Cl_2/hexane 40:60) to yield **S2** (362 mg, 79%) as a yellow solid.

^{1}H NMR (400 MHz, $CDCl_3$): δ = 8.54 (d, J = 9.2 Hz, 2H), 8.43 (s, 2H), 8.26 – 8.16 (m, 6H), 8.13 – 8.02 (m, 6H), 3.69 (s, 6H). ^{13}C NMR (101 MHz, $CDCl_3$): δ = 152.67, 131.53, 131.48, 130.17, 128.22, 127.84, 127.78, 127.35, 126.83, 126.42, 125.92, 125.13, 125.05, 125.03, 124.54, 122.03, 62.46. IR (neat): ν = 2924, 2852, 1730, 1597, 1464, 1246, 1006, 842, 830, 760. HR-MS (ESI^+): *m/z*: 463.1685 $[M+H]^+$ (calcd for $C_{34}H_{23}O_2$: 463.1698).

Compound 5:

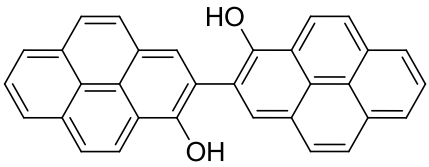

Under an Ar atmosphere, to a solution of **S2** (833 mg, 1.80 mmol) in anhydrous CH_2Cl_2 (80 mL) was added $BF_3{\cdot}SMe_2$ (2.30 mL, 21.6 mmol). The solution was stirred for 6 h at room temperature and then diluted with CH_2Cl_2 (200 mL). The mixture was washed with $HCl_{(aq)}$ (5%, 200 mL). Layers were separated and the aqueous one was extracted with CH_2Cl_2 (2 × 200 mL). The combined organic layers were dried over anhydrous Na_2SO_4 and the solvent was evaporated under reduced pressure. The crude material was purified by column chromatography (SiO_2, CH_2Cl_2/hexane 1:1 to 1:0, then acetone). Fractions containing the product were combined and concentrated. The resulting solid was washed with $CHCl_3$, filtered and collected to yield **5** (202 mg, 26%) as a brown solid.

^{1}H NMR (400 MHz, DMSO-d_6): δ = 9.79 (br, 2H), 8.55 (d, J = 9.2 Hz, 2H), 8.32 (s, 2H), 8.25 – 8.09 (m, 8H), 8.01 (m, 4H). ^{13}C NMR (101 MHz, DMSO-d_6): δ = 149.88, 131.32, 131.18, 128.89, 127.50, 126.23, 125.87, 125.07, 125.02, 124.40, 124.32, 124.11, 124.00, 123.75, 122.04, 119.37. IR (neat): ν = 2923, 2853, 1728, 1462, 1275, 1123, 841, 750. HR-MS (ESI^-): *m/z*: 433.1226 $[M-H]^-$ (calcd for $C_{32}H_{17}O_2$: 433.1229).

Compound 7:

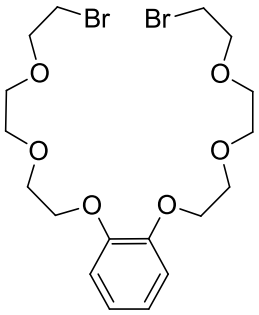

Under Ar, to a solution of **6** (455 mg, 0.666 mmol) in anhydrous acetone (5 mL) was added LiBr (1.13 g, 13.0 mmol). The suspension was refluxed overnight. The mixture was diluted with EtOAc (100 mL) and washed with brine (2 × 100 mL). The organic layer was dried over anhydrous Na_2SO_4 and the solvent was removed under vacuum. The crude material was purified by column chromatography (SiO_2, gradient from hexane/EtOAc 90:10 to 30:70) to afford **7** (307 mg, 92%) as a yellow oil.

^{1}H NMR (500 MHz, $CDCl_3$): δ = 6.89 (m, 4H), 4.14 (t, J = 6.2 Hz, 4H), 3.84 (t, J = 6.2 Hz, 4H), 3.78 (t, J = 6.3 Hz, 4H), 3.72 (m, 4H), 3.66 (m, 4H), 3.44 (t, J = 6.3 Hz, 4H). ^{13}C NMR (126 MHz, $CDCl_3$): δ = 148.97, 121.65, 114.97, 71.18, 70.79, 70.57, 69.86, 68.89, 30.44. IR (neat): ν = 2871, 1592, 1502, 1254, 1114, 1051, 930, 747. HR-MS (ESI$^+$): *m/z*: 521.0145 $[M+Na]^+$ (calcd for $C_{18}H_{28}Br_2O_6Na$: 521.0150).

Compound 8:

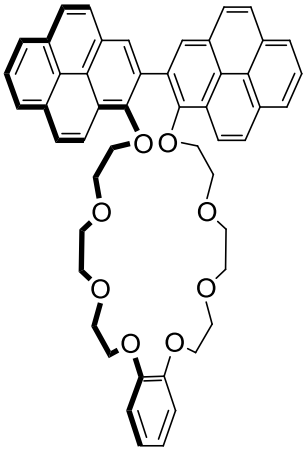

To a degassed solution of **5** (41 mg, 0.094 mmol) in anhydrous dioxane (150 mL) was added ^{t}BuOK (42 mg, 0.38 mmol). The solution was stirred for 20 min at room temperature and subsequently, were added **7** (47 mg, 0.094 mmol), KPF_6 (17 mg, 0.094 mmol) and a catalytic amount of ^{n}Bu$_4$NI. The mixture was refluxed for 24 h. The solvent was removed under reduced pressure, the solid was dissolved in CH_2Cl_2 (150 mL) and an excess of KPF_6 was added. The mixture was filtered and the solvent was evaporated under vacuum. The crude material was purified by column chromatography (SiO_2, CH_2Cl_2/MeOH 96:4), then by preparative TLC (SiO_2, CH_2Cl_2/MeOH 97:3) and finally by gel permeation chromatography (Bio-Beads® SX-1, CH_2Cl_2). The resulting solid was dissolved in CH_2Cl_2 (30 mL) and washed with an aqueous solution of Na_4EDTA (0.1 M, 5 × 50 mL) and H_2O (3 × 50 mL). The organic layer was dried over anhydrous Na_2SO_4 and the solvent was removed under vacuum to give **8** (25 mg, 34%) as a brown solid.

^{1}H NMR (500 MHz, $CDCl_3$): δ = 8.63 (d, J = 9.0 Hz, 2H), 8.40 (s, 2H), 8.18 (d, J = 7.6 Hz, 2H), 8.14 – 7.99 (m, 10H), 6.92 (m, 2H), 6.83 (m, 2H), 4.09 – 3.89 (m, 8H), 3.63 (m, 6H), 3.45 (m, 10H). ^{13}C NMR (126 MHz,

$CDCl_3$): δ = 151.49, 149.13, 131.48, 131.40, 130.23, 129.33, 128.27, 127.73, 127.70, 127.28, 126.76, 126.34, 125.73, 125.02, 124.99, 124.90, 122.31, 121.61, 114.64, 74.21, 70.90, 70.85, 70.39, 69.79, 69.20. IR (neat): ν = 3040, 2924, 2869, 1593, 1502, 1452, 1347, 1255, 1209, 1120, 1047, 844, 764, 749. HR-MS (ESI^+): *m/z*: 795.2936 $[M+Na]^+$ (calcd for $C_{50}H_{44}O_8Na$: 795.2934); 811.2678 $[M+K]^+$ (calcd for $C_{50}H_{44}O_8K$: 811.2673)

Compound S4:

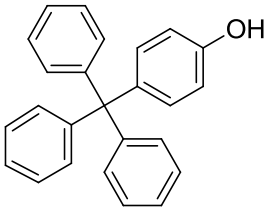

To a solution of **S3** (63.7 g, 0.245 mol) and phenol (350 g) at 160 ºC, was added $HCl_{(aq.)}$ (37%, 12 mL). The mixture was further stirred for 6 h at 160 ºC. Subsequently, toluene (500 mL) was added while the mixture was hot and the suspension was allowed to precipitate overnight at room temperature. The resulting solid was collected, washed with toluene (500 mL), cold Et_2O (300 mL) and dried under vacuum to give **S4** (49.1 g, 60%) as a white solid.

^{1}H NMR (400 MHz, DMSO-d_6): δ = 7.27 (t, *J* = 7.6 Hz, 6H), 7.21 – 7.10 (m, 9H), 6.90 (d, *J* = 8.8 Hz, 2H), 6.68 (d, *J* = 8.8 Hz, 2H). ^{13}C NMR (101 MHz, DMSO-d_6): δ = 155.26, 146.84, 136.57, 131.56, 130.46, 127.55, 125.80, 114.37, 63.74. IR (neat): ν = 3549, 3027, 1611, 1592, 1507, 1262, 1177, 1161, 764, 750, 701. HR-MS (ESI^-): *m/z*: 335.1435 $[M–H]^-$ (calcd for $C_{25}H_{19}O$: 335.1436).

Compound S5:

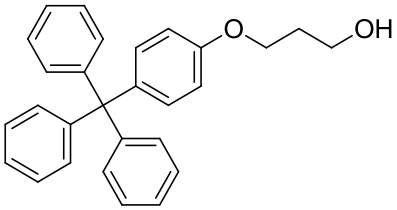

Under inert atmosphere, to a solution of **S4** (1.00 g, 2.97 mmol) in anhydrous acetone (100 mL) were added K_2CO_3 (2.06 g, 14.9 mmol) and 3-bromo-1-propanol (340 µL, 3.87 mmol). The suspension was refluxed for 24 h. The mixture was filtered and the solvent was removed under reduced pressure. The resulting solid was dissolved in a mixture of CH_2Cl_2/H_2O (1:1, 100 mL). Layers were separated and the aqueous one was extracted with CH_2Cl_2 (50 mL). The combined organic phases were dried over anhydrous Na_2SO_4 and the solvent was removed under vacuum. The crude material was purified by column chromatography (SiO_2, CH_2Cl_2) to afford **S5** (1.15 g, 98%) as a white solid.

^{1}H NMR (500 MHz, $CDCl_3$): δ = 7.27 – 7.17 (m, 15H), 7.11 (d, *J* = 8.9 Hz, 2H), 6.79 (d, *J* = 8.9 Hz, 2H), 4.11 (t, *J* = 5.9 Hz, 2H), 3.85 (t, *J* = 5.9 Hz, 2H), 2.04 (p, *J* = 5.9 Hz, 2H).^{13}C NMR (126 MHz, $CDCl_3$): δ = 156.80, 147.14, 139.36, 132.37, 131.25, 127.56, 125.99, 113.37, 65.84, 64.45, 60.81, 32.14. IR (neat): ν = 3323 (br), 1605, 1507, 1264, 1248, 1183, 1058, 1034, 825, 748, 700. HR-MS (ESI^+): *m/z*: 417.1830 $[M+Na]^+$ (calcd for $C_{28}H_{26}O_2Na$: 417.1830).

Compound S6:

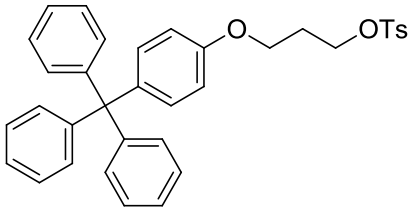

Under an Ar atmosphere, to a solution of **S5** (2.00 g, 5.07 mmol) in CH_2Cl_2 (200 mL) were added Et_3N (2.80 mL, 20.3 mmol), TsCl (1.93 g, 10.1 mmol) in three portions and a catalytic amount of DMAP. The solution was stirred overnight at room temperature. The solvent was removed under reduced pressure and the crude material was purified by column chromatography (SiO_2, hexane/CH_2Cl_2 60:40 to 40:60) to afford **S6** (2.41 g, 87%) as a white solid.

^{1}H NMR (500 MHz, $CDCl_3$): δ = 7.75 (d, J = 8.3 Hz, 2H), 7.27 – 7.17 (m, 17H), 7.08 (d, J = 8.9 Hz, 2H), 6.64 (d, J = 8.9 Hz, 2H), 4.23 (t, J = 6.1 Hz, 2H), 3.94 (t, J = 5.9 Hz, 2H), 2.35 (s, 3H), 2.10 (p, J = 6.0 Hz, 2H).^{13}C NMR (126 MHz, $CDCl_3$): δ = 156.54, 147.12, 144.89, 139.44, 132.98, 132.28, 131.23, 129.98, 128.03, 127.59, 126.03, 113.34, 67.26, 64.45, 63.15, 29.06, 21.76. IR (neat): ν = 3056, 1598, 1508, 1362, 1251, 1187, 1176, 948, 750, 702. HR-MS (ESI$^+$): *m/z*: 571.1923 $[M+Na]^+$ (calcd for $C_{35}H_{32}SO_2Na$: 571.1919).

Compound 12:

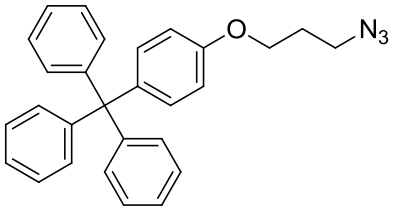

Caution! *NaN_3 is very toxic if swallowed, in contact with skin (readily absorbed) or inhaled. Therefore this reagent should be handled with care and adequate safety measures should be taken during the synthesis and large scale reactions should be avoided. Moreover, it forms explosive metal azides if it reacts with lead or copper.*

Under Ar, to a solution of **S6** (309 mg, 0.563 mmol) in anhydrous DMF (15 mL) was added NaN_3 (109 mg, 1.68 mmol). The suspension was stirred for 15 h at 70 ºC. The mixture was diluted with CH_2Cl_2 (30 mL) and washed with H_2O (3 × 30 mL). Subsequently, the aqueous phase was extracted with CH_2Cl_2 (2 × 70 mL). The combined organic layers were dried over anhydrous Na_2SO_4 and the solvent was evaporated under reduced pressure. The crude material was purified by column chromatography (SiO_2, hexane/CH_2Cl_2 60:40) to give **12** (172 mg, 73%) as a white solid.

^{1}H NMR (400 MHz, $CDCl_3$): δ = 7.27 – 7.15 (m, 15H), 7.10 (d, J = 8.9 Hz, 2H), 6.77 (d, J = 8.9 Hz, 2H), 4.02 (t, J = 5.9 Hz, 2H), 3.51 (t, J = 6.7 Hz, 2H), 2.03 (p, J = 6.3 Hz, 2H). ^{13}C NMR (101 MHz, $CDCl_3$): δ = 156.74, 147.14, 139.41, 132.37, 131.25, 127.57, 126.00, 113.38, 64.48, 64.46, 48.42, 28.98. IR (neat): ν = 3056, 2096, 1606, 1508, 1248, 1183, 764, 749, 701. Spectral data agree with those previously reported values. [S10]

Compound S7:

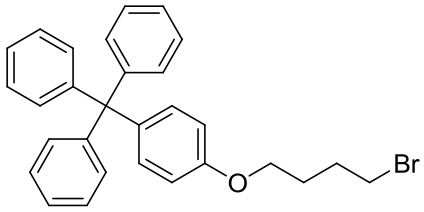

Under inert atmosphere, to a solution of **S4** (5.00 g, 14.9 mmol) in anhydrous CH_3CN (150 mL) were added K_2CO_3 (10.3 g, 74.5 mmol) and 1,4-dibromobutane (8.85 mL, 74.1 mmol). The suspension was stirred overnight at 75 ºC. The solvent was then removed under vacuum and the solid was dissolved in a mixture of CH_2Cl_2/H_2O (1:1, 400 mL). Layers were separated and the organic one was washed with H_2O (2 × 200 mL). The organic phase was dried over anhydrous Na_2SO_4 and the solvent was evaporated under reduced pressure. The crude material was purified by column chromatography (SiO_2, hexane to hexane/CH_2Cl_2 90:10) to afford **S7** (3.78 g, 54%) as a white solid.

^{1}H NMR (400 MHz, $CDCl_3$): δ = 7.27 – 7.16 (m, 15H), 7.10 (d, J = 8.9 Hz, 2H), 6.76 (d, J = 8.9 Hz, 2H), 3.97 (t, J = 6.0 Hz, 2H), 3.48 (t, J = 6.6 Hz, 2H), 2.06 (m, 2H), 1.93 (m, 2H). ^{13}C NMR (101 MHz, $CDCl_3$): δ = 156.96, 147.18, 139.22, 132.36, 131.26, 127.56, 125.99, 113.35, 66.83, 64.47, 33.63, 29.68, 28.12. IR (neat): ν = 3055, 1607, 1507, 1251, 1183, 1035, 827, 764, 750, 702. HR-MS (EI$^+$): *m/z*: 470.1245 $[M]^+$ (calcd for $C_{29}H_{27}OBr$: 470.1245).

Compound S9:

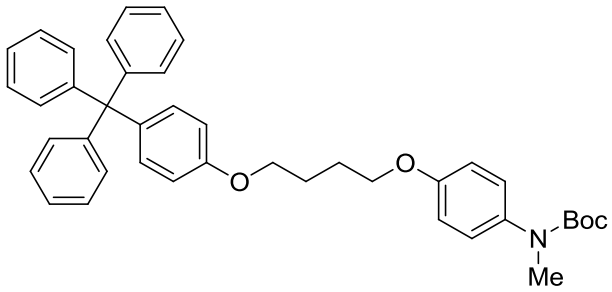

Under an Ar atmosphere, to a solution of **S7** (4.00 g, 8.48 mmol) in anhydrous DMF (15 mL) were added Cs_2CO_3 (6.97 g, 21.4 mmol) and **S8** (1.60 g, 7.17 mmol). The suspension was stirred overnight at 70 ºC. The mixture was diluted with EtOAc (100 mL) and washed with H_2O (3 × 100 mL) and brine (2 × 100 mL). The organic layer was dried over anhydrous Na_2SO_4 and concentrated to dryness. The crude material was purified by column chromatography (SiO_2, hexane to hexane/EtOAc 60:40) to yield **S9** (2.58 g, 59%) as a white solid.

^{1}H NMR (500 MHz, $CDCl_3$): δ = 7.27 – 7.16 (m, 15H), 7.13 – 7.08 (m, 4H), 6.83 (d, J = 8.9 Hz, 2H), 6.77 (d, J = 8.9 Hz, 2H), 4.01 (m, 4H), 3.21 (s, 3H), 1.96 (m, 4H), 1.43 (s, 9H). ^{13}C NMR (126 MHz, $CDCl_3$): δ = 157.06, 156.81, 155.28, 147.19, 139.07, 137.02, 132.34, 131.26, 127.55, 127.04, 125.98, 114.56, 113.35, 80.11, 67.83, 67.44, 64.45, 37.80, 28.52, 26.21. IR (neat): ν = 2950, 1696, 1510, 1365, 1244, 1150, 830, 764, 749, 702. HR-MS (ESI$^+$): *m/z*: 636.3093 $[M+Na]^+$ (calcd for $C_{41}H_{43}NO_4Na$: 636.3090).

Compounds (*R*)/(*S*)-9:

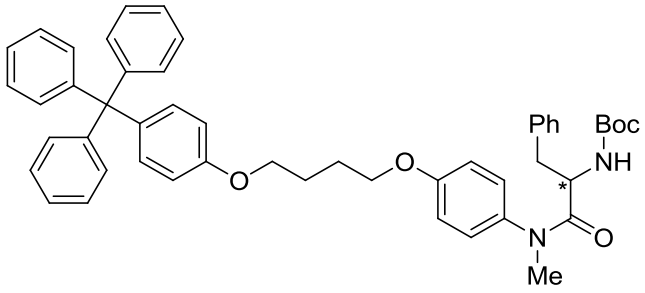

For the synthesis of (*R*)-**9**: To a solution of **S9** (515 mg, 0.839 mmol) in CH_2Cl_2 (5 mL) was added CF_3CO_2H (1 mL). The solution was stirred for 4 h at room temperature. The solvent was evaporated under reduced pressure. Subsequently, the solid was redissolved in toluene (3 × 20 mL) and concentrated to dryness. The solid was then dissolved in anhydrous CH_2Cl_2 (10 mL). Under Ar, to this solution were added Boc-D-Phe-OH (222 mg, 0.839 mmol), HOBt (113 mg, 0.839 mmol), EDCI (250 mg, 0.839 mmol) and DIPEA (145 µL, 0.839 mmol), while cooling in a water-ice bath. The mixture was stirred for 1 h at 0-4 ºC and for 18 h at room temperature. The solution was concentrated to dryness. The crude was dissolved in EtOAc (100 mL) and washed with successively with an aqueous solution of citric acid (10%, 2 × 50 mL), a saturated solution of $NaHCO_{3(aq)}$ (2 × 100 mL), $K_2CO_{3(aq)}$ (2 M, 2 × 100 mL) and brine (100 mL). The organic phase was dried over anhydrous Na_2SO_4 and the solvent was removed under reduced pressure. The crude material was purified by column chromatography (SiO_2, hexane/EtOAc 98:2 to 50:50) to give (*R*)-**9** (383 mg, 60%) as a white solid.

For the synthesis of (*S*)-**9**: This enantiomer was obtained following the same procedure starting from **S9** (500 mg, 0.815 mmol), employing Boc-L-Phe-OH and affording (*S*)-**9** (407 mg, 66%) as a white solid.

^{1}H NMR (500 MHz, $CDCl_3$): δ = 7.26 – 7.16 (m, 20H), 7.11 (d, *J* = 8.7 Hz, 2H), 6.95 (d, *J* = 5.5 Hz, 2H), 6.84 – 6.68 (m, 4H), 5.20 (d, *J* = 9.1 Hz, 1H), 4.52 (q, *J* = 7.9 Hz, 1H), 4.03 (m, 4H), 3.17 (s, 3H), 2.89 (dd, *J* = 13.3, 7.4 Hz, 1H), 2.71 (dd, *J* = 13.3, 7.4 Hz, 1H), 1.98 (m, 4H), 1.38 (s, 9H). ^{13}C NMR (126 MHz, $CDCl_3$): δ = 172.19, 158.54, 157.02, 154.85, 147.15, 139.07, 136.78, 135.27, 132.32, 131.23, 129.55, 128.47, 128.41, 127.52, 126.74, 125.95, 115.39, 113.34, 79.47, 67.80, 67.36, 64.42, 52.20, 39.96, 37.83, 28.43, 26.15, 26.13. IR (neat): ν = 3307, 2922, 2852, 1711, 1652, 1509, 1245, 1172, 764, 750, 702. HR-MS (ESI$^+$): *m/z*: 783.3771 $[M+Na]^+$ (calcd for $C_{50}H_{52}N_2O_5Na$: 783.3774); 761.3951 $[M+H]^+$ (calcd for $C_{50}H_{53}N_2O_5$: 761.3954). Spectral data are similar for both enantiomers except for the optical rotation: (*R*)-**9**: $[\alpha]_D^{20}$ = –4.2º (*c* 1, CH_2Cl_2); (*S*)-**9**: $[\alpha]_D^{20}$ = +4.0º (*c* 1, CH_2Cl_2).

Compounds (*R*)/(*S*)-S10:

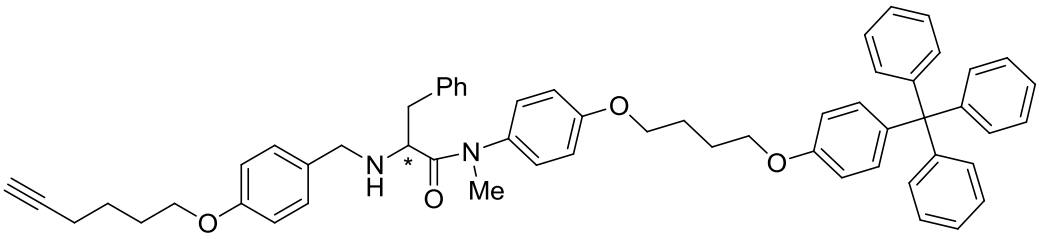

For the synthesis of (*R*)-**S10**: To a solution of (*R*)-**9** (226 mg, 0.297 mmol) in CH_2Cl_2 (10 mL) was added CF_3CO_2H (4 mL). The mixture was stirred for 4 h at room temperature and the solvent was evaporated under reduced pressure. The solid was dissolved in anhydrous MeOH (15 mL). Under an Ar atmosphere, Et_3N (1.6 mL) and **10** (60 mg, 0.297 mmol) were added. The mixture was stirred for 24 h at room temperature. Subsequently, $NaBH_4$ (50 mg, 1.33 mmol) and anhydrous THF (5 mL) were added. The solution was stirred for 18 h at room temperature. Then, H_2O (15 mL) was added and the solution was stirred for another 30 min at room temperature. The product was extracted with CH_2Cl_2 (3 × 30 mL). The combined organic phases were dried over anhydrous

Na_2SO_4 and the solvent was evaporated under vacuum. The crude material was purified by column chromatography (SiO_2, Hexane/EtOAc 40:60 to 20:80) to yield (*R*)-**S10** (80 mg, 32%) as a white solid.

For the synthesis of (*S*)-**S10**: This enantiomer was synthesized following the same procedure starting from (*S*)-**9** (163 mg, 0.214 mmol) and affording (*S*)-**S10** (62 mg, 34%) as a white solid.

^{1}H NMR (500 MHz, $CDCl_3$): δ = 7.26 – 7.15 (m, 20H), 7.11 (m, 4H), 6.99 (d, *J* = 6.4 Hz, 2H), 6.77 (d, *J* = 8.3 Hz, 4H), 6.64 (d, *J* = 8.4 Hz, 2H), 4.03 – 3.93 (m, 6H), 3.70 (d, *J* = 12.6 Hz, 1H), 3.49 – 3.40 (m, 2H), 3.16 (s, 3H), 2.84 (dd, *J* = 12.9, 8.3 Hz, 1H), 2.77 (dd, *J* = 13.0, 6.2 Hz, 1H), 2.26 (td, *J* = 7.1, 2.6 Hz, 2H), 1.99 – 1.83 (m, 7H), 1.71 (p, *J* = 7.2 Hz, 2H). ^{13}C NMR (126 MHz, $CDCl_3$): δ = 174.83, 158.26, 158.12, 156.99, 147.13, 139.13, 138.28, 135.57, 132.33, 132.13, 131.21, 129.72, 129.27, 128.57, 128.30, 127.53, 126.50, 125.97, 115.10, 114.40, 113.31, 84.21, 68.78, 67.84, 67.42, 67.36, 64.42, 59.38, 51.22, 40.61, 37.67, 28.44, 26.13, 25.19, 18.29. IR (neat): ν = 3297, 2923, 2852, 1658, 1509, 1245, 1180, 1032, 831, 750, 701. HR-MS (ESI$^+$): *m/z*: 847.4476 $[M+H]^+$ (calcd for $C_{58}H_{59}N_2O_4$: 847.4475). Spectral data are similar for both enantiomers except for the optical rotation: (*R*)-**S10**: $[\alpha]_D^{20}$ = –32.8º (*c* 0.5, CH_2Cl_2); (*S*)-**S10**: $[\alpha]_D^{20}$ = +32.1º (*c* 0.5, CH_2Cl_2).

Compounds (*R*)/(*S*)-11-H$^+$·PF$_6^-$:

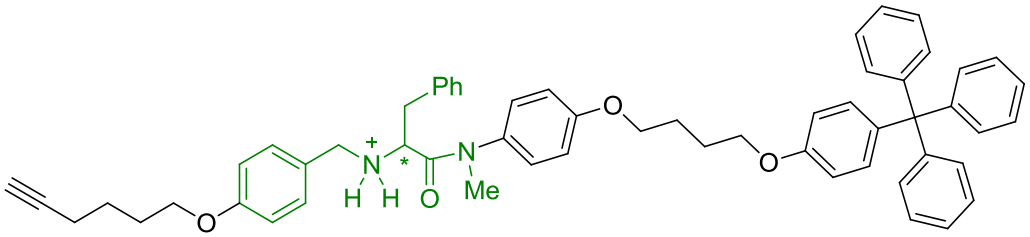

For the synthesis of (*R*)-**11-H**$^+$·PF_6^-: Under an Ar atmosphere, to a solution of (*R*)-**S10** (80 mg, 0.094 mmol) in CH_2Cl_2 (5 mL) was added HCl (1.0 M in Et_2O, 1.4 mL, 1.4 mmol). The solution was stirred for 8 h at room temperature. Subsequently the solvent was removed under reduced pressure and the solid was dissolved in CH_2Cl_2 (5 mL). To this solution were added acetone (10 mL), H_2O (10 mL) and an excess of KPF_6. The mixture was stirred for 16 h at room temperature. The resulting mixture was diluted with H_2O (50 mL) and extracted with CH_2Cl_2 (3 × 50 mL). The combined extracts were dried over anhydrous Na_2SO_4 and the solvent was evaporated under vacuum to yield (*R*)-**11-H**$^+$·PF_6^- (92 mg, 98%) as a white solid.

For the synthesis of (*S*)-**11-H**$^+$·PF_6^-: This enantiomer was synthesized following the same procedure starting from (*S*)-**S10** (134 mg, 0.158 mmol) and yielding (*S*)-**11-H**$^+$·PF_6^- (143 mg, 91%) as a white solid.

^{1}H NMR (500 MHz, $CDCl_3$): δ = 7.27 – 7.14 (m, 22H), 7.11 (d, *J* = 8.9 Hz, 2H), 6.86 – 6.76 (m, 8H), 4.17 (d, *J* = 13.0 Hz, 1H), 4.11 – 3.91 (m, 8H), 3.21 (s, 3H), 3.07 (d, *J* = 6.9 Hz, 2H), 2.26 (td, *J* = 7.0, 2.6 Hz, 2H), 2.03 – 1.85 (m, 7H), 1.69 (p, *J* = 7.1 Hz, 2H). ^{13}C NMR (126 MHz, $CDCl_3$): δ = 167.17, 160.47, 159.42, 157.01, 147.16, 139.17, 132.97, 132.90, 132.36, 131.40, 131.24, 129.48, 129.46, 128.28, 128.20, 127.56, 125.99, 120.87, 116.11, 115.49, 113.34, 84.06, 68.97, 68.15, 67.62, 67.37, 64.45, 58.74, 51.44, 38.82, 36.56, 28.28, 26.15, 26.13, 25.09, 18.30. IR (neat): ν = 3295, 2937, 1648, 1509, 1248, 1181, 837, 750, 701. HR-MS (ESI$^+$): *m/z*: 847.4479 $[M–PF_6^-]^+$ (calcd for $C_{58}H_{59}N_2O_4$: 847.4475). Spectral data are similar for both enantiomers except for the optical rotation: (*R*)-**11-H**$^+$·PF_6^-: $[\alpha]_D^{20}$ = –46.8º (*c* 0.25, CH_2Cl_2); (*S*)-**11-H**$^+$·PF_6^-: $[\alpha]_D^{20}$ = +42.7º (*c* 0.25, CH_2Cl_2).

Compounds (*R*)/(*S*)-14-$H^+ \cdot PF_6^-$:

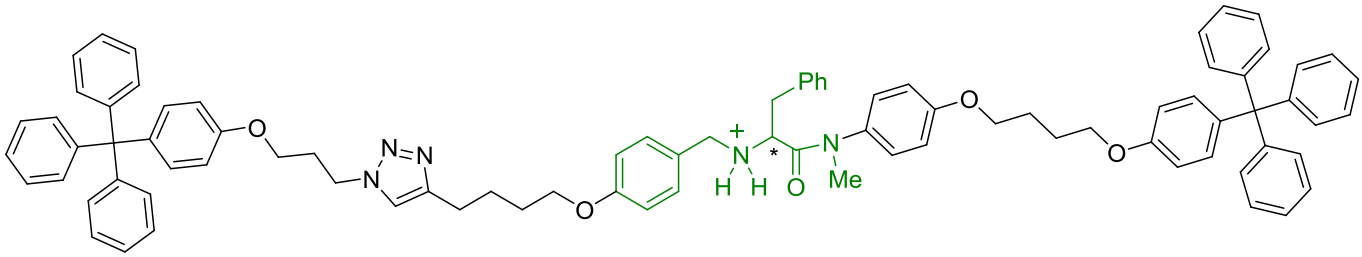

For the synthesis of (*R*)-**14**-$H^+ \cdot PF_6^-$: To a degassed solution of (*R*)-**11**-$H^+ \cdot PF_6^-$ (14 mg, 0.014 mmol) in anhydrous CH_2Cl_2 (3 mL) were added **12** (12 mg, 0.028 mmol), $Cu(CH_3CN)_4PF_6$ (3 mg, 0.007 mmol) and TBTA (4 mg, 0.007 mmol). The solution was stirred for 48 h at room temperature. The mixture was diluted with CH_2Cl_2 (40 mL) and washed with an aqueous solution of Na_4EDTA (0.1 M, 3 × 25 mL). The organic layer was dried over Na_2SO_4 and the solvent was removed under reduced pressure. The crude material was purified by gel permeation chromatography (Bio-Beads® S-X1, CH_2Cl_2). The resulting solid was dissolved in CH_2Cl_2 (10 mL) and HCl (1.0 M in Et_2O, 1.0 mL) was added under inert atmosphere. The solution was stirred for 3 h at room temperature. The solvent was then evaporated under vacuum. Subsequently, the solid was dissolved in CH_2Cl_2 (5 mL) and acetone (10 mL), H_2O (10 mL) and an excess of KPF_6 were added. The mixture was stirred overnight at room temperature. The resulting mixture was diluted with H_2O (20 mL) and extracted with CH_2Cl_2 (2 × 25 mL). The combined organic layers were dried over anhydrous Na_2SO_4 and concentrated to dryness to yield (*R*)-**14**-$H^+ \cdot PF_6^-$ (19 mg, 95%) as a white solid.

For the synthesis of (*S*)-**14**-$H^+ \cdot PF_6^-$: This enantiomer was obtained following the same procedure starting from (*S*)-**11**-$H^+ \cdot PF_6^-$ (62 mg, 0.062 mmol) and yielding (*S*)-**14**-$H^+ \cdot PF_6^-$ (52 mg, 59%) as a white solid.

^{1}H NMR (500 MHz, $CDCl_3$): δ = 7.33 (s, 1H), 7.25 – 7.15 (m, 37H), 7.10 (m, 4H), 6.89 (m, 2H), 6.81 – 6.71 (m, 8H), 4.51 (t, *J* = 6.9 Hz, 2H), 4.19 – 4.12 (m, 2H), 4.06 – 3.85 (m, 9H), 3.22 (s, 3H), 3.09 (d, *J* = 7.2 Hz, 2H), 2.66 (br, 2H), 2.33 (p, *J* = 6.4 Hz, 2H), 1.98 (br, 4H), 1.74 (br, 4H). ^{13}C NMR (126 MHz, $CDCl_3$): δ = 167.11, 160.43, 159.37, 157.04, 156.54, 147.78, 147.17, 147.08, 139.59, 139.12, 133.12, 132.94, 132.40, 132.34, 131.50, 131.27, 131.24, 131.20, 129.58, 129.37, 128.23, 128.18, 127.57, 127.55, 126.02, 125.98, 121.70, 121.06, 116.11, 115.43, 113.36, 68.14, 67.76, 67.40, 64.44, 64.19, 59.12, 51.41, 47.31, 38.74, 36.72, 30.12, 29.84, 28.64, 26.14, 26.10, 25.92, 25.18. IR (neat): ν = 2936, 1658, 1608, 1509, 1275, 1257, 1182, 844, 764, 750, 702. HR-MS (ESI$^+$): *m/z*: 1266.6466 $[M-PF_6^-]^+$ (calcd for $C_{86}H_{84}N_5O_5$: 1266.6472). Spectral data are similar for both enantiomers except for the optical rotation: (*R*)-**14**-$H^+ \cdot PF_6^-$: $[\alpha]_D^{20}$ = –22.3º (*c* 0.33, $CHCl_3$); (*S*)-**14**-$H^+ \cdot PF_6^-$: $[\alpha]_D^{20}$ = +22.1º (*c* 0.33, $CHCl_3$).

Compounds (*R*)/(*S*)-2-$H^+ \cdot 2PF_6^-$:

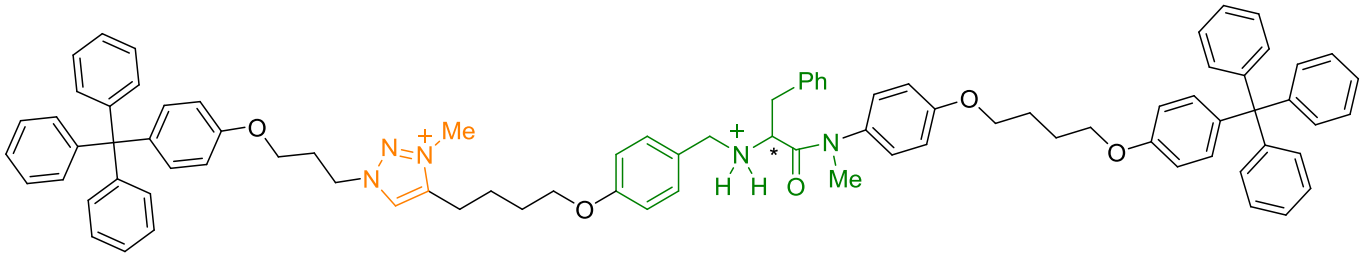

Compounds (*R*)- and (*S*)-**2**-$H^+ \cdot 2PF_6^-$ were prepared adpating the method reported by Zhu:[S11] For the synthesis of (*R*)-**2**-$H^+ \cdot 2PF_6^-$: Under Ar, a solution of (*R*)-**14**-$H^+ \cdot PF_6^-$ (17 mg, 12 μmol) in iodomethane (4 mL) was stirred for 4 days at room temperature. The solvent was removed under reduced pressure. Then, the solid was dissolved in

CH_2Cl_2 (5 mL) and acetone (10 mL), H_2O (10 mL) and an excess of KPF_6 were added. The mixture was stirred for 18 h at room temperature. The resulting mixture was diluted with H_2O (25 mL) and extracted with CH_2Cl_2 (3 × 30 mL). The combined extracts were dried over anhydrous Na_2SO_4 and were concentrated to dryness. The crude material was purified by preparative TLC (SiO_2, CH_2Cl_2/MeOH 98:2). The resulting solid was dissolved in CH_2Cl_2 (10 mL) and HCl (1.0 M in Et_2O, 1.0 mL) was added under inert atmosphere. The solution was stirred for 5 h at room temperature. The solvent was then evaporated under vacuum. Subsequently, the solid was dissolved in CH_2Cl_2 (2.5 mL) and acetone (5 mL), H_2O (5 mL) and an excess of KPF_6 were added. The mixture was stirred overnight at room temperature. The mixture was diluted with H_2O (10 mL) and extracted with CH_2Cl_2 (2 × 20 mL). The combined organic layers were dried over anhydrous Na_2SO_4 and the solvent was evaporated under vacuum to yield (*R*)-**2**-$\mathbf{H}^+\cdot 2PF_6^-$ (11 mg, 58%) as a white solid.

For the synthesis of (*S*)-**2**-$\mathbf{H}^+\cdot 2PF_6^-$: This enantiomer was synthetized following the same procedure starting from (*S*)-**14**-$\mathbf{H}^+\cdot PF_6^-$ (21 mg, 15 µmol) and affording (*S*)-**2**-$\mathbf{H}^+\cdot 2PF_6^-$ (23 mg, 98%) as a white solid.

^{1}H NMR (500 MHz, $CDCl_3$): δ = 8.12 (s, 1H), 7.25 – 7.13 (m, 37H), 7.09 (m, 4H), 6.94 (br, 2H), 6.79 – 6.66 (m, 8H), 4.67 (t, *J* = 7.0 Hz, 2H), 4.08 – 3.83 (m, 14H), 3.20 – 3.13 (m, 5H), 2.76 (t, *J* = 7.7 Hz, 2H), 2.40 (m, 2H), 1.96 (br, 4H), 1.81 (m, 4H). ^{13}C NMR (126 MHz, $CDCl_3$): δ = 166.82, 160.24, 159.35, 157.06, 156.30, 147.18, 147.08, 144.83, 139.69, 139.09, 133.11, 132.86, 132.38, 132.33, 131.59, 131.24, 131.17, 129.63, 129.41, 128.19, 128.09, 127.60, 127.56, 126.01, 125.98, 116.10, 115.58, 113.38, 113.36, 68.11, 67.46, 67.25, 64.46, 63.87, 59.58, 51.37, 47.74, 38.75, 37.32, 32.07, 29.60, 29.51, 29.42, 29.09, 28.12, 26.15, 26.09. IR (neat): ν = 2925, 1654, 1608, 1509, 1275, 1259, 1182, 837, 764, 750, 702, 558. HR-MS (ESI$^+$): *m/z*: 1280.6637 [M–H^+–$2PF_6^-$]$^+$ (calcd for $C_{87}H_{86}N_5O_5$: 1280.6629); 1426.6366 [M–PF_6^-]$^+$ (calcd for $C_{87}H_{87}N_5O_5PF_6$: 1426.6349). Spectral data are similar for both enantiomers except for the optical rotation: (*R*)-**2**-$\mathbf{H}^+\cdot 2PF_6^-$: $[\alpha]_D^{20}$ = –5.5° (*c* 0.3, $CHCl_3$); (*S*)-**2**-$\mathbf{H}^+\cdot 2PF_6^-$: $[\alpha]_D^{20}$ = +3.9° (*c* 0.3, $CHCl_3$).

Compounds (*R*)/(*S*)-13-$\mathbf{H}^+\cdot\mathbf{PF_6^-}$:

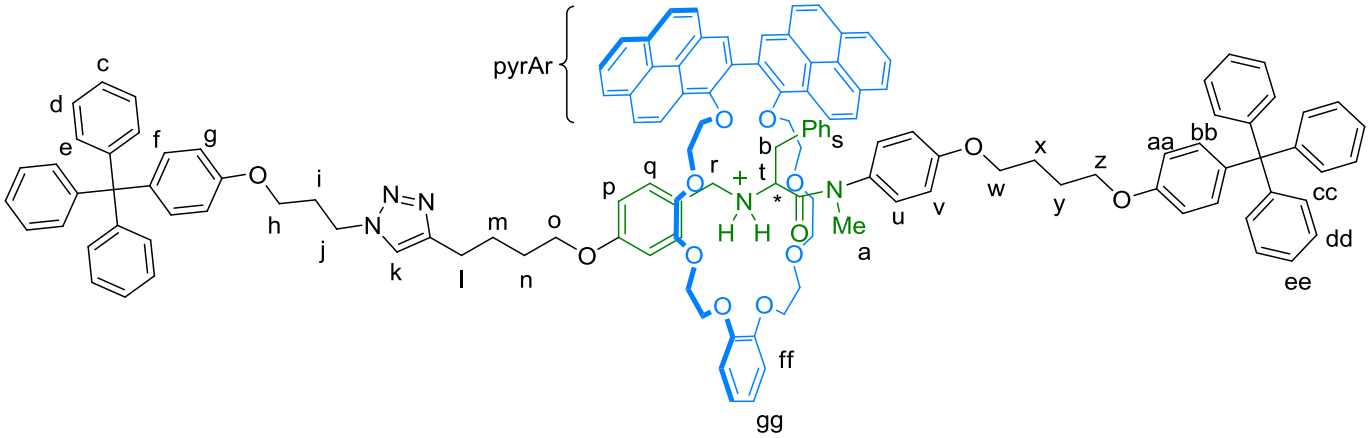

For the synthesis of (*R*)-**13**-$\mathbf{H}^+\cdot PF_6^-$: A solution of (*R*)-**11**-$\mathbf{H}^+\cdot PF_6^-$ (17 mg, 0.017 mmol) and **8** (26 mg, 0.034 mmol) in CH_2Cl_2 (8 mL) was stirred for 10 min at room temperature. The solvent was removed under reduced pressure and the solid was redissolved in CH_2Cl_2 (1.5 mL). Under Ar, to this solution were added **12** (14 mg, 0.034 mmol), $Cu(CH_3CN)_4PF_6$ (3 mg, 0.008 mmol) and TBTA (5 mg, 0.008 mmol). The mixture was stirred for 3 days at room temperature. The resulting solution was diluted with CH_2Cl_2 (25 mL) and washed with an aqueous solution of Na_4EDTA (0.1 M, 2 × 25 mL). The organic layer was dried over Na_2SO_4 and the solvent was evaporated under vacuum. The crude material was purified by gel permeation chromatography (Bio-Beads® S-X1, CH_2Cl_2) to afford (*R*)-**13**-$\mathbf{H}^+\cdot PF_6^-$ (13 mg, 35%) as a brown solid.

For the synthesis of (*S*)-**13-H**$^+$·PF_6^-: This enantiomer was synthetized following the same procedure starting from (*S*)-**11-H**$^+$·PF_6^- (17 mg, 0.017 mmol) and affording (*S*)-**13-H**$^+$·PF_6^- (7 mg, 19%) as a brown solid.

^{1}H NMR (500 MHz, $CDCl_3$) δ = 8.57 – 8.45 (m, 2H, H_{pyrAr}), 8.38 – 7.86 (m, 14H, H_{pyrAr}), 7.48 (m, 1H, H_k), 7.28 – 7.15 (m, 37H, $H_{c+d+e+q+s+u+cc+dd+ee}$), 7.09 (m, 4H, H_{f+bb}), 6.94 – 6.57 (m, 12H, $H_{g+aa+ff+gg+p/v/s}$), 5.97 (d, *J* = 7.1 Hz, 1H, $H_{p/v/s}$), 5.63 (d, *J* = 7.9 Hz, 1H, $H_{p/v/s}$), 4.58 (br, 2H, H_j), 4.36 – 3.08 (m, 35H, $H_{macCH2+h+o+r+t+w+z}$), 2.75 (br, 4H, H_{l+b}), 2.41 (m, 2H, H_i), 2.32 (s, 3H, H_a), 2.05 – 1.93 (m, 4H, H_{x+y}), 1.71 – 1.48 (m, 4H, H_{m+n}). ^{13}C NMR (126 MHz, $CDCl_3$) δ = 165.98, 159.65, 158.67, 157.01, 156.63, 152.46, 150.52, 147.89, 147.13, 146.94, 139.44, 139.22, 132.37, 131.76, 131.22, 130.00, 129.60, 128.92, 128.66, 128.13, 127.86, 127.56, 127.19, 127.05, 126.91, 126.78, 126.60, 125.99, 125.76, 125.61, 125.44, 125.29, 125.17, 124.88, 124.71, 124.35, 122.46, 122.33, 122.20, 121.60, 114.08, 113.89, 113.44, 113.34, 76.00, 74.54, 73.28, 72.60, 71.63, 70.72, 70.00, 67.54, 67.42, 66.80, 64.43, 58.68, 50.12, 38.44, 37.95, 37.80, 37.44, 32.07, 30.30, 29.84, 28.64, 26.28, 25.37. IR (neat): *v*=2924, 1599, 1505, 1451, 1275, 1258, 1118, 1046, 843, 764, 750, 702. HR-MS (ESI$^+$): *m/z*: 2038.9519 [M–PF_6^-]$^+$ (calcd for $C_{136}H_{128}N_5O_{13}$: 2038.9509). Spectral data are similar for both enantiomers except for the optical rotation: (*R*)-**13-H**$^+$·PF_6^-: $[\alpha]_D^{20}$ = –2.9º (*c* 0.2, CH_2Cl_2); (*S*)-**13-H**$^+$·PF_6^-: $[\alpha]_D^{20}$ = +4.7º (*c* 0.2, CH_2Cl_2).

Compounds (*R*)/(*S*)-1-H$^+$·2PF_6^-:

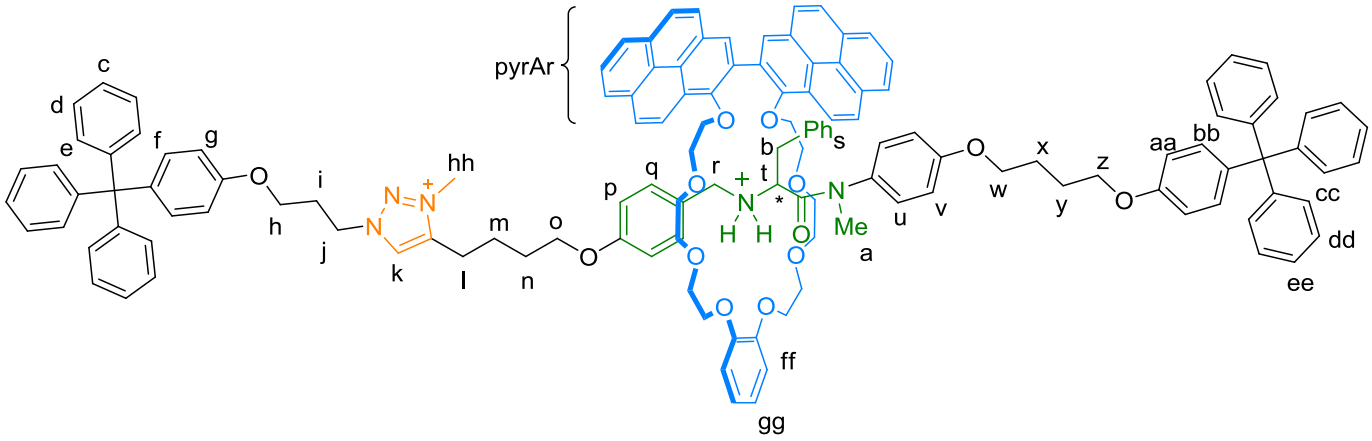

For the synthesis of (*R*)-**1-H**$^+$·2PF_6^-: Under inert atmosphere, a solution of (*R*)-**13-H**$^+$·PF_6^- (4 mg, 1.9 µmol) in iodomethane (4 mL) was stirred for 4 days at room temperature protected from light. The solvent was evaporated under vacuum. Subsequently, the solid was dissolved in CH_2Cl_2 (2 mL) and acetone (5 mL), H_2O (5 mL) and an excess of KPF_6 were added. The mixture was stirred for 5 h at room temperature protected from light. The resulting mixture was diluted with H_2O (10 mL) and extracted with CH_2Cl_2 (3 × 25 mL). The combined organic layers were dried over anhydrous Na_2SO_4 and the solvent was removed under reduced pressure. The crude material was purified by preparative TLC (SiO_2, CH_2Cl_2/MeOH 96:4) to yield (*R*)-**1-H**$^+$·2PF_6^- (3 mg, 68%) as a brown solid.

For the synthesis of (*S*)-**1-H**$^+$·2PF_6^-: This enantiomer was synthetized following the same procedure starting from (*S*)-**13-H**$^+$·PF_6^- (5 mg, 2.3 µmol) and affording (*S*)-**1-H**$^+$·2PF_6^- (3 mg, 55%) as a brown solid.

^{1}H NMR (400 MHz, $CDCl_3$) δ = 8.64 – 7.96 (m, 17H, $H_{pyrAr+k}$), 7.34 – 7.04 (m, 41H, $H_{c+d+e+f+q+s+u+bb+cc+dd+ee}$), 6.95 – 6.69 (m, 12H, $H_{g+aa+ff+gg+p/v/s}$), 5.94 (br, 2H, $H_{p/v/s}$), 4.33 – 3.15 (m, 44H, H $H_{macCH2+h+j+l+o+r+t+b+w+z+hh}$), 2.36 (m, 2H, H_i), 2.31 (s, 3H, H_a), 2.06 – 1.95 (m, 4H, H_{x+y}), 1.66 (br, 4H, H_{m+n}). ^{13}C NMR (126 MHz, $CDCl_3$) δ = 147.17, 147.12, 132.52, 132.41, 132.38, 132.21, 131.49, 131.44, 131.24, 131.05, 130.21, 129.61, 128.63, 127.81, 127.59, 127.40, 127.32, 127.22, 127.09, 126.05, 125.98, 125.78, 125.08, 125.03, 124.98, 124.94, 122.35, 113.72, 113.67, 113.34, 113.23, 74.21, 72.66, 70.87, 70.72, 70.43, 69.85, 64.46, 64.28, 61.40, 40.32, 37.96, 32.08, 30.29, 29.85, 29.51, 28.63, 26.30, 22.86. IR (neat): *v* = 2922, 2853, 1660, 1506, 1456, 1254, 1109, 841, 753, 702, 558. HR-MS (ESI$^+$): *m/z*: 2052.9675 [M–H$^+$–2PF_6^-]$^+$ (calcd for $C_{137}H_{130}N_5O_{13}$: 2052.9665); 2198.9368 [M–PF_6^-]$^+$ (calcd for

$C_{137}H_{131}N_5O_{13}PF_6$: 2198.9385). Spectral data are similar for both enantiomers except for the optical rotation: (*R*)-**1-H**$^+$·2PF_6^-: $[\alpha]_D^{20}$ = +14.1° (*c* 0.1, $CHCl_3$); (*S*)-**1-H**$^+$·2PF_6^-: $[\alpha]_D^{20}$ = –14.2 ° (*c* 0.1, $CHCl_3$).

Compound 1·PF_6^-

To obtain **1**·PF_6^- for the NMR experiments: An excess of K_2CO_3 was added to a degassed solution of **1-H**$^+$·2PF_6^- (1.2 mg, 0.51 μmol) in $CDCl_3$ (400 μL). The suspension was shaken for 1 min and subsequently filtered through a 0.2 μm filter to remove the excess of base. The resulting solution was analyzed by NMR.

2. Additional NMR Supporting Figures

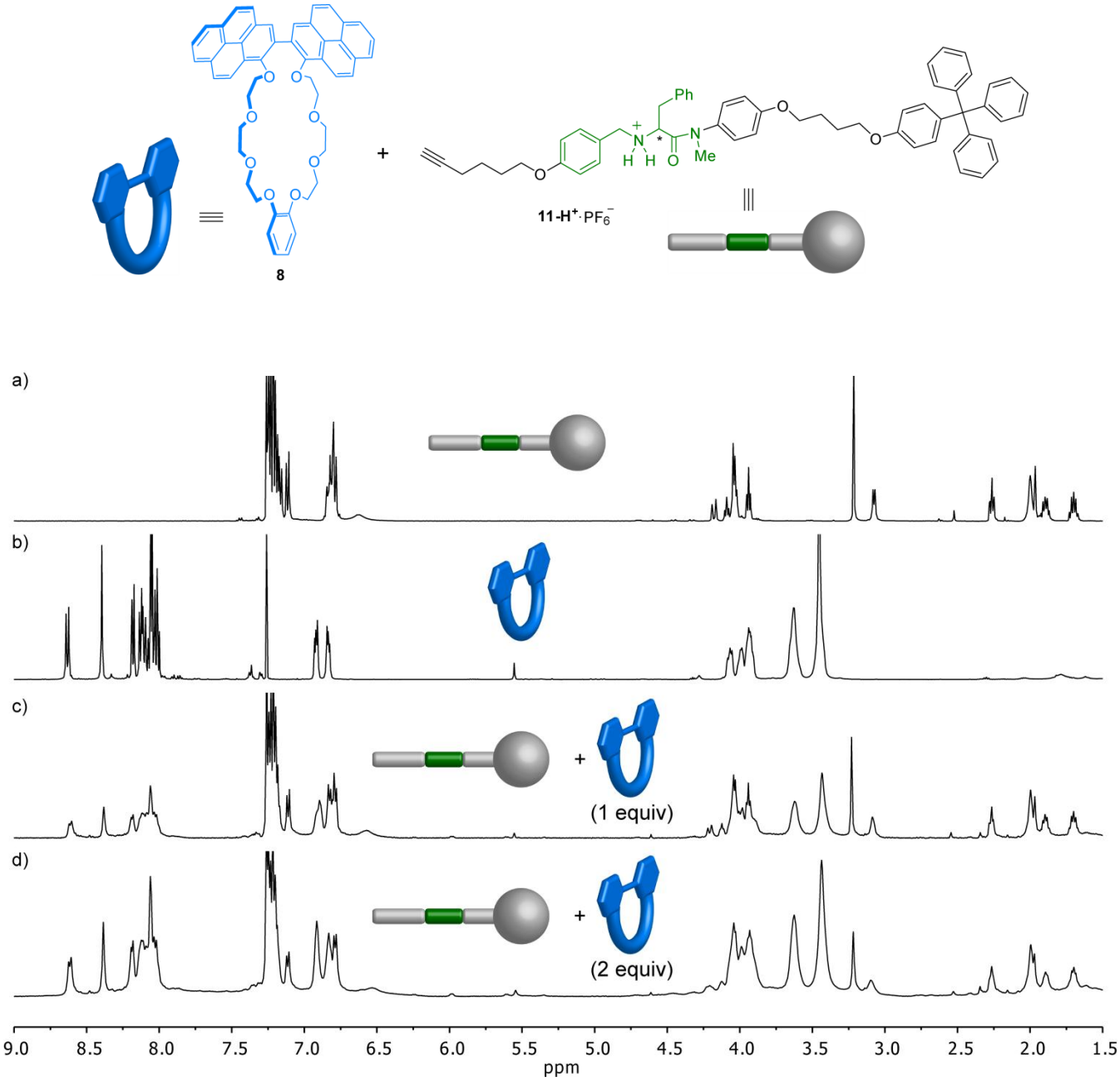

Figure S1: Study of the pseudorotaxane formation monitored by ^{1}H NMR (500 MHz, $CDCl_3$) spectroscopy: (a) **11-H**$^{+}\cdot PF_6^{-}$; (b) macrocycle **8**; (c) **11-H**$^{+}\cdot PF_6^{-}$ (8.0 mM) after addition of **8** (1 equiv); (d) **11-H**$^{+}\cdot PF_6^{-}$ (8.0 mM) after addition of **8** (2 equiv).

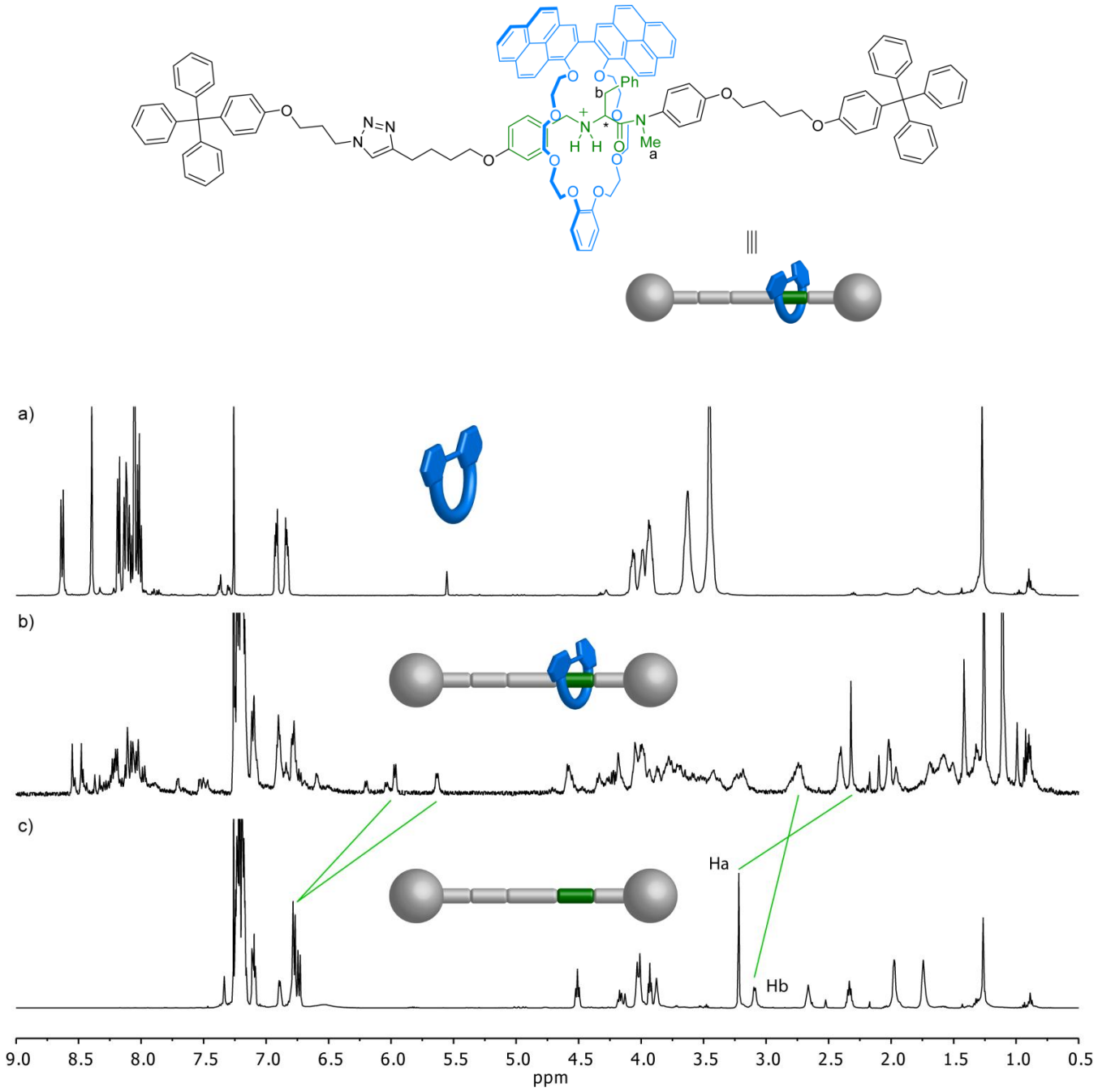

Figure S2: ^{1}H NMR (500 MHz, $CDCl_3$) spectra of: (a) macrocycle **8**; (b) rotaxane **13-H**$^{+}\cdot PF_6^{-}$; (c) thread **14-H**$^{+}\cdot PF_6^{-}$.

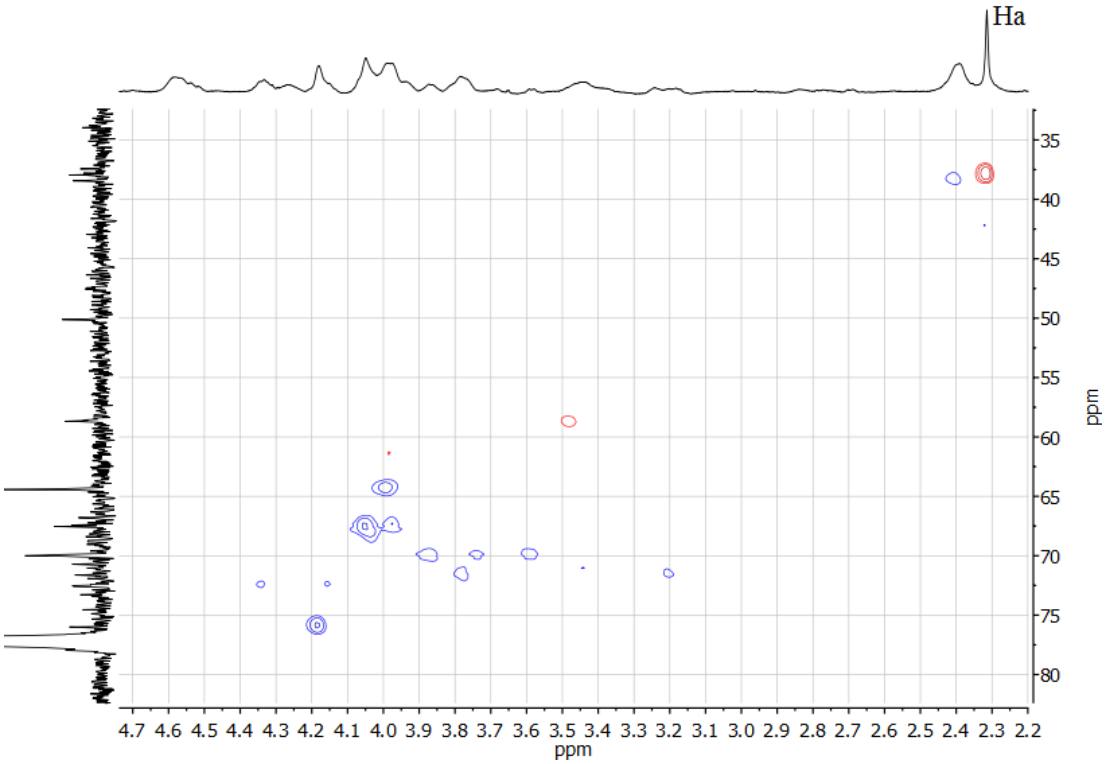

Figure S3: Partial HSQC NMR (500 MHz and 126 MHz, $CDCl_3$) spectrum of rotaxane **13-H**$^+$·PF_6^- showing a signal at 2.3 ppm in the CH/CH_3 phase, supporting its assignment as the *N*-methyl amide group Ha.

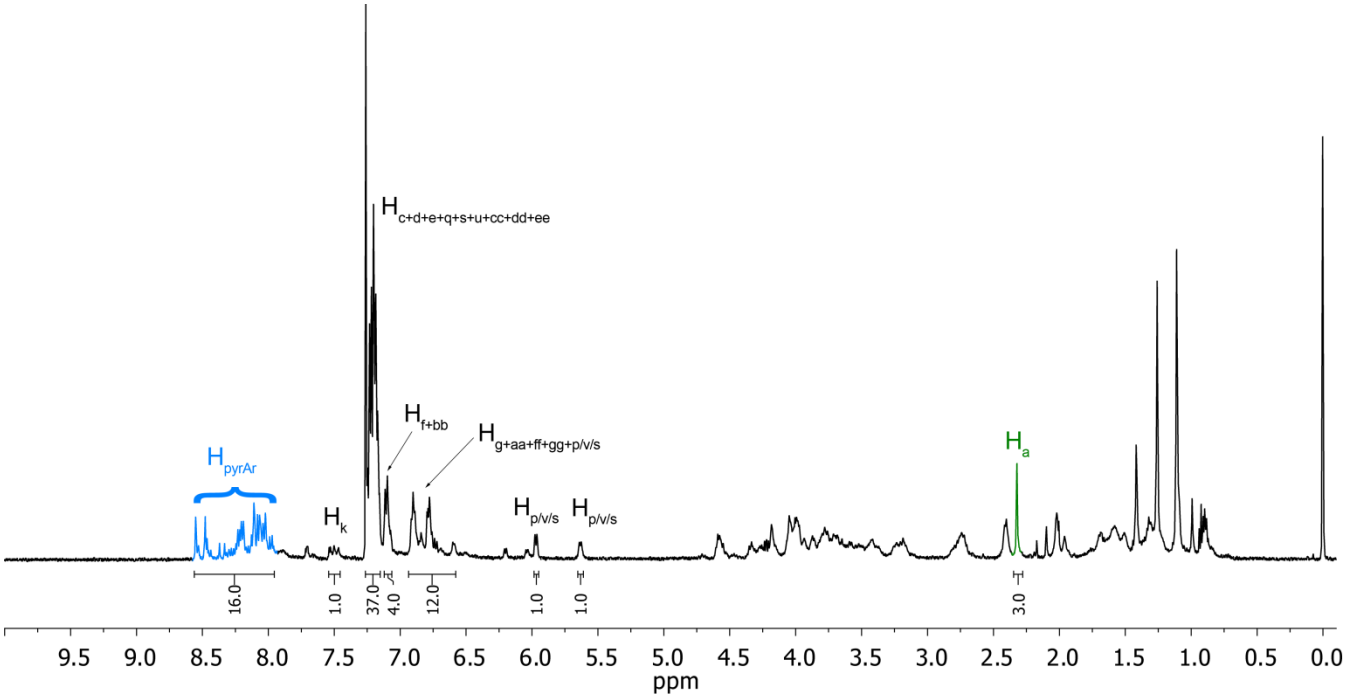

Figure S4: ^{1}H NMR (500 MHz, $CDCl_3$) spectrum of rotaxane **13-H**$^+$·PF_6^- showing the correct integration of the signal of Ha in comparison with those of the aromatic H atoms of the molecule.

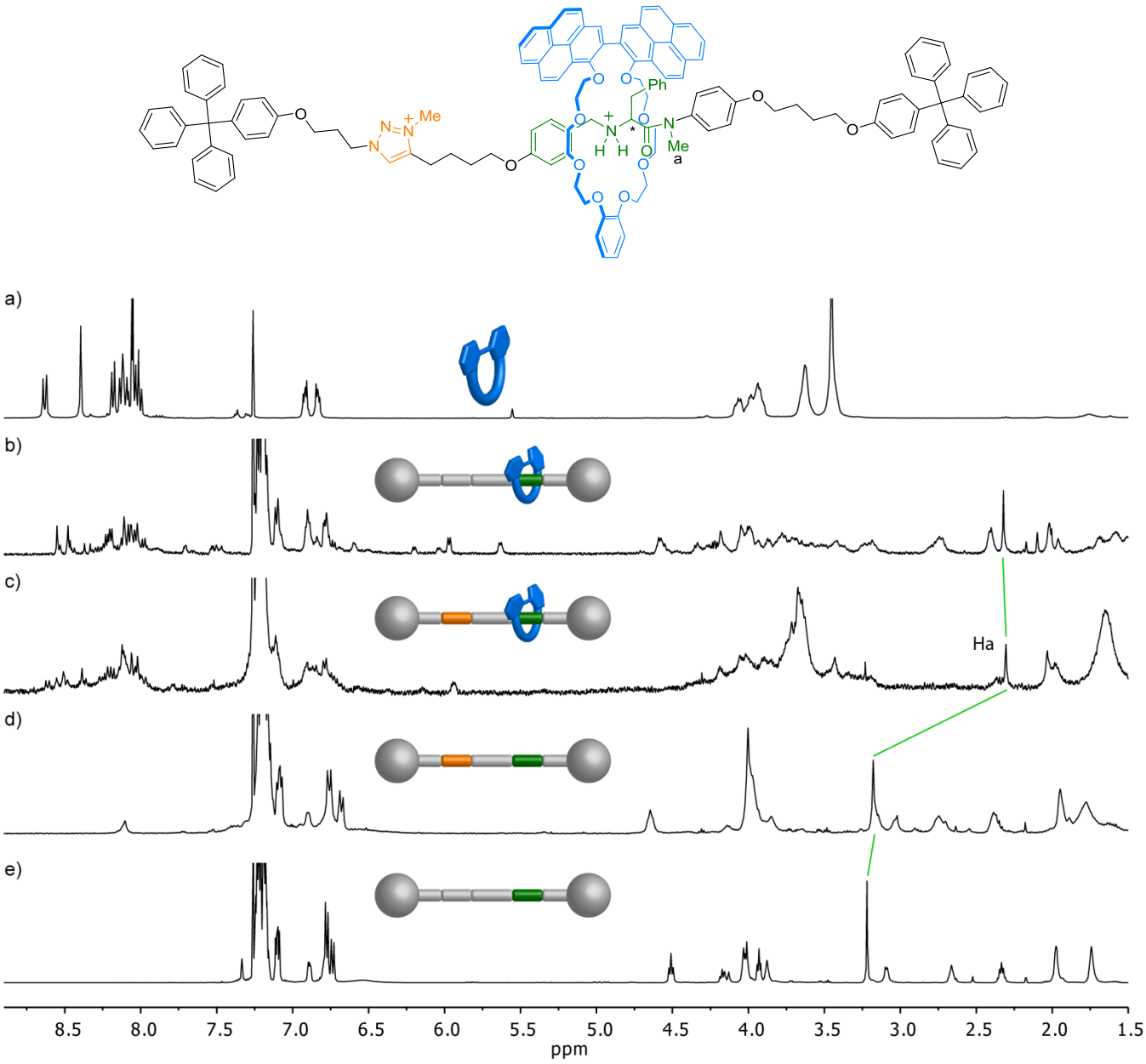

Figure S5: ^{1}H NMR (400 MHz, $CDCl_3$) spectra of: (a) macrocycle **8**; (b) rotaxane **13-H**$^{+}$·PF_6^{-}; (c) rotaxane **1-H**$^{+}$·$2PF_6^{-}$; (d) thread **2-H**$^{+}$·$2PF_6^{-}$; (e) thread **14-H**$^{+}$·PF_6^{-}.

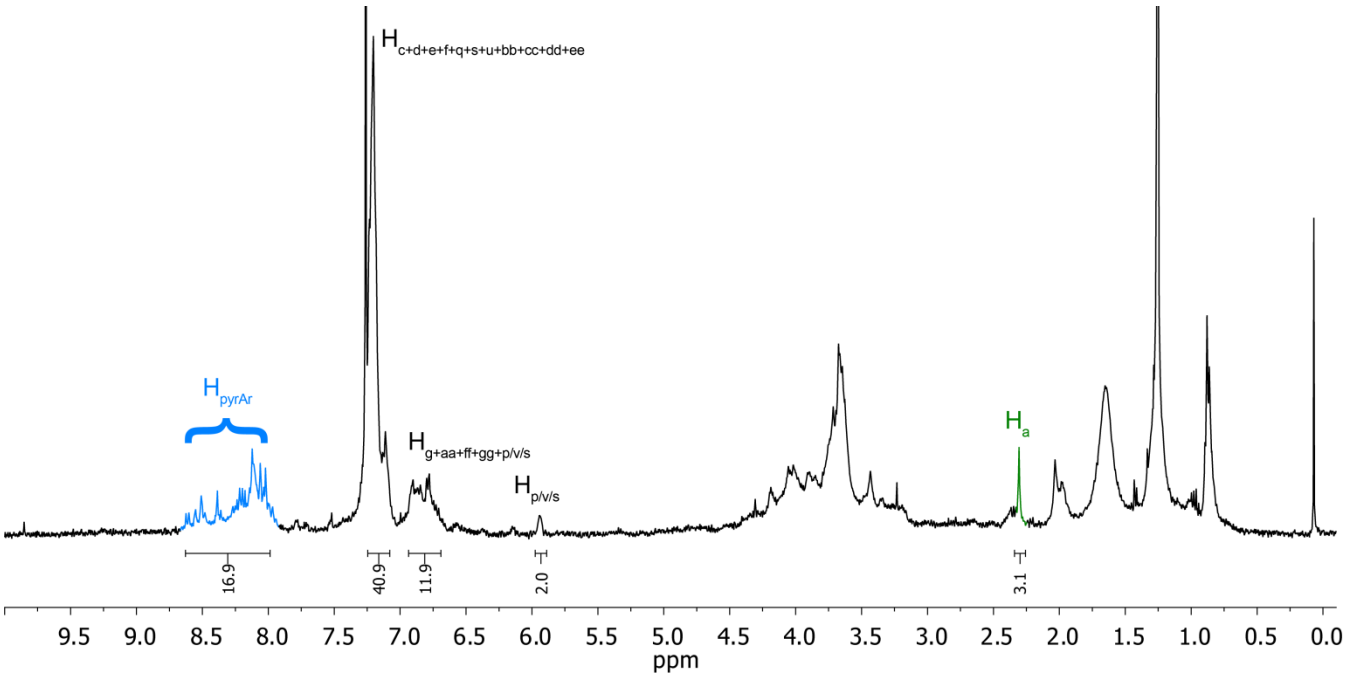

Figure S6: ^{1}H NMR (500 MHz, $CDCl_3$) spectrum of rotaxane **1-H**$^{+}$·2PF_6^- showing the correct integration of the signal of Ha in comparison with those of the aromatic H atoms of the molecule.

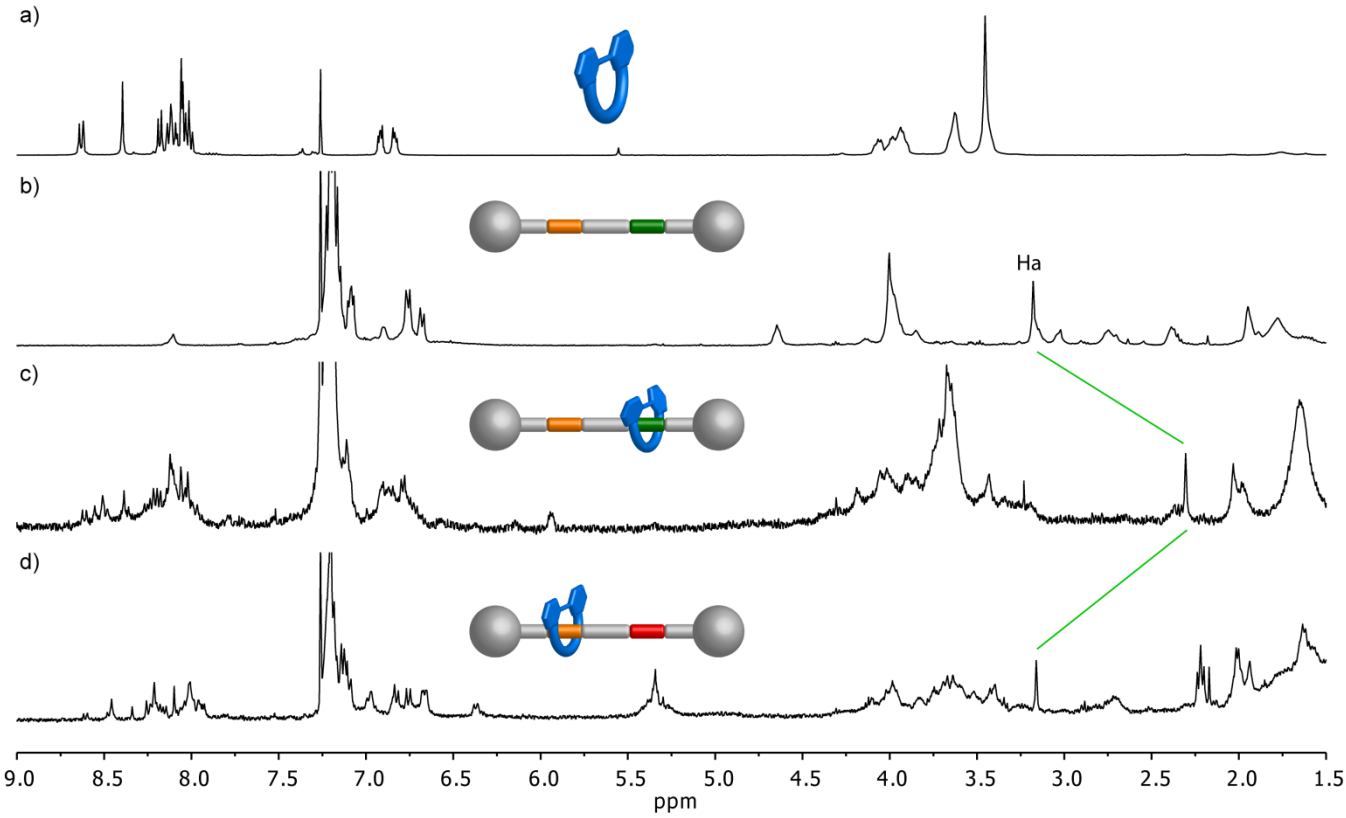

Figure S7: ^{1}H NMR (400 MHz, $CDCl_3$) spectra of: (a) macrocycle **8**; (b) thread **2-H**$^{+}$·2PF_6^-; (c) rotaxane **1-H**$^{+}$·2PF_6^-; (d) rotaxane **1**·PF_6^-.

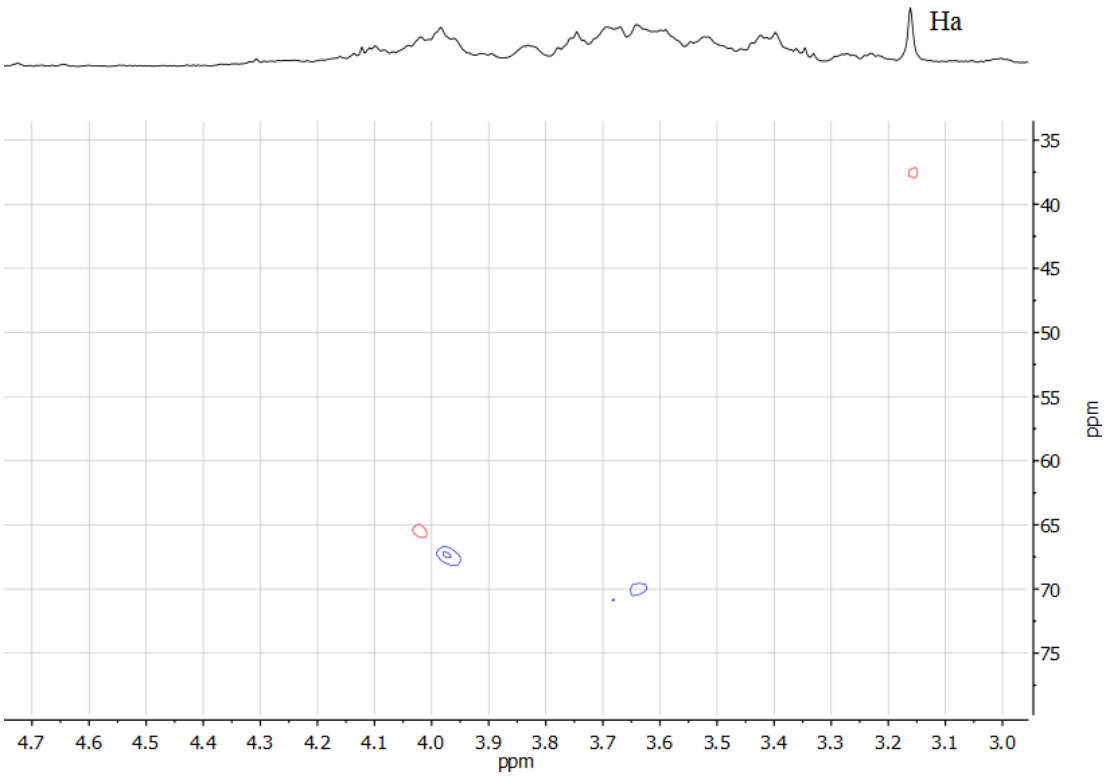

Figure S8: Partial HSQC NMR (500 MHz and 126 MHz, $CDCl_3$) spectrum of rotaxane **1**·PF_6^- showing a signal at 3.16 ppm in the CH/CH_3 phase, supporting its assignment as the *N*-methyl amide group Ha

3. NMR spectra of new compounds

Compound 4:

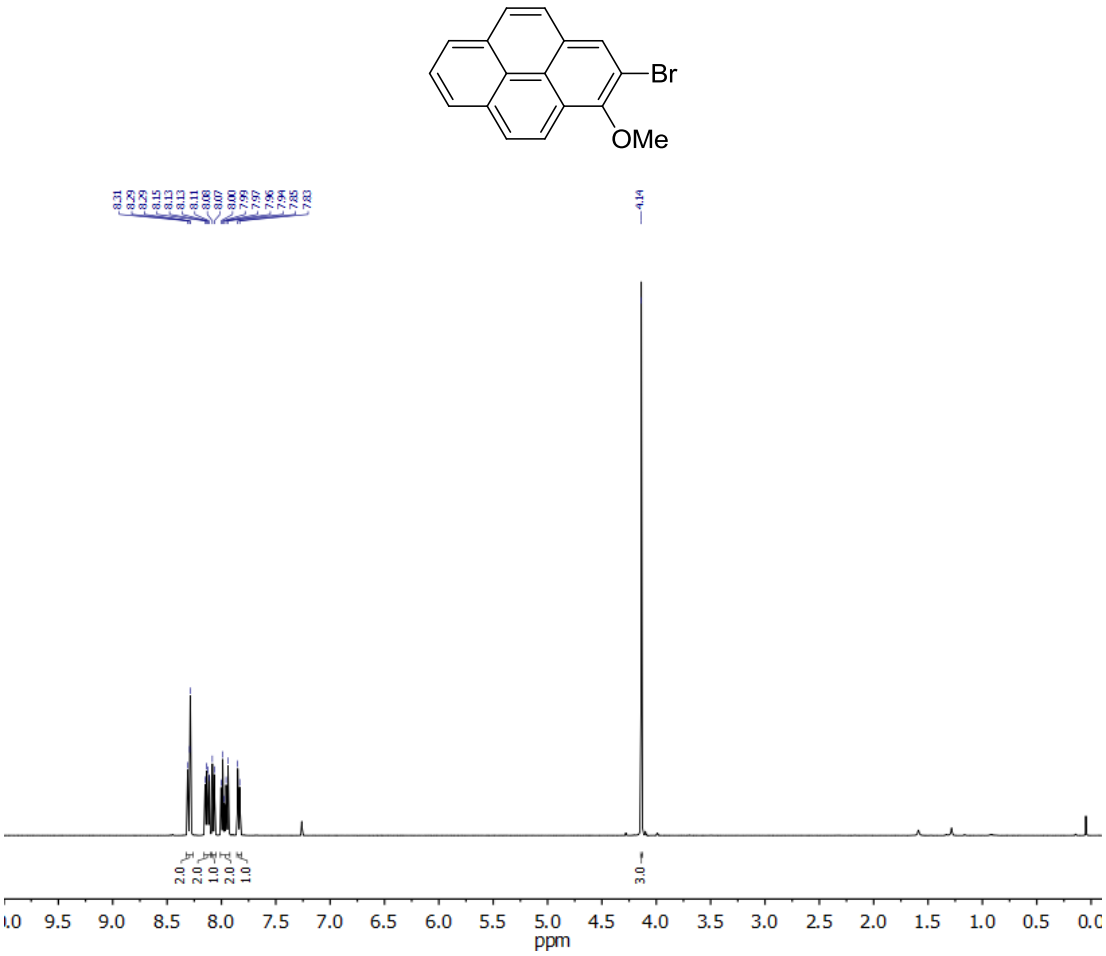

Figure S9: ^{1}H NMR (500 MHz, $CDCl_3$) spectrum of **4**.

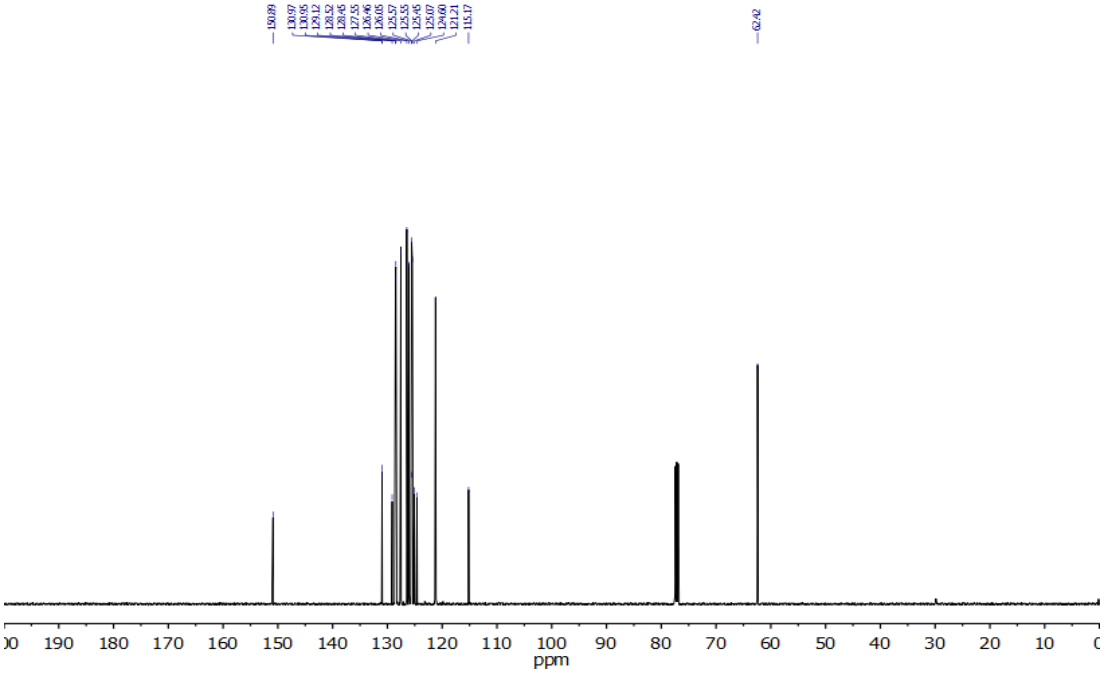

Figure S10: ^{13}C NMR (126 MHz, $CDCl_3$) spectrum of **4**.

Compound S2:

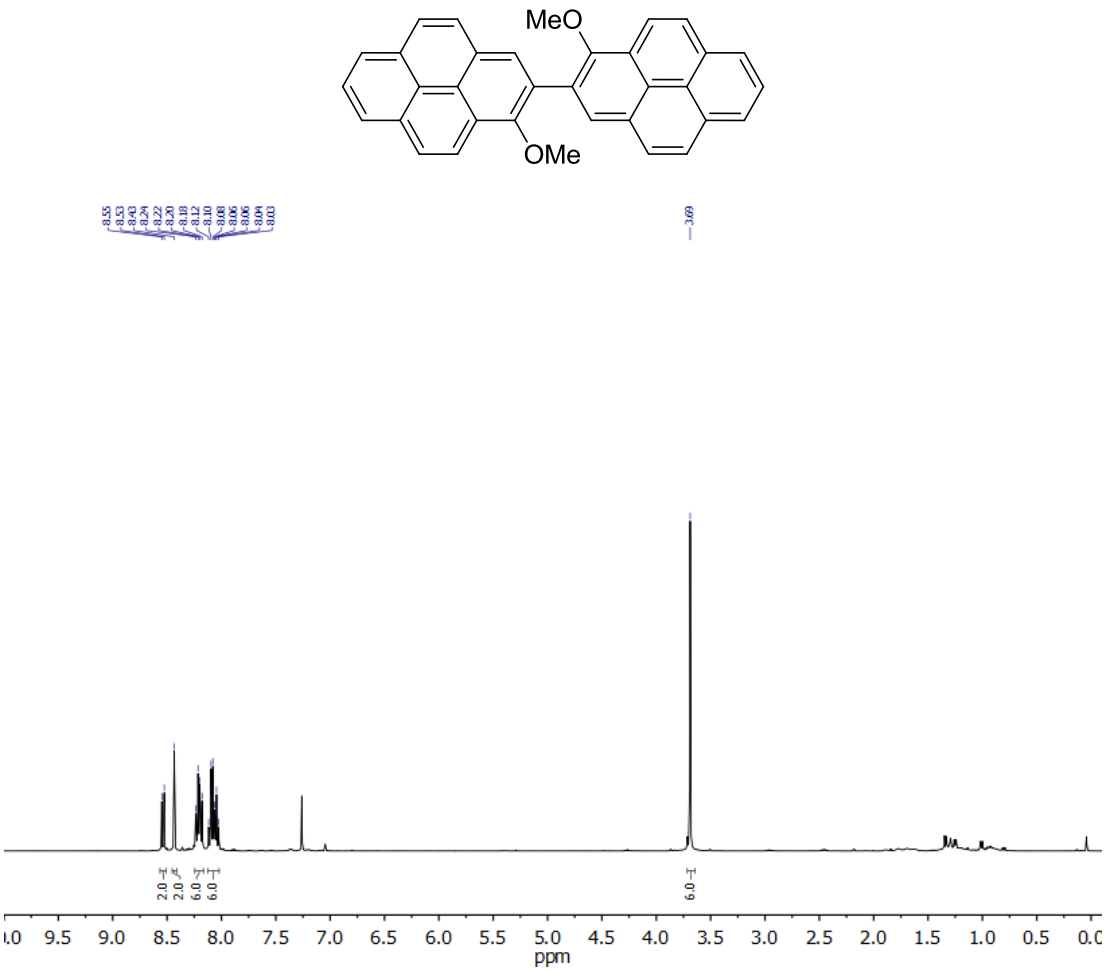

Figure S11: ^{1}H NMR (400 MHz, $CDCl_3$) spectrum of **S2**.

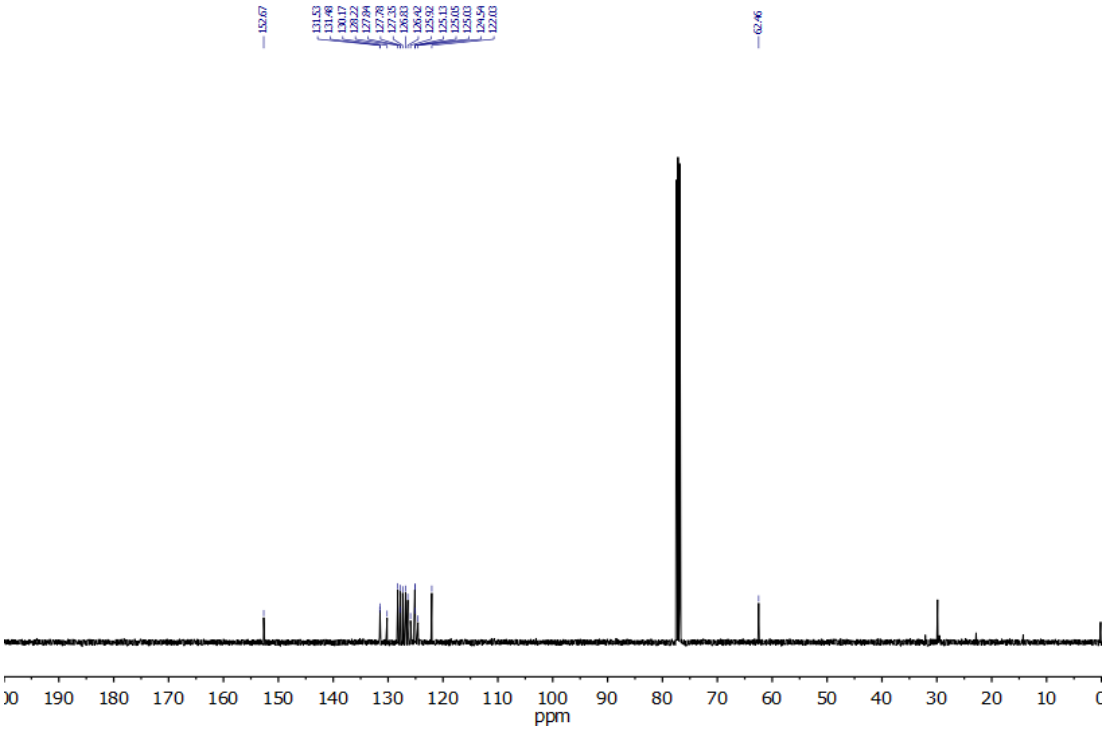

Figure S12: ^{13}C NMR (101 MHz, $CDCl_3$) spectrum of **S2**.

Compound 5:

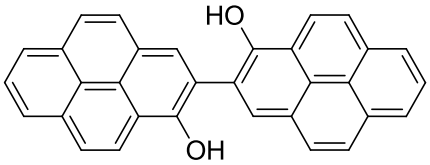

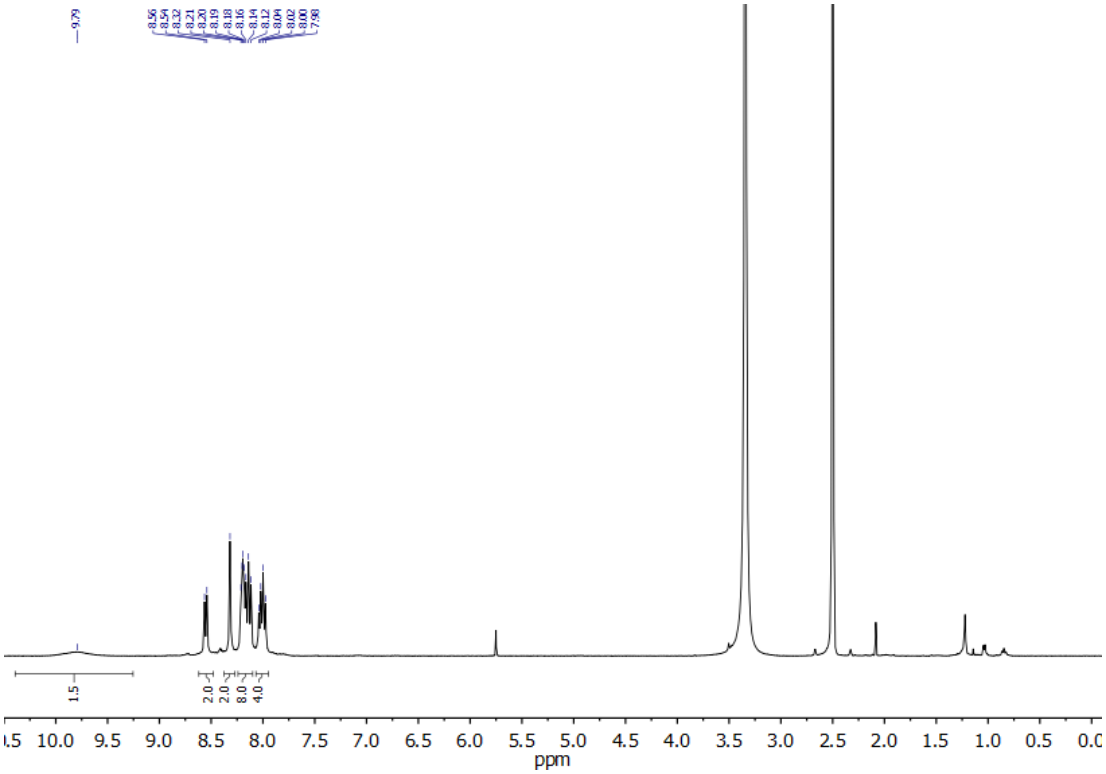

Figure S13: ^{1}H NMR (400 MHz, DMSO-d_6) spectrum of **5**.

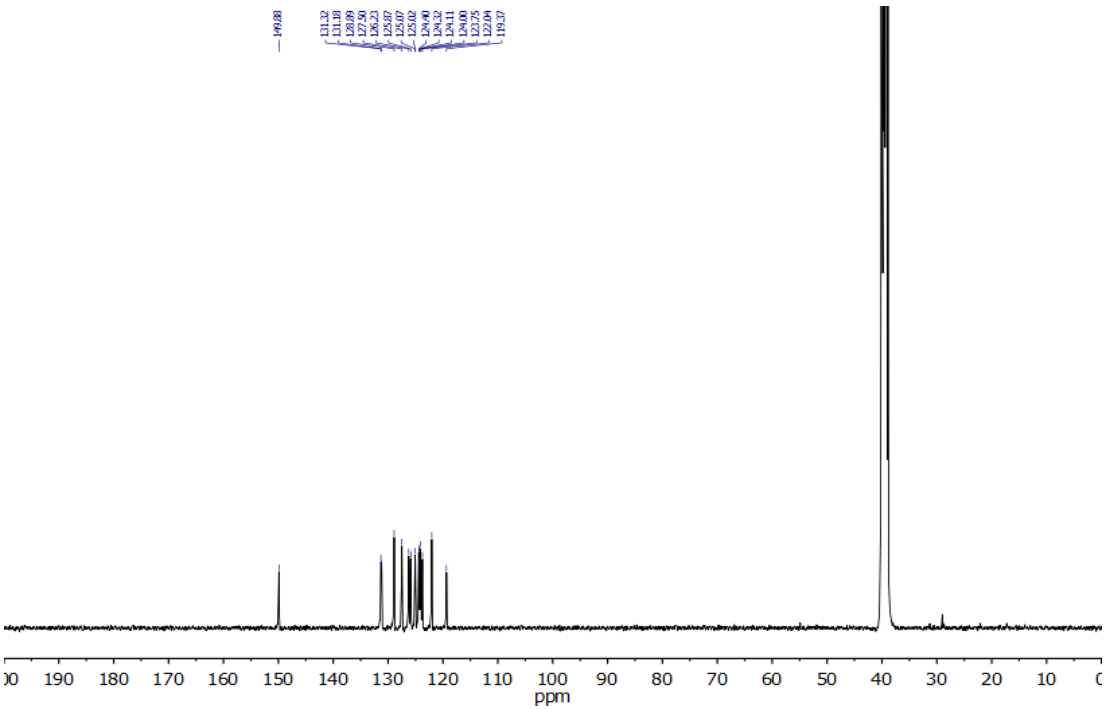

Figure S14: ^{13}C NMR (101 MHz, DMSO-d_6) spectrum of **5**.

Compound 7:

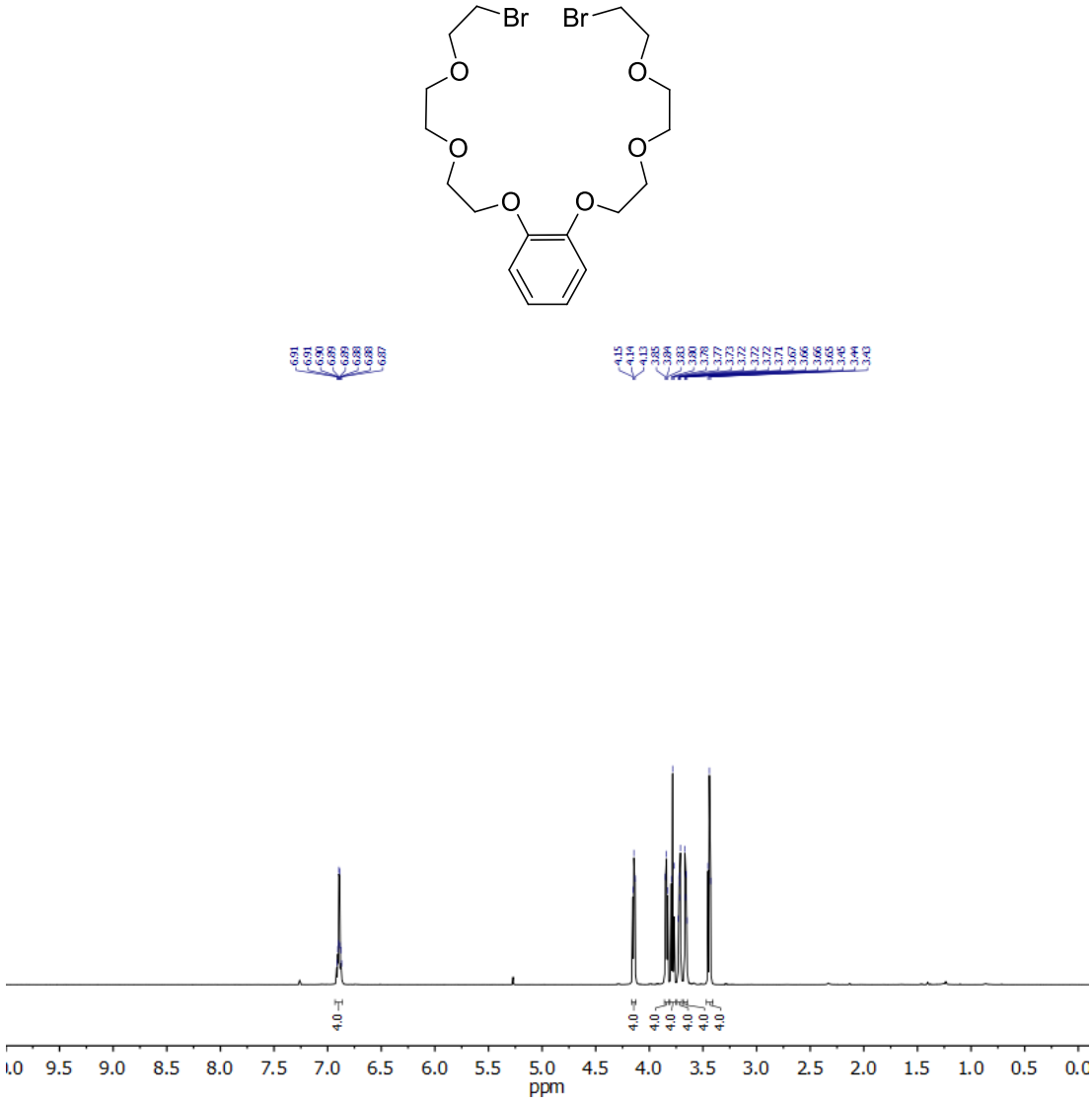

Figure S15: ^{1}H NMR (500 MHz, $CDCl_3$) spectrum of **7**.

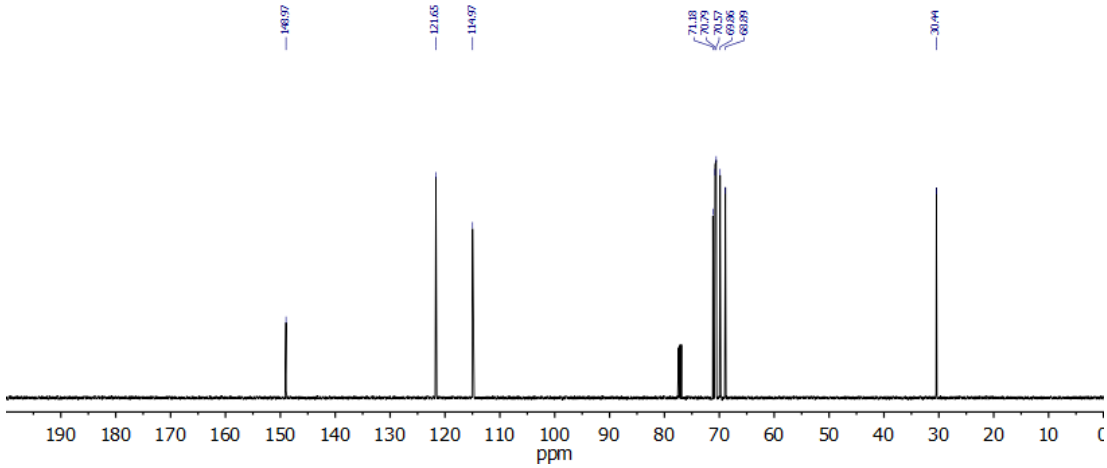

Figure S16: ^{13}C NMR (126 MHz, $CDCl_3$) spectrum of **7**.

Compound 8:

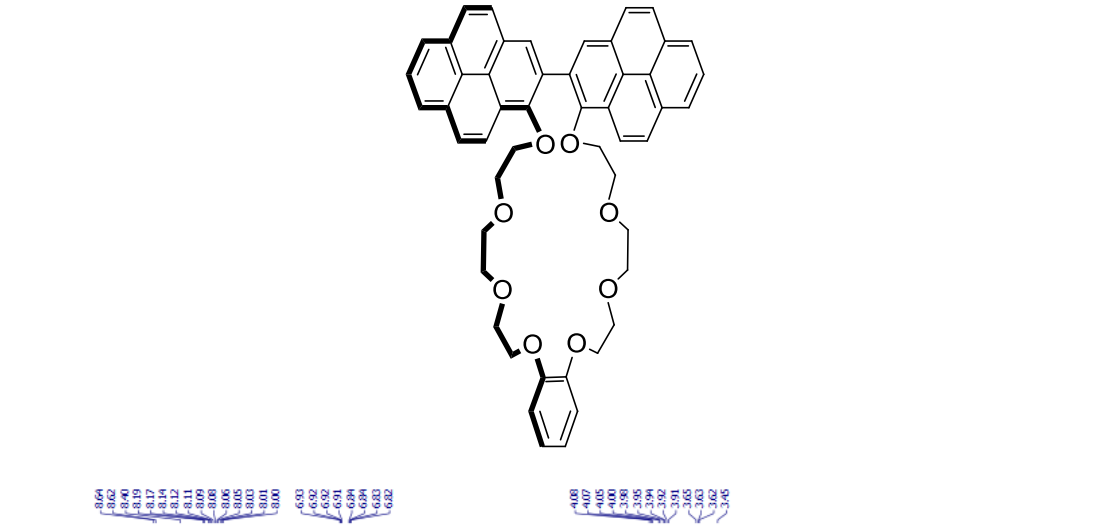

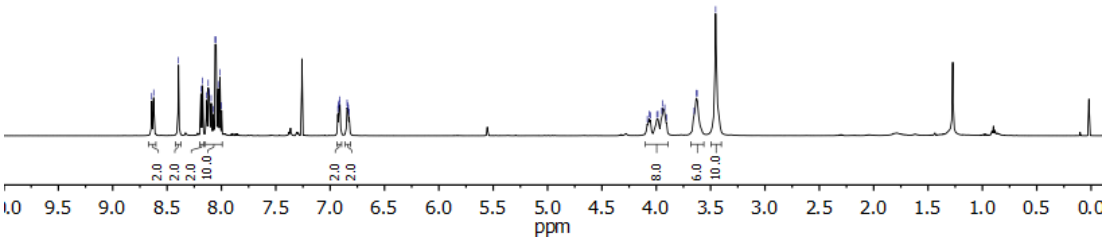

Figure S17: ^{1}H NMR (500 MHz, $CDCl_3$) spectrum of **8**.

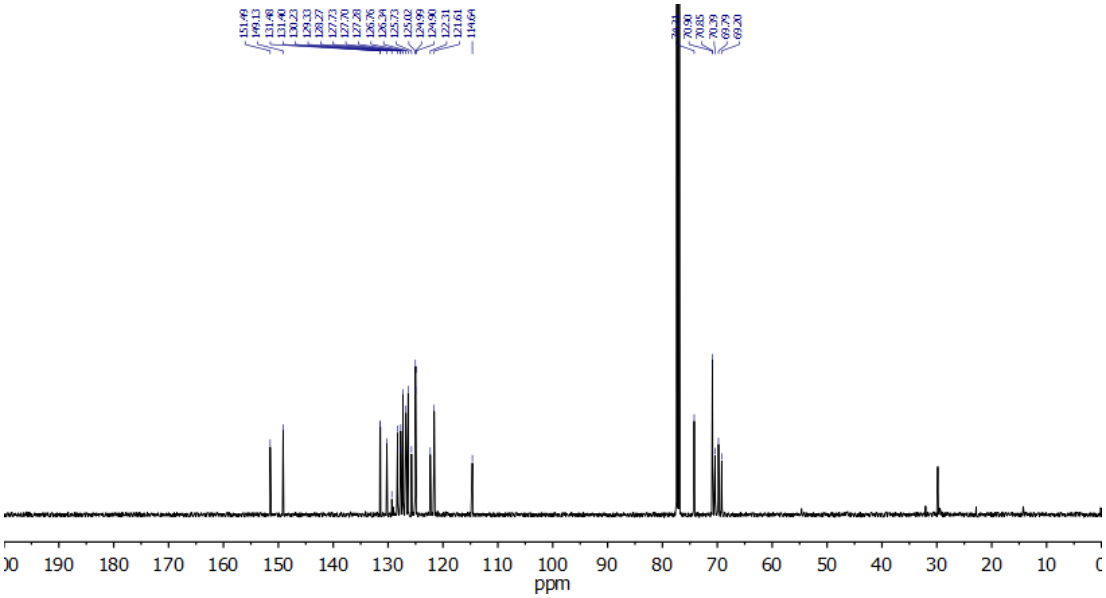

Figure S18: ^{13}C NMR (126 MHz, $CDCl_3$) spectrum of **8**.

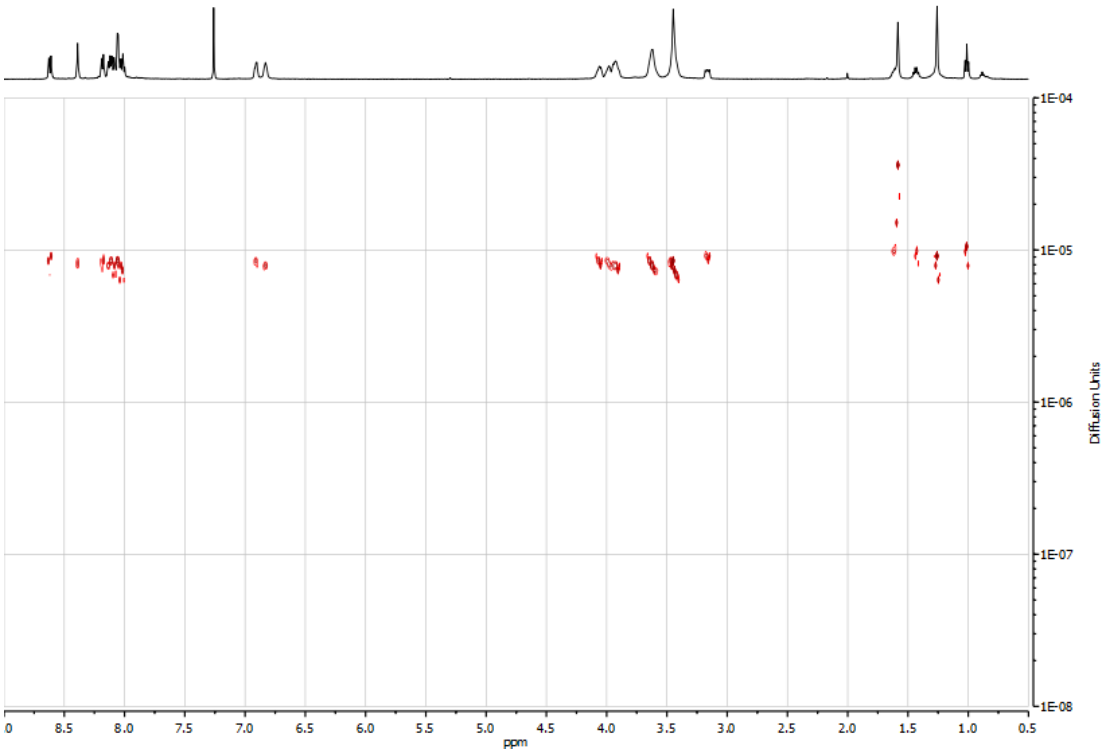

Figure S19: DOSY NMR (500 MHz, $CDCl_3$) spectrum of **8**.

Compound 8·K$^+$:

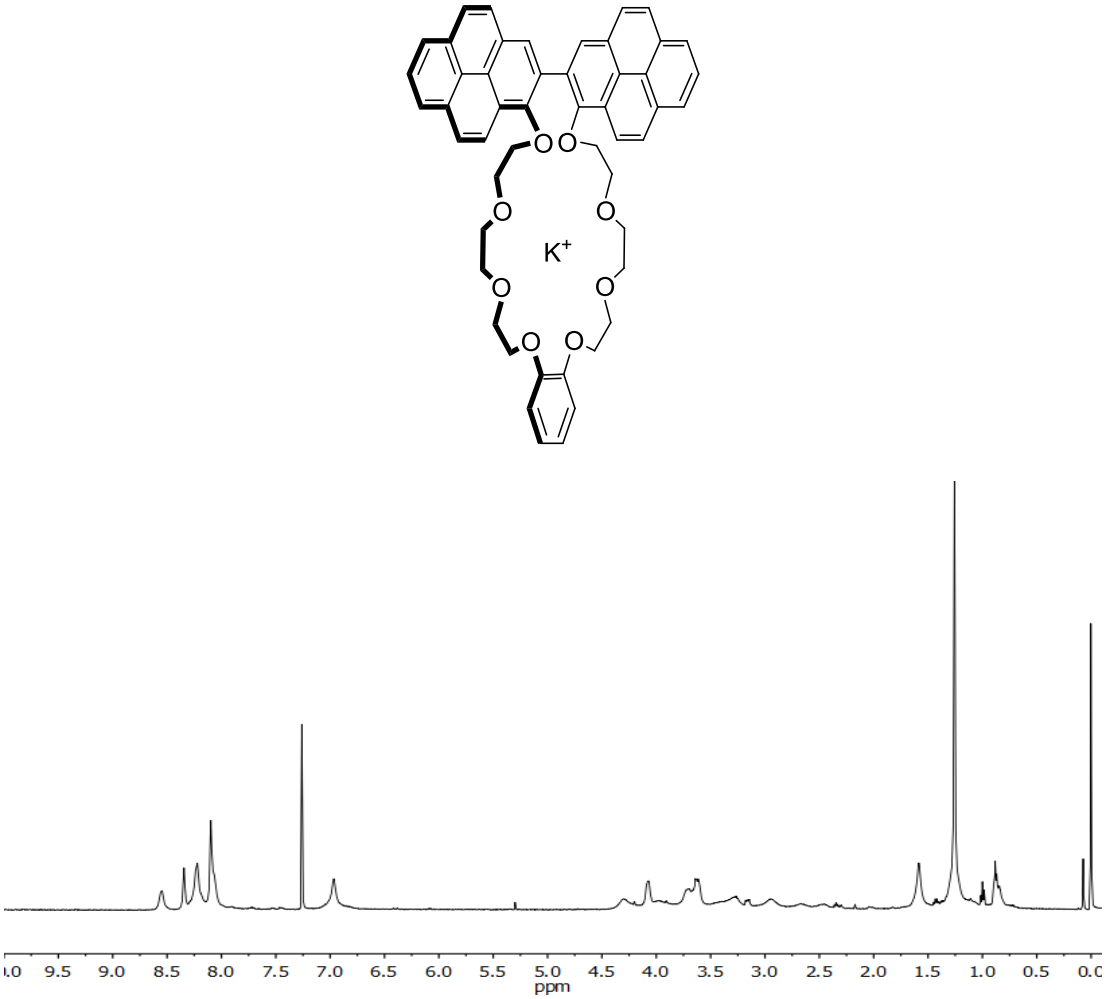

Figure S20: ^{1}H NMR (500 MHz, $CDCl_3$) spectrum of **8⊂K$^+$**.

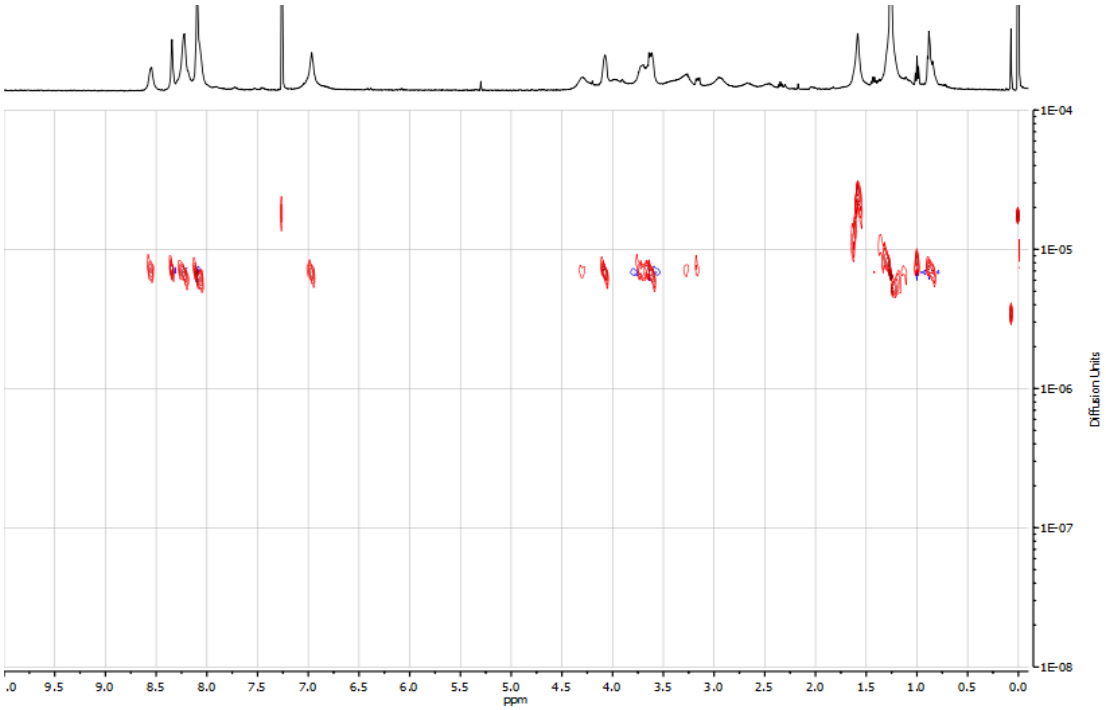

Figure S21: DOSY NMR (500 MHz, $CDCl_3$) spectrum of **8⊂K$^+$**.

Compound S4:

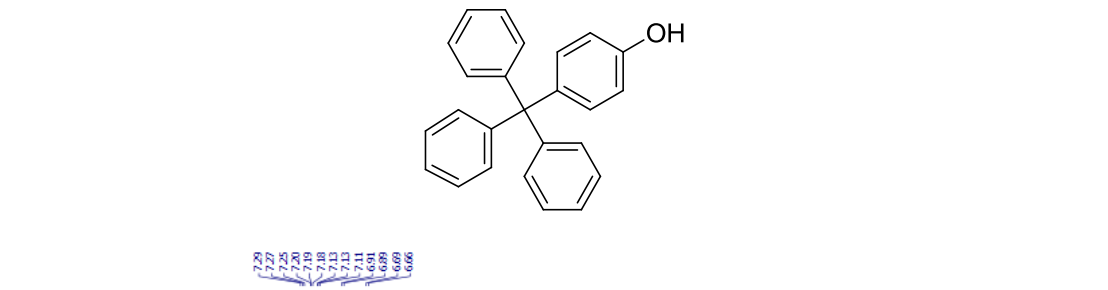

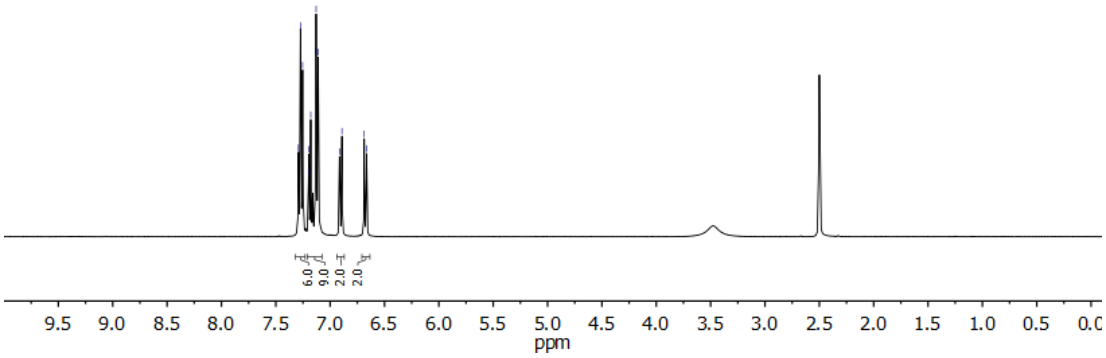

Figure S22: ^{1}H NMR (400 MHz, DMSO-d_6) spectrum of **S4**.

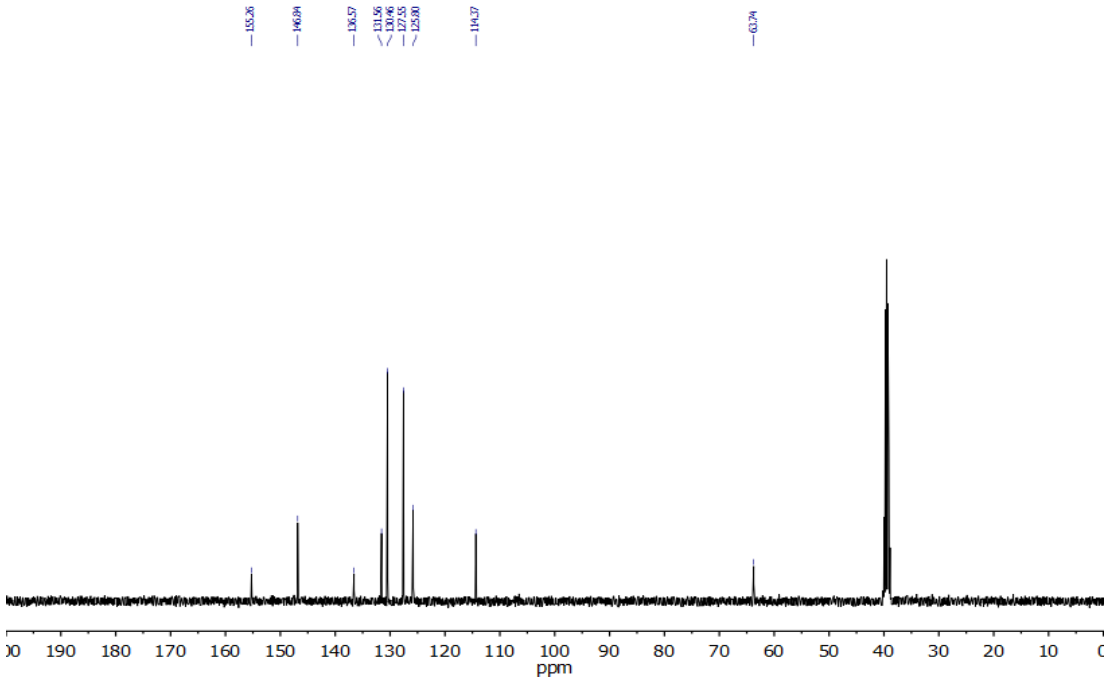

Figure S23: ^{13}C NMR (101 MHz, DMSO-d_6) spectrum of **S4**.

Compound S5:

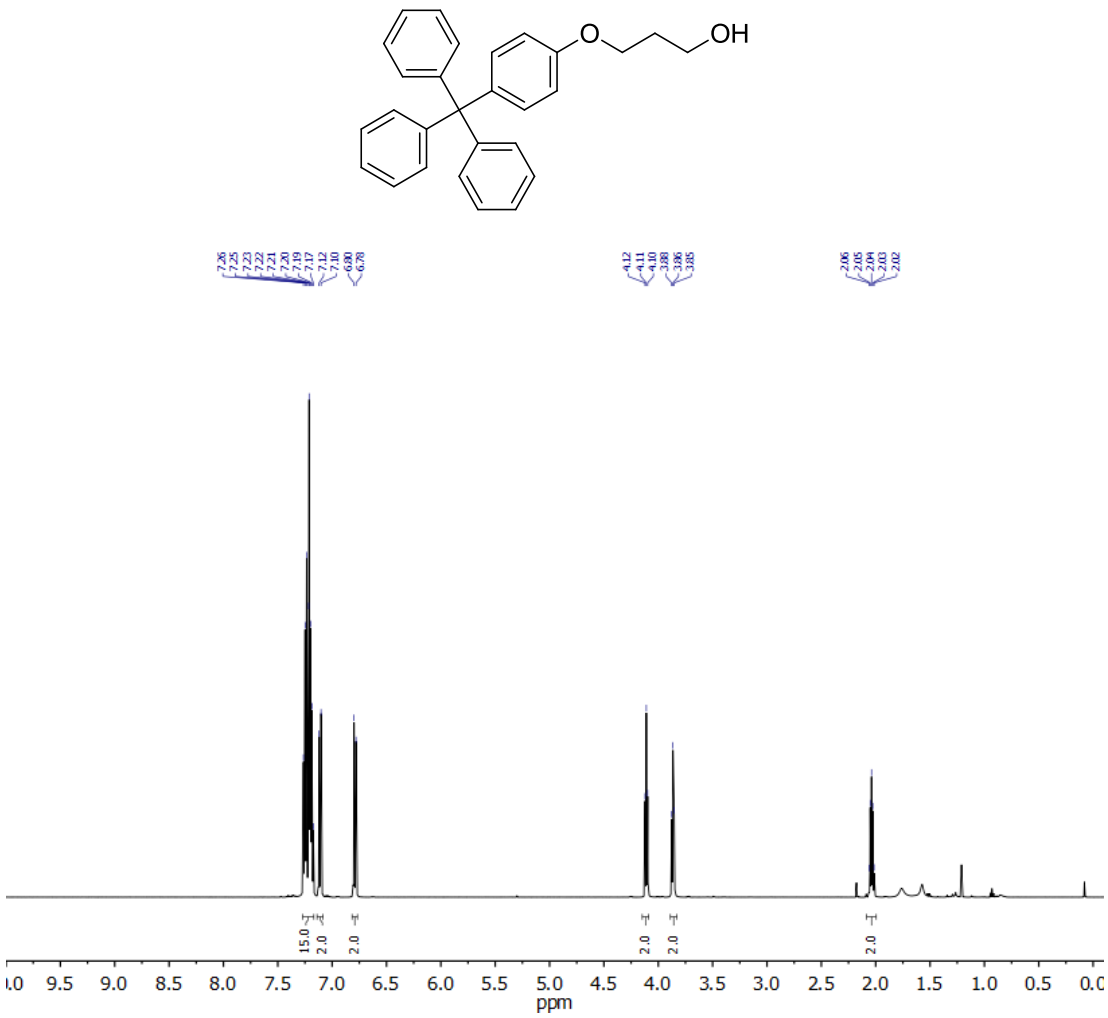

Figure S24: ^{1}H NMR (500 MHz, $CDCl_3$) spectrum of **S5**.

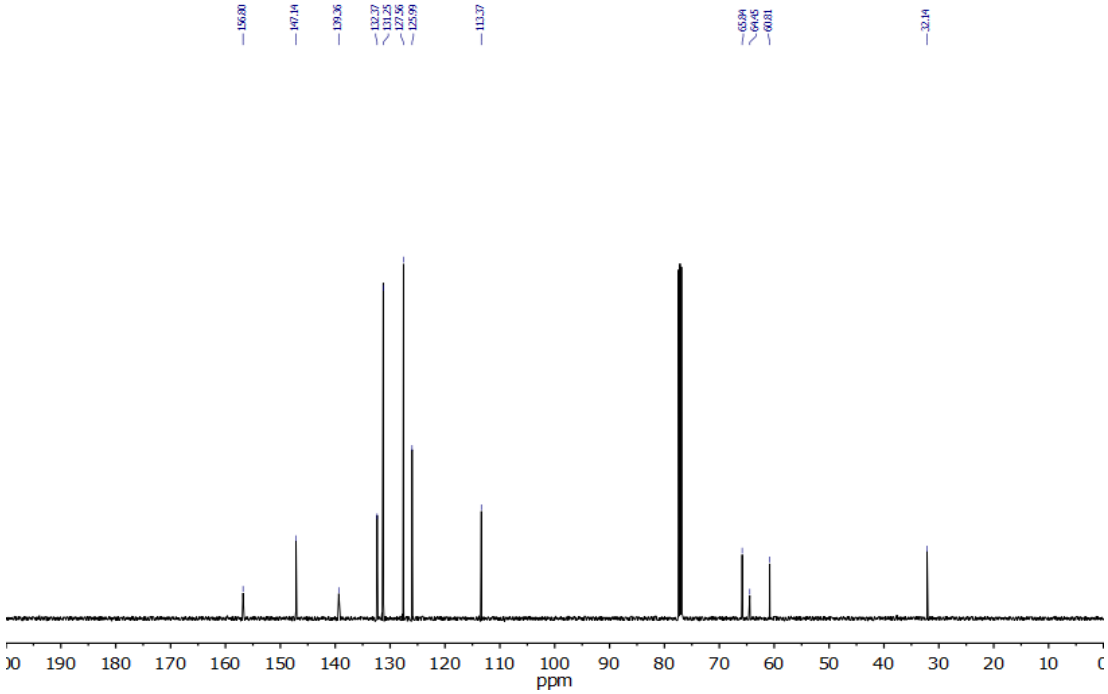

Figure S25: ^{13}C NMR (126 MHz, $CDCl_3$) spectrum of **S5**.

Compound S6:

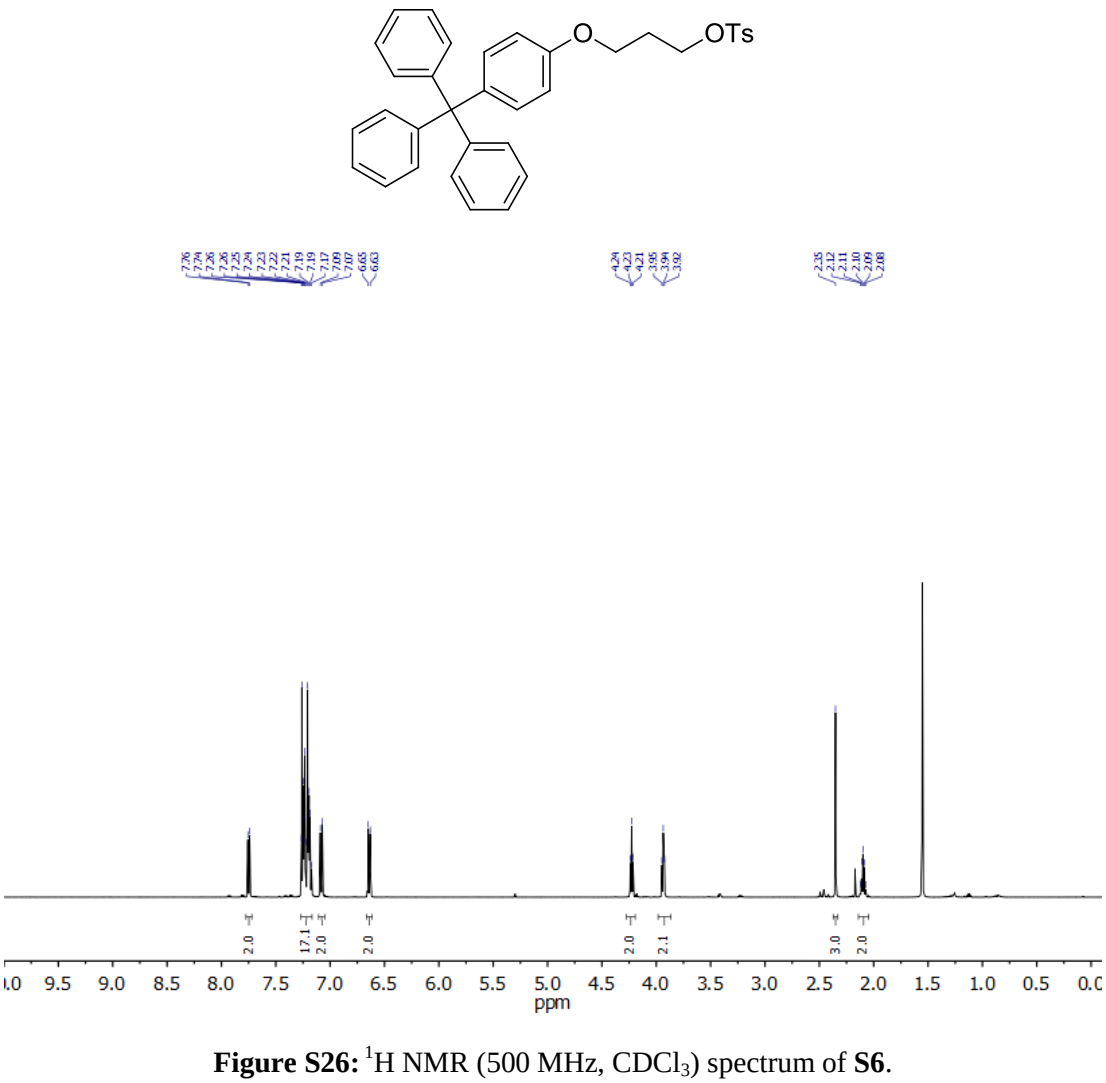

Figure S26: ^{1}H NMR (500 MHz, $CDCl_3$) spectrum of **S6**.

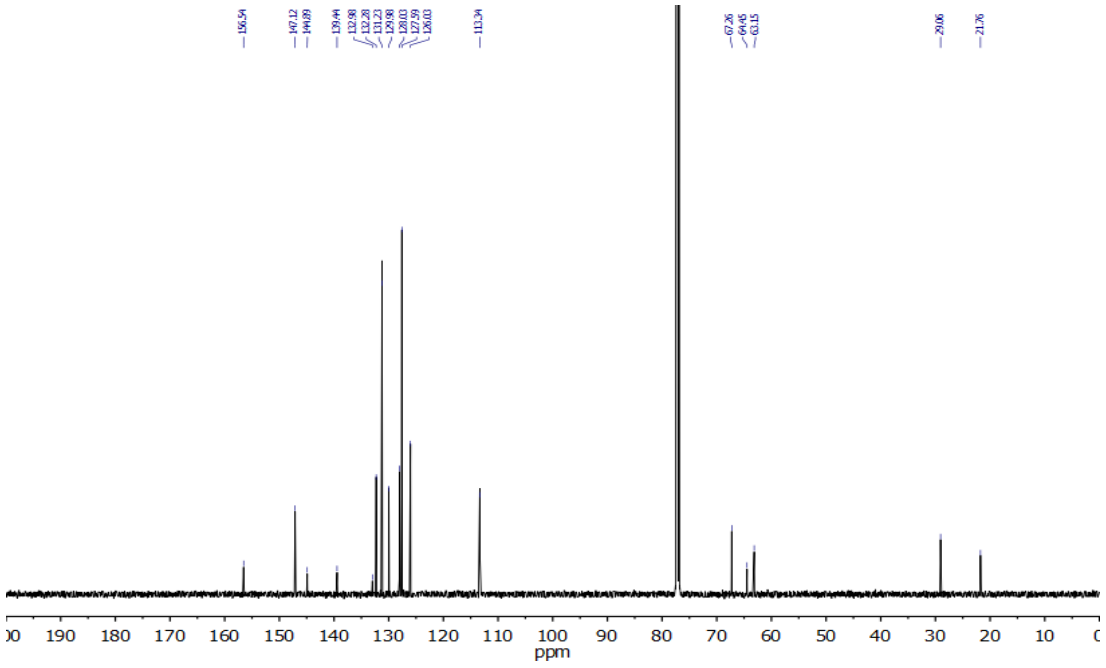

Figure S27: ^{13}C NMR (126 MHz, $CDCl_3$) spectrum of **S6**.

Compound 12:

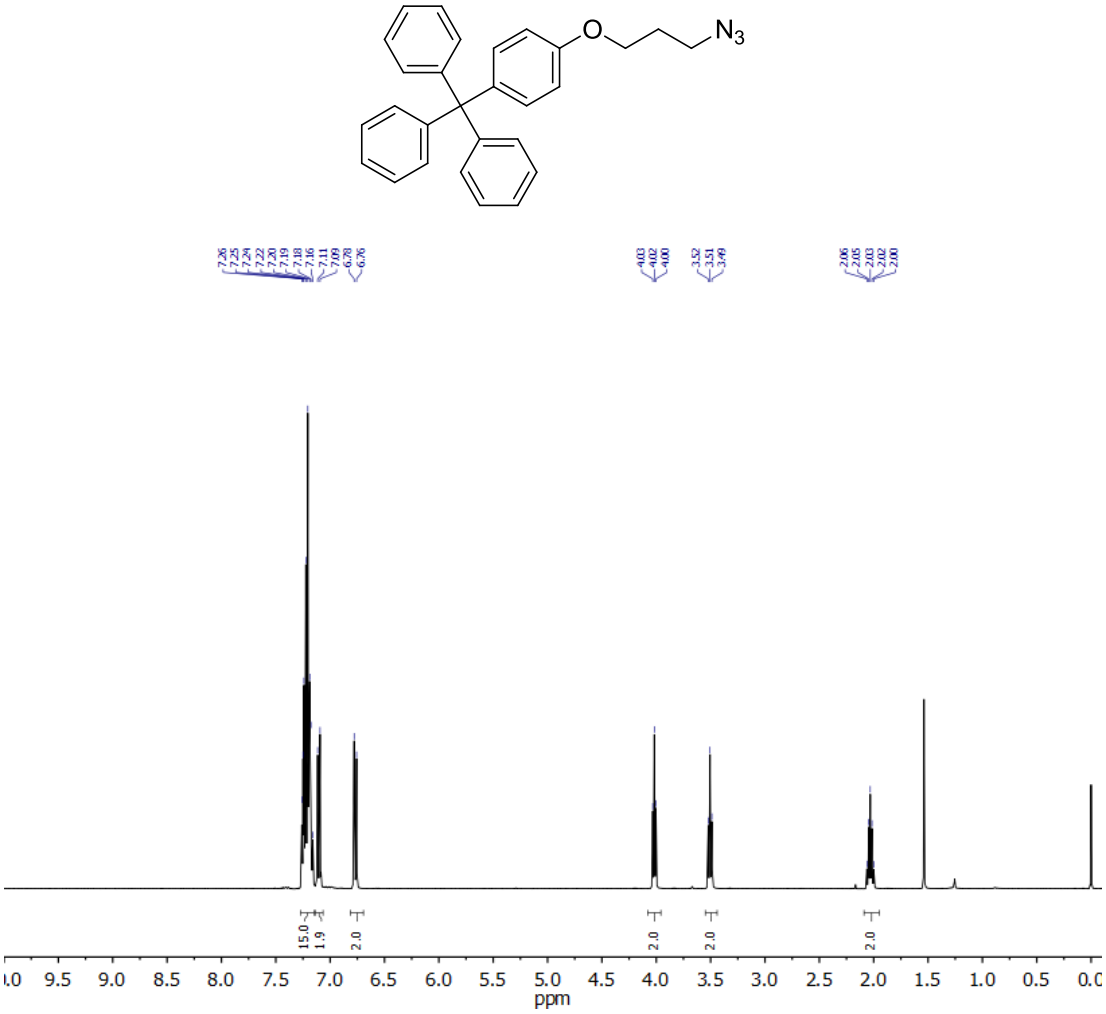

Figure S28: ^{1}H NMR (400 MHz, $CDCl_3$) spectrum of **12**.

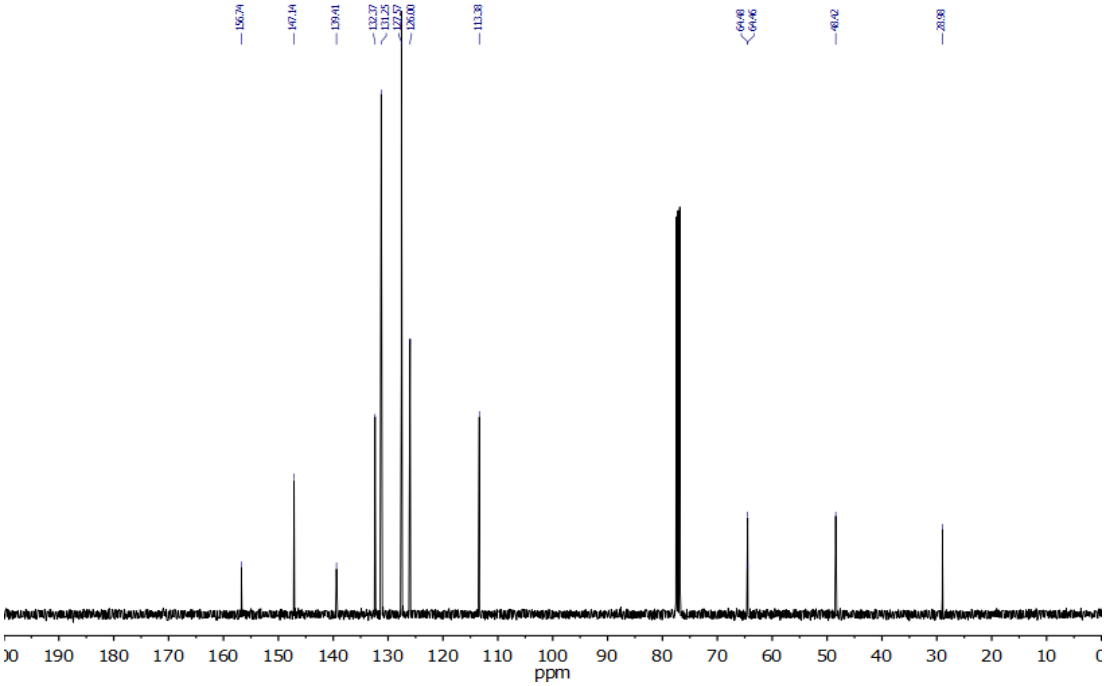

Figure S29: ^{13}C NMR (101 MHz, $CDCl_3$) spectrum of **12**.

Compound S7:

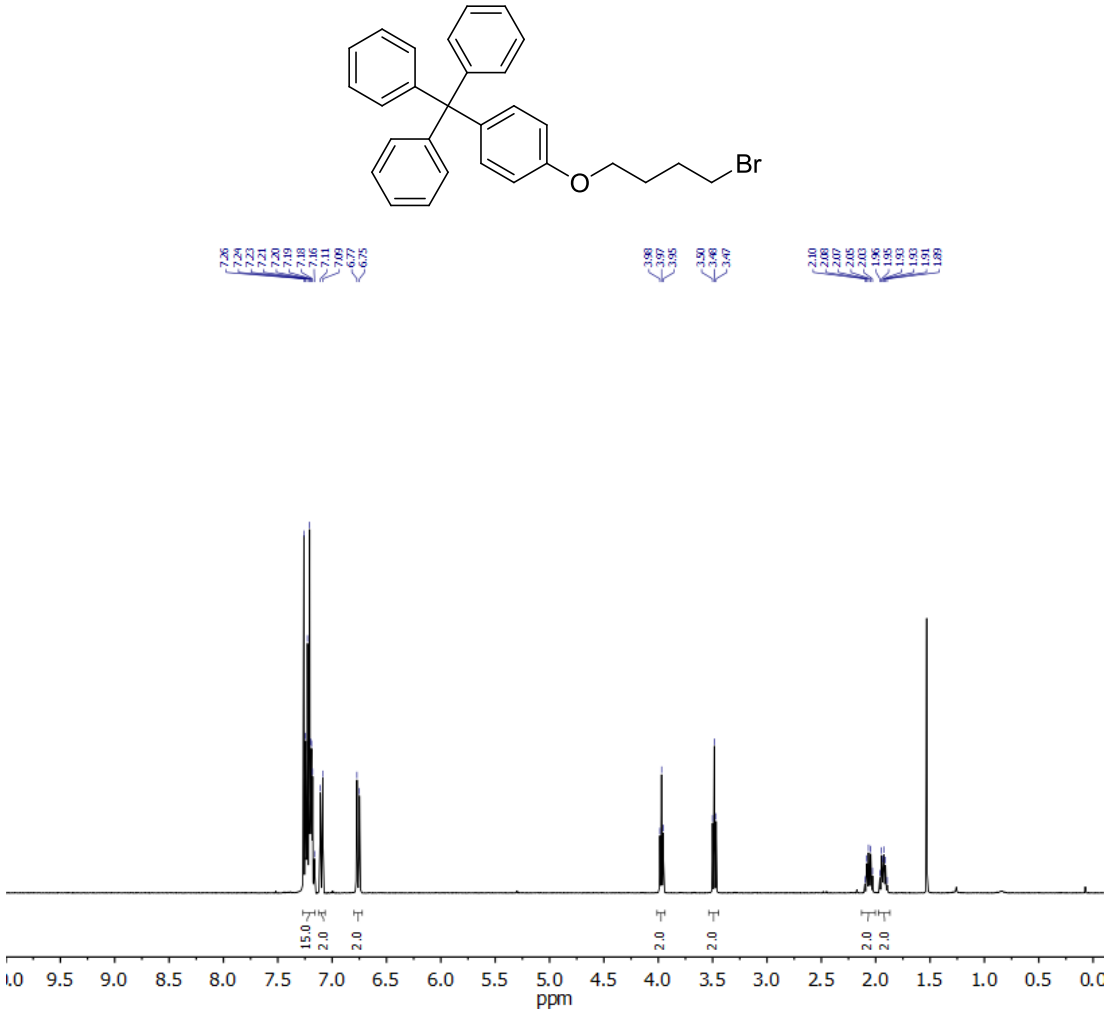

Figure S30: ^{1}H NMR (400 MHz, $CDCl_3$) spectrum of **S7**.

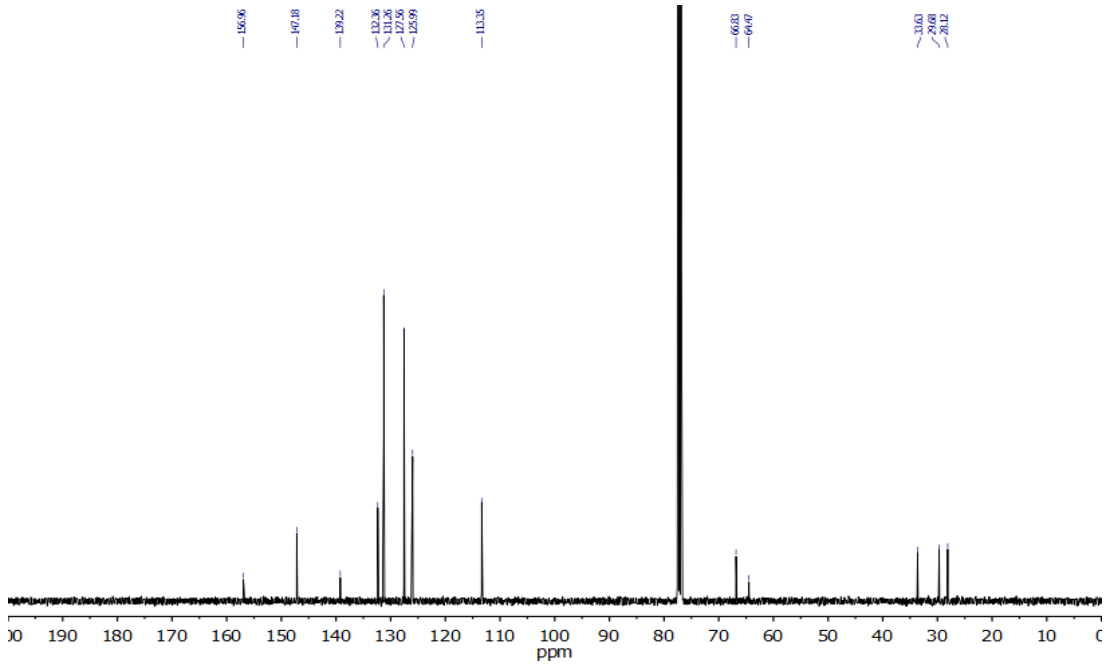

Figure S31: ^{13}C NMR (101 MHz, $CDCl_3$) spectrum of **S7**.

Compound S9:

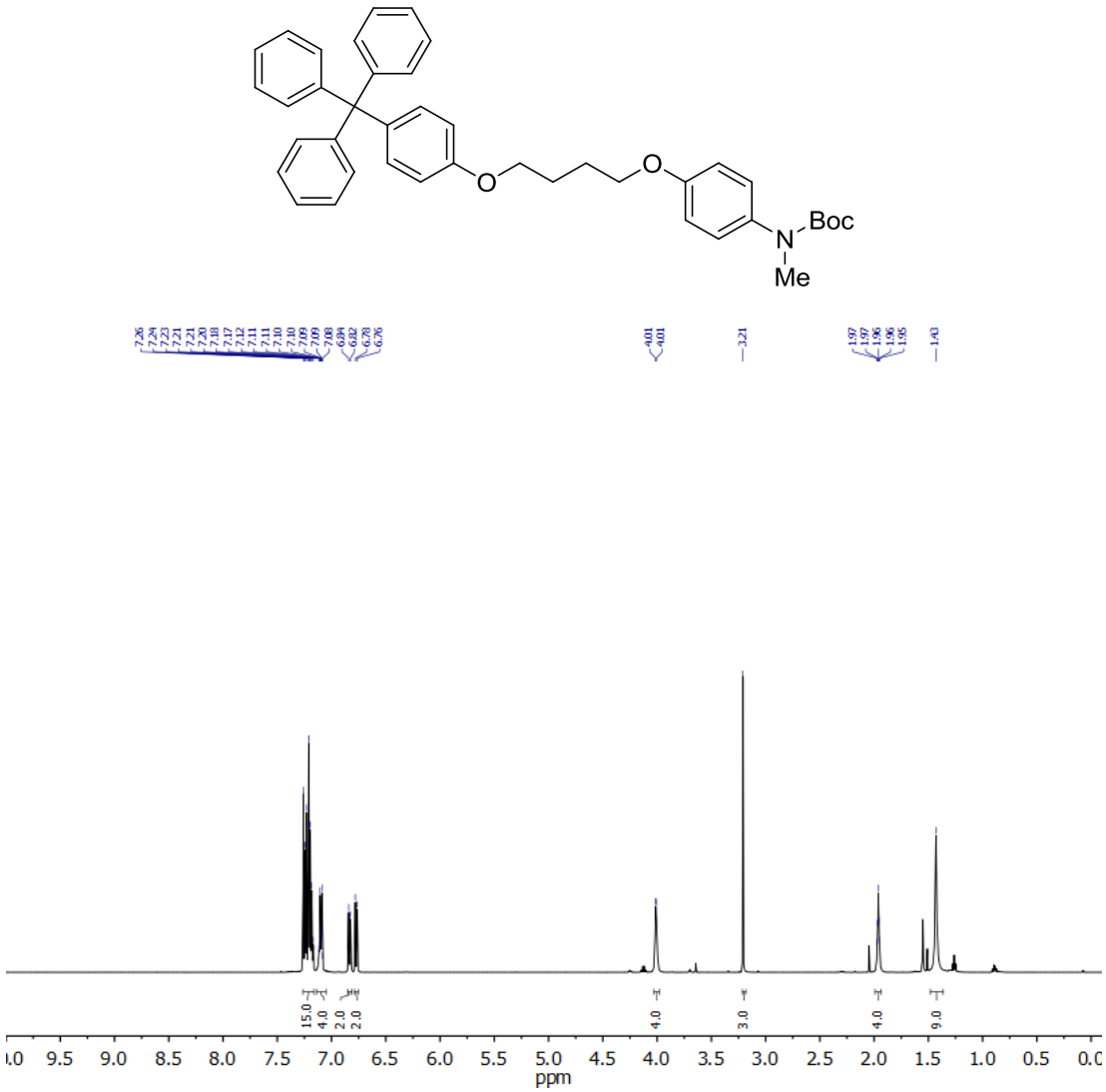

Figure S32: ^{1}H NMR (500 MHz, $CDCl_3$) spectrum of **S9**.

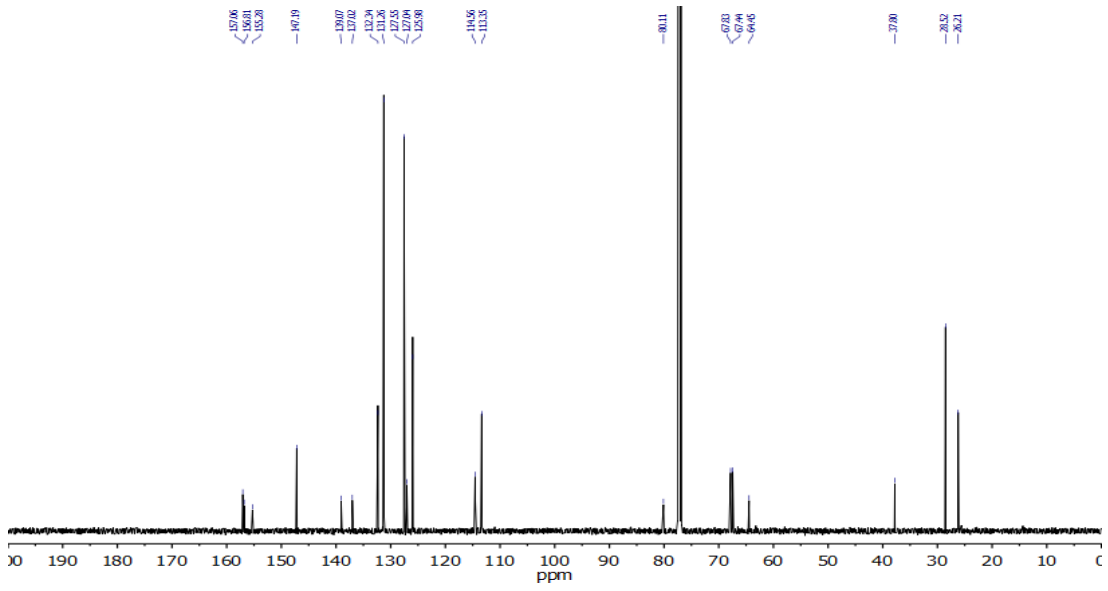

Figure S33: ^{13}C NMR (126 MHz, $CDCl_3$) spectrum of **S9**.

Compound 9:

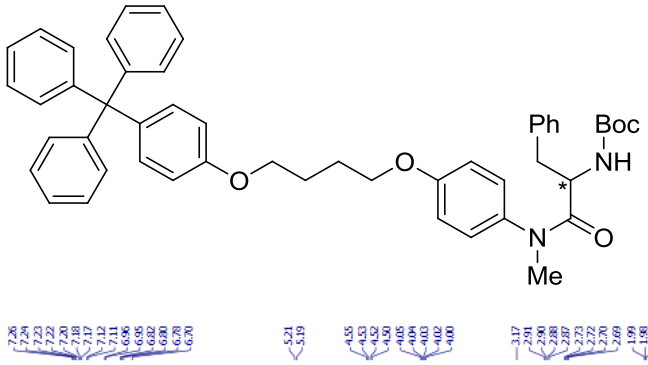

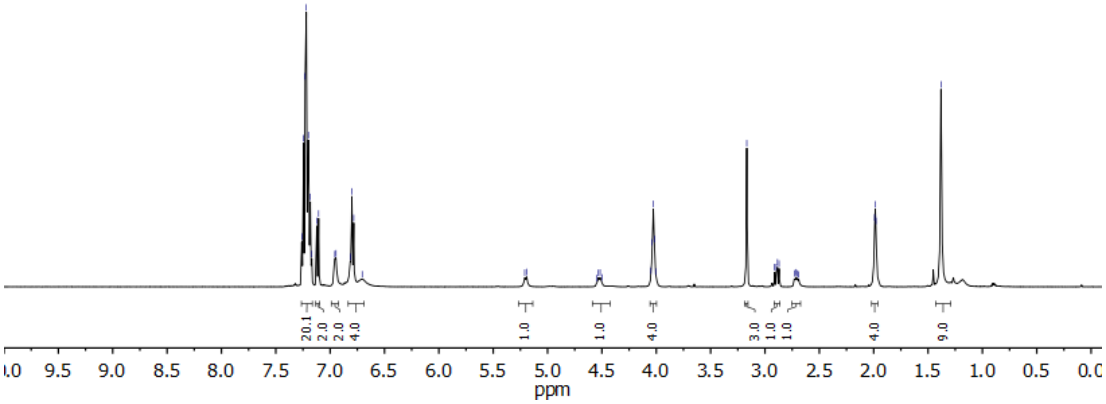

Figure S34: ^{1}H NMR (500 MHz, $CDCl_3$) spectrum of **9**.

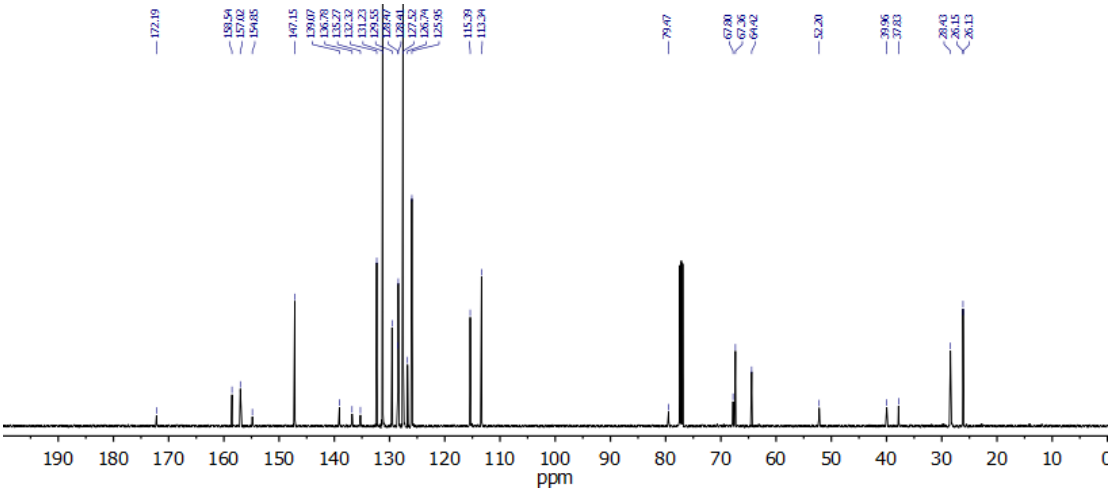

Figure S35: ^{13}C NMR (126 MHz, $CDCl_3$) spectrum of **9**.

Compound S10:

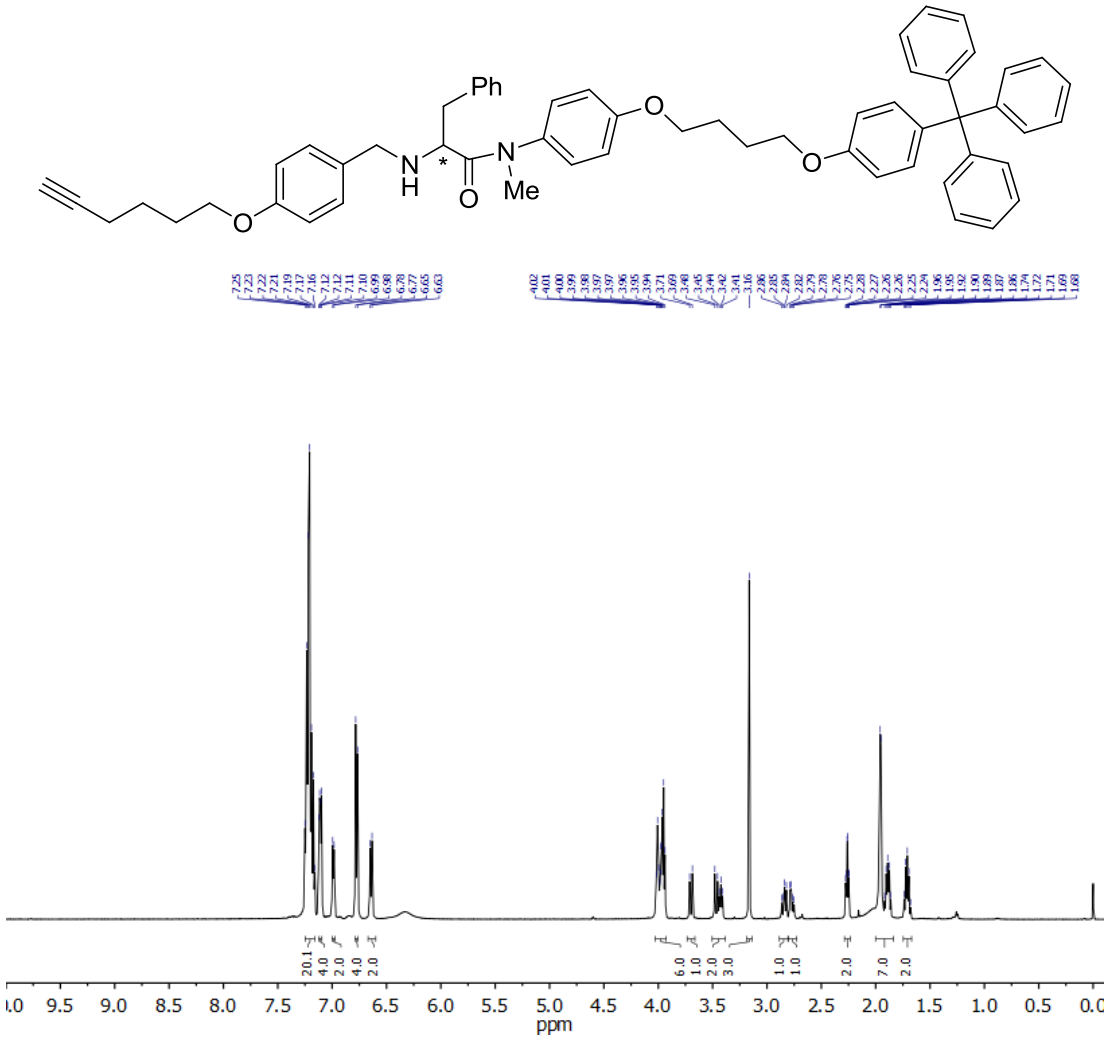

Figure S36: ^{1}H NMR (500 MHz, $CDCl_3$) spectrum of **S10**.

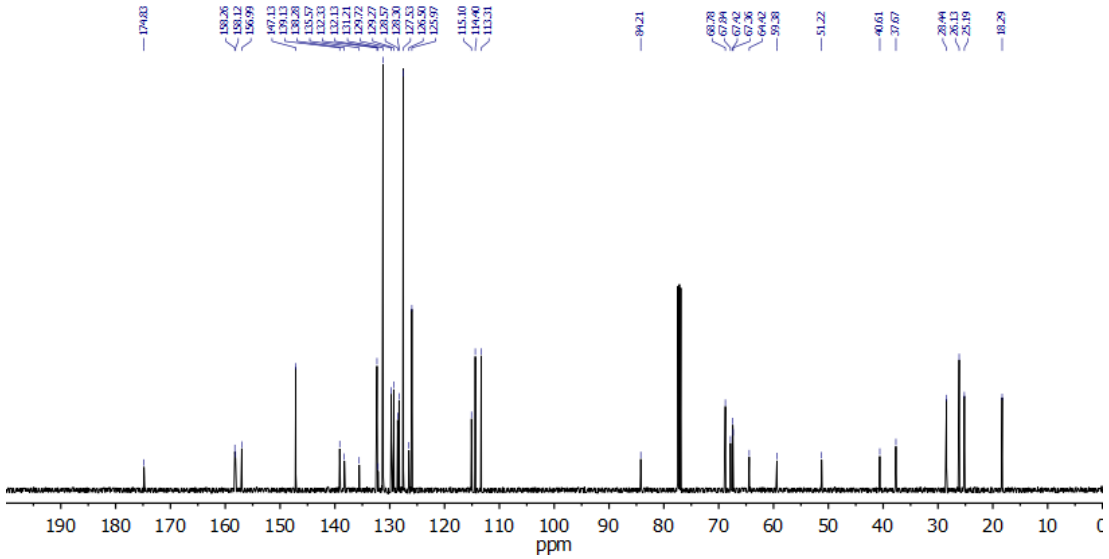

Figure S37: ^{13}C NMR (126 MHz, $CDCl_3$) spectrum of **S10**.

Compound 11-$H^+ \cdot PF_6^-$:

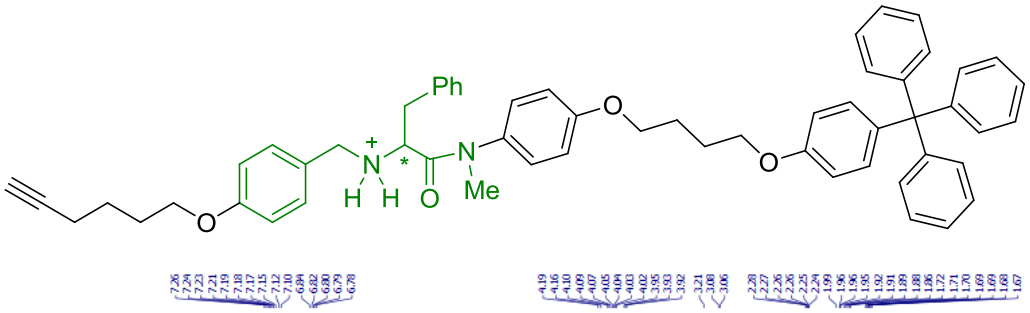

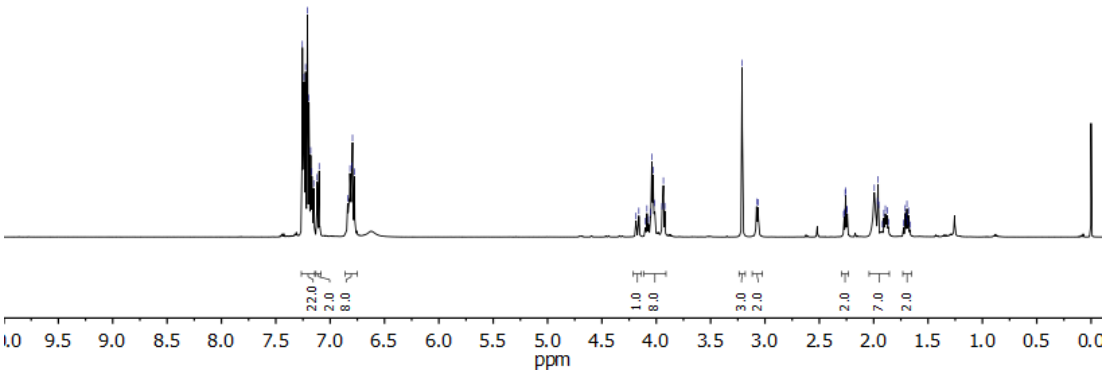

Figure S38: ^{1}H NMR (500 MHz, $CDCl_3$) spectrum of **11-$H^+ \cdot PF_6^-$**.

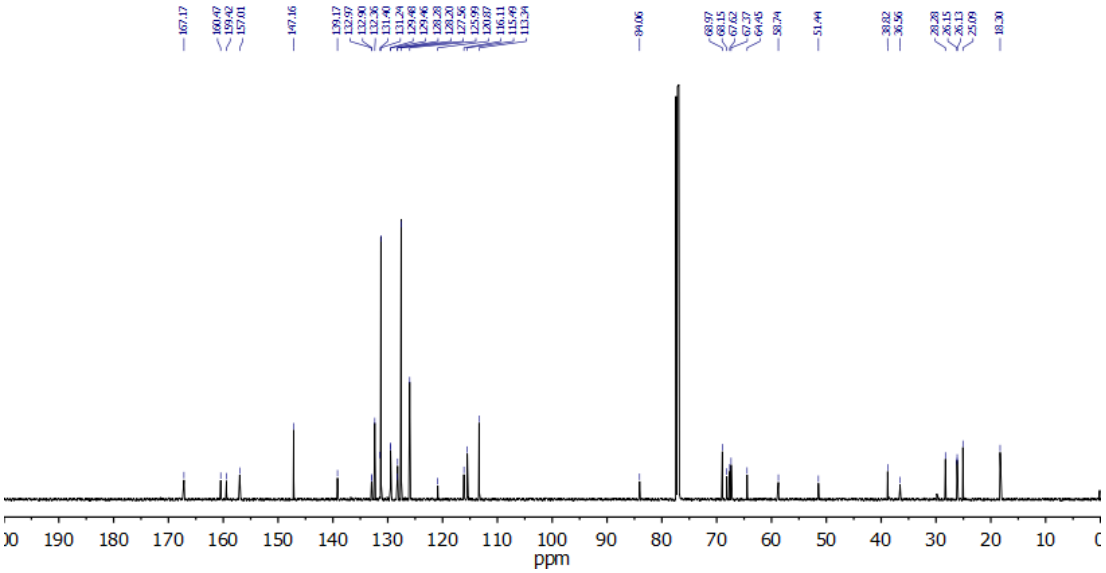

Figure S39: ^{13}C NMR (126 MHz, $CDCl_3$) spectrum of **11-$H^+ \cdot PF_6^-$**.

Compound 14-H$^+$·PF$_6^-$:

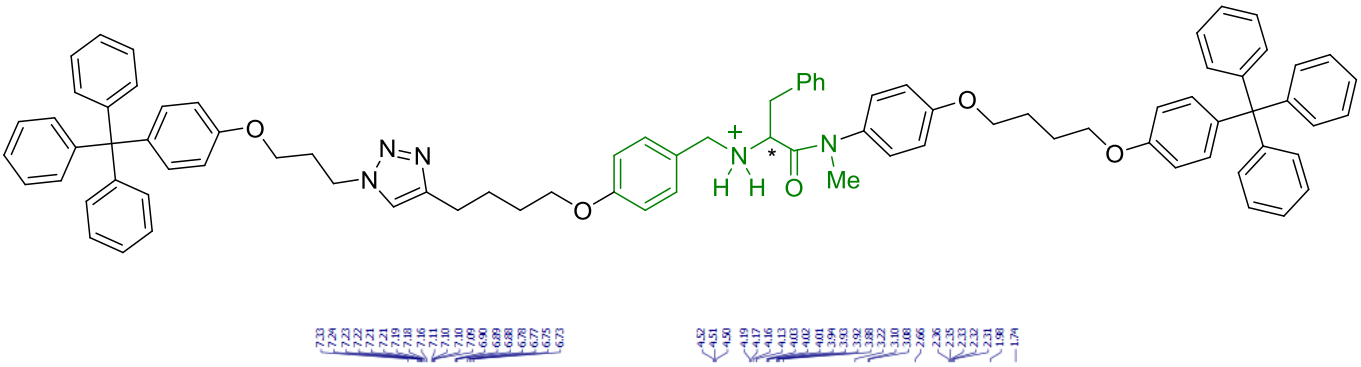

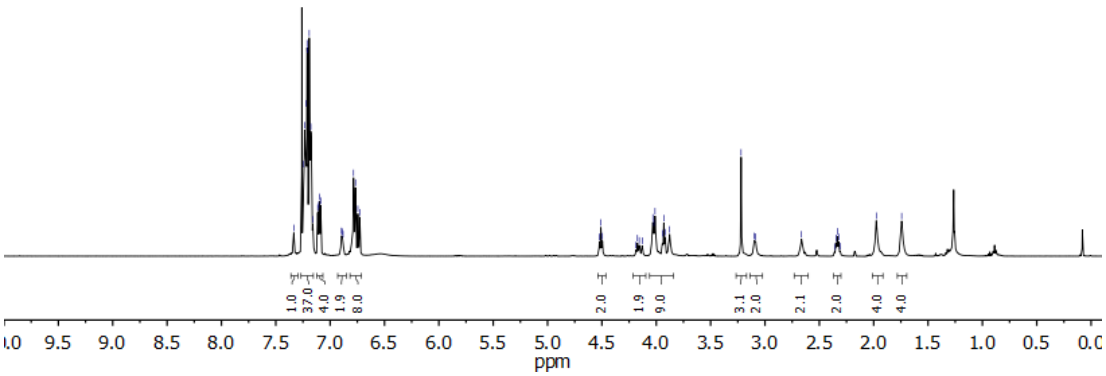

Figure S40: ^{1}H NMR (500 MHz, $CDCl_3$) spectrum of **14-H$^+$·PF$_6^-$**.

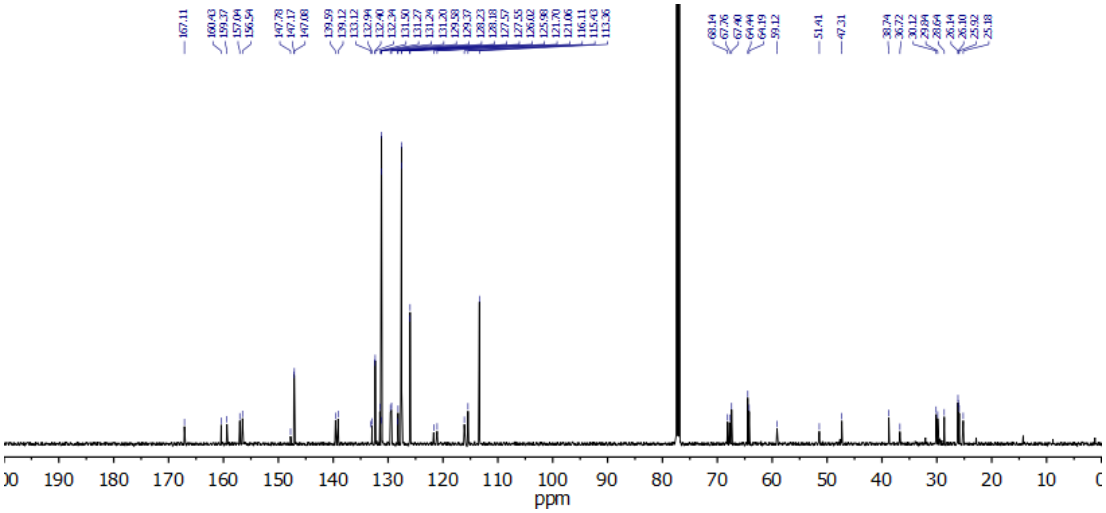

Figure S41: ^{13}C NMR (126 MHz, $CDCl_3$) spectrum of **14-H$^+$·PF$_6^-$**.

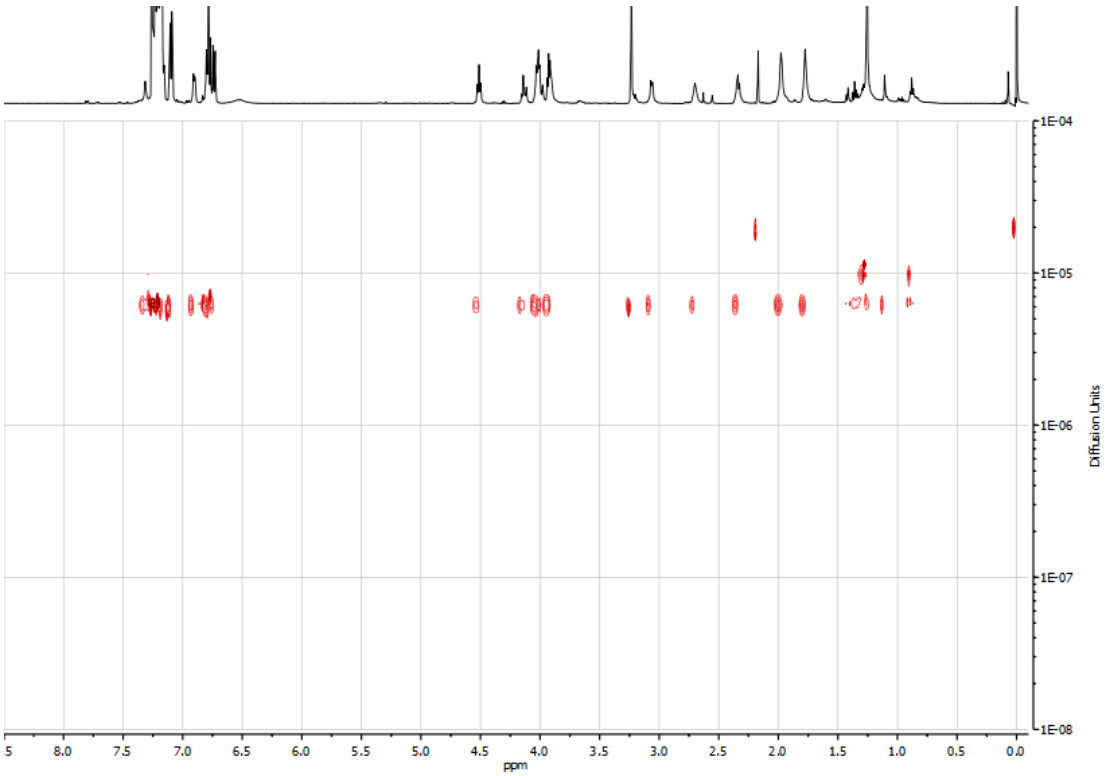

Figure S42: DOSY NMR (500 MHz, $CDCl_3$) spectrum of **14-H**$^+$·PF_6^-.

Compound 2-H$^+$·2PF$_6^-$:

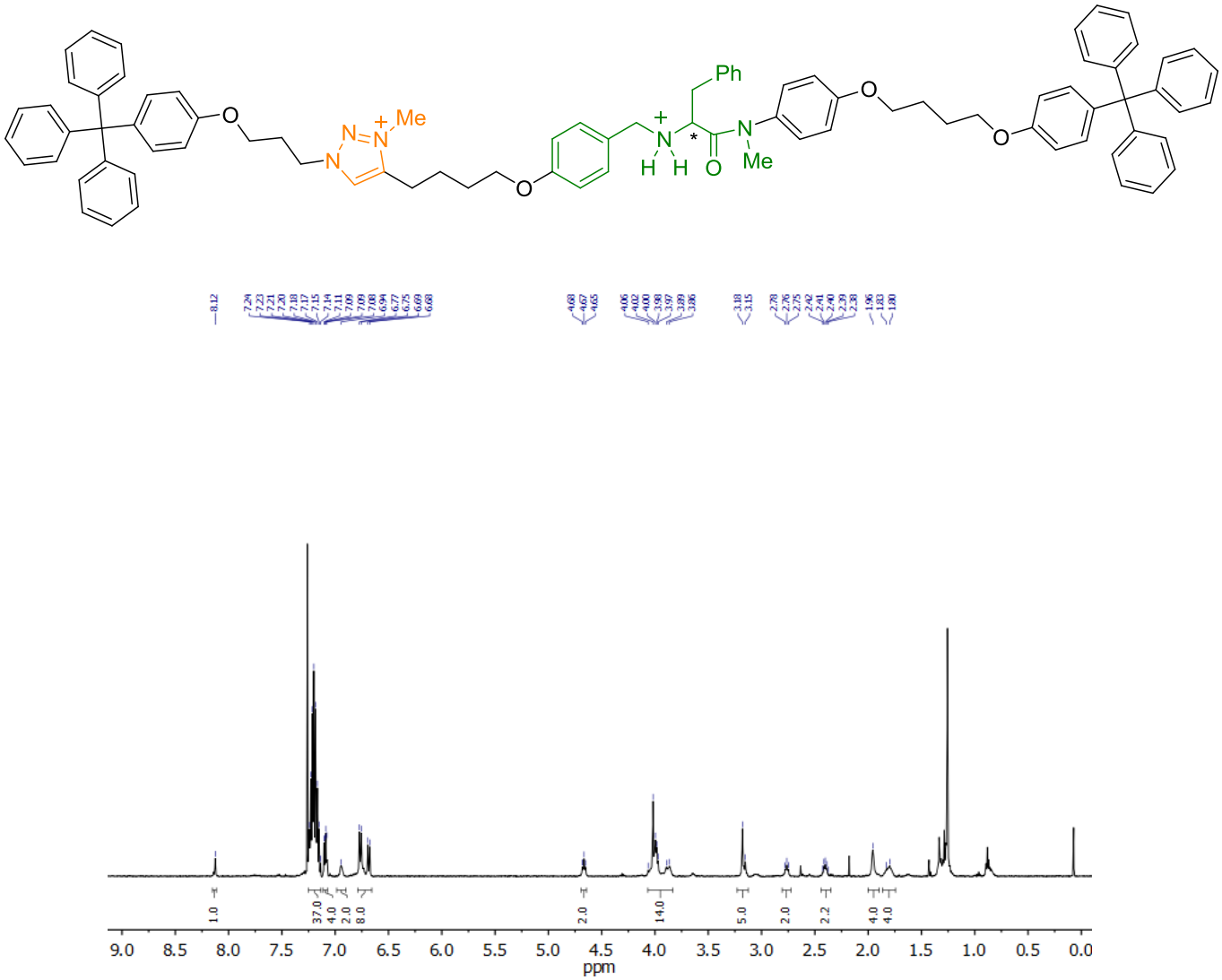

Figure S43: ^{1}H NMR (500 MHz, $CDCl_3$) spectrum of **2-H**$^+$·2PF$_6^-$.

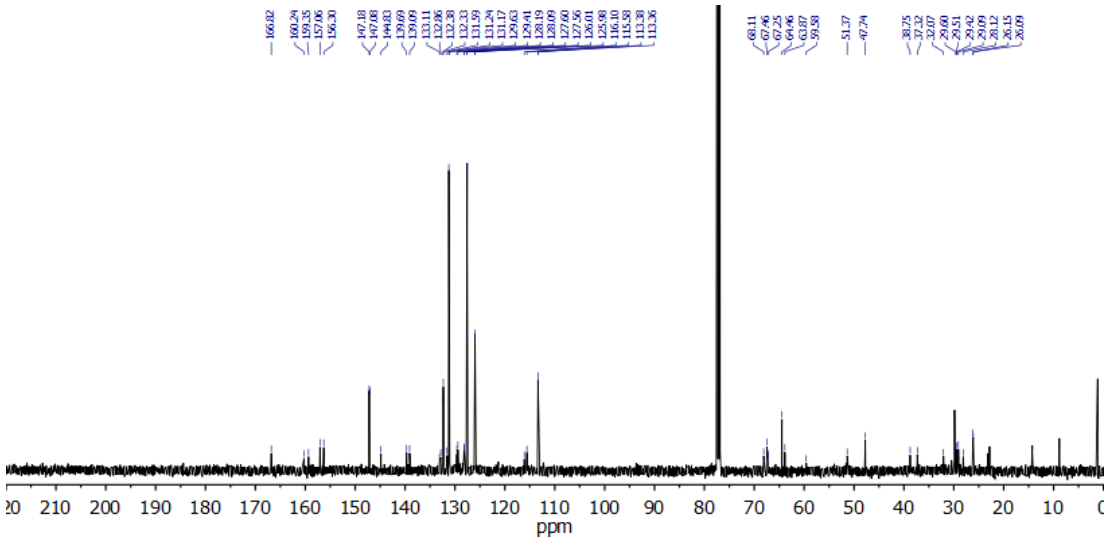

Figure S44: ^{13}C NMR (126 MHz, $CDCl_3$) spectrum of **2-H**$^+$·2PF$_6^-$.

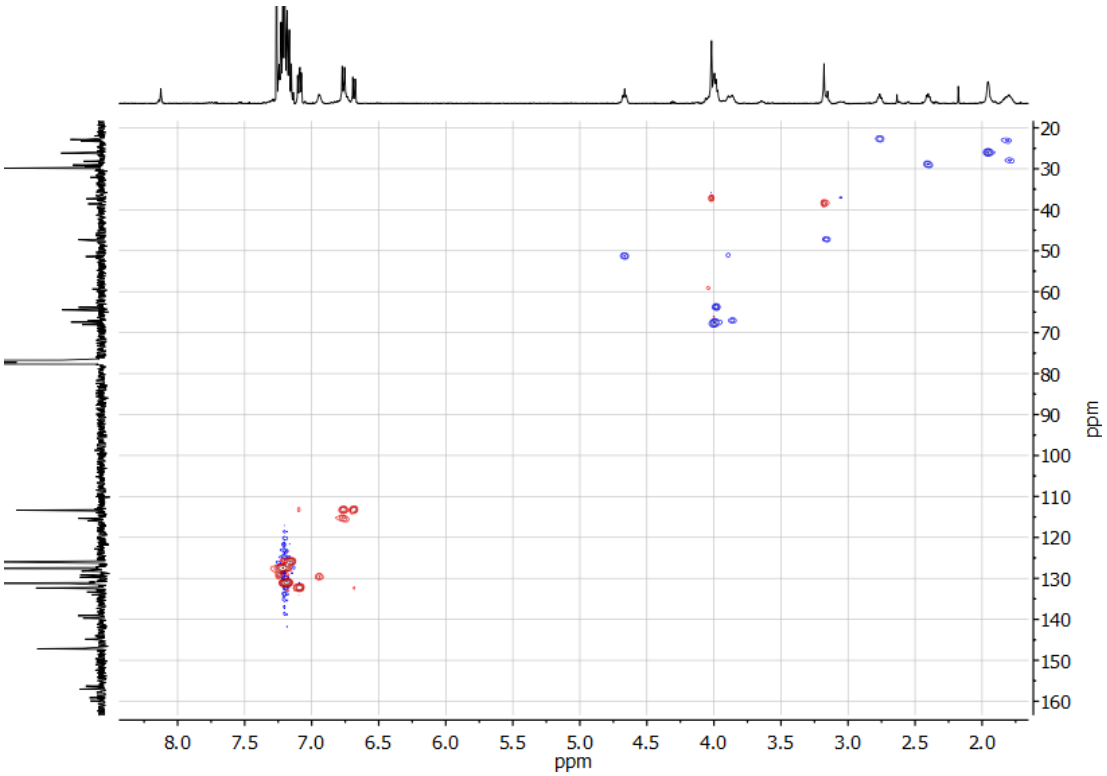

Figure S45: HSQC NMR (500 MHz and 126 MHz, $CDCl_3$) spectrum of **2-H**$^+$·2PF_6^-.

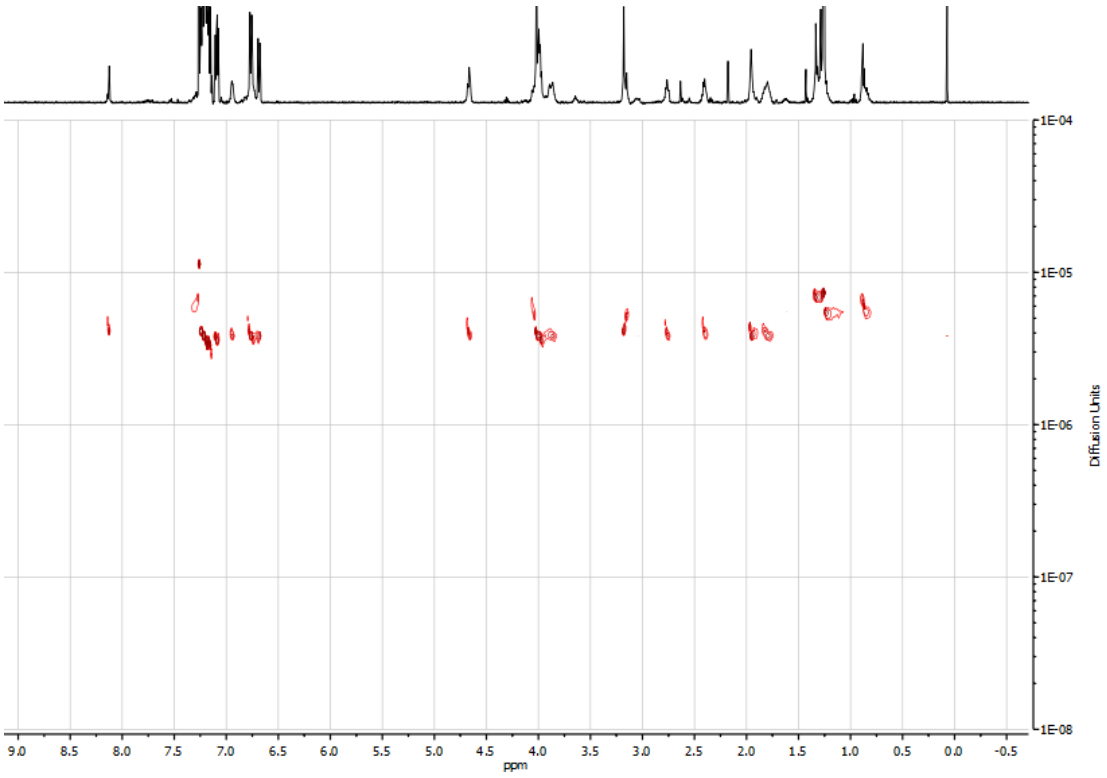

Figure S46: DOSY NMR (500 MHz, $CDCl_3$) spectrum of **2-H**$^+$·2PF_6^-.

Compound 13-$H^+ \cdot PF_6^-$:

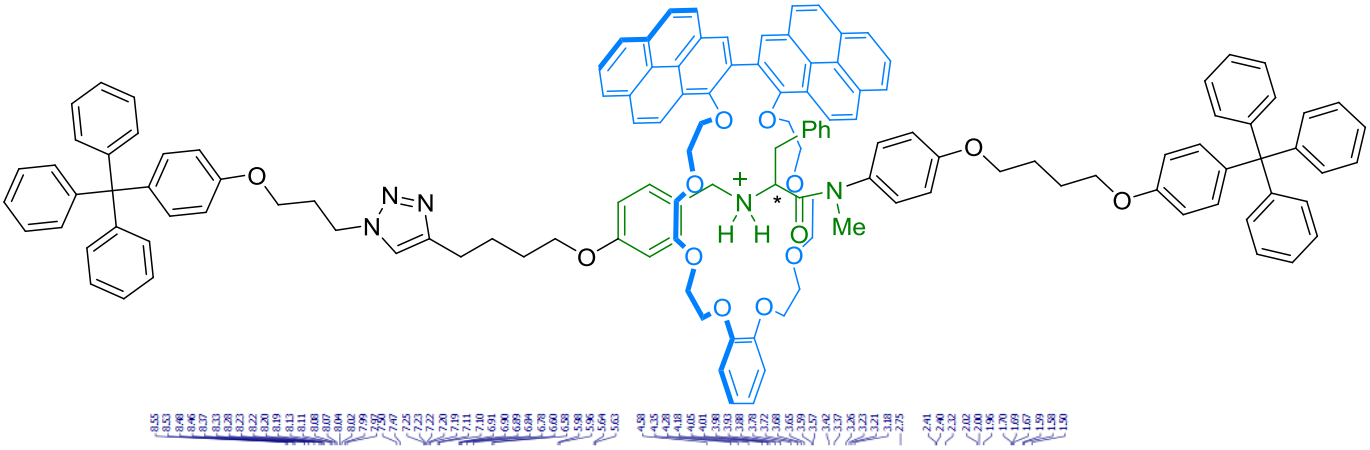

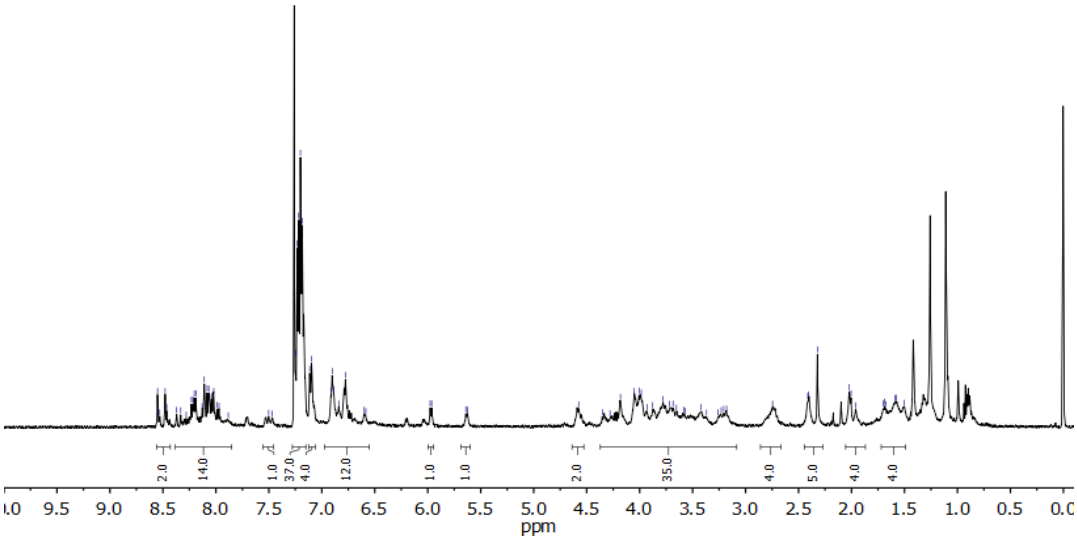

Figure S47: ^{1}H NMR (500 MHz, $CDCl_3$) spectrum of **13-$H^+ \cdot PF_6^-$**.

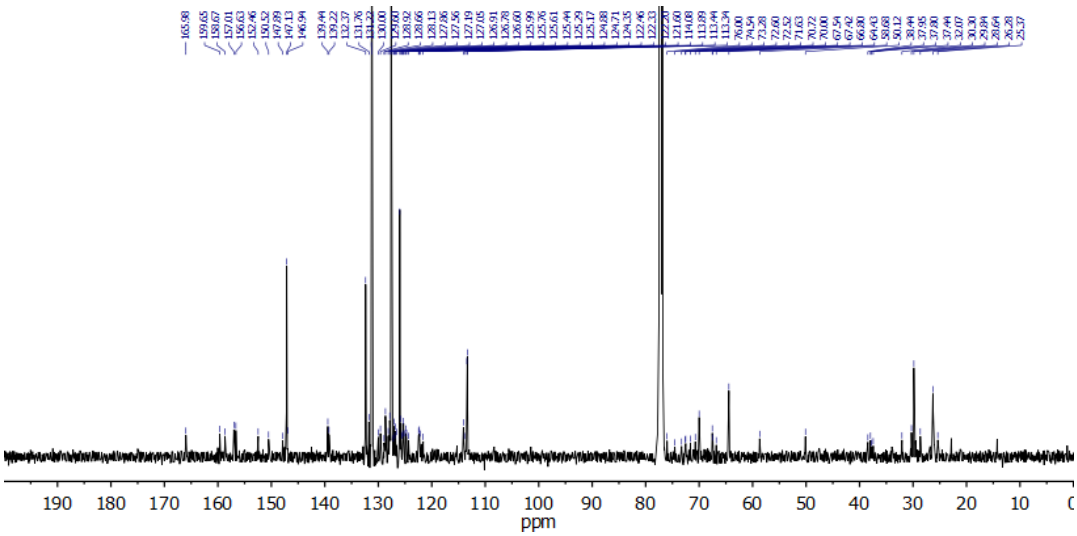

Figure S48: ^{13}C NMR (126 MHz, $CDCl_3$) spectrum of **13-$H^+ \cdot PF_6^-$**.

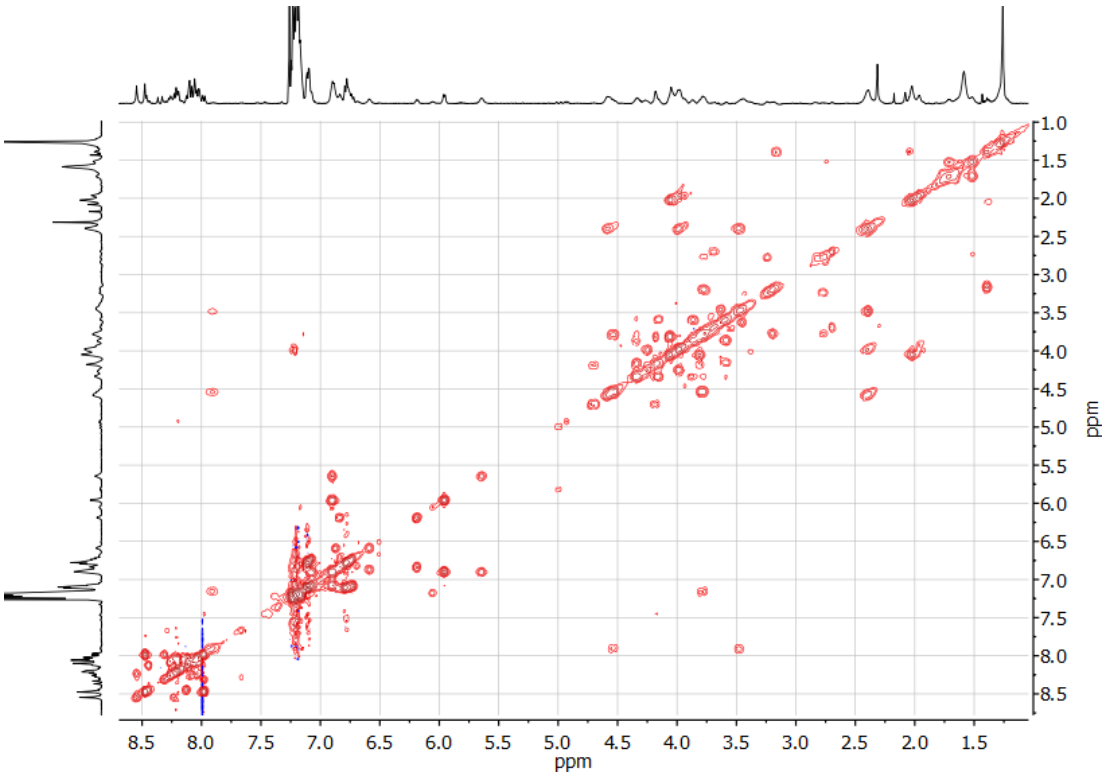

Figure S49: COSY NMR (500 MHz, $CDCl_3$) spectrum of **13-H**$^+$·PF_6^-.

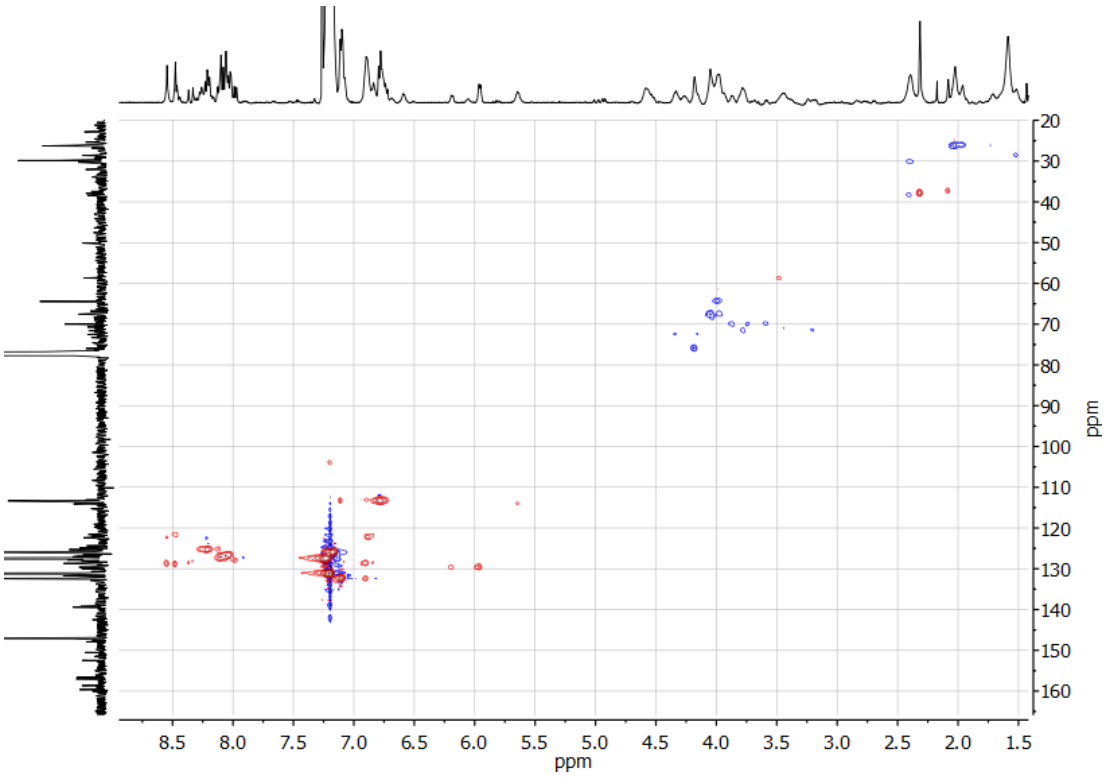

Figure S50: HSQC NMR (500 MHz and 126 MHz, $CDCl_3$) spectrum of **13-H**$^+$·PF_6^-.

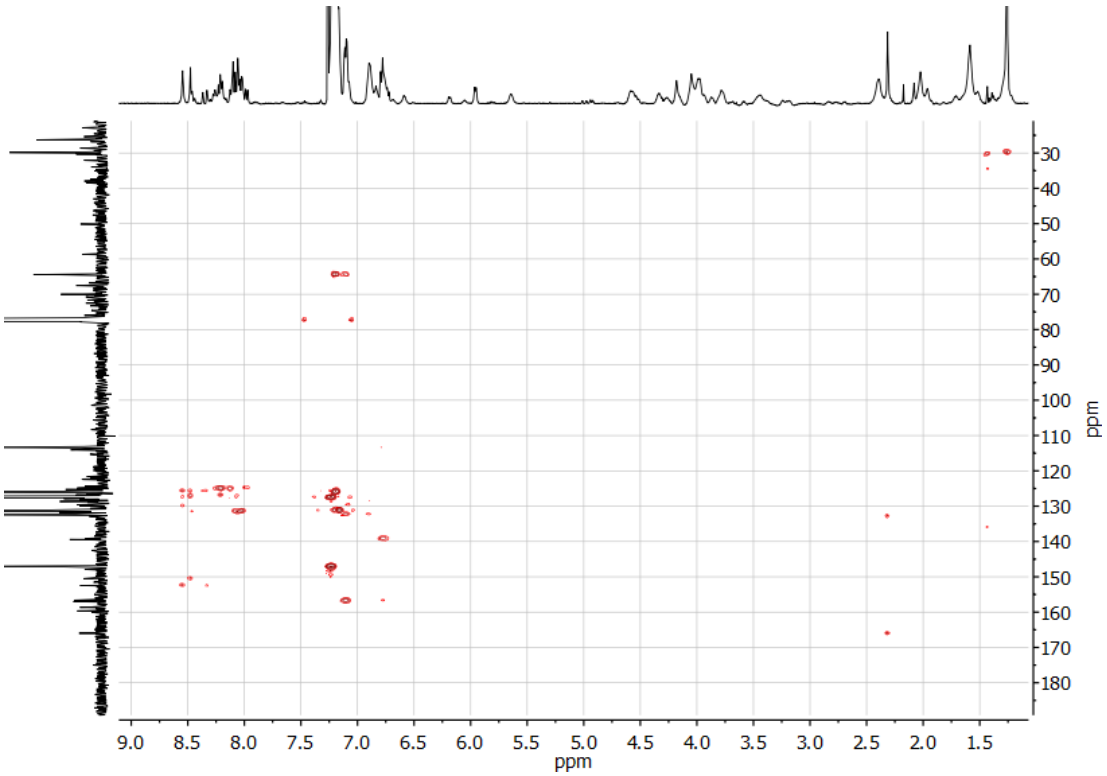

Figure S51: HMBC NMR (500 MHz and 126 MHz, $CDCl_3$) spectrum of **13-H**$^+$·PF_6^-.

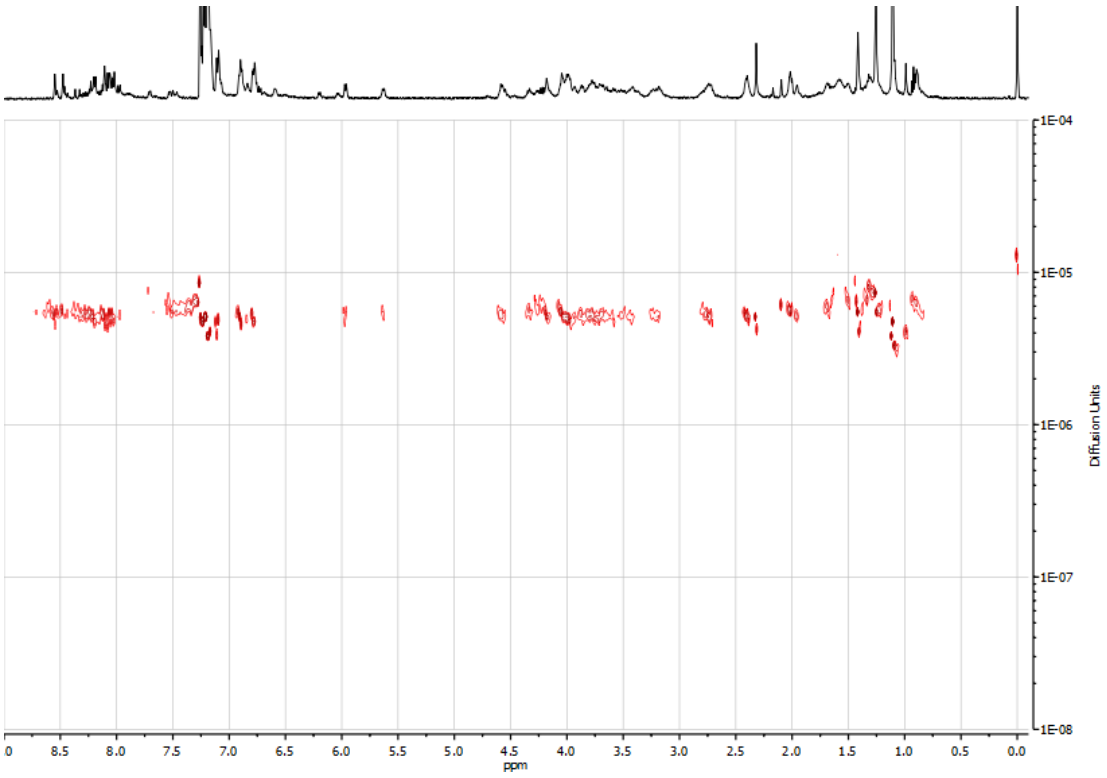

Figure S52: DOSY NMR (500 MHz, $CDCl_3$) spectrum of **13-H**$^+$·PF_6^-.

Compound 1-$H^+ \cdot 2PF_6^-$:

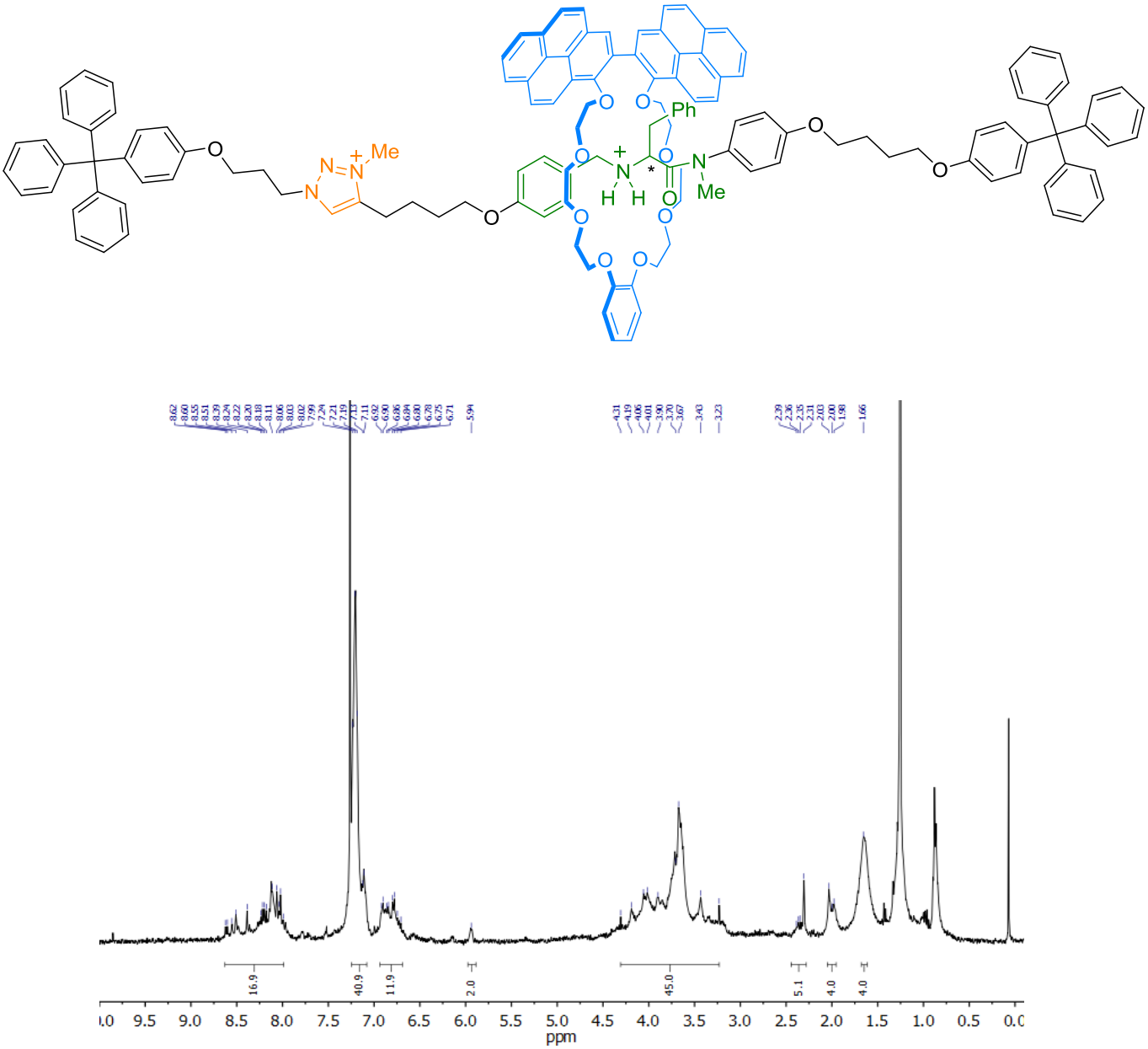

Figure S53: ^{1}H NMR (400 MHz, $CDCl_3$) spectrum of **1-$H^+ \cdot 2PF_6^-$**.

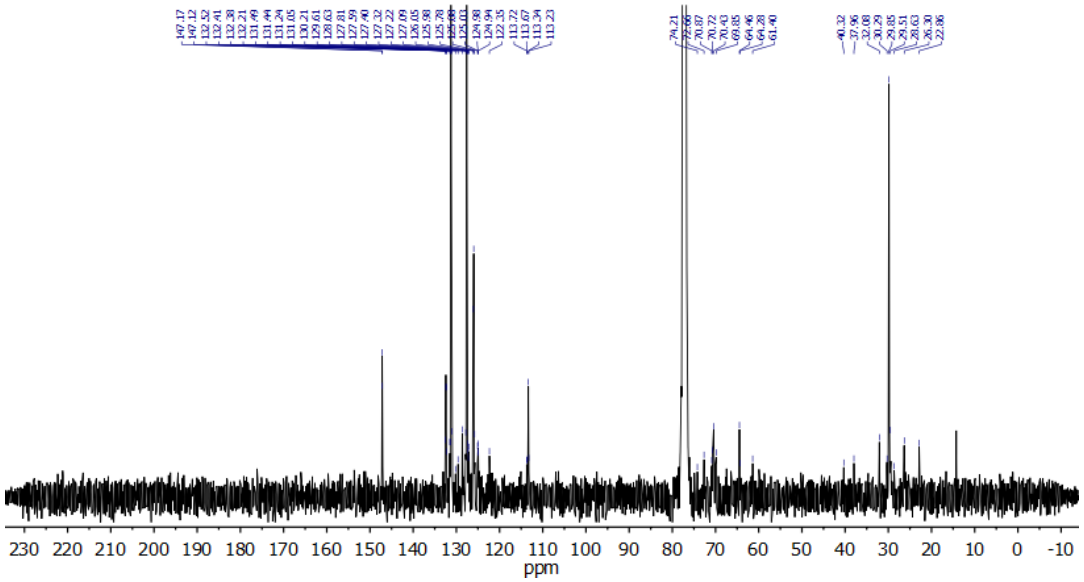

Figure S54: ^{13}C NMR (126 MHz, $CDCl_3$) spectrum of **1-H**$^{+}$·2PF_6^-.

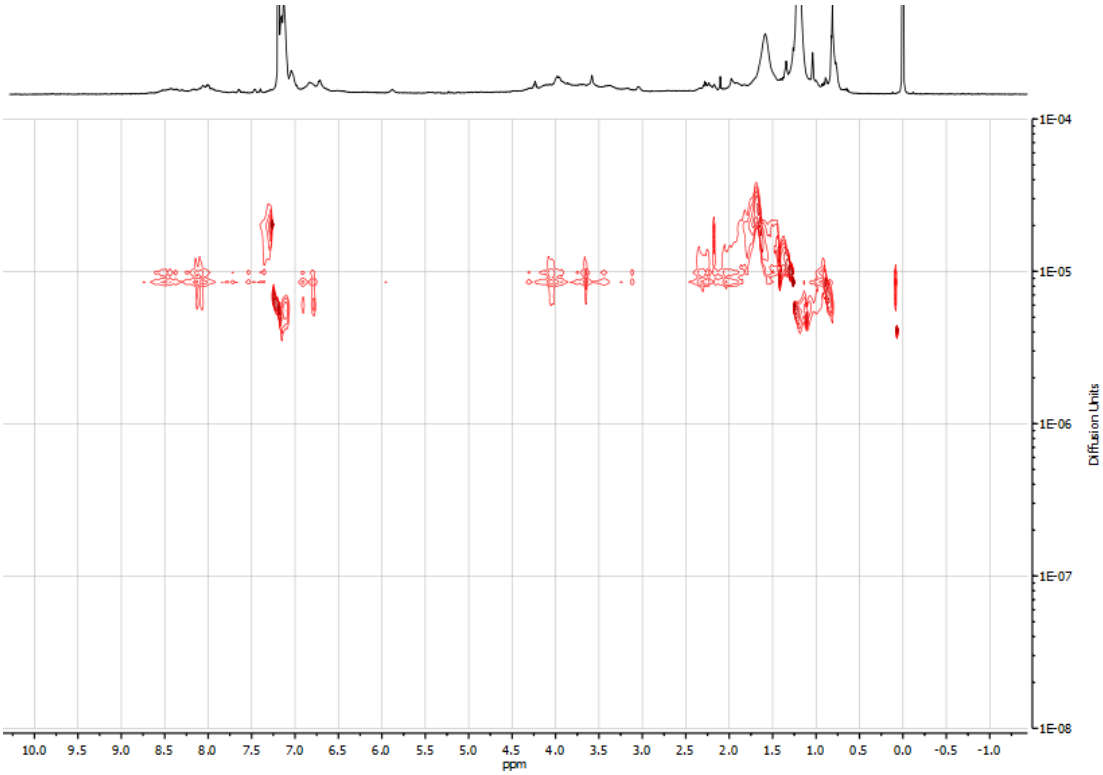

Figure S55: DOSY NMR (500 MHz, $CDCl_3$) spectrum of **1-H**$^{+}$·2PF_6^-.

Compound 1·PF_6^-:

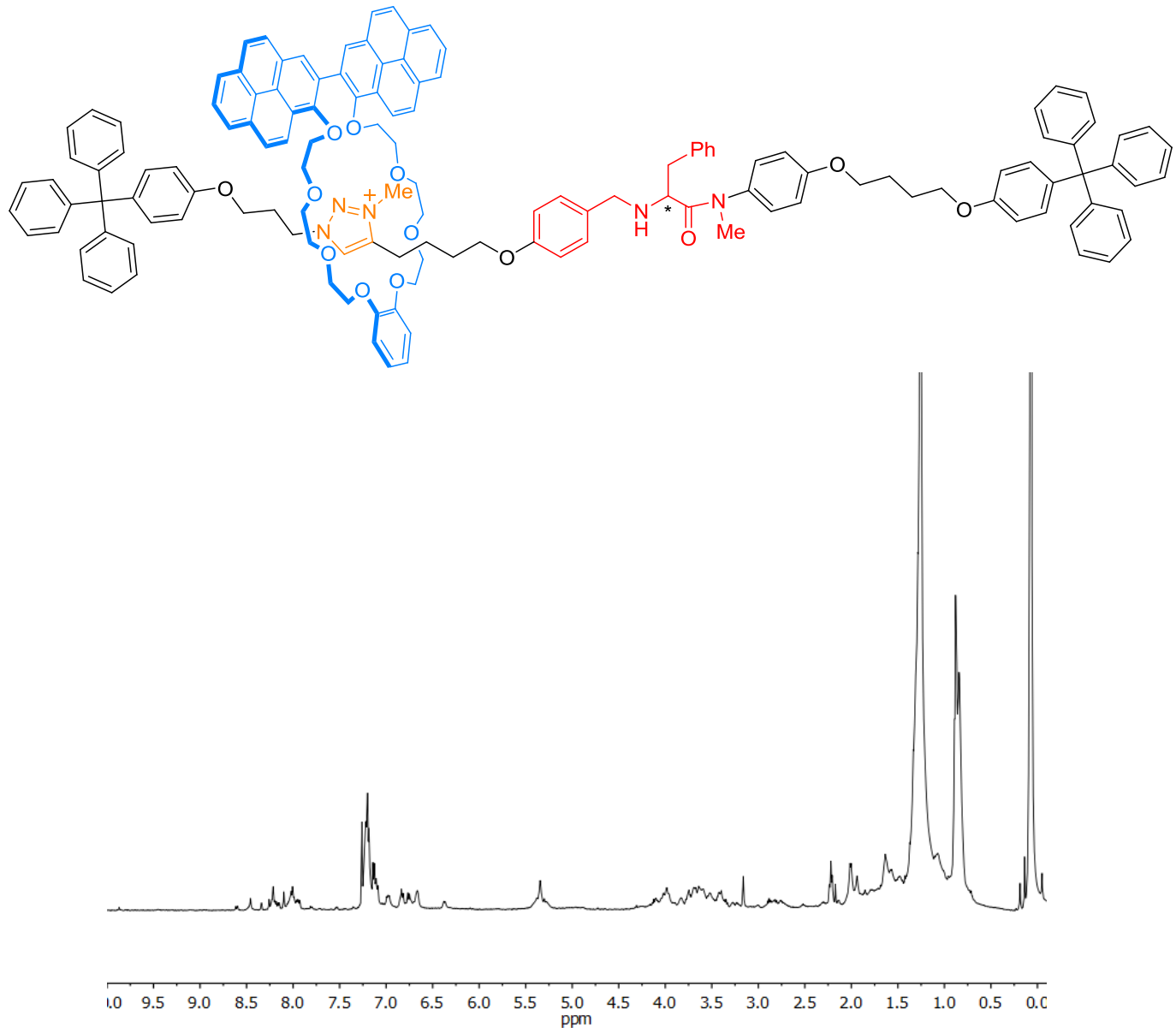

Figure S56: ^{1}H NMR (500 MHz, $CDCl_3$) spectrum of **1**·PF_6^-.

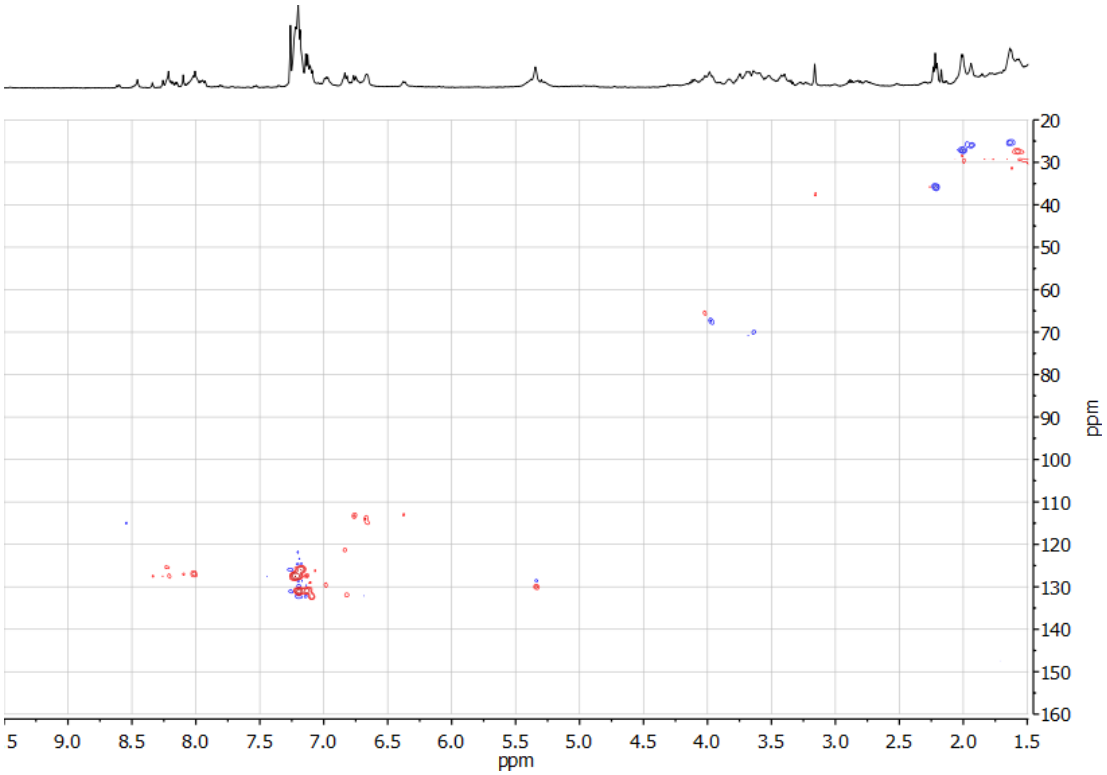

Figure S57: HSQC NMR (500 MHz and 126 MHz, $CDCl_3$) spectrum of **1**·PF_6^-.

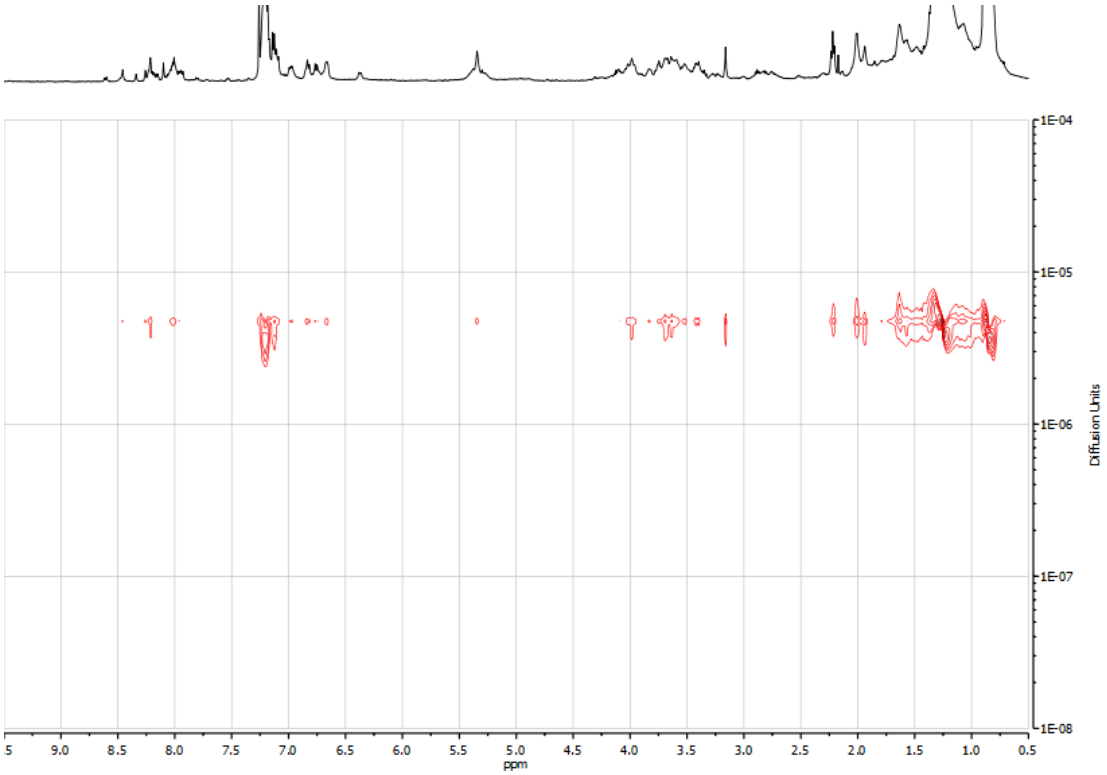

Figure S58: DOSY NMR (500 MHz, $CDCl_3$) spectrum of **1**·PF_6^-.

4. HRMS spectra of rotaxanes

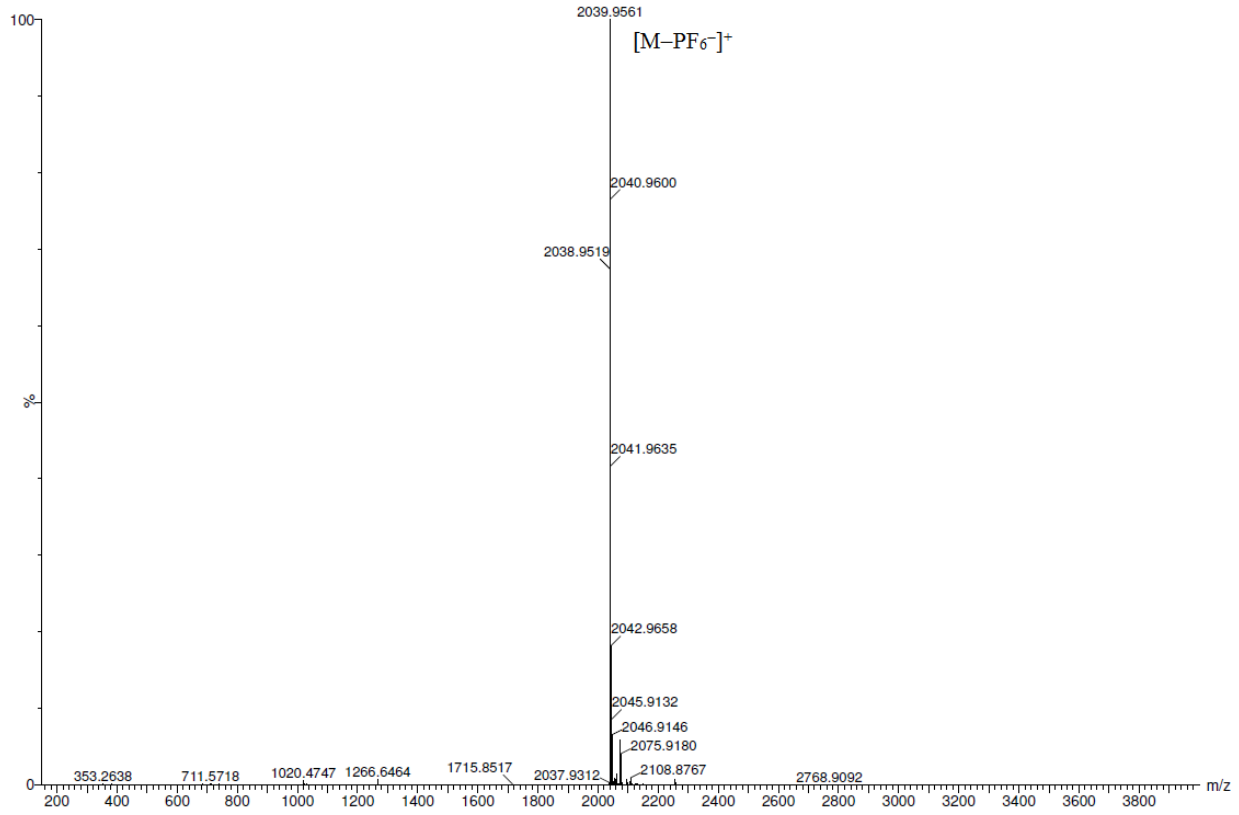

Figure S59: HRMS (ESI$^+$) spectrum of **13-H**$^+$·PF_6^-.

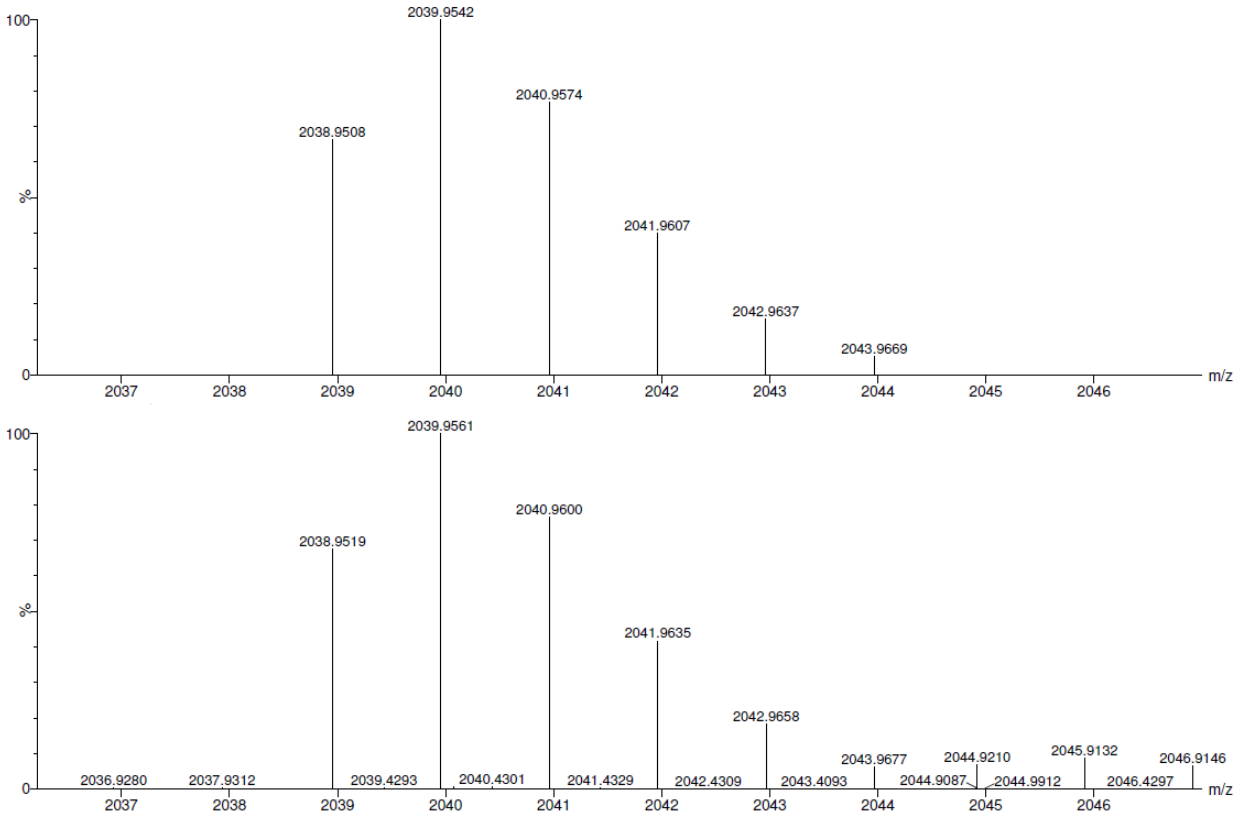

Figure S60: Observed (bottom) and calculated (top) isotopic distribution for [**13–**PF_6^-]$^+$.

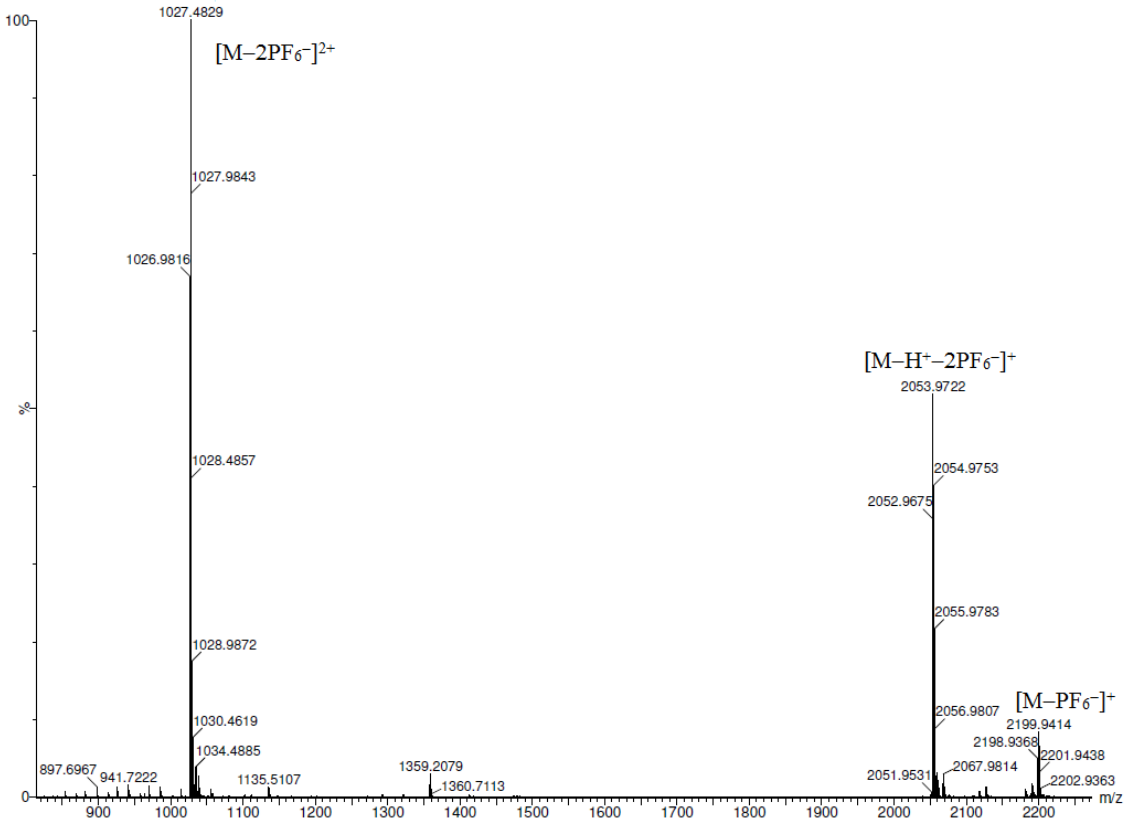

Figure S61: HRMS (ESI$^+$) spectrum of **1**-**H**$^+$·2PF$_6^-$.

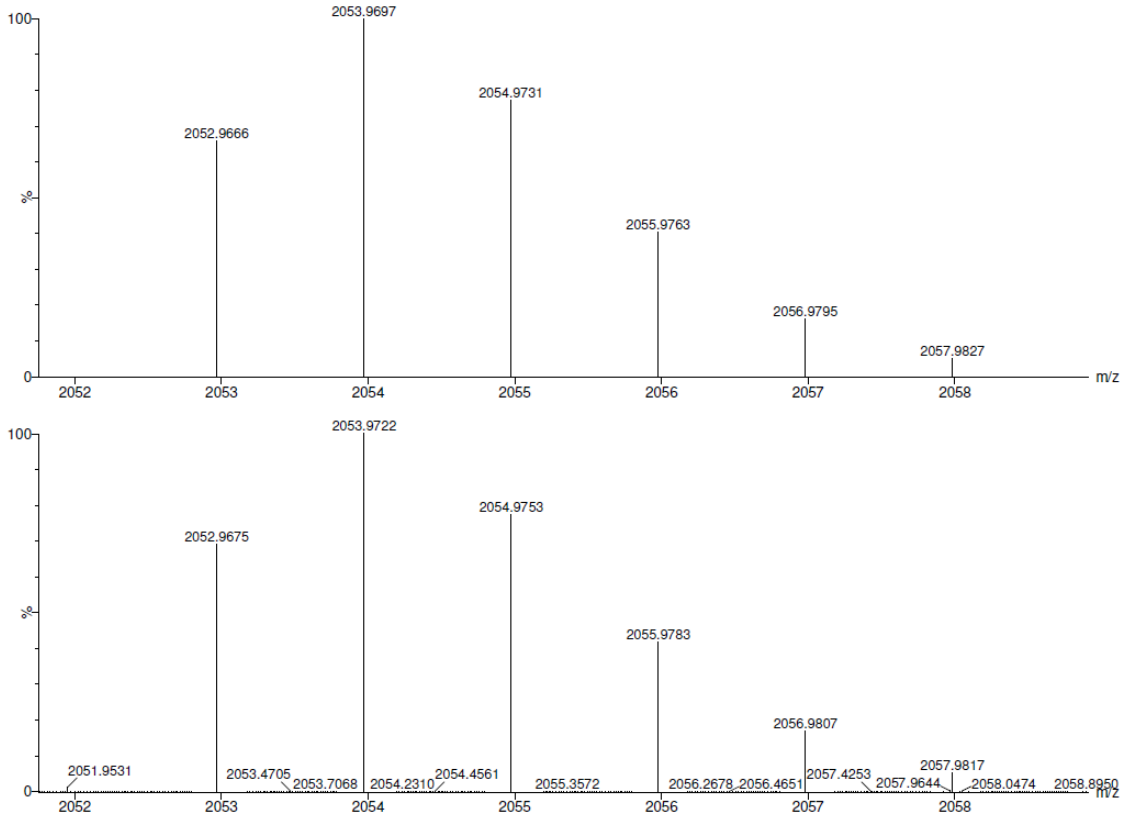

Figure S62: Observed (bottom) and calculated (top) isotopic distribution for [**1**–H$^+$–2PF$_6^-$]$^+$.

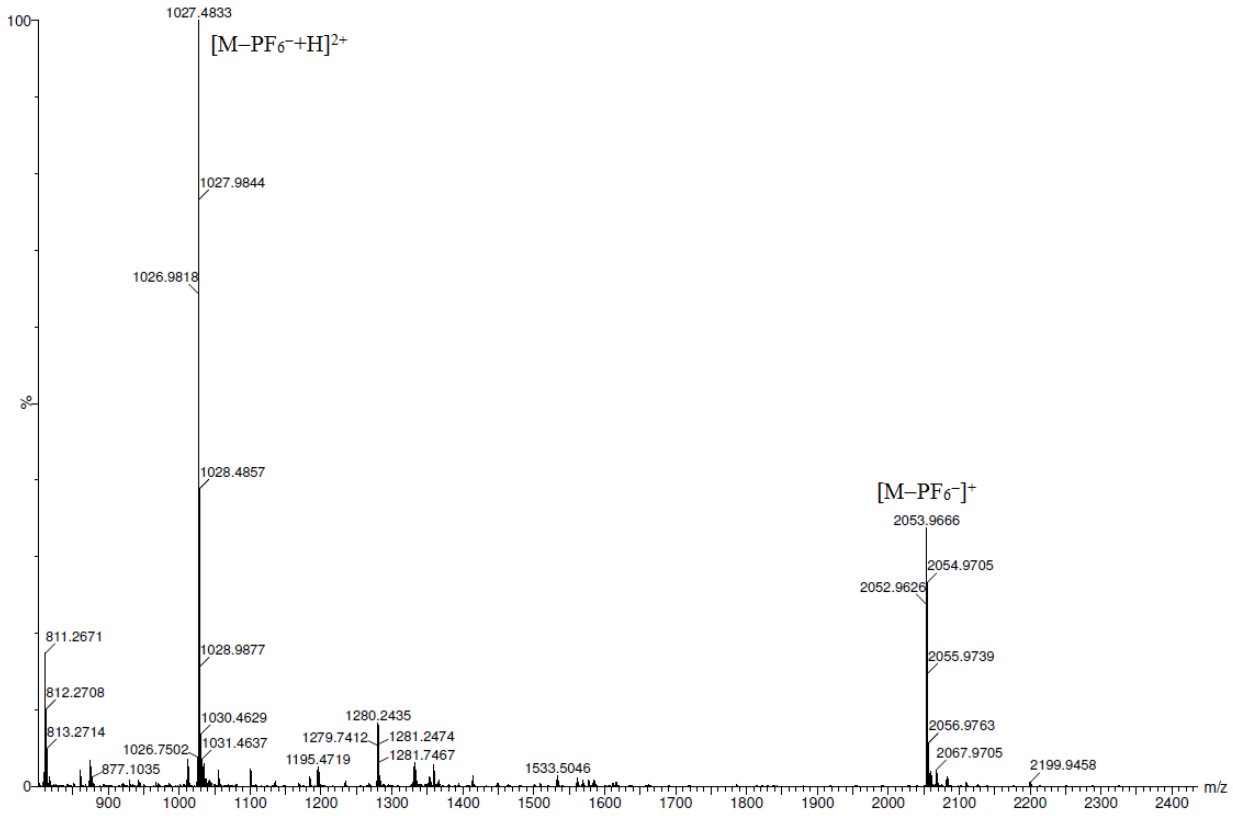

Figure S63: HRMS (ESI$^+$) spectrum of **1**·PF_6^- used for the OFF state CPL measurement, showing peaks corresponding to: *m/z*: 2052.9626 $[M–PF_6^-]^+$ (calcd for $C_{137}H_{130}N_5O_{13}$: 2052.9665); 1026.9818 $[M+H–PF_6^-]^{2+}$ (calcd for $[C_{137}H_{131}N_5O_{13}]^{2+}$: 1026.9872).

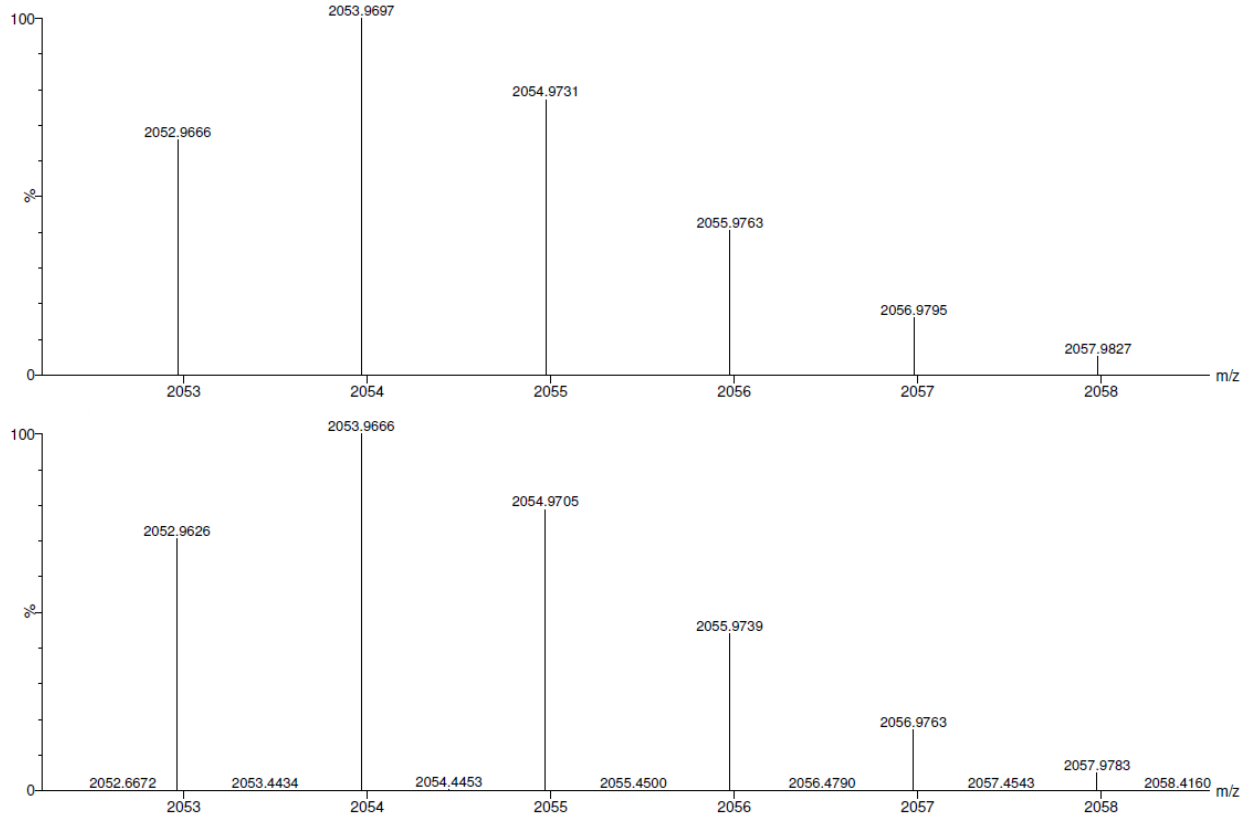

Figure S64: Observed (bottom) and calculated (top) isotopic distribution for [**1**–PF_6^-]$^+$.

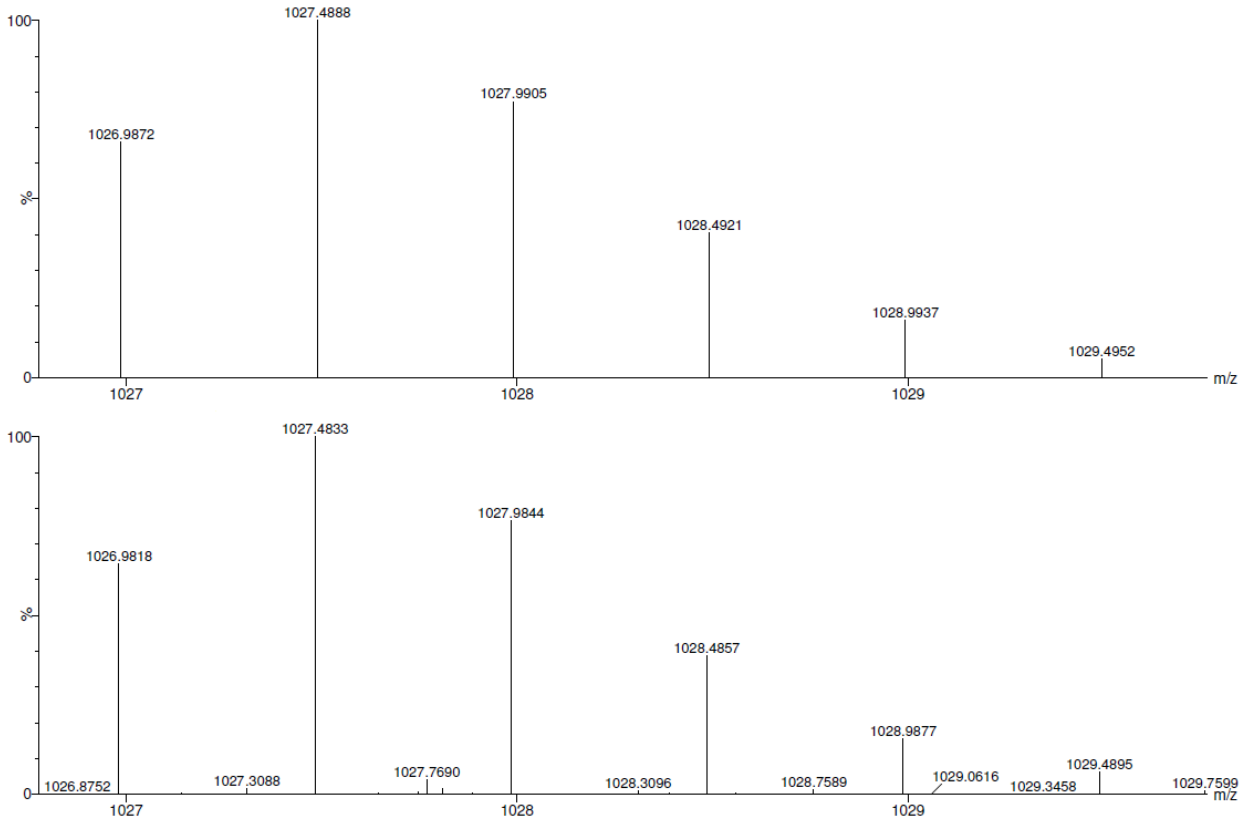

Figure S65: Observed (bottom) and calculated (top) isotopic distribution for [**1**–PF_6^-+H]$^{2+}$.

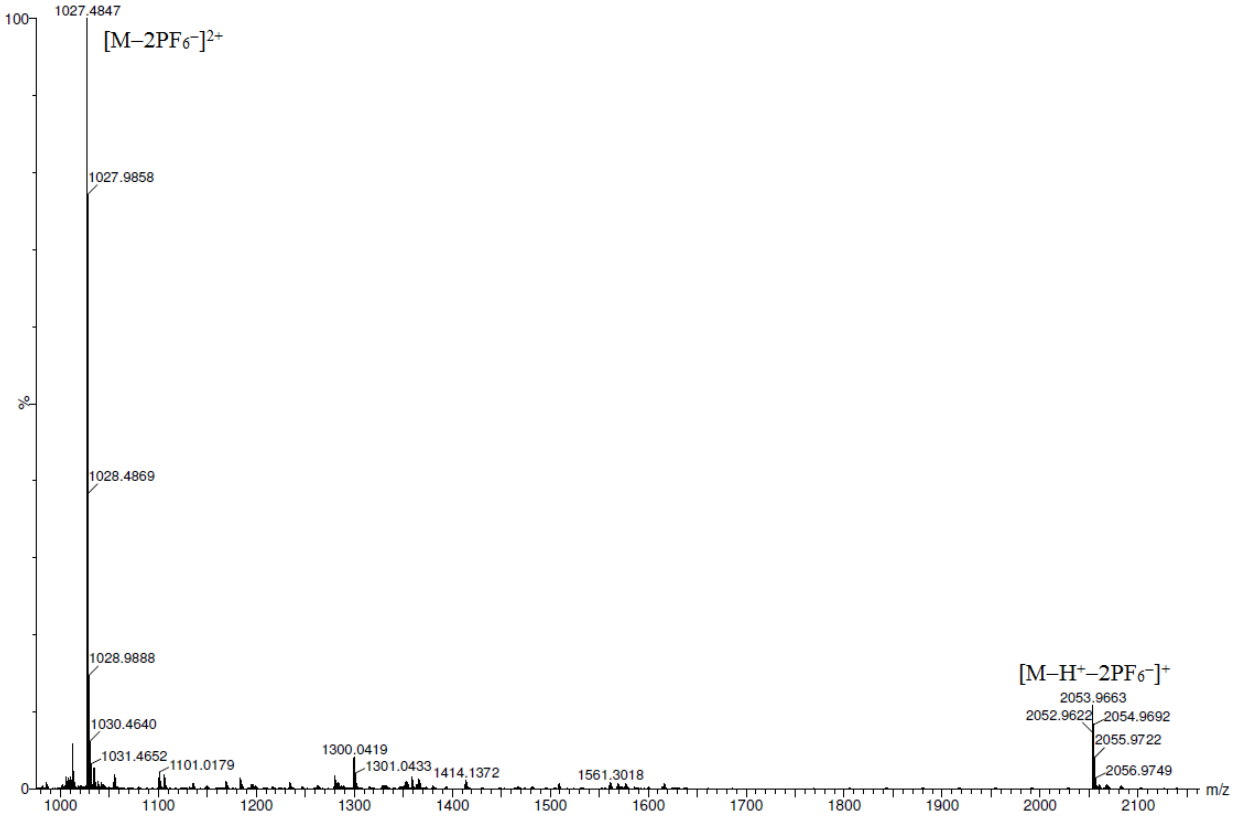

Figure S66: HRMS (ESI$^+$) spectrum of **1**-**H**$^+$ used for the second cycle ON state CPL measurement, showing peaks corresponding to: *m/z*: 2052.9622 [M–H^+–2PF_6^-]$^+$ (calcd for $C_{137}H_{130}N_5O_{13}$: 2052.9665); 1026.9829 [M–2PF_6^-]$^{2+}$ (calcd for $[C_{137}H_{131}N_5O_{13}]^{2+}$: 1026.9872).

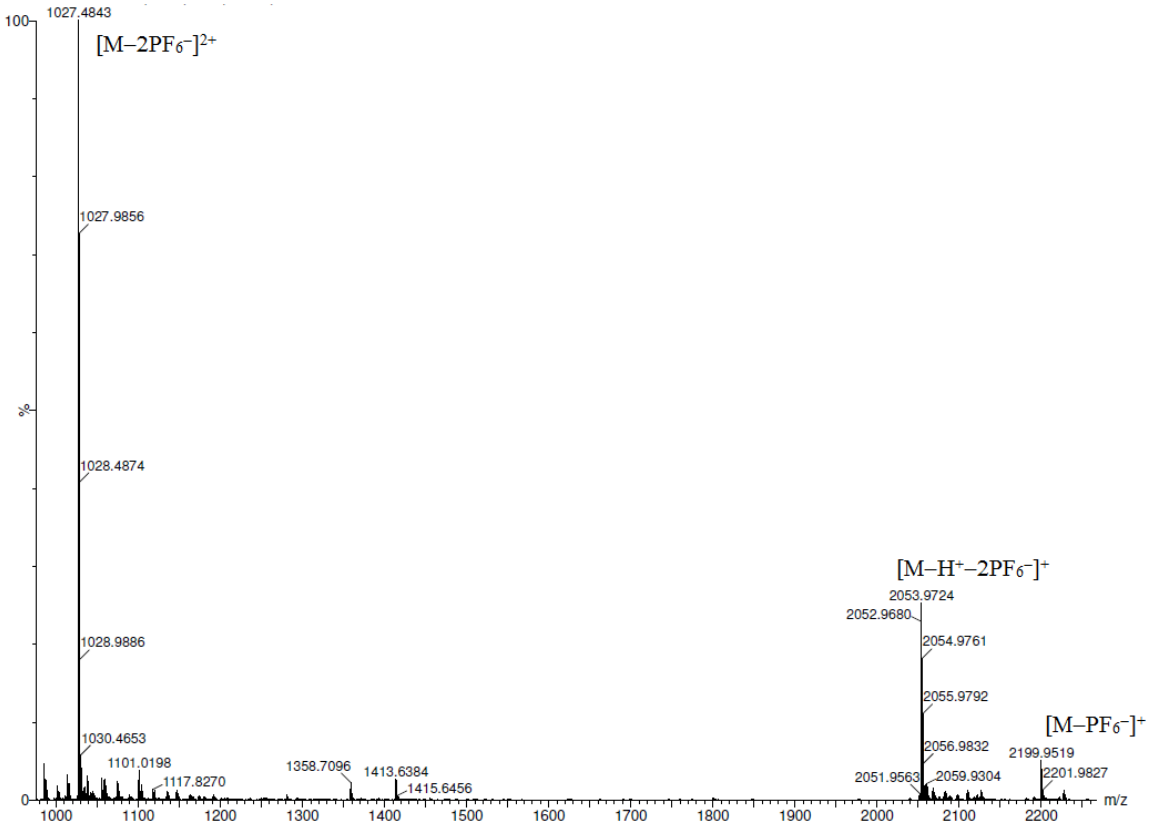

Figure S67: HRMS (ESI$^+$) spectrum of **1-H**$^+$·2PF$_6^-$ obtained by protonation of **1**·PF$_6^-$ with CF_3CO_2H and counterion exchange with KPF_6, showing peaks corresponding to: *m/z*: 2052.9680 [M–H$^+$–2PF$_6^-$]$^+$ (calcd for $C_{137}H_{130}N_5O_{13}$: 2052.9665); 2198.9424 [M–PF$_6^-$]$^+$ (calcd for [$C_{137}H_{131}N_5O_{13}PF_6$]$^+$: 2198.9385).

5. HPLC traces

HPLC experiments were carried out using an HPLC Agilent 1200 Infinity Series with a LiChroCART® 250-4 LiChrospher® 100 RP-8 (5 µm) analytical column. The column temperature was set at 20.0 ºC. The wavelength selected for the peak detection was 280 nm and the flow was constant during the operation: 1.000 mL/min. The mobile phase gradient used is shown in Table S1.

Table S1: Solvent gradient used for the HPLC analysis.

Time (min)	CH_2Cl_2	Methanol
0	100	0
15	99	1
20	98	2
25	96	4
30	95	5
35	92	8
40	90	10
43	85	15
47	93	7
50	100	0

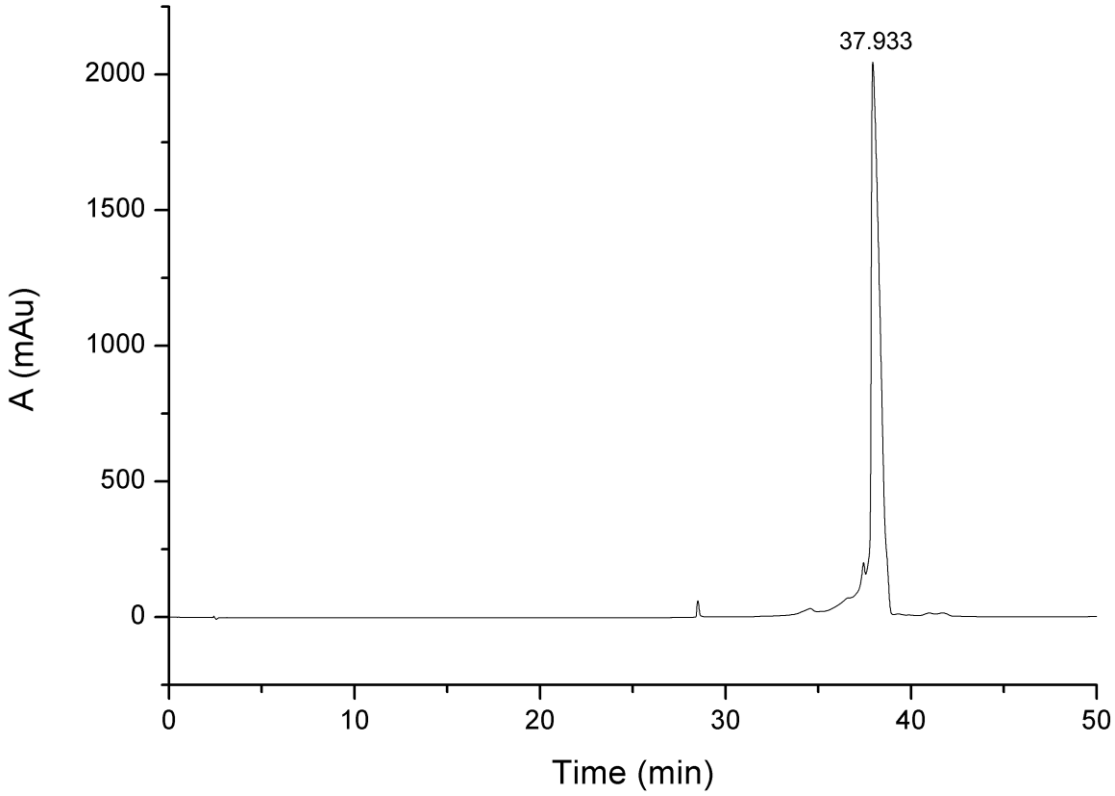

Figure S68: HPLC chromatogram of **8**.

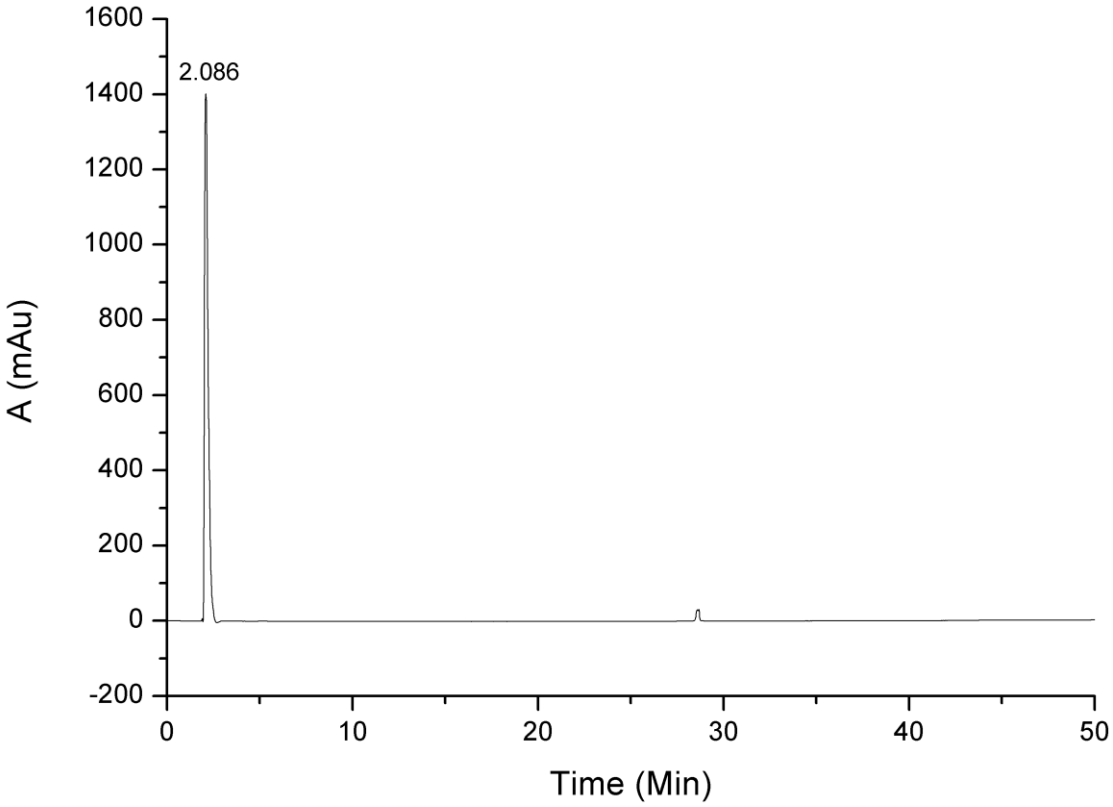

Figure S69: HPLC chromatogram of **12**.

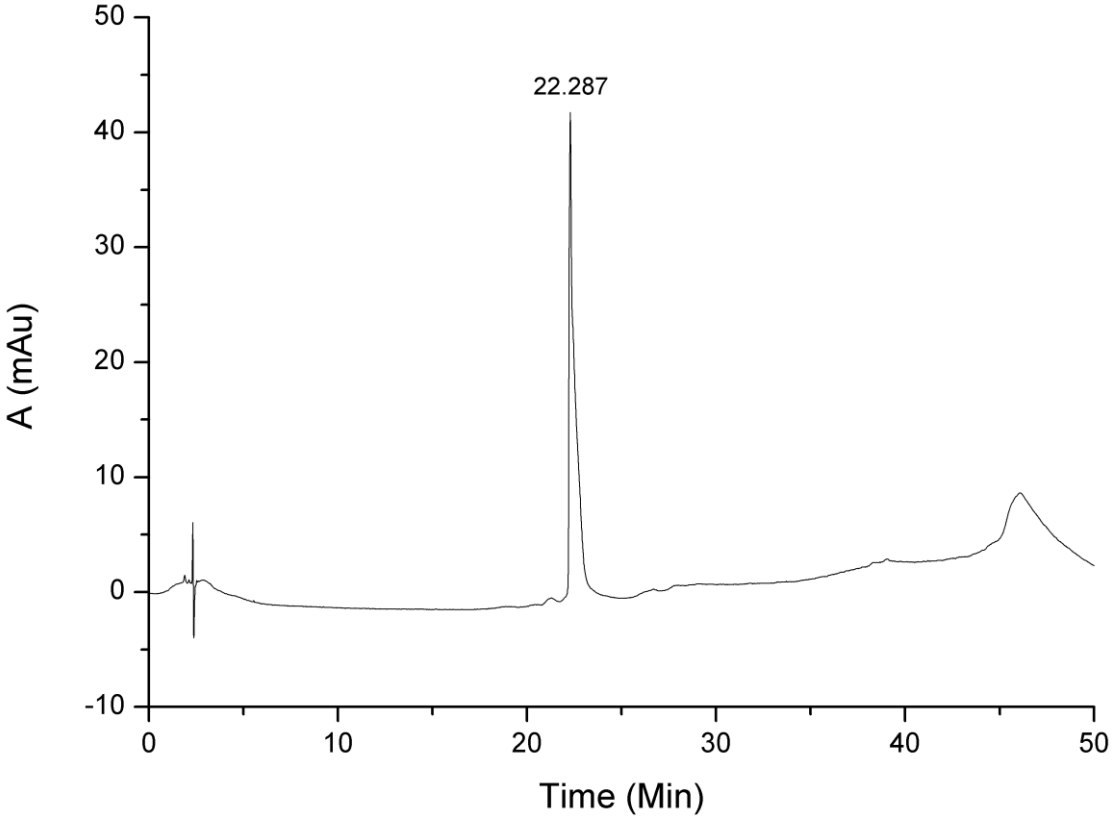

Figure S70: HPLC chromatogram of **11-H**$^{+}$·PF_6^{-}.

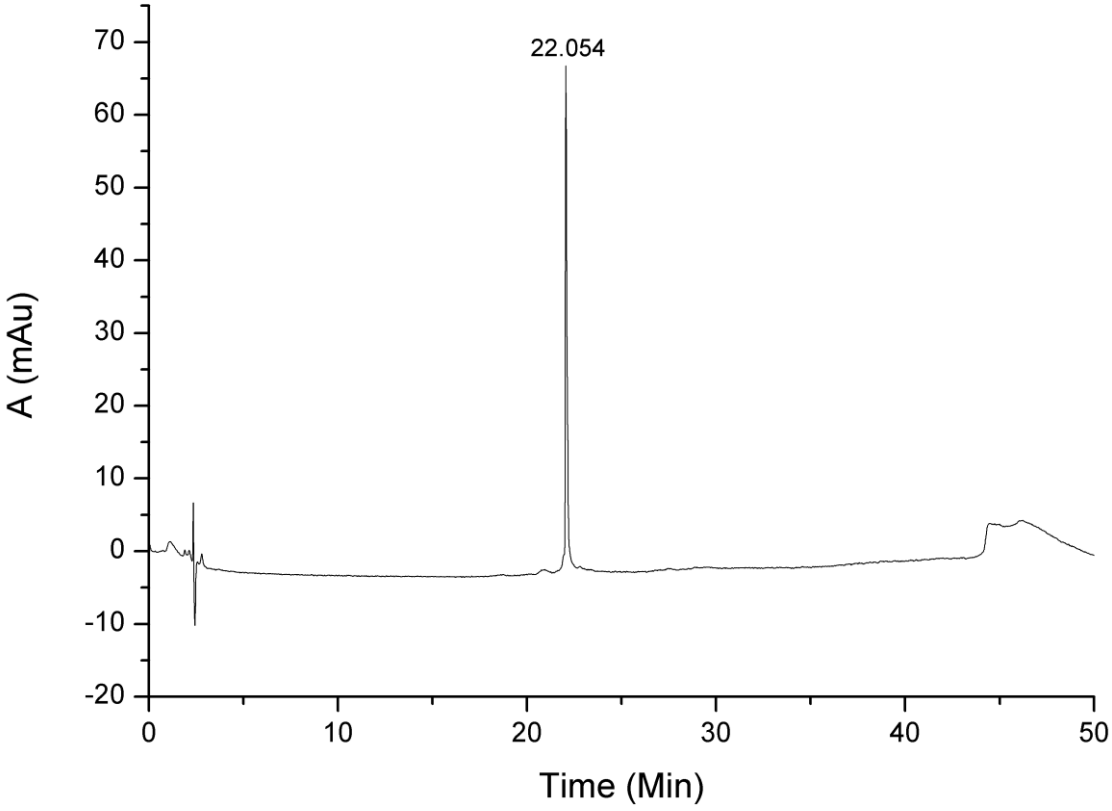

Figure S71: HPLC chromatogram of **14-H**$^{+}$·PF_6^{-}.

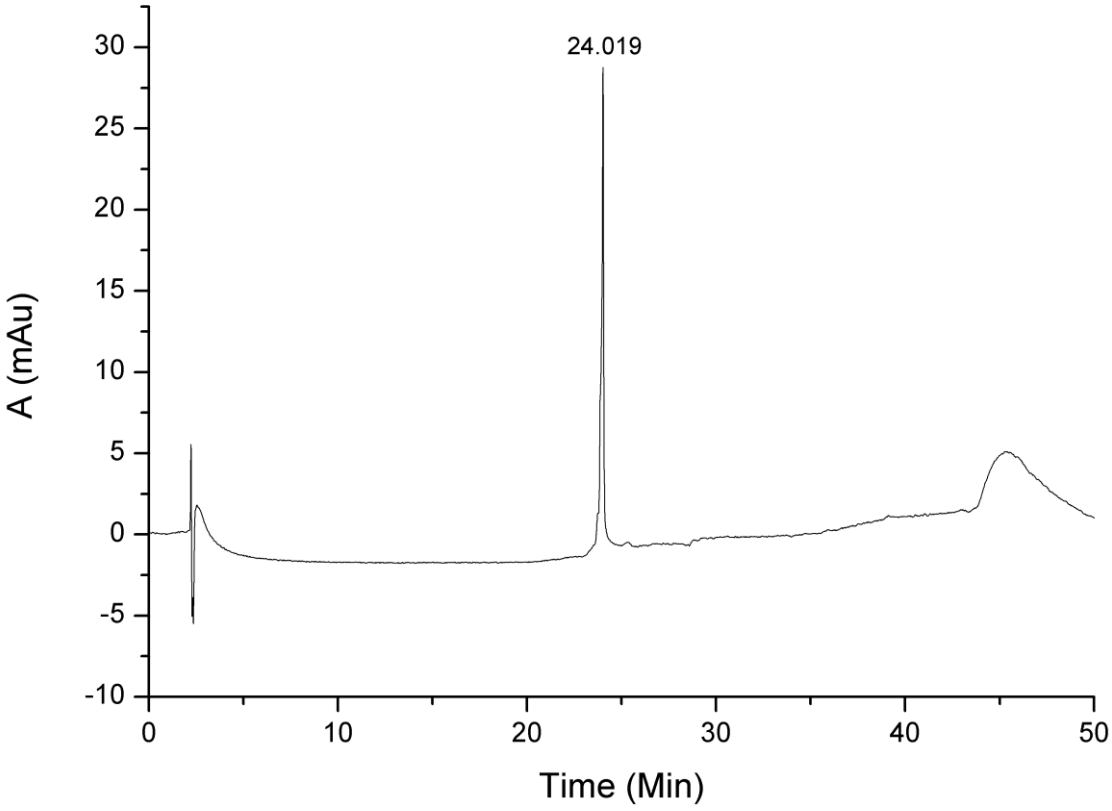

Figure S72: HPLC chromatogram of **2-H**$^{+}$·$2PF_6^{-}$.

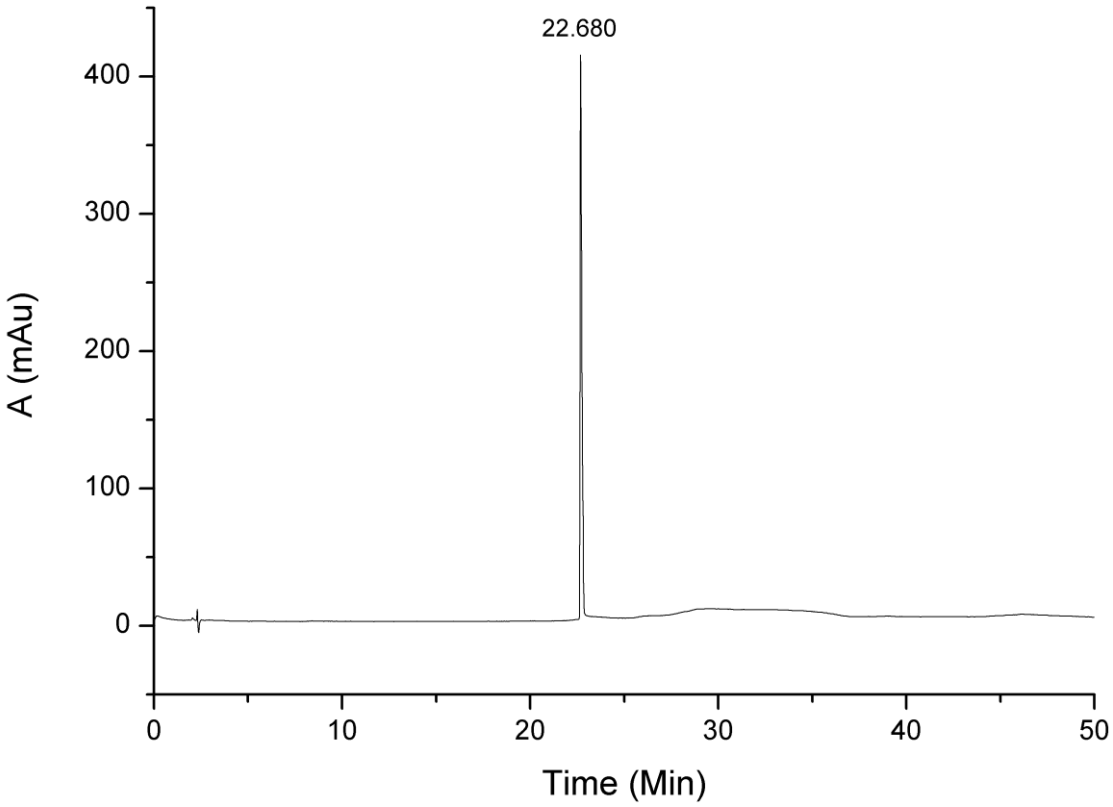

Figure S73: HPLC chromatogram of **13-H**$^{+}$·PF_6^{-}.

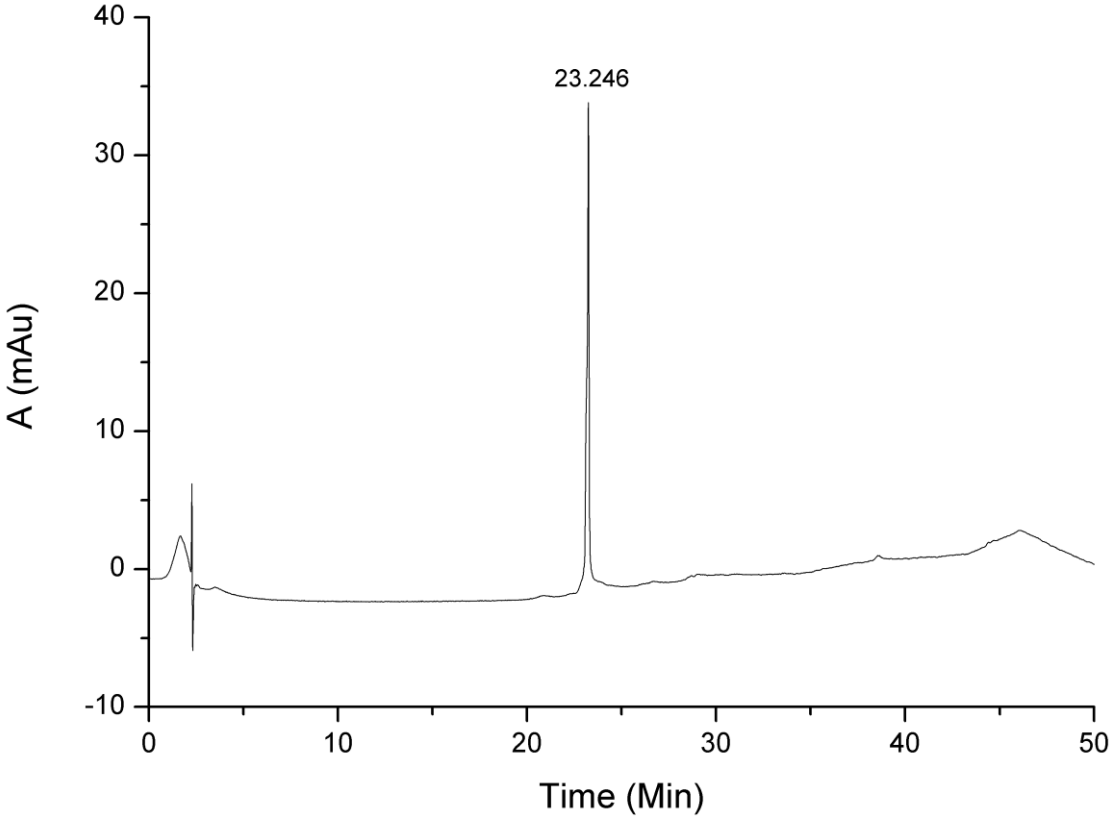

Figure S74: HPLC chromatogram of **1-H**$^{+}$·$2PF_6^{-}$.

6. Photophysical properties

UV-Vis absorption, fluorescence, electronic circular dichroism (ECD) and circularly polarized luminescence (CPL) spectra were recorded on an Olis DSM172 spectrophotometer equipped with a 150 W Xenon lamp. The spectra were recorded at *ca*. 1×10^{-5} M (for (*R*)/(*S*)-**1-H**$^+$·2PF$_6^-$, (*R*)/(*S*)-**1**·PF$_6^-$, **8** and (*R*)/(*S*)-**13-H**$^+$·PF$_6^-$,) and *ca*. 1×10^{-4} M (for (*R*)/(*S*)-**2-H**$^+$·2PF$_6^-$, (*R*)/(*S*)-**14-H**$^+$·PF$_6^-$ and the partial UV-Vis and ECD spectra of (*R*)/(*S*)-**1-H**$^+$·2PF$_6^-$ and (*R*)/(*S*)-**13-H**$^+$·PF$_6^-$) in HPLC grade $CHCl_3$ at 20 ºC. For absorbance and fluorescence measurements, a fixed slit-width of 1 mm and 0.5 s of integration time were selected. For ECD measurements, a fixed slit-width of 1.000 mm and 0.5 s of integration time were selected. The ECD spectra shown correspond each one to an average spectrum of 30 scans. For CPL measurements, a fixed slit-width of 3.000 mm, a fixed excitation wavelength of 355 nm and 1.0 s of integration time were selected. Each CPL spectra correspond to an average spectrum calculated after 200 scans. UV-Vis absorption, fluorescence, ECD and CPL spectra of (*R*)/(*S*)-**1-H**$^+$·2PF$_6^-$, (*R*)/(*S*)-**1**·PF$_6^-$, (*R*)/(*S*)-**1-H**$^+$ (from the protonation of (*R*)/(*S*)-**1**·PF$_6^-$) and the switching experiments were carried out under Ar with degassed solvent.

Quantum yields were determined by measuring both absorbance and fluorescence of compounds **1-H**$^+$·2PF$_6^-$, **1**·PF$_6^-$, **1-H**$^+$ (from the protonation of **1**·PF$_6^-$), **8**, **13-H**$^+$·PF$_6^-$ in $CHCl_3$, using anthracene in EtOH as standard (Φ_r = 0.27).[S12] For the relative determination of the fluorescence quantum yield Φ in a series of solvents, eq. 1 was used.[S13, S14]

$$\Phi_x = \Phi_r \times \frac{F_x}{F_r} \times \frac{1-10^{-A_r(\lambda_{ex})}}{1-10^{-A_x(\lambda_{ex})}} \times \frac{n_x^2}{n_r^2} \quad \text{(Eq. 1)}$$

The subscripts *x* and *r* refer respectively to the sample and a reference (standard) fluorophore with known quantum yield Φ_r in a specific solvent; *F* stands for the spectrally corrected, integrated fluorescence spectra; $A(\lambda_{ex})$ denotes the absorbance at the used excitation wavelength λ_{ex}; and *n* represents the refractive index of the solvent (in principle at the average emission wavelength). To minimize inner filter effects, the absorbance at the excitation wavelength λ_{ex} was kept under 0.3. The measurements were performed using 10×10 mm cuvettes on non-degassed samples for **8** and **13-H**$^+$·PF$_6^-$ and on degassed samples for **1-H**$^+$·2PF$_6^-$, **1**·PF$_6^-$ and **1-H**$^+$ (from the protonation of **1**·PF$_6^-$).

Table S2: Quantum yields of rotaxanes and macrocycle.

Compound	Φ
1-H$^+$·2PF$_6^-$	0.11
1·PF$_6^-$	0.11
1-H$^+$ (from the protonation of **1**·PF$_6^-$)	0.11
8	0.18
13-H$^+$·PF$_6^-$	0.19

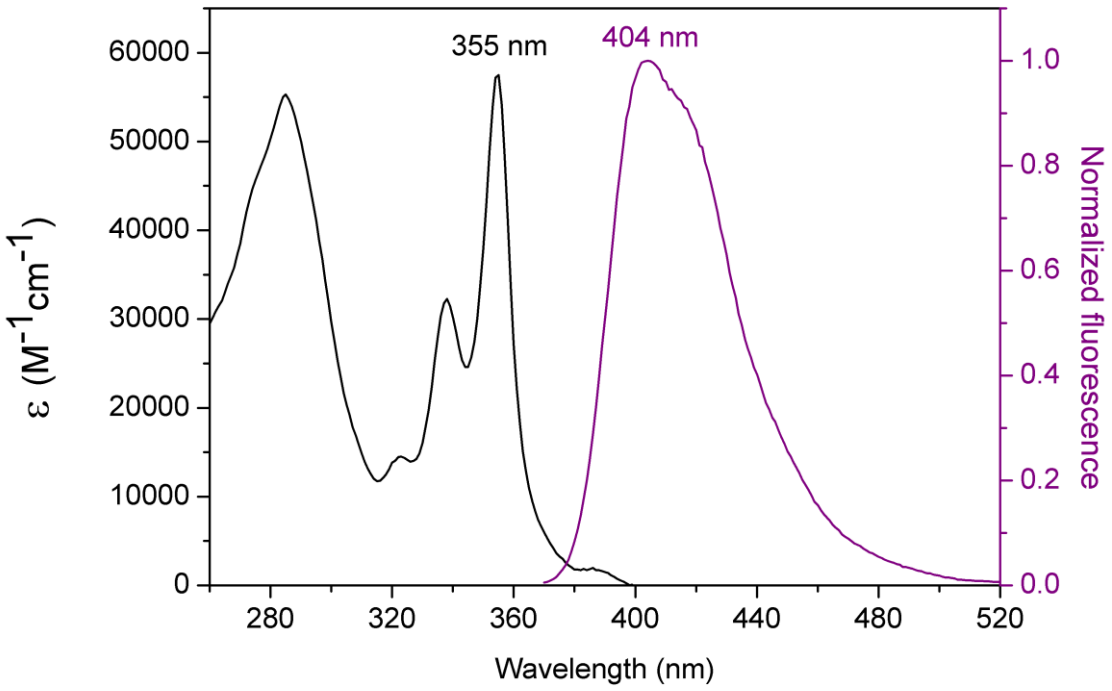

Figure S75: UV-Vis absorption (black line) and emission (purple line, λ_{exc} = 355 nm) spectra of macrocycle **8**.

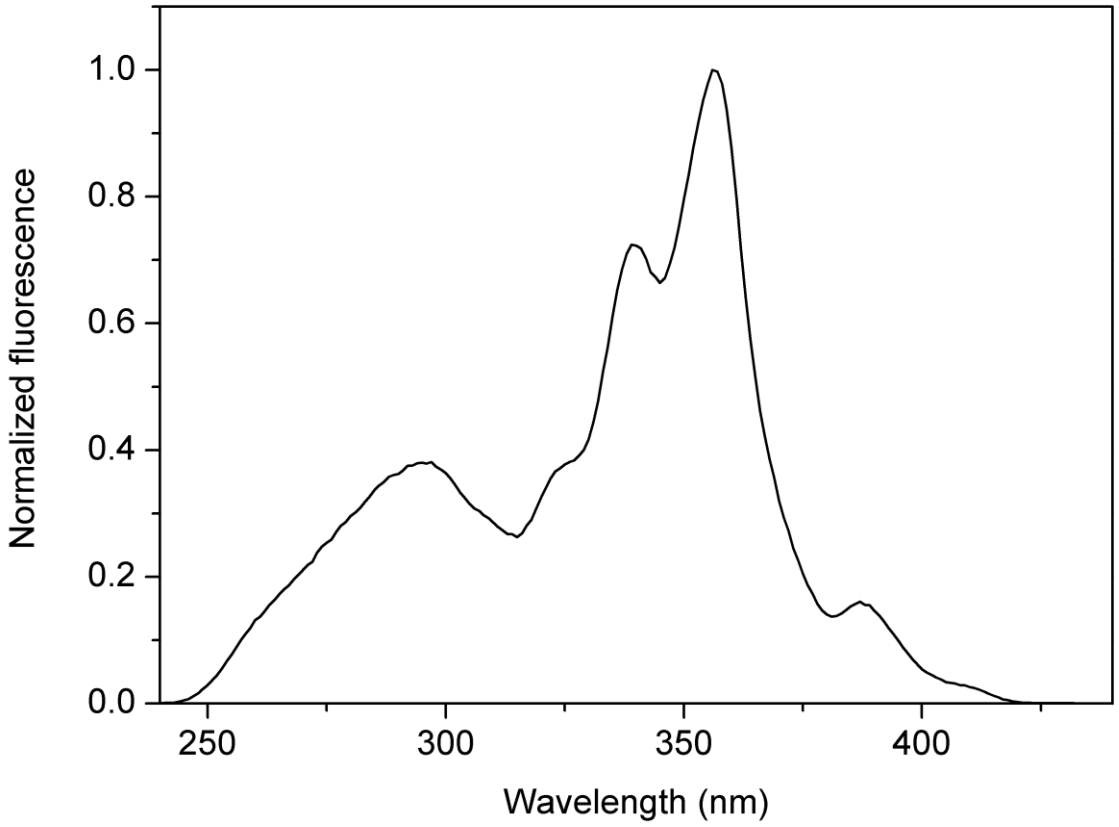

Figure S76: Excitation spectrum (λ_{emi} = 404 nm) of macrocycle **8**.

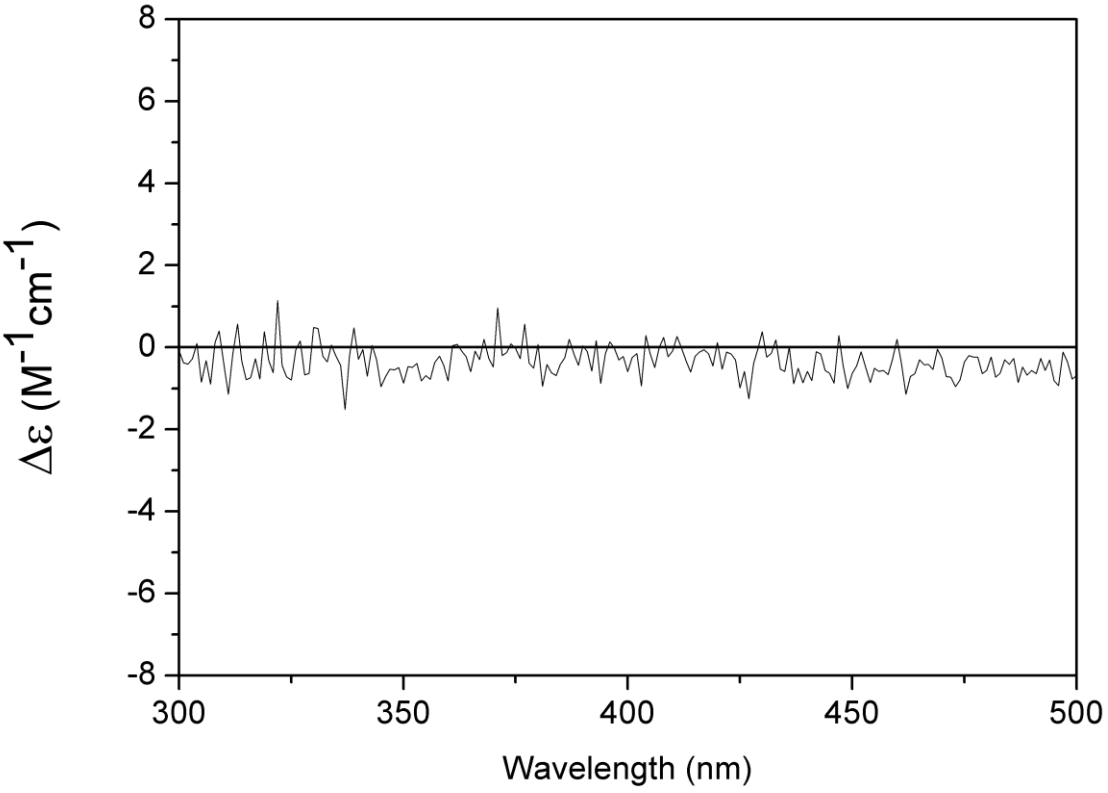

Figure S77: ECD spectrum of macrocycle **8** showing the absence of response.

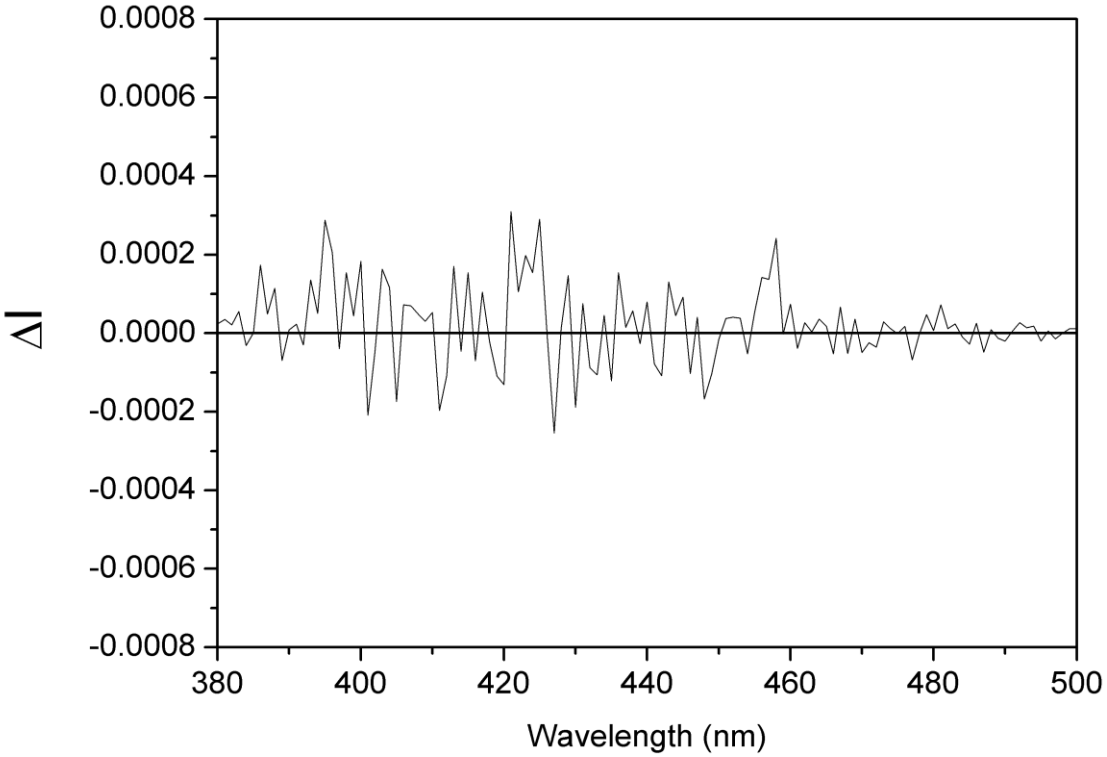

Figure S78: CPL (λ_{exc} = 355 nm) spectrum of macrocycle **8** demonstrating the absence of response.

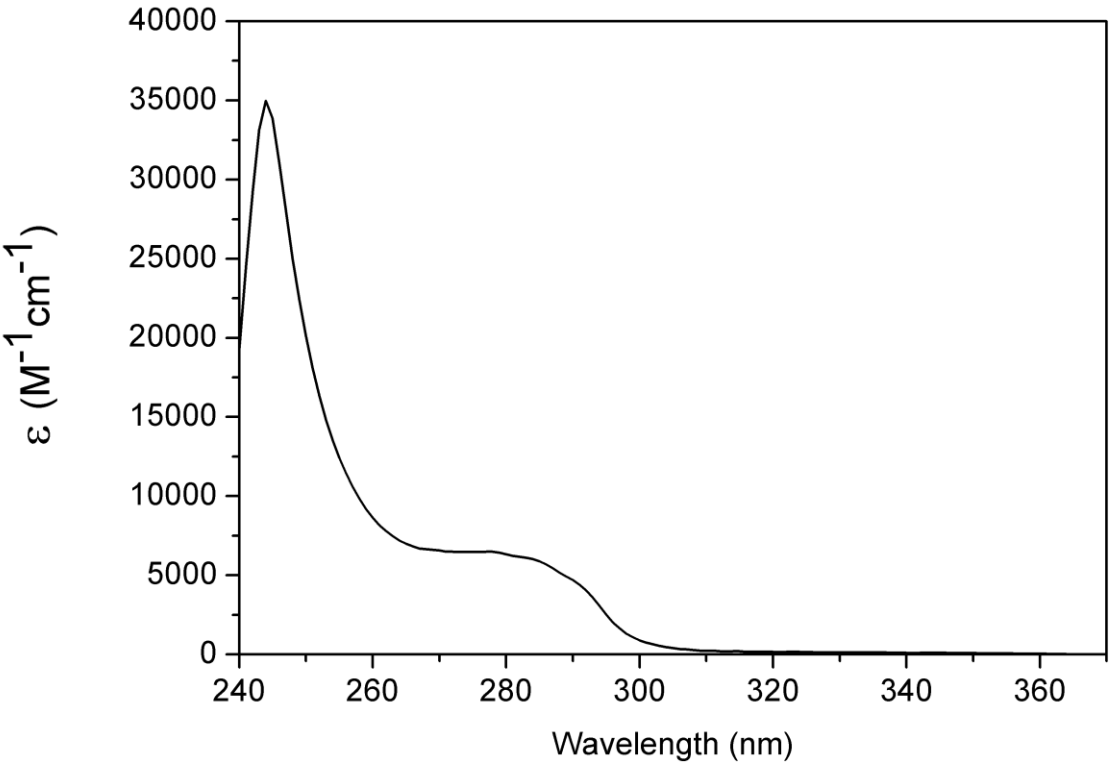

Figure S79: UV-Vis absorption spectrum of thread **14-H**$^{+}$·PF_6^{-}.

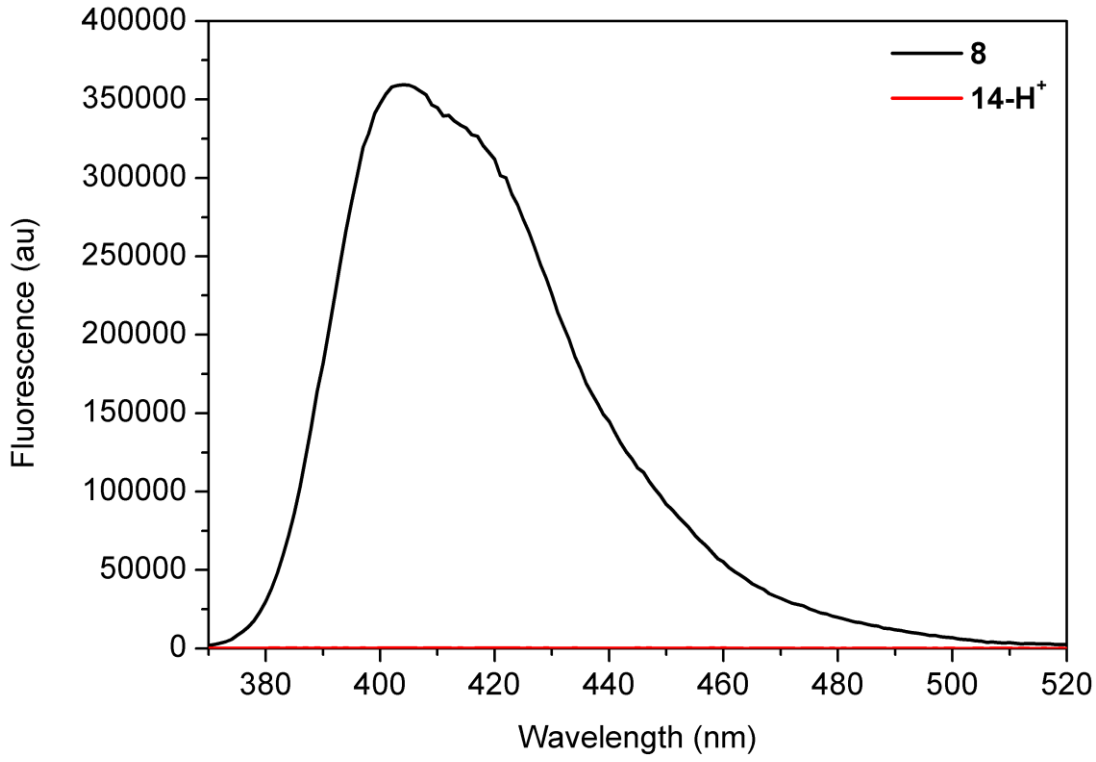

Figure S80: Emission (λ_{exc} = 355 nm) spectra of macrocycle **8** and thread **14-H**$^{+}$·PF_6^{-} showing no fluorescence response for the thread.

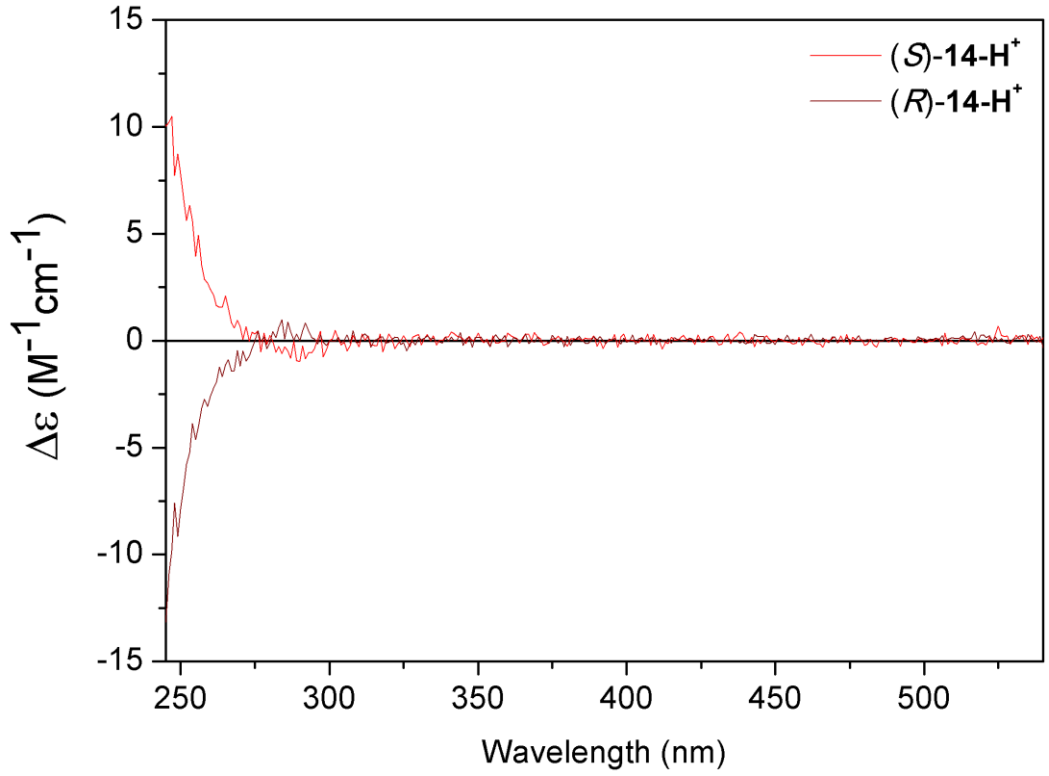

Figure S81: ECD spectra of threads (*R*)/(*S*)-**14-H**$^{+}$·PF_6^{-}.

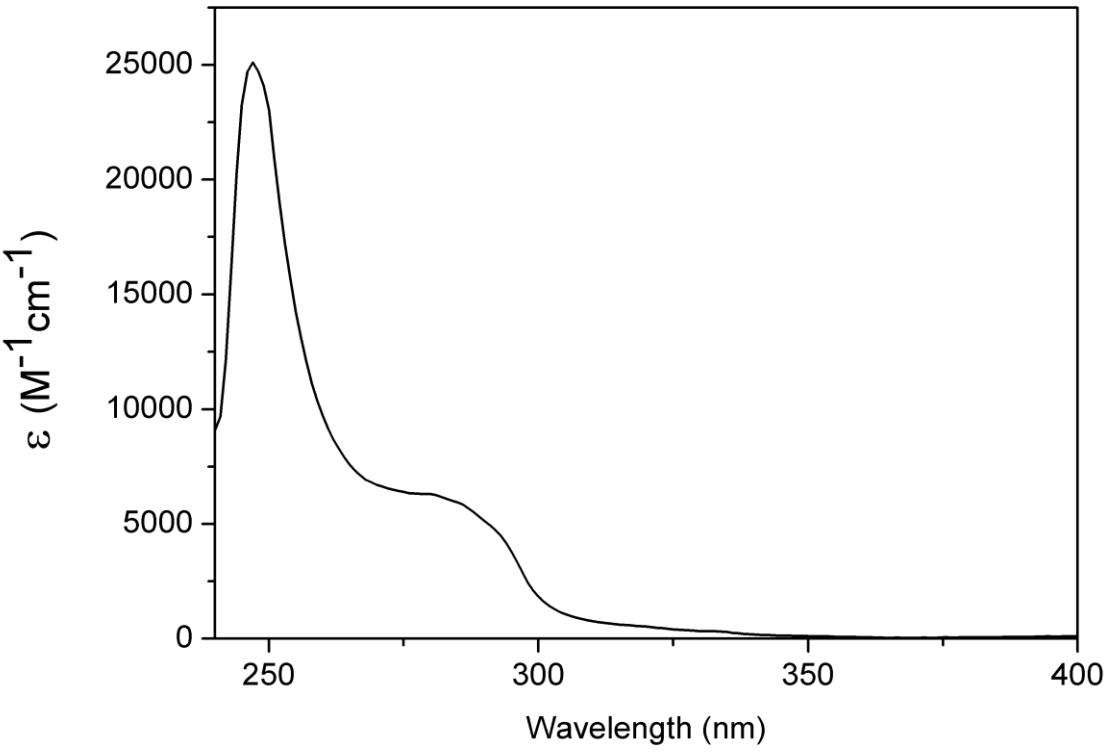

Figure S82: UV-Vis absorption spectrum of thread **2-H**$^{+}$·$2PF_6^{-}$.

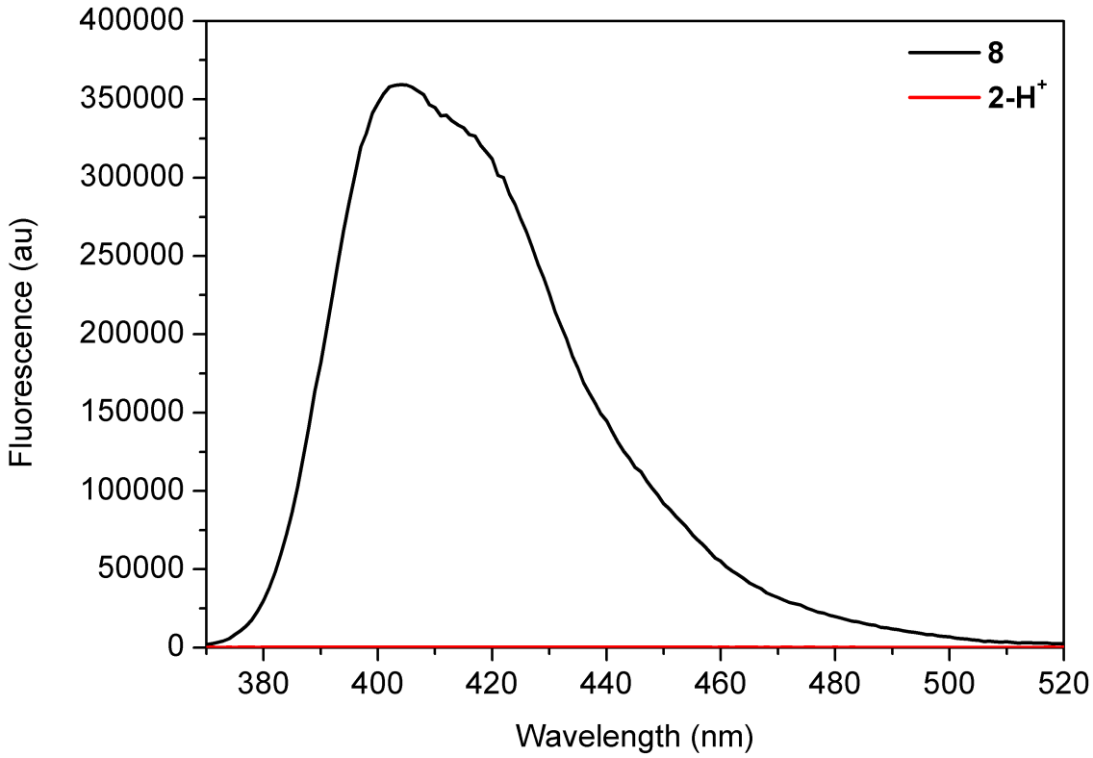

Figure S83: Emission (λ_{exc} = 355 nm) spectra of macrocycle **8** and thread **2-H**$^{+}$·2PF$_6^-$ showing no fluorescence response for the thread.

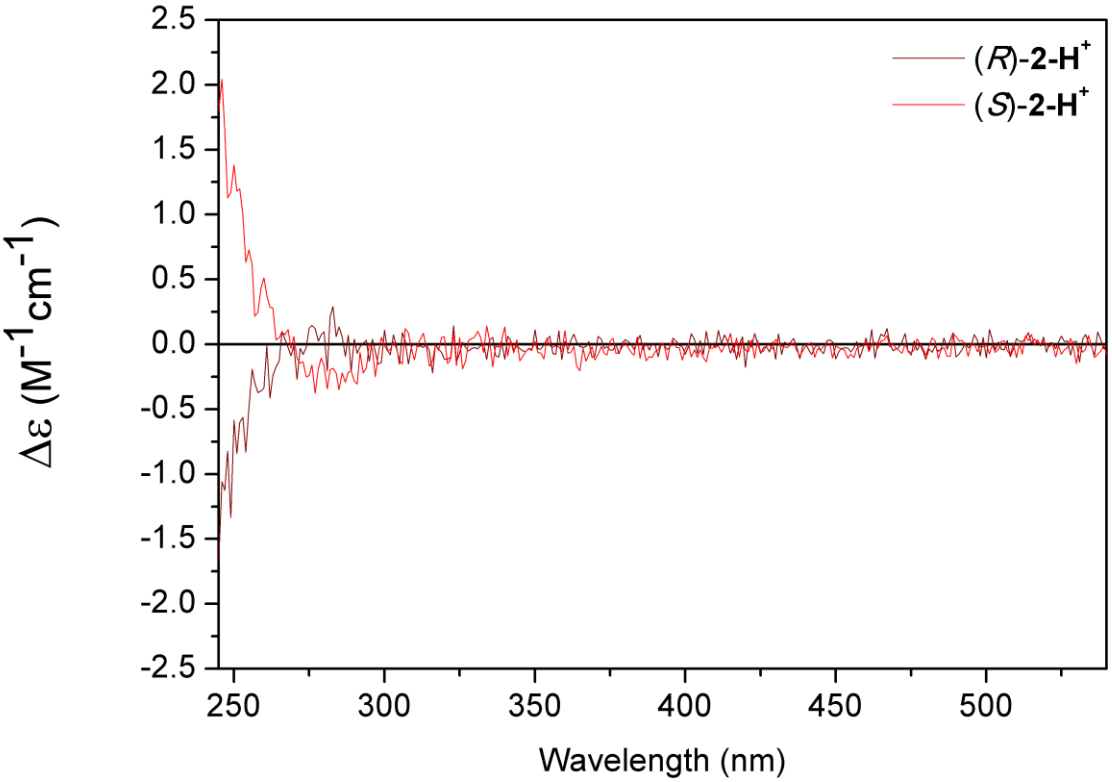

Figure S84: ECD spectra of threads (*R*)/(*S*)-**2-H**$^{+}$·2PF$_6^-$.

Since (*R*)/(*S*)-**2-H**$^{+}$·2PF$_6^-$ and (*R*)/(*S*)-**14-H**$^{+}$·PF$_6^-$ were not found to be fluorescent, no CPL was recorded.

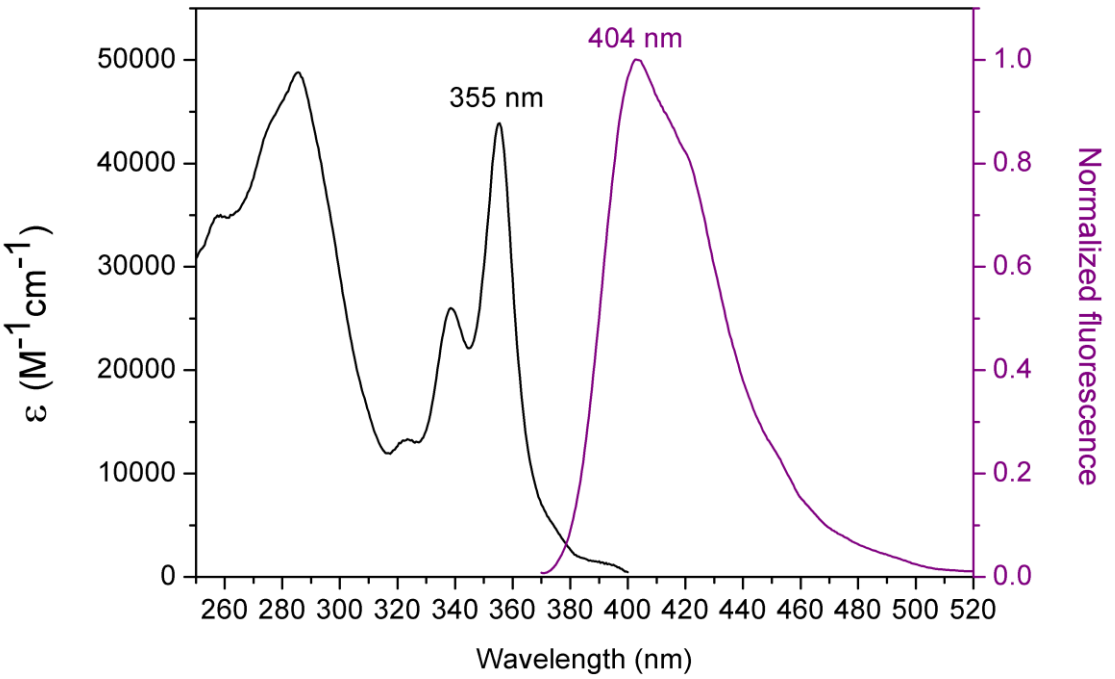

Figure S85: UV-Vis absorption (black line) and emission (purple line, λ_{exc} = 355 nm) spectra of rotaxane **13-H**$^{+}\cdot PF_6^{-}$.

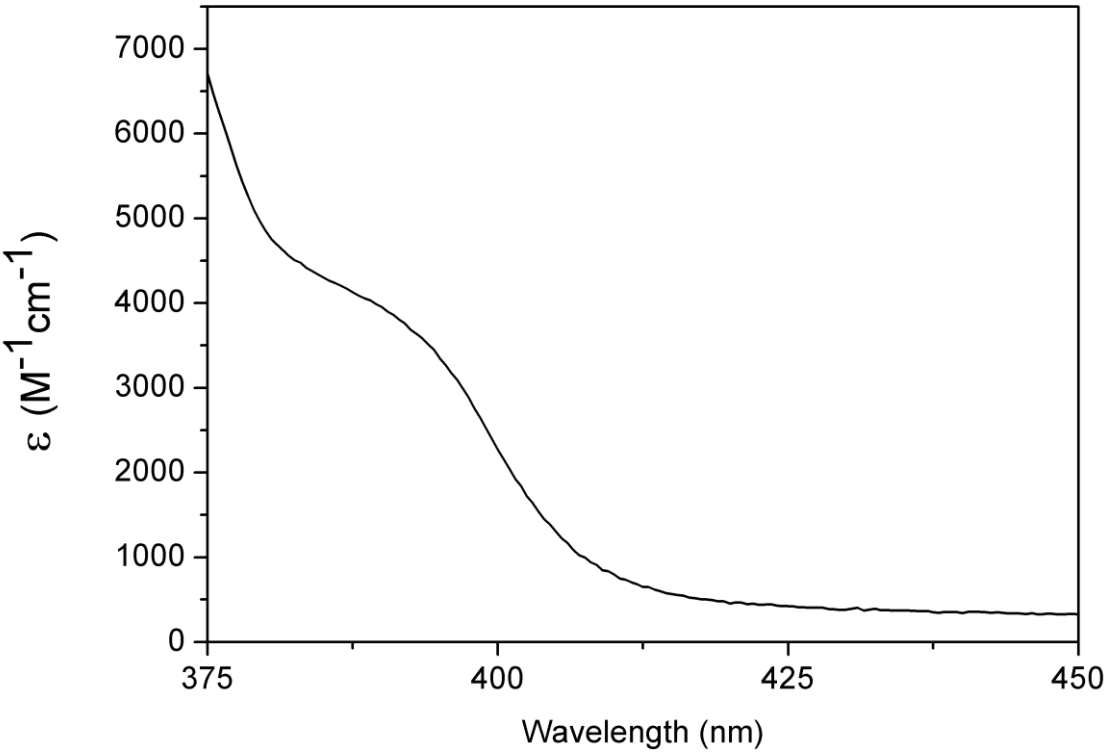

Figure S86: Partial UV-Vis absorption spectrum of rotaxane **13-H**$^{+}\cdot PF_6^{-}$.

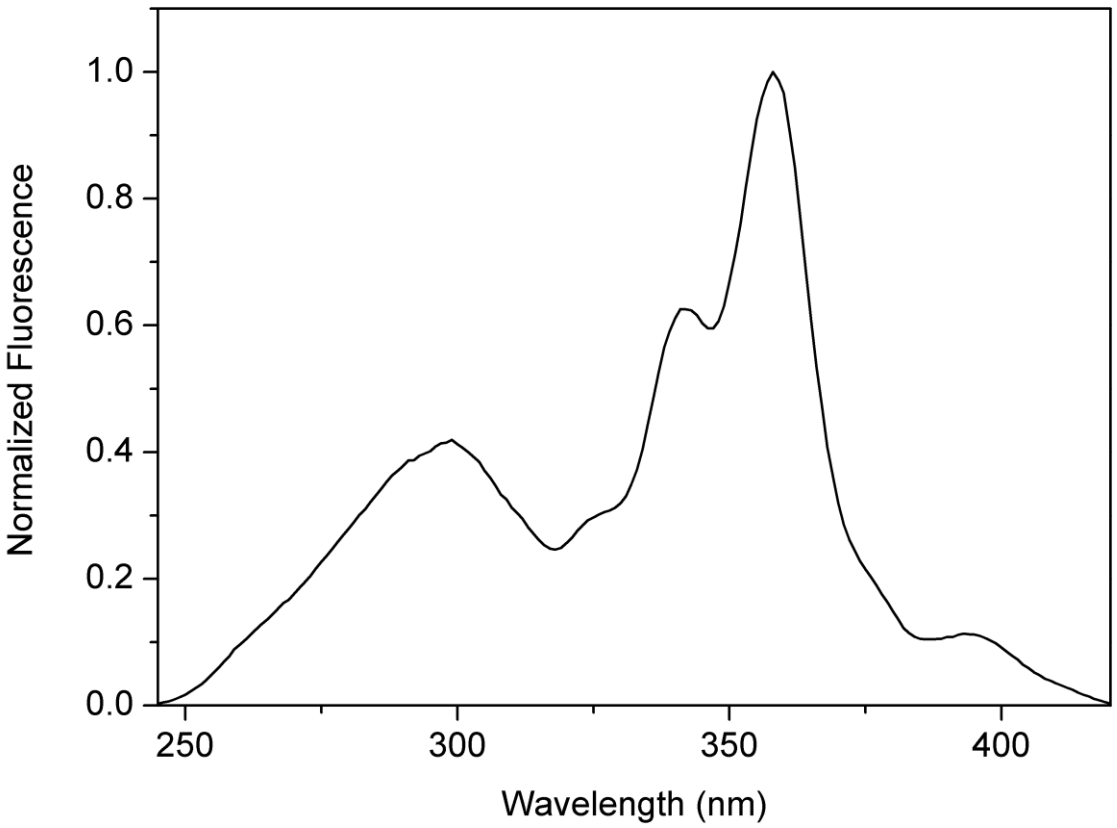

Figure S87: Excitation spectrum (λ_{emi} = 403 nm) of rotaxane **13-H**$^{+}$·PF_6^{-}.

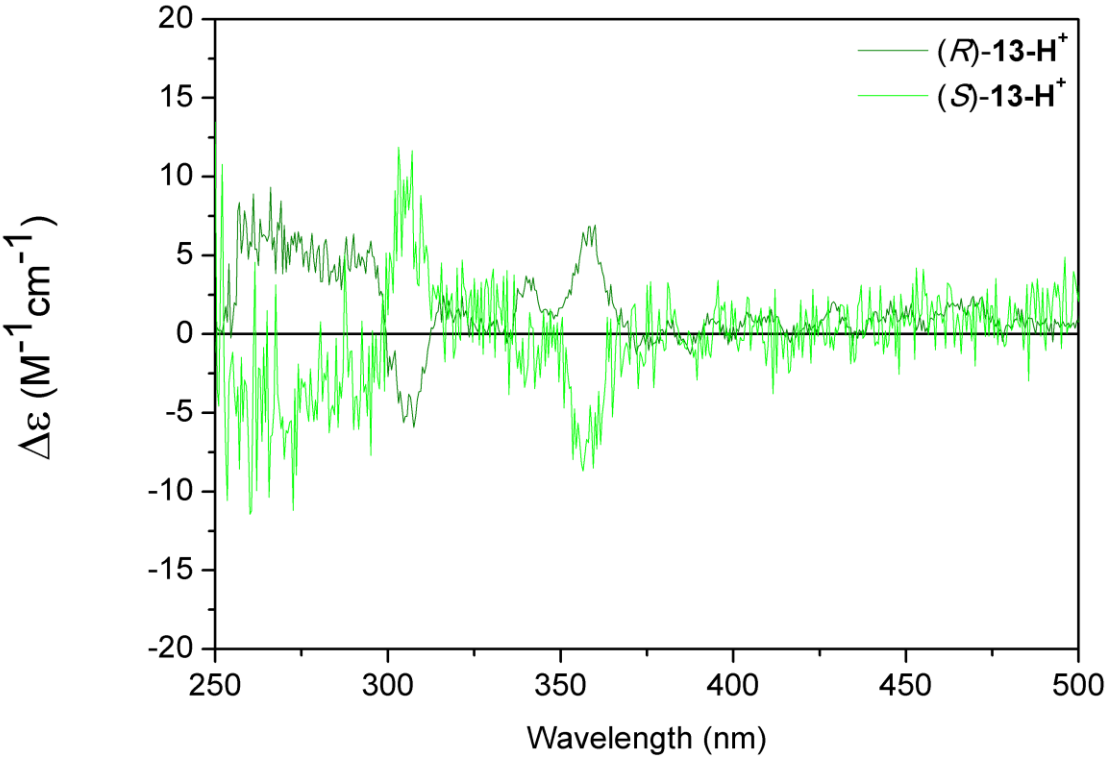

Figure S88: ECD spectra of rotaxane (*R*)/(*S*)-**13-H**$^{+}$·PF_6^{-}.

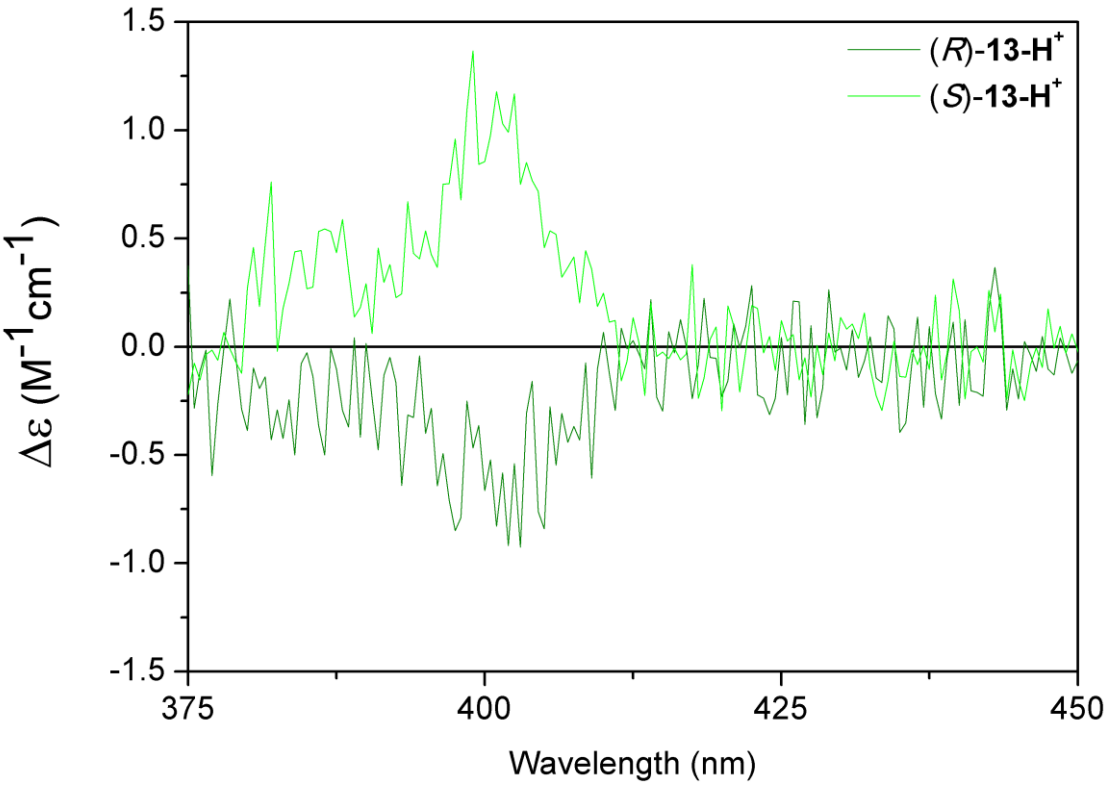

Figure S89: Partial ECD spectra of rotaxane (*R*)/(*S*)-**13-H**$^{+}$·PF_6^-.

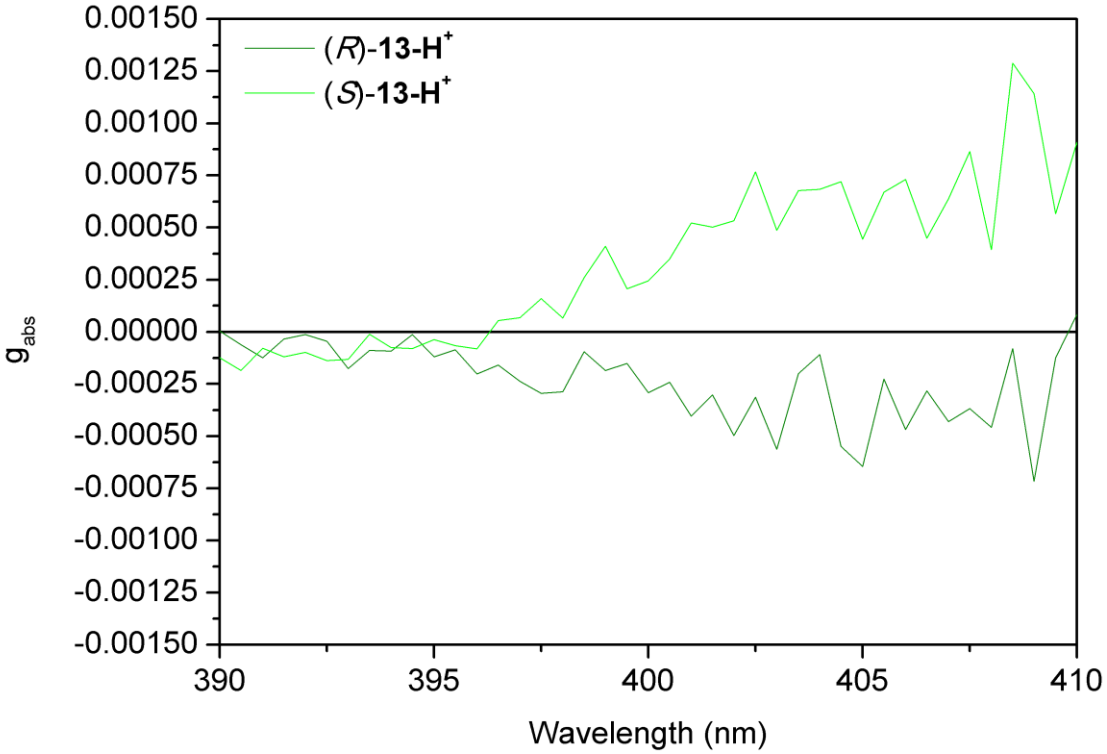

Figure S90: Partial g_{abs} spectra of rotaxane (*R*)/(*S*)-**13-H**$^{+}$·PF_6^- ($g_{abs} = 5 \times 10^{-4}$).

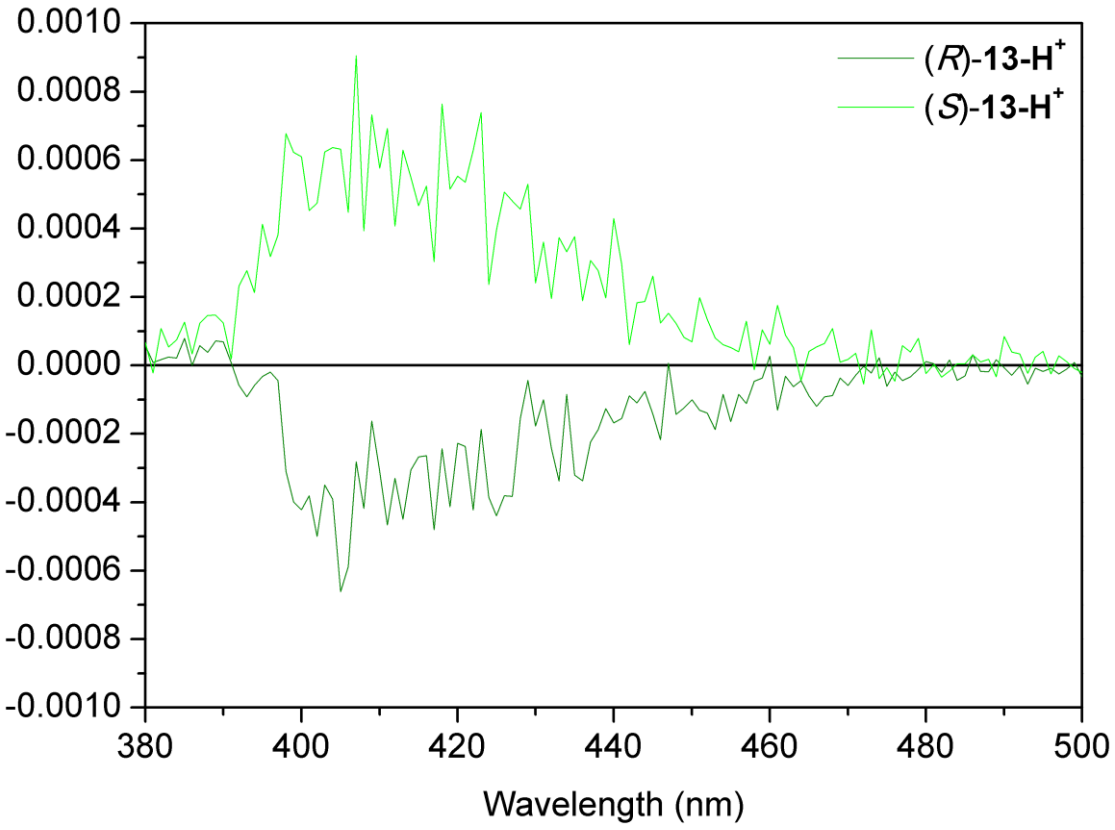

Figure S91: CPL (λ_{exc} = 355 nm) spectra of rotaxane (*R*)/(*S*)-**13-H**$^{+}$·PF_6^-.

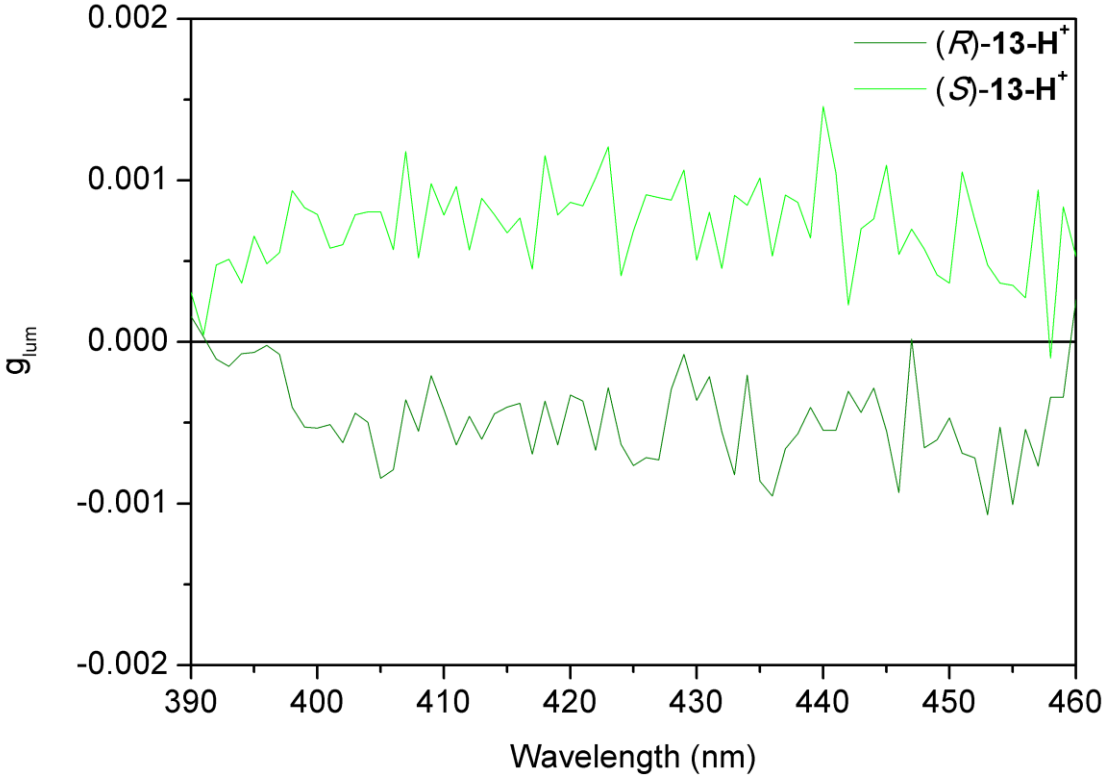

Figure S92: g_{lum} (λ_{exc} = 355 nm) spectra of rotaxane (*R*)/(*S*)-**13-H**$^{+}$·PF_6^- ($g_{lum} = 5 \times 10^{-4}$).

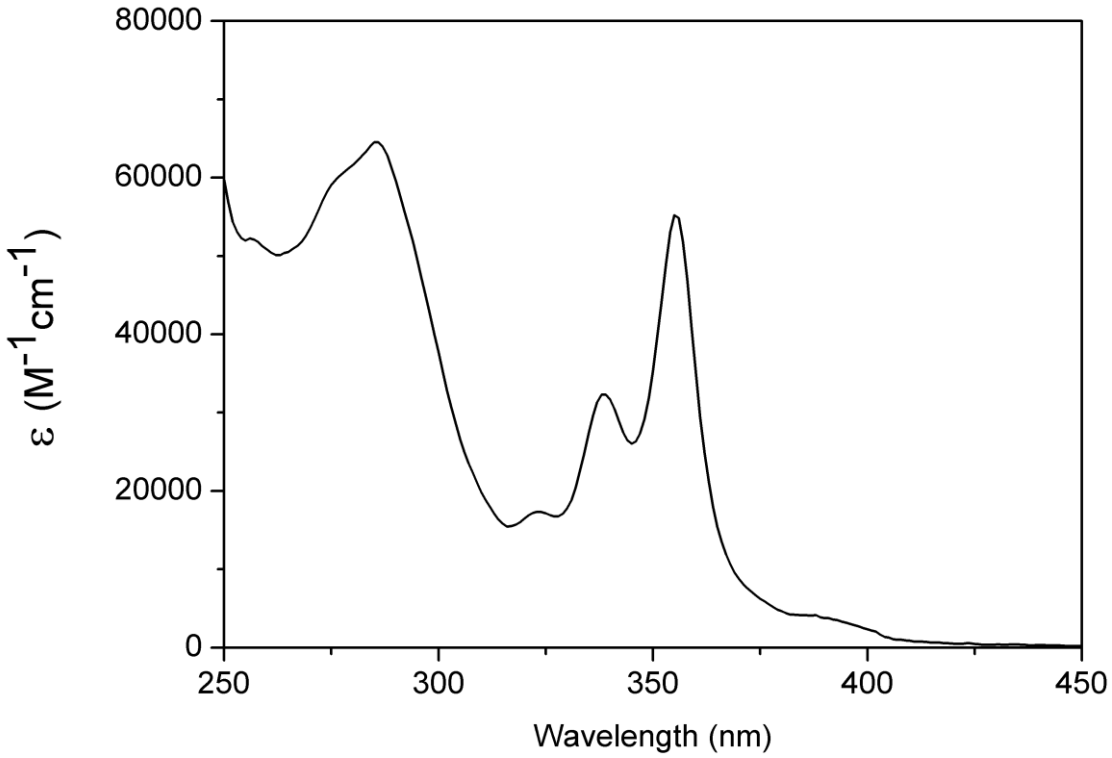

Figure S93: UV-Vis absorption spectrum of rotaxane **1-H**$^{+}$·2PF_6^-.

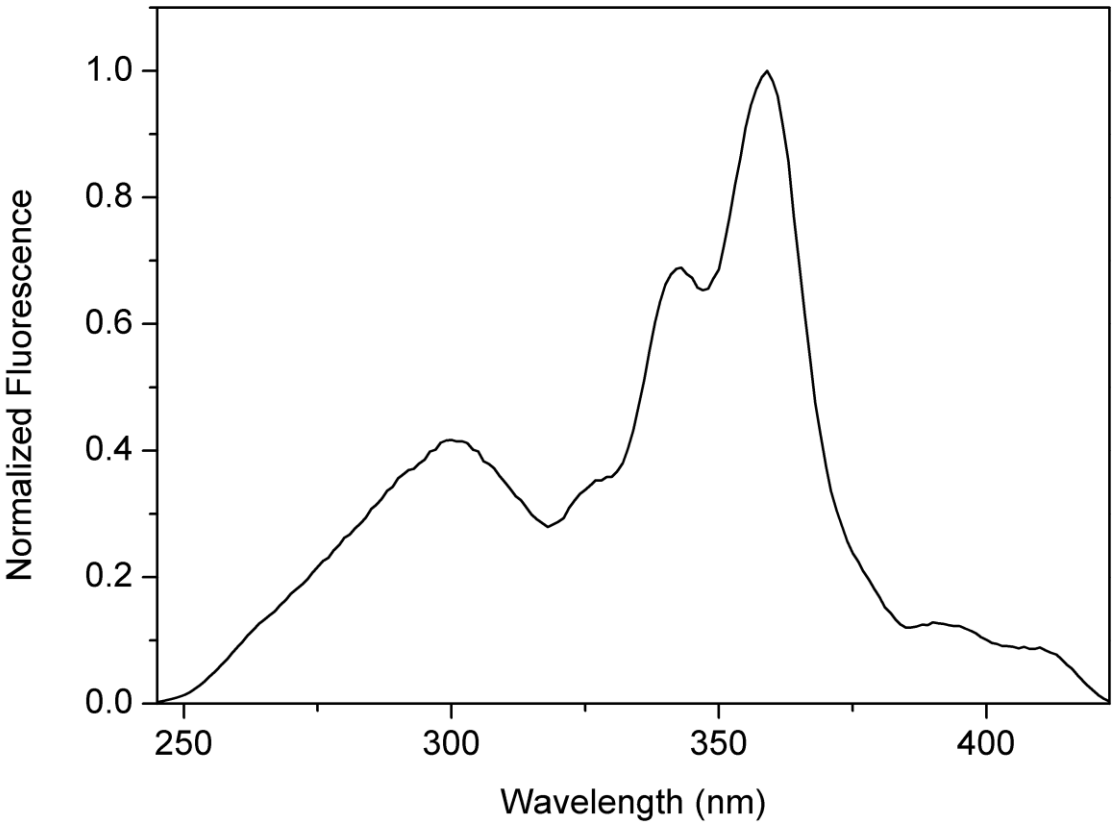

Figure S94: Excitation spectrum (λ_{emi} = 404 nm) of rotaxane **1-H**$^{+}$·2PF_6^-.

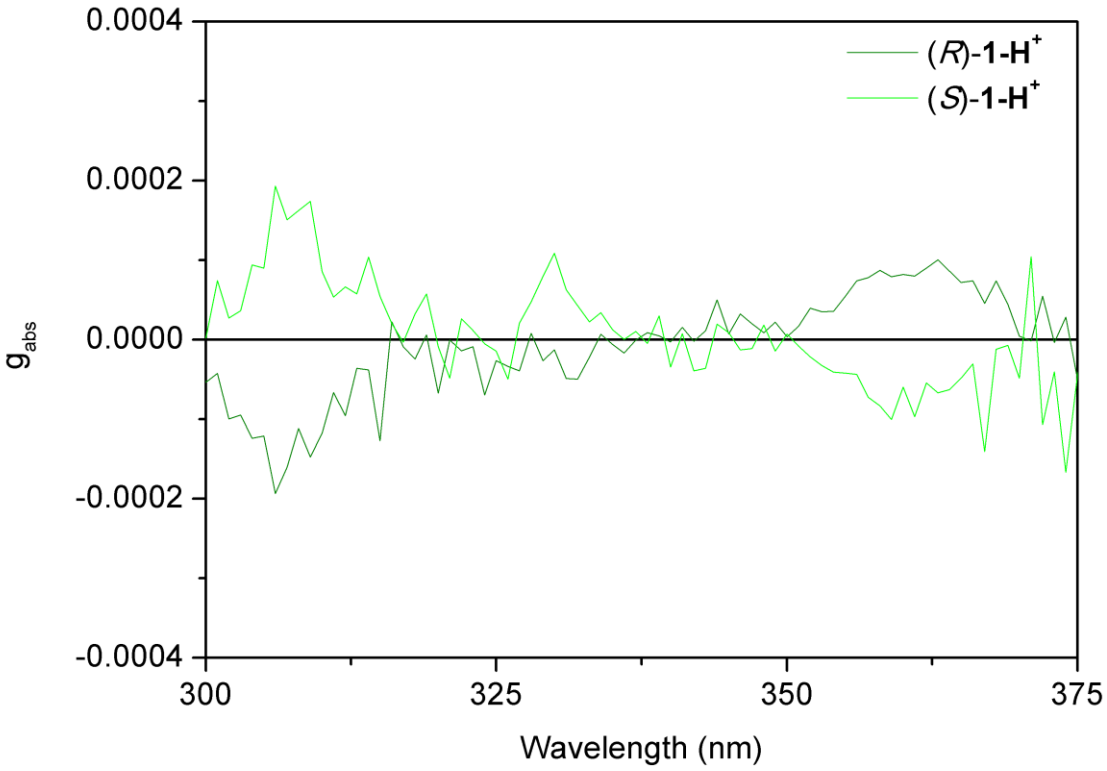

Figure S95: g_{abs} spectra of rotaxane (*R*)/(*S*)-**1**-$H^+ \cdot 2PF_6^-$.

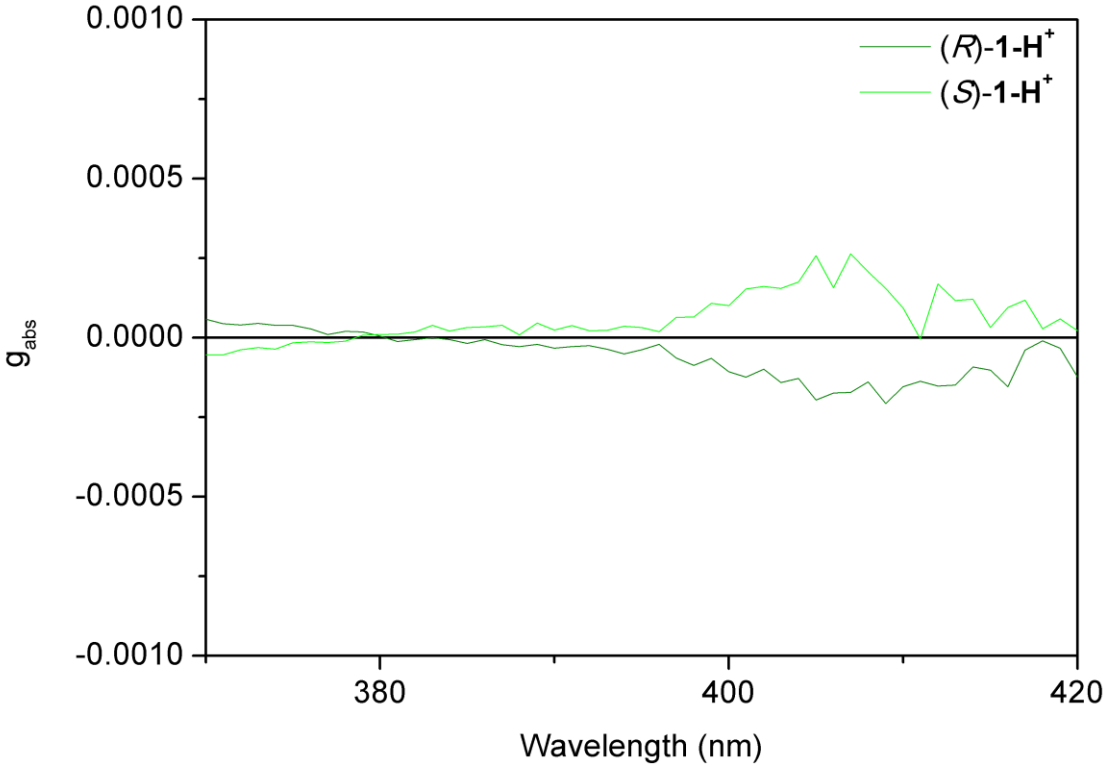

Figure S96: Partial g_{abs} spectra of rotaxane (*R*)/(*S*)-**1**-$H^+ \cdot 2PF_6^-$ ($g_{abs} = 3 \times 10^{-4}$).

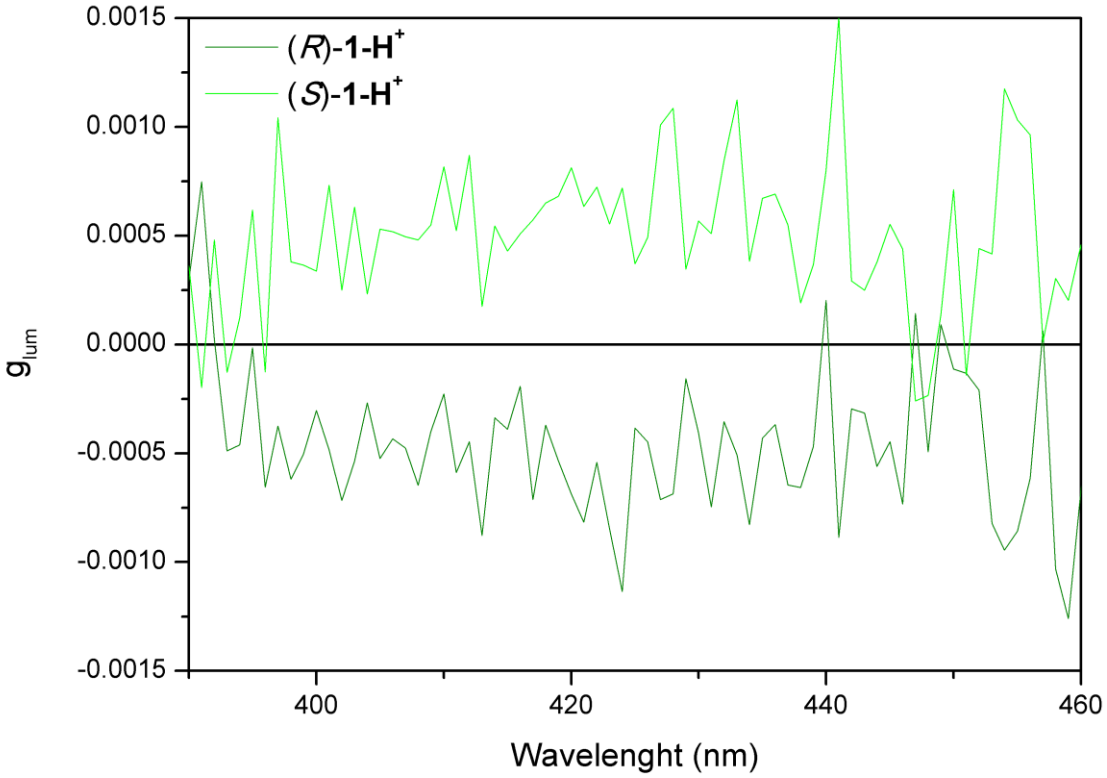

Figure S97: g_{lum} (λ_{exc} = 355 nm) spectra of rotaxane (*R*)/(*S*)-**1**-$H^+ \cdot 2PF_6^-$ ($g_{lum} = 5 \times 10^{-4}$).

Switching experiments:

To obtain (*S*)-**1**$\cdot PF_6^-$ for photophysical measurements: Under an Ar atmosphere, an excess of K_2CO_3 was added to a solution of (*S*)-**1**-$H^+ \cdot 2PF_6^-$ in $CHCl_3$ (1.2×10^{-5} mol L^{-1}, 2.5 mL). The suspension was shaken for 2 min and subsequently filtered through a 0.2 μm filter to remove the excess of base.

(*R*)-**1**$\cdot PF_6^-$ was obtained following the same procedure starting from (*R*)-**1**-$H^+ \cdot 2PF_6^-$.

To obtain (*S*)-**1**-H^+ for photophysical measurements: Under inert atmosphere, to a solution of (*S*)-**1**$\cdot PF_6^-$ in $CHCl_3$ (1.2×10^{-5} mol L^{-1}, 2.5 mL) was added a degassed solution of CF_3CO_2H in $CHCl_3$ (0.2 %, 17.3 μL, 15 equiv.). The resulting solution was shaken for 1 min.

(*R*)-**1**-H^+ was obtained following the same procedure starting from (*R*)-**1**$\cdot PF_6^-$.

The *in situ* switching was carried out by repeatedly following the procedures described above on the same sample.

Election of the base for the switching experiments:

For the switching mechanism we also tried other bases such as NaOH, a phosphazene-bound base (BEMP resin), Et_3N and DBU in addition to the chosen K_2CO_3. The use of NaOH or the phosphazene resin resulted in the decomposition of the system. Therefore, these bases were discarded. To deprotonate the system with Et_3N, 50 equivalents were required as monitored by CD measurements, thus generating a large amount of salts upon reprotonation. As a result, the "on" state that did not show a better CPL response than that observed when using K_2CO_3. Finally, although DBU and K_2CO_3 gave very similar results, we chose K_2CO_3 as it resulted more convenient. K_2CO_3 is solid and it has very poor solubility in CH_3Cl so it can be used in excess as this surplus can be easily removed by filtration, has no effects on the concentration of the solution and the control of the stoichiometry added was less critical.

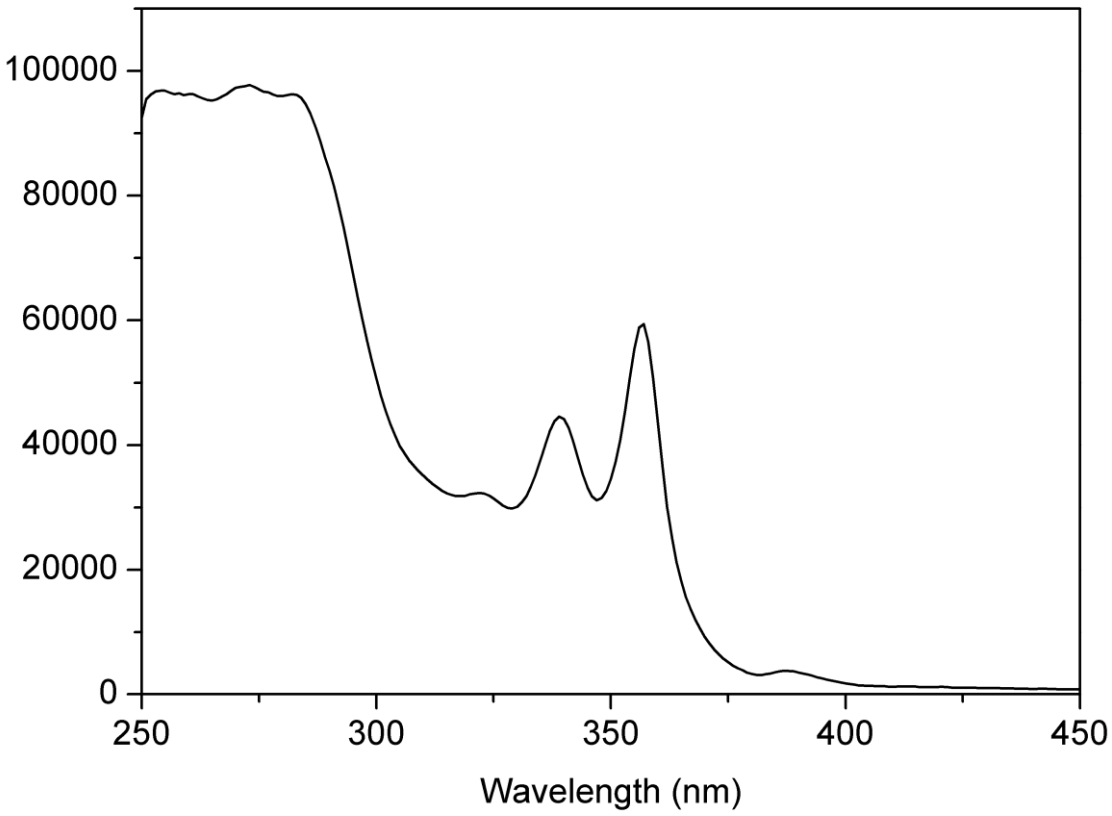

Figure S98: UV-Vis absorption spectrum of rotaxane **1**·PF_6^-.

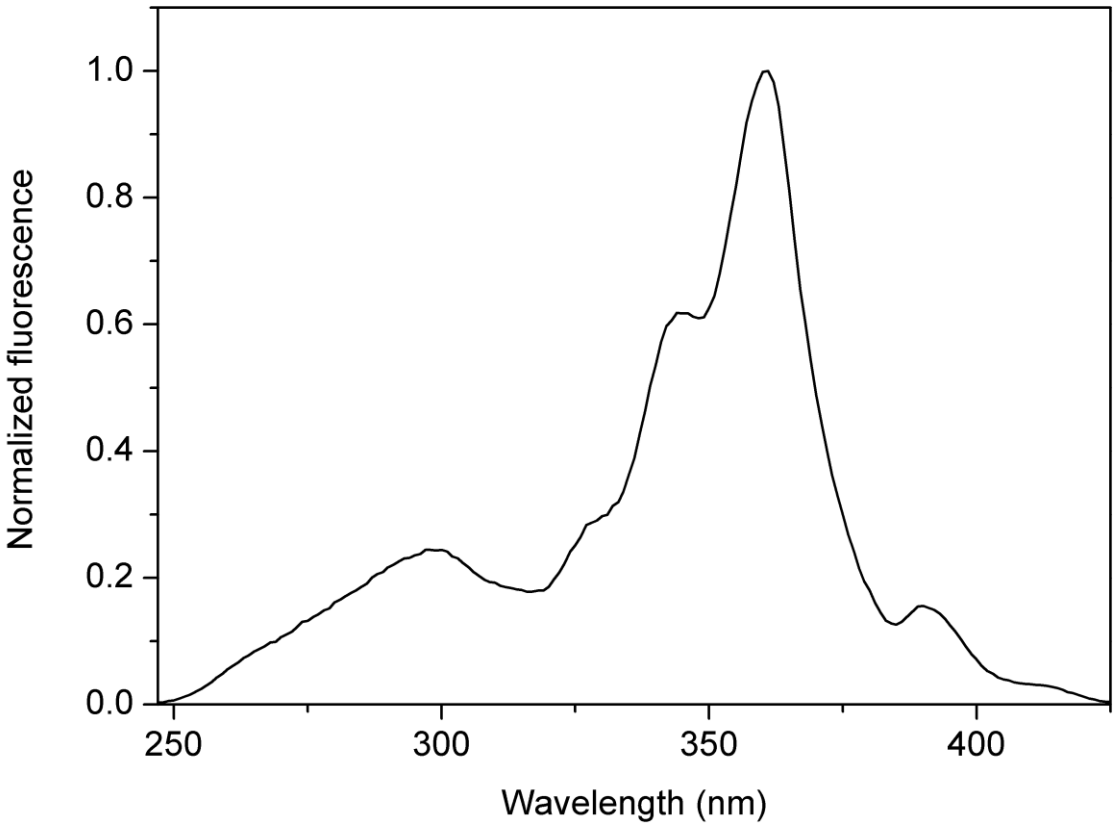

Figure S99: Excitation spectrum (λ_{em} = 404 nm) of rotaxane **1**·PF_6^-.

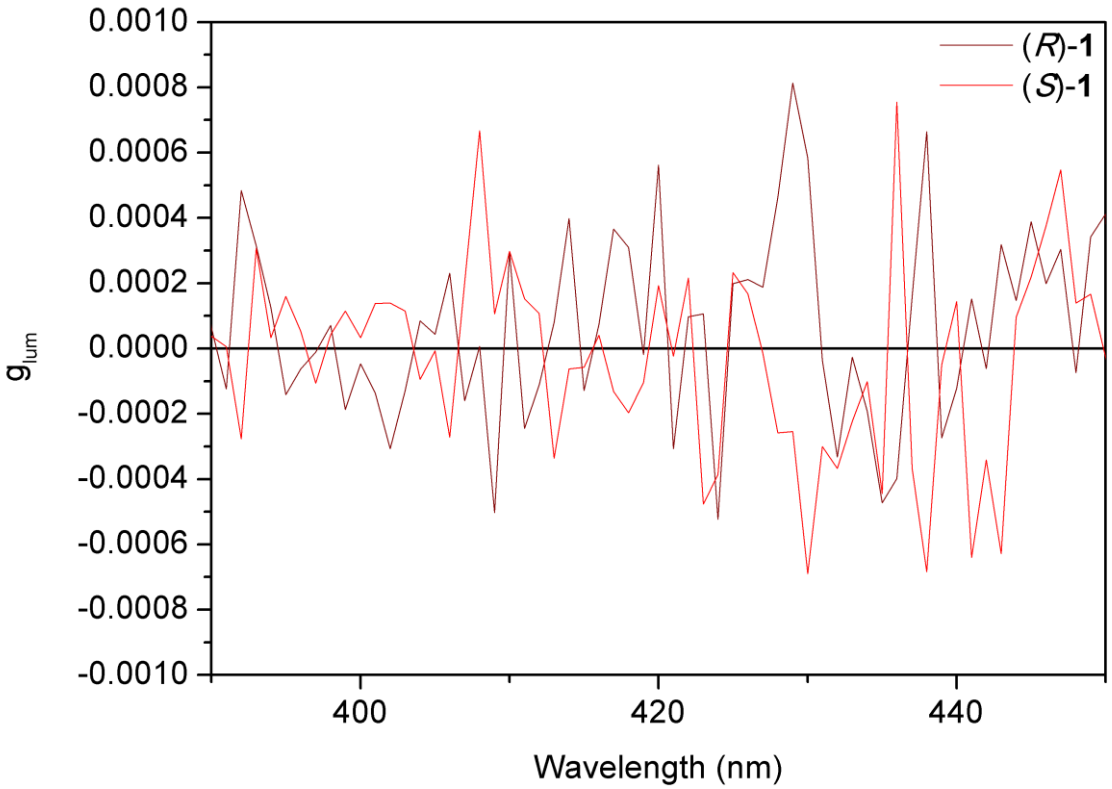

Figure S100: g_{lum} (λ_{exc} = 355 nm) spectra of rotaxane (*R*)/(*S*)-**1**·PF_6^- (g_{lum} = 0).

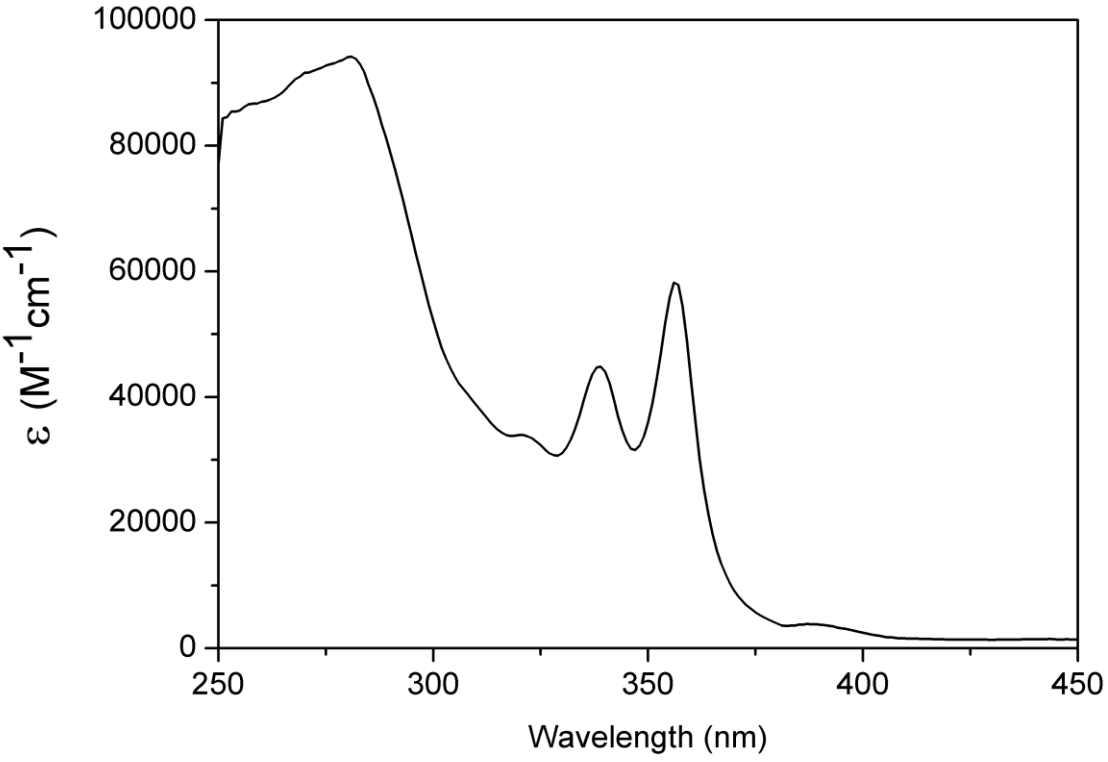

Figure S101: UV-Vis absorption spectrum of rotaxane **1**-H^+ (from the protonation of **1**·PF_6^-).

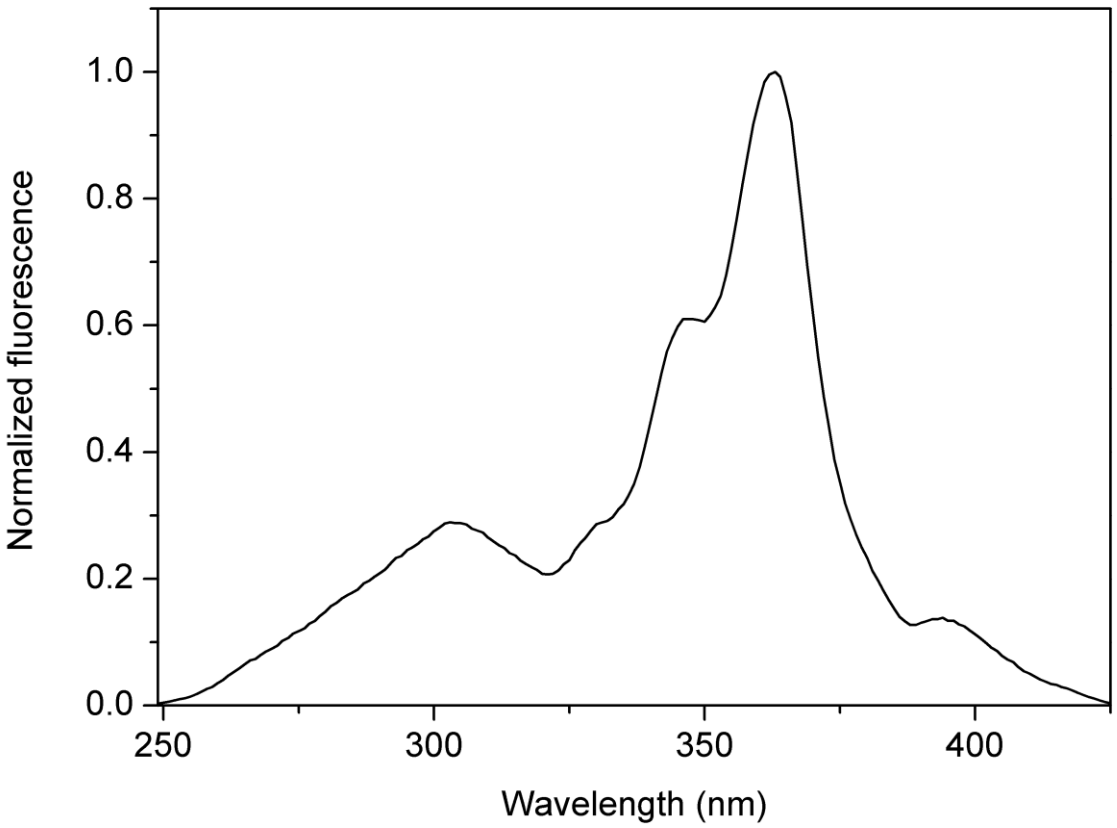

Figure S102: Excitation spectrum (λ_{emi} = 404 nm) of rotaxane **1-H**$^+$ (from the protonation of **1**·PF_6^-).

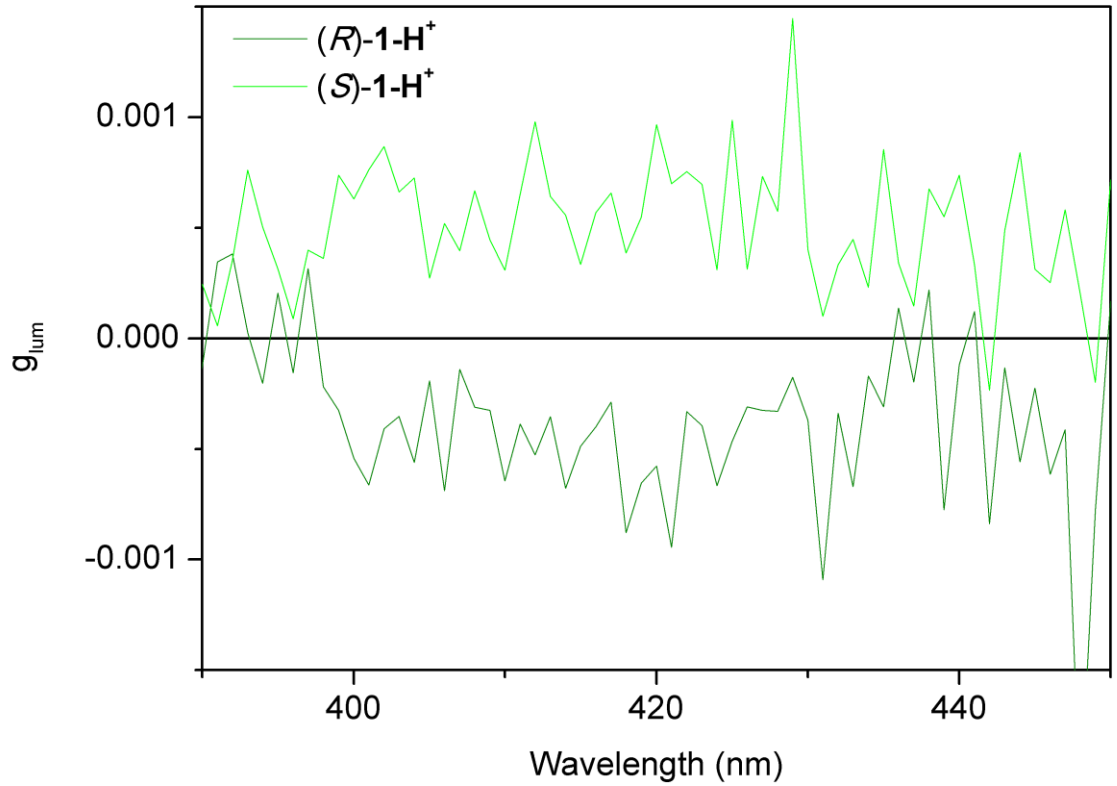

Figure S103: g_{lum} (λ_{exc} = 355 nm) spectra of rotaxanes (*R*)/(*S*)-**1-H**$^+$ (from the protonation of **1**·PF_6^-, g_{lum} = 5 × 10^{-4}).

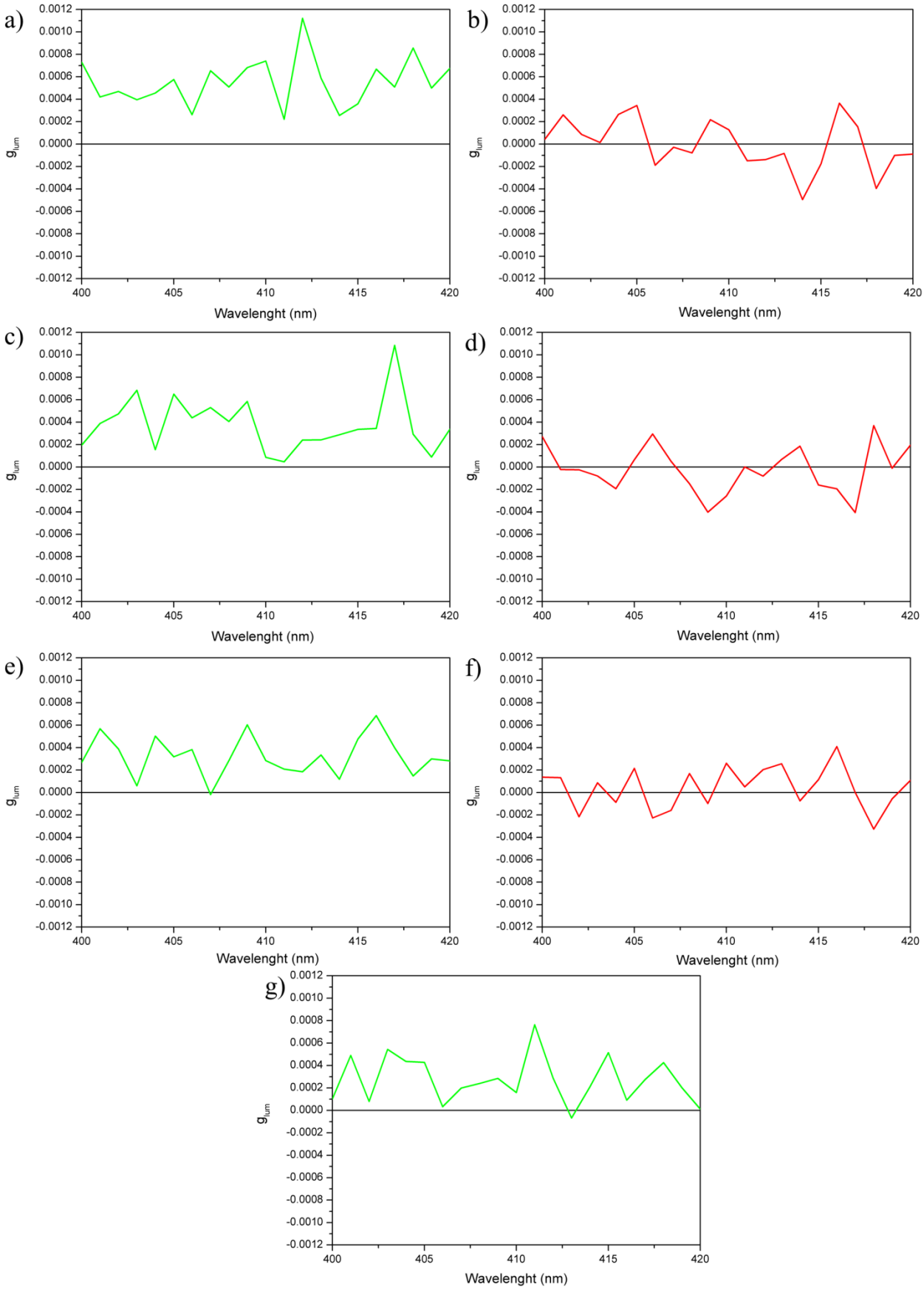

Figure S104: *In situ* CPL switching experiment. g_{lum} (λ_{exc} = 355 nm) spectra of rotaxane (*S*)-**1-H**$^{+}$·2PF_6^{-}: (a) (*S*)-**1-H**$^{+}$·2PF_6^{-}; (b) solution (a) after addition of K_2CO_3; (c) solution (b) after addition of CF_3CO_2H; (d) solution (c) after addition of K_2CO_3; (e) solution (d) after addition of CF_3CO_2H; (f) solution (e) after addition of K_2CO_3; (g) solution (f) after addition of CF_3CO_2H.

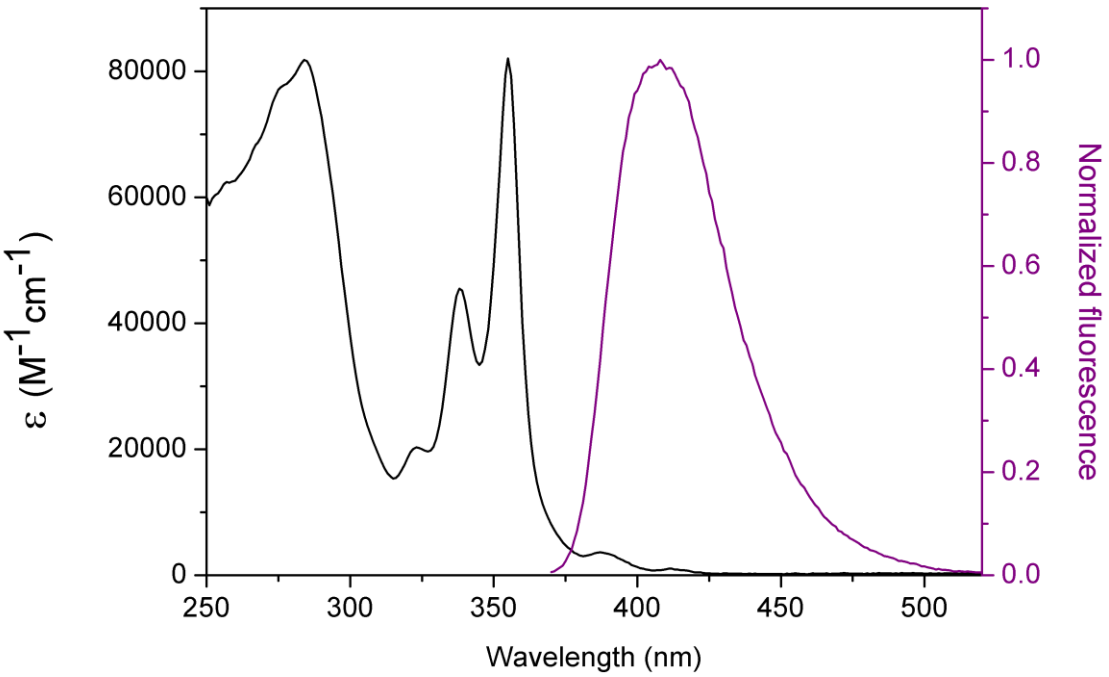

Figure S105: UV-Vis absorption (black line) and emission (purple line, λ_{exc} = 355 nm) spectra of an equimolar solution of thread (*S*)-**2**-$\mathbf{H}^{+}\cdot 2PF_6^-$ (*ca*. 1 × 10^{-5} M) and macrocycle **8** (*ca*. 1 × 10^{-5} M).

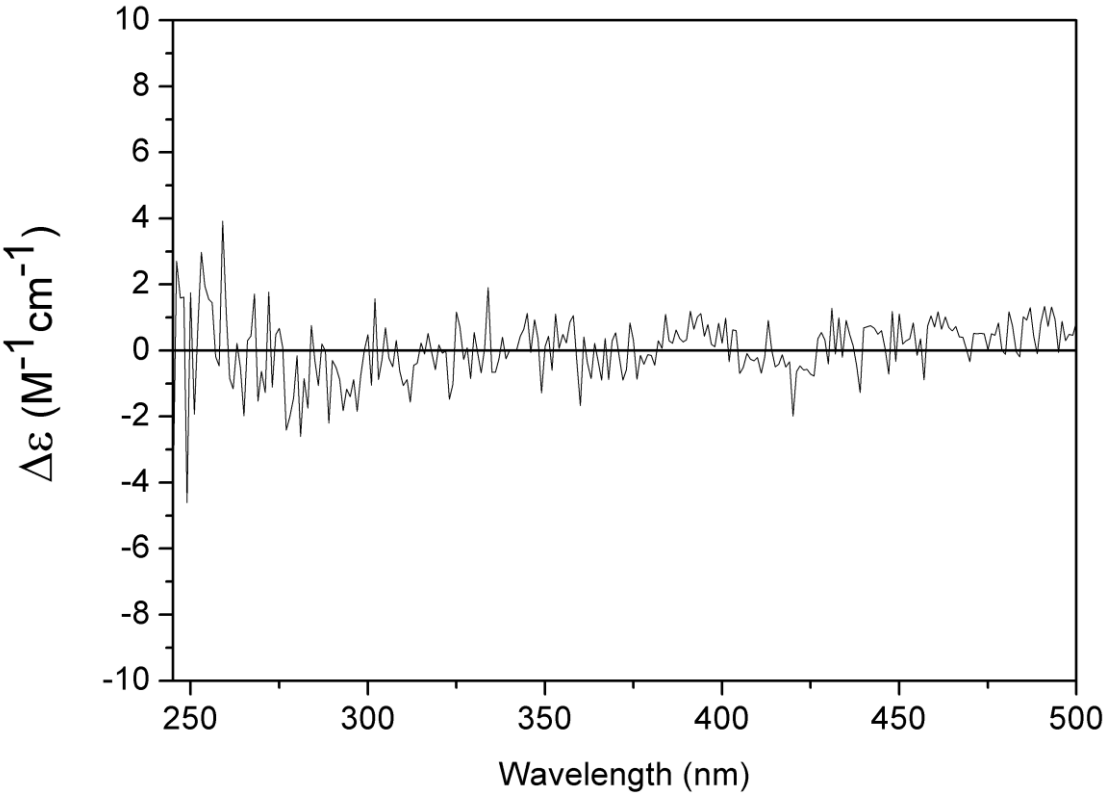

Figure S106: ECD spectrum of an equimolar solution of thread (*S*)-**2**-$\mathbf{H}^{+}\cdot 2PF_6^-$ (*ca*. 1 × 10^{-5} M) and macrocycle **8** (*ca*. 1 × 10^{-5} M).

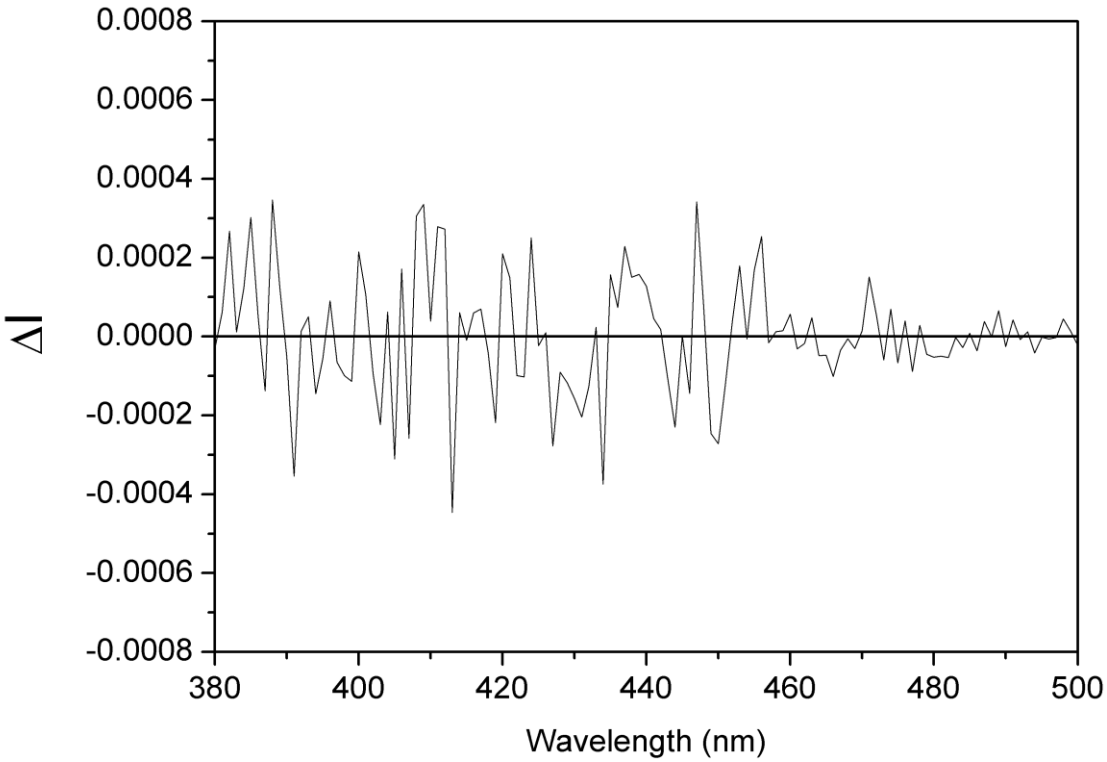

Figure S107: CPL (λ_{exc} = 355 nm) spectrum of an equimolar solution of thread (*S*)-**2-H**$^{+}$·2PF_6^- (*ca*. 1 × 10^{-5} M) and macrocycle **8** (*ca*. 1 × 10^{-5} M).

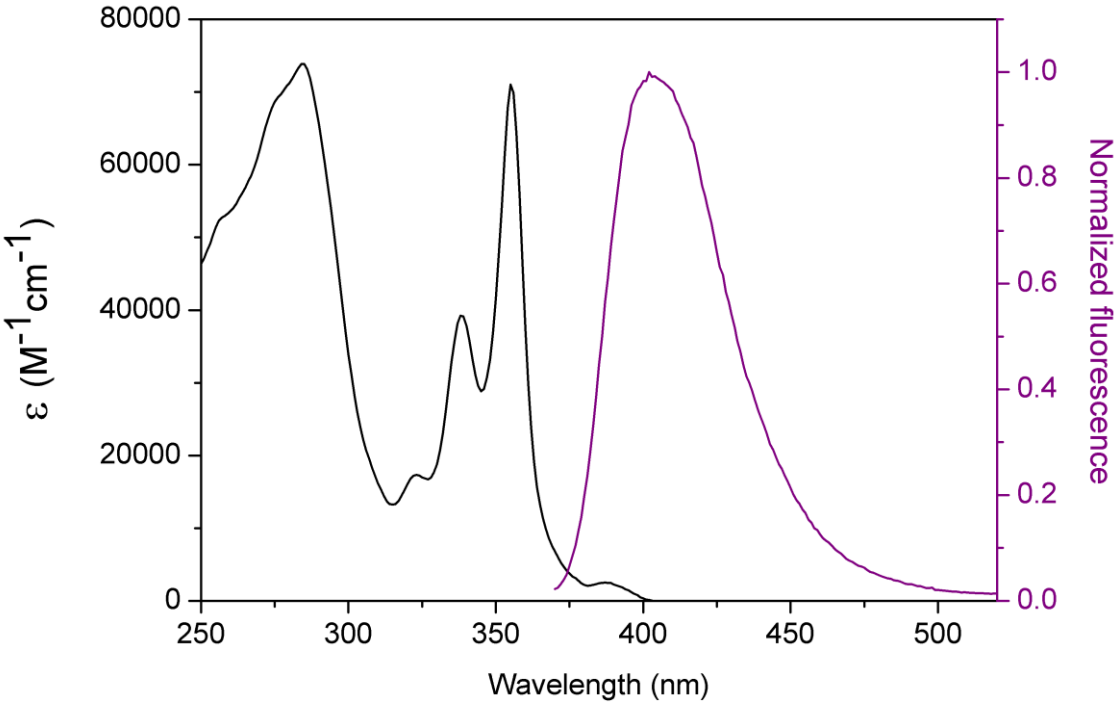

Figure S108: UV-Vis absorption (black line) and emission (purple line, λ_{exc} = 355 nm) spectra of an equimolar solution of (*S*)-**11-H**$^{+}$·PF_6^- (*ca*. 1 × 10^{-5} M) and macrocycle **8** (*ca*. 1 × 10^{-5} M).

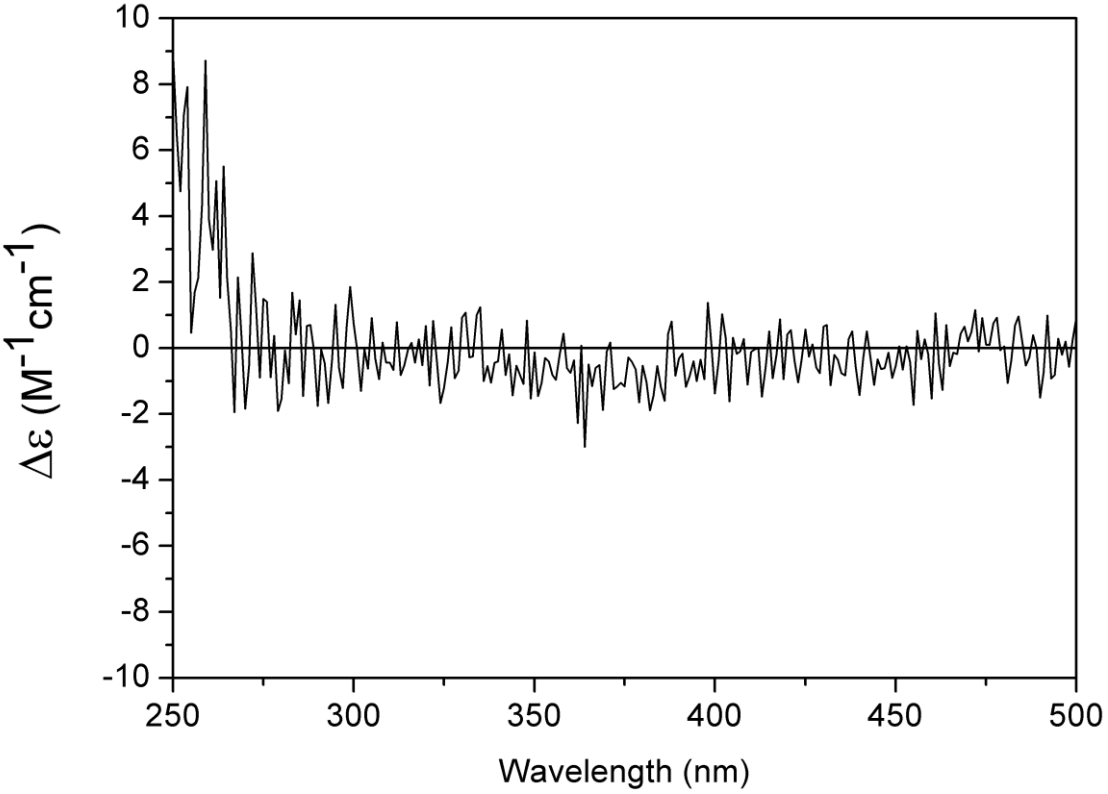

Figure S109: ECD spectrum of an equimolar solution of (*S*)-**11-H**$^{+}\cdot PF_6^-$ (*ca*. 1×10^{-5} M) and macrocycle **8** (*ca*. 1×10^{-5} M).

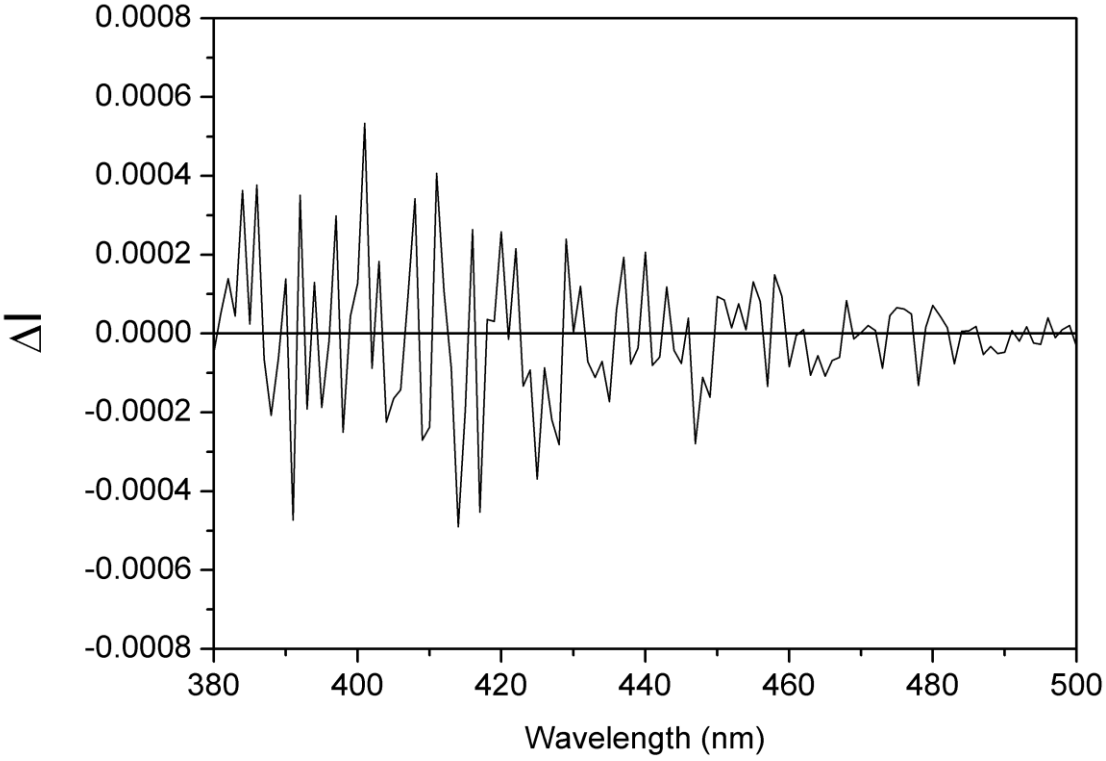

Figure S110: CPL (λ_{exc} = 355 nm) spectrum of an equimolar solution of (*S*)-**11-H**$^{+}\cdot PF_6^-$ (*ca*. 1×10^{-5} M) and macrocycle **8** (*ca*. 1×10^{-5} M).

7. Statistical Analysis of the CPL data

7.1. Statistical analysis of the CPL spectra of rotaxane (*S*)-1

For the statistical analysis of the CPL spectra of (*S*)-**1**-$\mathbf{H}^+\cdot 2PF_6^-$, (*S*)-**1**$\cdot PF_6^-$ and (*S*)-**1**-$\mathbf{H}^+$ obtained by reprotonation of (*S*)-**1**$\cdot PF_6^-$ with CF_3CO_2H we used the data of non-normalized ΔI (i. e. $I_L - I_R$) as recorded. The different CPL spectra represented in ΔI before normalization are shown in Figure S111. As discussed in section 6, each spectrum is the average of 200 scans.

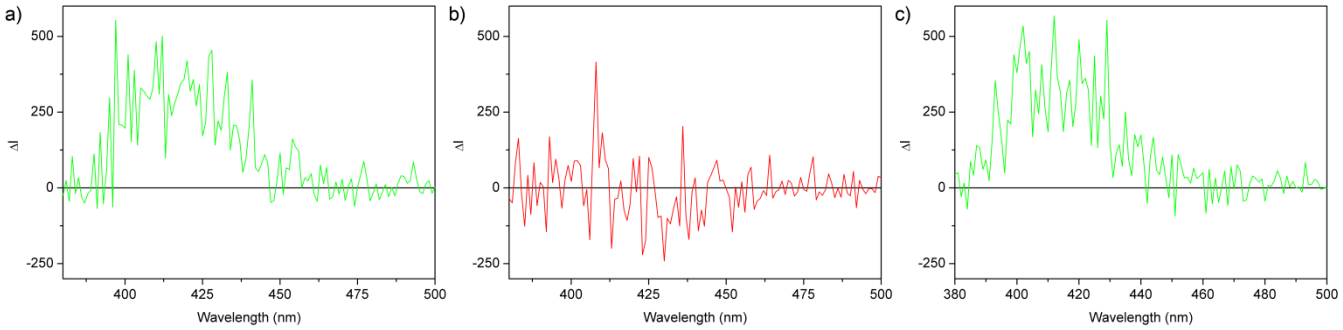

Figure S111: CPL (λ_{exc} = 355 nm) (*ca.* 1×10^{-5} M) spectra in non-normalized ΔI scale ($CHCl_3$) of: (a) (*S*)-**1**-$\mathbf{H}^+\cdot 2PF_6^-$; (b) (*S*)-**1**$\cdot PF_6^-$; (c) (*S*)-**1**-$\mathbf{H}^+$, obtained by protonation of **1**$\cdot PF_6^-$ with a solution of CF_3CO_2H in $CHCl_3$.

In this case, two different approaches were used, one based on the areas of the different spectra and the second one based on the ΔI values in a region of 26 nm width around the emission λ_{max}.

7.1.1. Statistical analysis based on the area

For this approach, we divided the spectra of the 200 scans recorded into 10 groups of 20 scans and calculated the corresponding average areas. With this 10 area values, a mean area and their standard deviations for the spectra of each compound were calculated. The data are shown in Table S3 and Figure S112.

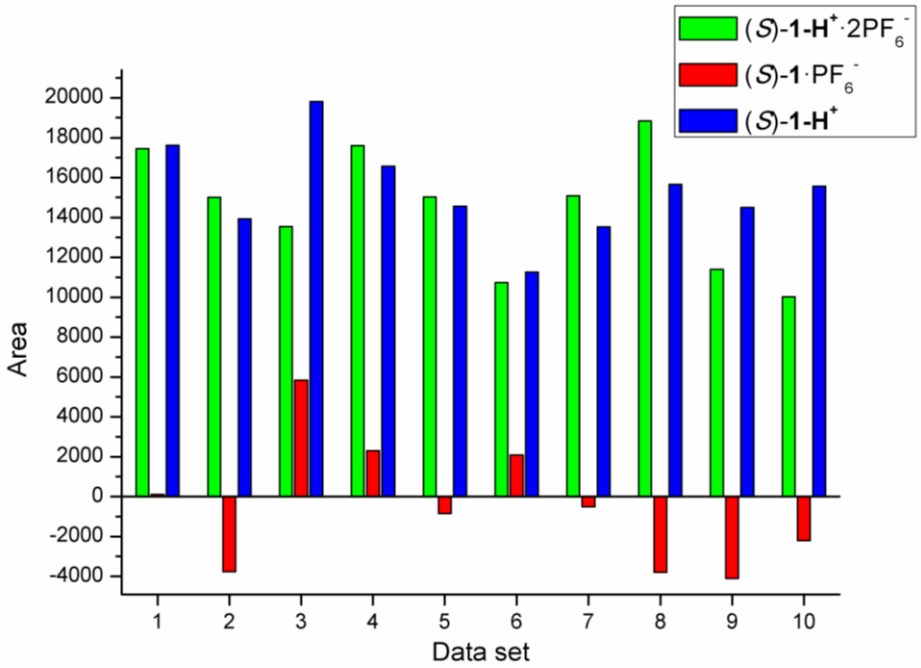

Figure S112: Mean areas for the average CPL spectra of each group of 20 scans recorded for (*S*)-**1**-$\mathbf{H}^+\cdot 2PF_6^-$; (*S*)-**1**$\cdot PF_6^-$; and (*S*)-**1**-$\mathbf{H}^+$, obtained by protonation of **1**$\cdot PF_6^-$ with a solution of CF_3CO_2H in $CHCl_3$

Table S3. Statistic parameters for the areas obtained from CPL spectra

	(*S*)-**1**-$\mathbf{H}^+$·2PF_6^-	(*S*)-**1**·PF_6^-	(*S*)-**1**-$\mathbf{H}^+$ after reprotonation
Average area ($\bar{x}$)	14469.250	−488.960[a]	15300.45
Standard deviation (s)	3034.379	3209.730	2362.28
Variance (s^2)	9207455,916	10302366,673	5580366,798
Number of data	10	10	10

[a] As the CPL signals can be positive or negative, negative values indicate that the spectra delimits a net area in the negative part of the scale.

- **F-test**

$F = \frac{s_1^2}{s_2^2}$ ($s_1 > s_2$)

$H_0 \equiv s_1^2 = s_2^2$ ($F_{calc} < F_{tab}$) Variances are not significantly different
$H_1 \equiv s_1^2 \neq s_2^2$ ($F_{calc} \geq F_{tab}$) Variances are significantly different

Table S4. F-test for the area data[a]

	$\mathbf{F_{calc}}$	**Conclusion**
(*S*)-**1**-$\mathbf{H}^+$·2PF_6^- vs (*S*)-**1**·PF_6^-	1.119	$F_{calc} < F_{tab} \rightarrow H_0$
(*S*)-**1**·PF_6^- vs (*S*)-**1**-$\mathbf{H}^+$ after reprotonation	1.846	$F_{calc} < F_{tab} \rightarrow H_0$
(*S*)-**1**-$\mathbf{H}^+$·2PF_6^- vs (*S*)-**1**-$\mathbf{H}^+$ after reprotonation	1.650	$F_{calc} < F_{tab} \rightarrow H_0$

[a] F_{tab} ($\alpha = 0.05$; $n_1=n_2= 10$; $df_1 = df_2 = 9$) = 3.18

Therefore, in all cases is concluded that the variances do not significantly differ.

- **t-test**

$t = \frac{|\bar{x}_1 - \bar{x}_2|}{s_p\sqrt{\frac{1}{n_1}+\frac{1}{n_2}}}$ $\left(s_p = \sqrt{\frac{(n_1-1)s_1^2+(n_2-1)s_2^2}{n_1+n_2-2}}\right)$

- *Comparison between "on" and "off" states*

$H_0 \equiv \bar{x}_1$ (on) $\leq \bar{x}_2$ (off) ($t_{calc} < t_{tab}$) Means are not significantly different
$H_1 \equiv \bar{x}_1$ (on) $> \bar{x}_2$ (off) ($t_{calc} \geq t_{tab}$) Means are significantly different with the "on" state ((*S*)-**1**-$\mathbf{H}^+$) giving a higher signal that the "off" state ((*S*)-**1**)

Table S5. t-test for the area data of "on" and "off" states[a]

	$\mathbf{t_{calc}}$	**Conclusion**
(*S*)-**1**-$\mathbf{H}^+$·2PF_6^- vs (*S*)-**1**·PF_6^-	10.71	$t_{calc} > t_{tab} \rightarrow H_1$
(*S*)-**1**·PF_6^- vs (*S*)-**1**-$\mathbf{H}^+$ after reprotonation	12.53	$t_{calc} > t_{tab} \rightarrow H_1$

[a] t_{tab} (one-tailed, 0.05; $n_1=n_2= 10$; df = 18) = 1.734; t_{tab} (one-tailed, 0.001; $n_1=n_2= 10$; df = 18) = 3.610

Therefore, the tests (Tables S4-S5) show that, at 95% confidence, and even at 99.9%, the signals observed for (*S*)-**1**-$\mathbf{H}^+\cdot 2PF_6^-$ ("on I" state) and (*S*)-**1**-$\mathbf{H}^+$ obtained by protonation of **1**$\cdot PF_6^-$ with a solution of CF_3CO_2H ("on II" state) are significantly higher from the signals of (*S*)-**1**$\cdot PF_6^-$ ("off" state).

- *Comparison between "on" states*

We also compared the signals of (*S*)-**1**-$\mathbf{H}^+\cdot 2PF_6^-$ and (*S*)-**1**-$\mathbf{H}^+$ after reprotonation with CF_3CO_2H.

$H_0 \equiv \bar{x}_1 = \bar{x}_2$ ($t_{calc} < t_{tab}$) Means are not significantly different

$H_1 \equiv \bar{x}_1 \neq \bar{x}_2$ ($t_{calc} \geq t_{tab}$) Means are significantly different

Table S6. t-test for the area data of (*S*)-**1**-$\mathbf{H}^+\cdot 2PF_6^-$ and reprotonated (*S*)-**1**-$\mathbf{H}^+$

	t_{calc}	Conclusion
(*S*)-**1**-$\mathbf{H}^+\cdot 2PF_6^-$ vs (*S*)-**1**-$\mathbf{H}^+$ after reprotonation	0.68	$t_{calc} < t_{tab} \rightarrow H_0$

[a] t_{tab} (two-tailed, 0.05; $n_1=n_2= 10$; df = 18) = 2.101; t_{tab} (two-tailed, 0.001; $n_1=n_2= 10$; df = 18) = 3.922

On the contrary, at the same level of confidence as the comparison between "on" and "off sates" there are no significant differences between the signals of both "on" states ((*S*)-**1**-$\mathbf{H}^+\cdot 2PF_6^-$ and reprotonated (*S*)-**1**-$\mathbf{H}^+$) (Table S6).

If we assume that due to the degradation, the signal of (*S*)-**1**-$\mathbf{H}^+$ after reprotonation can only diminish due to the degration, then $H_1 \equiv \bar{x}_1 > \bar{x}_2$, and a one-tailed test would be the appropriate and the reference t values shown in table S5 would have to be considered. However, the conclusion of the test would remain unaltered.

7.1.1. Statistical analysis based on the intensity

For this approach, we analyzed the non-normalized ΔI values between 400 and 425 nm (26 points). The data are shown in Figure S113 and Table S7.

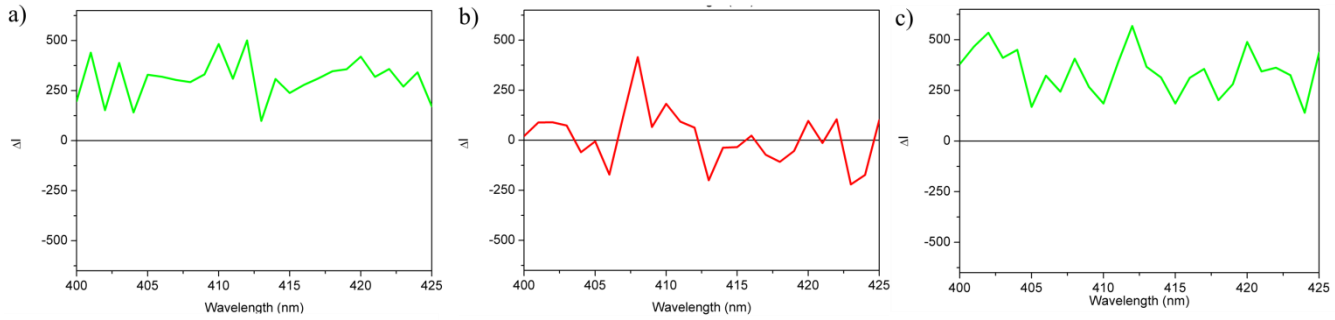

Figure S113: Partial CPL (λ_{exc} = 355 nm) (*ca.* 1×10^{-5} M) spectra in non-normalized ΔI scale ($CHCl_3$) of: (a) (*S*)-**1**-$\mathbf{H}^+\cdot 2PF_6^-$; (b) (*S*)-**1**$\cdot PF_6^-$; (c) (*S*)-**1**-$\mathbf{H}^+$, obtained by protonation of (*S*)-**1**$\cdot PF_6^-$ with a solution of CF_3CO_2H in $CHCl_3$.

Table S7. Statistic parameters for the non-normalized ΔI values obtained from CPL spectra

	(*S*)-**1**-$\mathbf{H}^+\cdot 2PF_6^-$	(*S*)-**1**$\cdot PF_6^-$	(*S*)-**1**-$\mathbf{H}^+$ after reprotonation
Average ΔI ($\bar{x}$)	308.08	15.39	342.34
Standard deviation (s)	97.56	132.92	110.97
Variance (s^2)	9517.387	17668.095	12315.404
Number of data	26	26	26

- **F-test**

$F = \frac{s_1^2}{s_2^2}$ ($s_1 > s_2$)

$H_0 \equiv s_1^2 = s_2^2$ ($F_{calc} < F_{tab}$) Variances are not significantly different
$H_1 \equiv s_1^2 \neq s_2^2$ ($F_{calc} \geq F_{tab}$) Variances are significantly different

Table S8. F-test for the ΔI data[a]

	F_{calc}	Conclusion
(*S*)-**1**-$\mathbf{H}^+$·$2PF_6^-$ vs (*S*)-**1**·PF_6^-	1.856	$F_{calc} < F_{tab} \rightarrow H_0$
(*S*)-**1**·PF_6^- vs (*S*)-**1**-$\mathbf{H}^+$ after reprotonation	1.435	$F_{calc} < F_{tab} \rightarrow H_0$
(*S*)-**1**-$\mathbf{H}^+$·$2PF_6^-$ vs (*S*)-**1**-$\mathbf{H}^+$ after reprotonation	1.294	$F_{calc} < F_{tab} \rightarrow H_0$

[a] F_{tab} ($\alpha = 0.05$; $n_1=n_2= 26$; $df_1 = df_2 = 25$) = 1.96

Therefore, in all cases is concluded that the variances do not significantly differ.

- **t-test**

$t = \frac{|\bar{x}_1 - \bar{x}_2|}{s_p\sqrt{\frac{1}{n_1}+\frac{1}{n_2}}}$ $\left(s_p = \sqrt{\frac{(n_1-1)s_1^2+(n_2-1)s_2^2}{n_1+n_2-2}}\right)$

- *Comparison between "on" and "off" states*

$H_0 \equiv \bar{X}_1$ (on) $\leq \bar{X}_2$ (off) ($t_{calc} < t_{tab}$) Means are not significantly different
$H_1 \equiv \bar{X}_1$ (on) $> \bar{X}_2$ (off) ($t_{calc} \geq t_{tab}$) Means are significantly different with the "on" state ((*S*)-**1**-$\mathbf{H}^+$) giving a higher signal that the "off" state ((*S*)-**1**)

As we are comparing the data of the different (*S*)-**1** species, we consider the signal of the "on" state positive and higher than that of the "off" state.

Table S9. t-test for the ΔI data of "on" and "off" states[a]

	t_{calc}	Conclusion
(*S*)-**1**-$\mathbf{H}^+$·$2PF_6^-$ vs (*S*)-**1**·PF_6^-	9.05	$t_{calc} > t_{tab} \rightarrow H_1$
(*S*)-**1**·PF_6^- vs (*S*)-**1**-$\mathbf{H}^+$ after reprotonation	9.63	$t_{calc} > t_{tab} \rightarrow H_1$

[a] t_{tab} (one-tailed, 0.05; $n_1=n_2= 26$; df = 50) = 1.676; t_{tab} (one-tailed, 0.001; $n_1=n_2= 26$; df = 50) = 3.262

Therefore, the tests based on ΔI (tables S8-S9) bring the same conclusions than those based on the areas of the spectra. At 95% and even at 99.9% confidence level, the signal observed for (*S*)-**1**·PF_6^- ("off" state) is significantly different from the signals of (*S*)-**1**-$\mathbf{H}^+$·$2PF_6^-$ ("on I" state) and (*S*)-**1**-$\mathbf{H}^+$ obtained by protonation of (*S*)-**1**·PF_6^- with a solution of CF_3CO_2H ("on II" state).

- *Comparison between "on" states*

$H_0 \equiv \bar{X}_1 = \bar{X}_2$ ($t_{calc} < t_{tab}$) Means are not significantly different
$H_1 \equiv \bar{X}_1 \neq \bar{X}_2$ ($t_{calc} \geq t_{tab}$) Means are significantly different

Table S10. t-test for the ΔI data of (*S*)-**1-H**$^+$·2PF_6^- and reprotonated (*S*)-**1-H**$^+$

	t_{calc}	Conclusion
(*S*)-**1-H**$^+$·2PF_6^- vs (*S*)-**1-H**$^+$ after reprotonation	1.18	$t_{calc} < t_{tab} \rightarrow H_0$

[a] t_{tab} (two-tailed, 0.05; n_1=n_2= 26; df = 50) = 2.009; t_{tab} (two-tailed, 0.001; n_1=n_2= 26; df = 50) = 3.497

On the contrary, there are no significant differences between the signals of both "on" states ((*S*)-**1-H**$^+$·2PF_6^- and reprotonated (*S*)-**1-H**$^+$) (Table S10).

If we assume that due to the degradation, the signal of (*S*)-**1-H**$^+$ after reprotonation can only diminish due to the degration, then $H_1 \equiv \bar{x}_1 > \bar{x}_2$, and a one-tailed test would be the appropriate and the reference t values shown in table S9 would have to be considered. However, the conclusion of the test would remain unaltered.

7.2. Statistical analysis of the CPL data of the operation cycles

Finally, we performed the statistical analysis of the CPL data obtained during the cycles of *in situ* switching of the CPL response. Having obtained the same conclusions eihter using areas or non-normalized ΔI intensities for (*S*)-**1-H**$^+$·2PF_6^-, (*S*)-**1**·PF_6^- and reprotonated (*S*)-**1-H**$^+$, we used the non-normalized ΔI data between 400 and 420 nm (21 points). The data are shown in Table S11 and Figure S114.

Table S11. Statistic parameters for the non-normalized ΔI values obtained from CPL spectra

	Average ΔI ($\bar{x}$)	Standard deviation (s)	Variance (s^2)	Number of data
(*S*)-**1-H**$^+$·2PF_6^- (Cycle 0)[a]	366.998	136.348	18590.7588	21
(*S*)-**1**·PF_6^- (Cycle 0.5)[a]	1.725	131.501	17292.6318	21
(*S*)-**1-H**$^+$ (Cycle 1)[a]	236.414	146.668	21511.3817	21
(*S*)-**1** (Cycle 1.5)[a]	−15.402	122.639	15040.3481	21
(*S*)-**1-H**$^+$ (Cycle 2)[a]	198.093	108.888	11856.5789	21
(*S*)-**1** (Cycle 2.5)[a]	26.115	111.771	12492.8418	21
(*S*)-**1-H**$^+$ (Cycle 3)[a]	160.206	121.127	14671.6321	21

[a] The cycle number corresponds to that shown in Figure 7 in the main text.

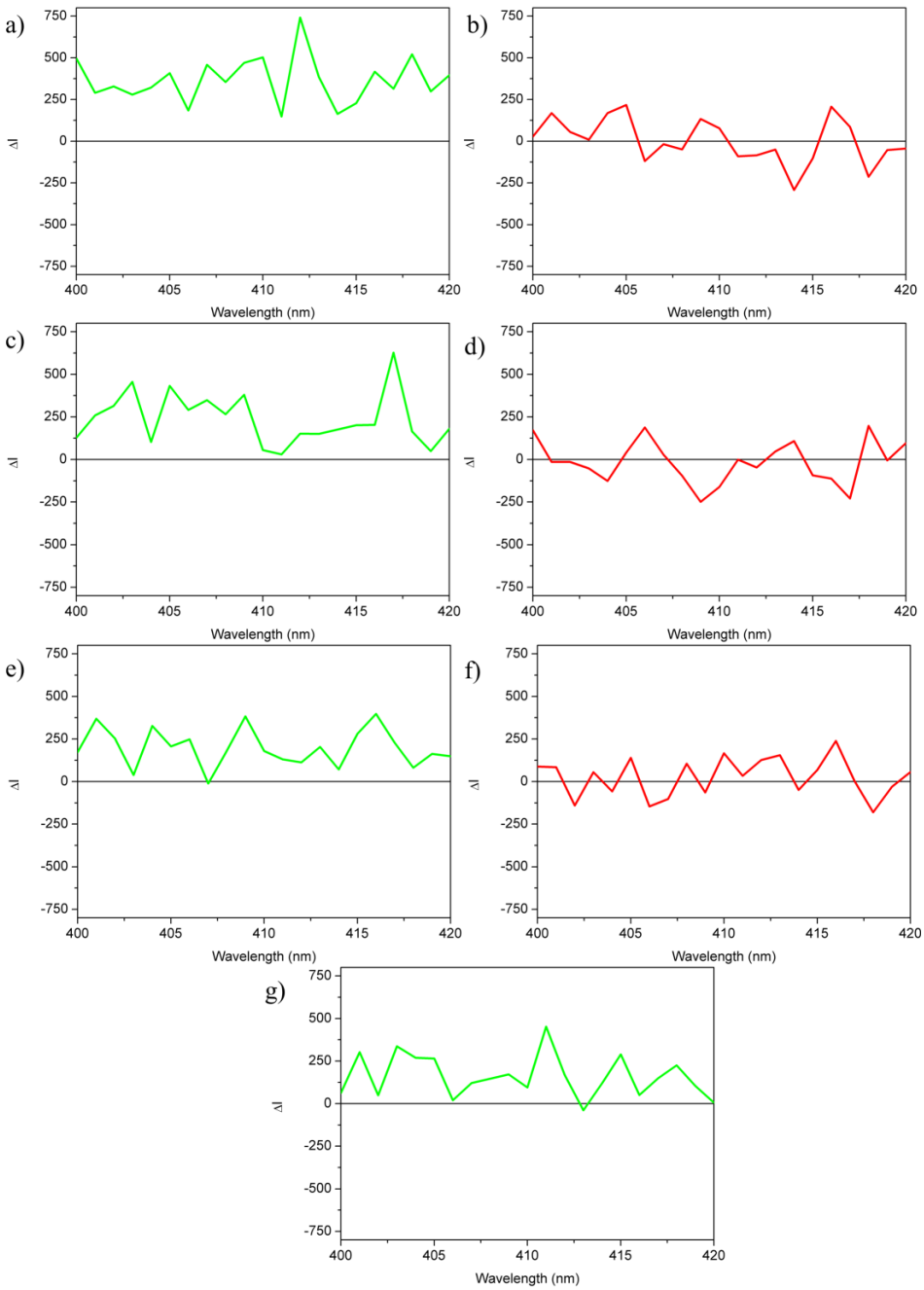

Figure S114: *In situ* CPL switching experiment. Non-normalized ΔI spectra of rotaxane (*S*)-**1-H**$^{+}$·2PF_6^-: (a) (*S*)-**1-H**$^{+}$·2PF_6^-; (b) solution (a) after addition of K_2CO_3; (c) solution (b) after addition of CF_3CO_2H; (d) solution (c) after addition of K_2CO_3; (e) solution (d) after addition of CF_3CO_2H; (f) solution (e) after addition of K_2CO_3; (g) solution (f) after addition of CF_3CO_2H

- **F-test**

$$F = \frac{s_1^2}{s_2^2} \quad (s_1 > s_2)$$

$H_0 \equiv {s_1}^2 = {s_2}^2$ $(F_{calc} < F_{tab})$ Variances are not significantly different
$H_1 \equiv {s_1}^2 \neq {s_2}^2$ $(F_{calc} \geq F_{tab})$ Variances are significantly different

Table S12. F-test for the cycles ΔI data[a]

"on" state vs "off" state	F_{calc}	Conclusion
Cycle 0 vs Cycle 0.5	1.075	$F_{calc} < F_{tab} \rightarrow H_0$
Cycle 0.5 vs Cycle 1	1.244	$F_{calc} < F_{tab} \rightarrow H_0$
Cycle 1 vs Cycle 1.5	1.430	$F_{calc} < F_{tab} \rightarrow H_0$
Cycle 1.5 vs Cycle 2	1.269	$F_{calc} < F_{tab} \rightarrow H_0$
Cycle 2 vs Cycle 2.5	1.054	$F_{calc} < F_{tab} \rightarrow H_0$
Cycle 2.5 vs Cycle 3	1.174	$F_{calc} < F_{tab} \rightarrow H_0$

[a] F_{tab} (α = 0.05; n_1=n_2= 21; df_1 = df_2 = 20) = 2.12

Therefore, in all cases is concluded that the variances do not significantly differ.

- **t-test**

$$t = \frac{|\bar{x}_1 - \bar{x}_2|}{s_p\sqrt{\frac{1}{n_1}+\frac{1}{n_2}}} \qquad \left(s_p = \sqrt{\frac{(n_1-1)s_1^2+(n_2-1)s_2^2}{n_1+n_2-2}}\right)$$

$H_0 \equiv \bar{X}_1$ (on) $\leq \bar{X}_2$ (off) ($t_{calc} < t_{tab}$) Means are not significantly different

$H_1 \equiv \bar{X}_1$ (on) $> \bar{X}_2$ (off) ($t_{calc} \geq t_{tab}$) Means are significantly different with the "on" states giving a higher signal that the "off" states

Table S13. t-test for the cycles ΔI data[a]

"on" state vs "off" state	t_{calc}	Conclusion
Cycle 0 vs Cycle 0.5	8.84	$t_{calc} > t_{tab} \rightarrow H_1$
Cycle 0.5 vs Cycle 1	5.46	$t_{calc} > t_{tab} \rightarrow H_1$
Cycle 1 vs Cycle 1.5	6.04	$t_{calc} > t_{tab} \rightarrow H_1$
Cycle 1.5 vs Cycle 2	5.97	$t_{calc} > t_{tab} \rightarrow H_1$
Cycle 2 vs Cycle 2.5	5.05	$t_{calc} > t_{tab} \rightarrow H_1$
Cycle 2.5 vs Cycle 3	3.73	$t_{calc} > t_{tab} \rightarrow H_1$

[a] t_{tab} (one-tailed, 0.05; n_1=n_2= 21; df = 40) = 1.684; t_{tab} (one-tailed, 0.001; n_1=n_2= 21; df = 40) = 3.307

Therefore, the tests perfomed (Tables S12-S13) show that at 95%, and even 99.9%, confidence level, the signals observed for different "on" states (cycle 0, 1, 2 and 3) is significantly higher than those corresponding to the "off" states (cycle 0.5, 1.5 and 2.5). Therefore, although there is a degradation of the system among these cycles, the clear difference between both CPL response states is maintained.

8. Single crystal X-ray diffraction analysis

Suitable crystals for X-ray diffraction analysis of **8**⊂KPF_6 were grown by slow evaporation of a solution of the complex in $CHCl_3$. The diffraction data were collected on a Bruker SMART APEX diffractometer equipped with an APEX detector using a Mo radiation source. The structure was solved with SHELXT[S15] 2018 and refined using the full-matrix least-squares against F^2 procedure with SHELX 2018[S16] using the WinGX32[S17] software. C–H hydrogen atoms were placed in idealized positions (U_{eg}(H) = 1.2U_{eg}(C) or U_{eg}(H) = 1.5U_{eg}(C)) and were allowed to ride on their parent atoms.

The crystals obtained were of moderate quality, which, together with its low stability at low temperature that forced to collect the data at room temperature, meant that several restraints had to be used for some atom groups, especially for the PF_6 counterion. Hence, DANG, SADI, ISOR restraints had to be used. Moreover, for this PF_6 anion, some apparent disorder between two positions was found, which resulted in the use of PART instructions.

During the refinement the structure of the target molecule was established, but large residual electron density was still present. This electron density was located mainly in the void and corresponded to a disordered chloroform molecule, which could not be fully modeled. Therefore, the SQUEEZE[S18] routine included in PLATON[S19] was applied and a density of 446 e^-/cell in an approximate 1476 $Å^3$ volume was identified. Eight chloroform molecules per unit cell were introduced in the formula. This density was removed and the data refined against the model.

Summary of the X-ray diffraction measurement and refinement data: Chemical formula, $C_{52}H_{46}Cl_6F_6KO_8P$; *Mr*, 1195.66; crystal size [mm^3], 0.460 × 0.340 × 0.200; temperature, 293(2) K; wavelength [Å], 0.71073 (Mo Kα), crystal system, monoclinic; space group, *C*2/*c*; *a* [Å], 13.3866(12); *b* [Å], 22.472(2); *c* [Å], 18.1039(17); α [°], 90; β [°], 99.497(2); γ [°], 90; *V* [$Å^3$], 5371.3(9); *Z*, 4; ρ_{calcd} [Mg m^{-3}], 1.479; μ [mm^{-1}], 0.501; F(000), 2448; θ range [°], 1.789 to 28.053; *hkl* ranges, -17/17, -29/16, -23/23; reflections collected, 16688; independent reflections, 6016; R_{int}, 0.0241; completeness to θ = 25.242°, 99.9%; absorption correction, semi-empirical from equivalents; refinement method; full-matrix least-squares on F^2; Final *R* indices [$I>2\sigma(I)$], R_1 = 0.1142, wR_2 = 0.3619; *R* indices (all data), R_1 = 0.1546, wR_2 = 0.4004; goodness-of-fit on F^2, 1.343.

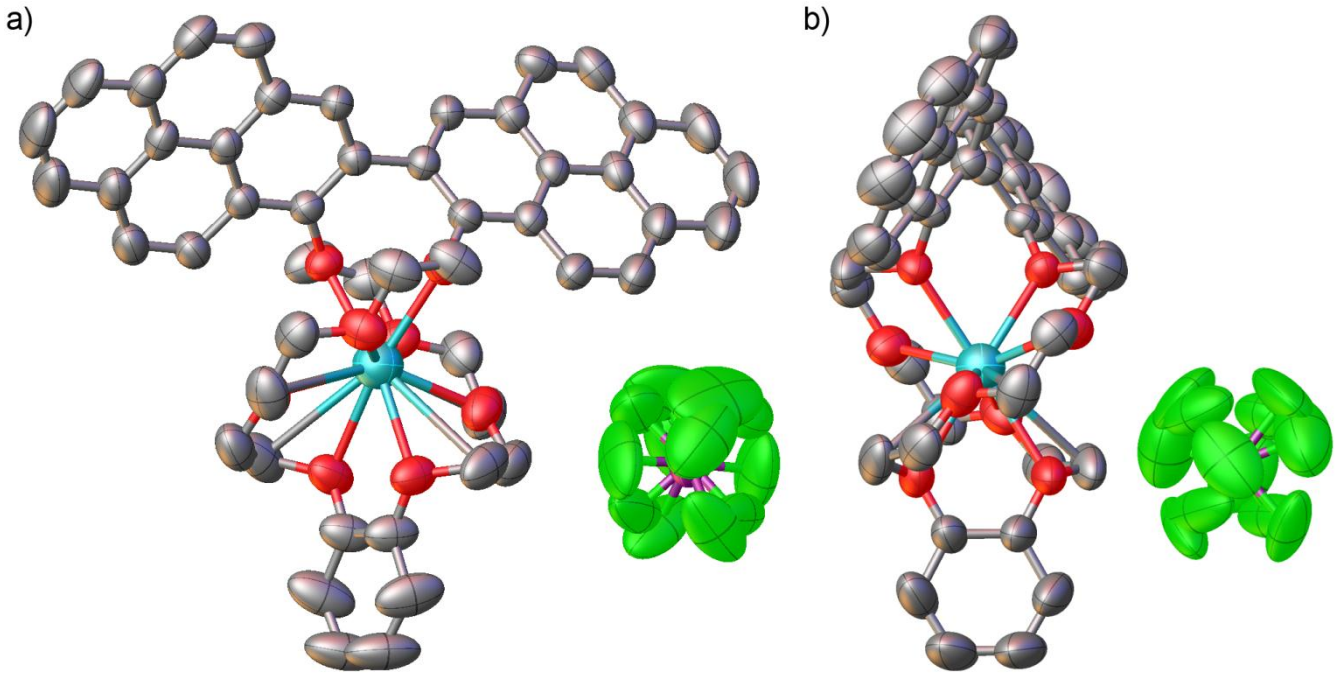

Figure S115. (a) Front and (b) side views of the ORTEP-type[S20] representation of the solid state structure of **8**⊂KPF_6 showing the ellipsoids at 50% probability: a) Color code: C: gray, O: red, K: light blue, P: violet, Cl: green. Hydrogen atoms have been omitted for clarity.

Table S14. Atomic coordinates for the X-ray diffraction structure of **8**⊂KPF_6

Atom	X	Y	Z
C	-0.6977	12.2915	12.9490
C	-1.6501	13.3232	12.9365
C	-1.4775	14.3924	12.0651
H	-2.1029	15.1070	12.0814
C	-0.4017	14.4450	11.1634
C	0.5407	13.3913	11.1795
C	0.4055	12.3230	12.0759
C	1.4111	11.2931	12.0901
H	1.3452	10.5793	12.7140
C	2.4548	11.3326	11.2206
H	3.1186	10.6537	11.2523
C	2.5654	12.3933	10.2474
C	3.5952	12.4405	9.2850
H	4.2571	11.7589	9.2742
C	3.6585	13.4472	8.3708
H	4.3520	13.4479	7.7229
C	2.7543	14.4338	8.3744
H	2.8316	15.1301	7.7333
C	1.6952	14.4720	9.2957
C	1.6074	13.4234	10.2206
C	0.7269	15.5034	9.3064
H	0.7710	16.1939	8.6557
C	-0.2343	15.5169	10.2028
H	-0.8374	16.2505	10.2202
C	-0.1983	11.2652	15.0453
H	0.2080	12.1608	15.1663
H	0.5263	10.5922	15.0718
C	-1.1311	11.0135	16.1077
H	-0.6488	10.9302	16.9676
H	-1.7717	11.7642	16.1799
C	-2.9662	9.5978	16.6505
H	-3.5826	10.3686	16.5606
H	-2.6797	9.5433	17.5966
C	-3.6418	8.4045	16.2880
H	-4.4512	8.2982	16.8480
H	-3.0508	7.6272	16.4495
C	-4.8135	7.3551	14.5221
H	-5.7530	7.5063	14.7966
H	-4.4920	6.5247	14.9571
C	-4.7258	7.2203	13.0133
H	-5.3113	6.4815	12.7082
H	-5.0360	8.0568	12.5841
C	-2.8371	5.7753	13.0061
C	-3.4111	4.5259	12.6365
H	-4.2305	4.5041	12.1552
C	-2.7967	3.3798	12.9651
H	-3.1215	2.5570	12.6175
O	-0.8636	11.2072	13.7814
O	-1.8343	9.7980	15.8222
O	-4.0142	8.4459	14.9131
O	-3.3557	6.9497	12.6256
K	-2.2403	9.1845	13.3918
C	-3.7829	12.2915	13.8347
C	-2.8305	13.3232	13.8472
C	-3.0031	14.3924	14.7185
H	-2.3777	15.1070	14.7022
C	-4.0789	14.4450	15.6202
C	-5.0213	13.3913	15.6042
C	-4.8861	12.3230	14.7078
C	-5.8917	11.2931	14.6935
H	-5.8258	10.5793	14.0697
C	-6.9354	11.3326	15.5631
H	-7.5992	10.6537	15.5314
C	-7.0460	12.3933	16.5362
C	-8.0758	12.4405	17.4987
H	-8.7377	11.7589	17.5094
C	-8.1391	13.4472	18.4129
H	-8.8326	13.4479	19.0608
C	-7.2349	14.4338	18.4093
H	-7.3122	15.1301	19.0504
C	-6.1758	14.4720	17.4879
C	-6.0880	13.4234	16.5630
C	-5.2075	15.5034	17.4772
H	-5.2516	16.1939	18.1280
C	-4.2463	15.5169	16.5809
H	-3.6432	16.2505	16.5634
C	-4.2823	11.2652	11.7384
H	-4.6886	12.1608	11.6174
H	-5.0069	10.5922	11.7119
C	-3.3495	11.0135	10.6760
H	-3.8318	10.9302	9.8161
H	-2.7090	11.7642	10.6037
C	-1.5144	9.5978	10.1332
H	-0.8980	10.3686	10.2230
H	-1.8009	9.5433	9.1870
C	-0.8388	8.4045	10.4956
H	-0.0294	8.2982	9.9356
H	-1.4298	7.6272	10.3342
C	0.3329	7.3551	12.2616
H	1.2724	7.5063	11.9870
H	0.0114	6.5247	11.8266

C	0.2452	7.2203	13.7704	F	3.7348	8.7753	12.6276
H	0.8307	6.4815	14.0754	F	3.3476	7.4292	14.4864
H	0.5554	8.0568	14.1996	F	5.2670	6.1843	14.0793
C	-1.6435	5.7753	13.7775	P	4.4530	7.4787	13.3918
C	-1.0695	4.5259	14.1471	F	5.1712	8.7753	14.1561
H	-0.2501	4.5041	14.6284	F	5.5584	7.4292	12.2973
C	-1.6839	3.3798	13.8186	F	3.6390	6.1843	12.7044
H	-1.3591	2.5570	14.1661	F	3.7885	7.9326	12.0187
O	-3.6170	11.2072	13.0022	F	3.3517	8.5079	13.5811
O	-2.6463	9.7980	10.9615	F	3.4024	6.4607	13.4865
O	-0.4664	8.4459	11.8705				
O	-1.1249	6.9497	14.1580				

9. References

(S1) Chan, T. R.; Hilgraf, R.; Sharpless, K. B.; Fokin, V. V., Polytriazoles as Copper(I)-Stabilizing Ligands in Catalysis. *Org. Lett.* **2004**, *6*, 2853-2855.

(S2) Takahashi, Y.; Ito, Ts.; Sakai, S.; Ishii, Y., A novel palladium(0) complex; bis(dibenzylideneacetone)palladium(0). *J. Chem. Soc. D* **1970**, 1065-1066.

(S3) Naganna, N.; Madhavan, N., Soluble Non-Cross-Linked Poly(norbornene) Supports for Peptide Synthesis with Minimal Reagents. *J. Org. Chem.* **2014**, *79*, 11549-11557.

(S4) Koreeda, M.; Gopalaswamy, R., Regio- and Stereocontrolled Synthesis of the Bay-Region anti-Diol Epoxide Metabolites of the Potent Carcinogens Benzo[a]pyrene and 7,12-Dimethylbenz[a]anthracene. *J. Am. Chem. Soc.* **1995**, *117*, 10595-10596.

(S5) Singh, S.; Gill, S.; Sharma, V. K.; Nagrath, S., NADH model studies. Part 2. Cationic hydrogenations using acridan derivatives as hindered NADH models. *J. Chem. Soc., Perkin Trans. 1* **1986**, 1273-1275.

(S6) Vlasceanu, A.; Jessing, M.; Kilburn J. P., BN/CC isosterism in borazaronaphthalenes towards phosphodiesterase 10A (PDE10A) inhibitors. *Bioorg. Med. Chem.* **2015**, *23*, 4453-4461.

(S7) Cantrill, S. J.; Youn, G. J.; Stoddart, J. F.; Williams, D. J., Supramolecular Daisy Chains. *J. Org. Chem.* **2001**, *66*, 6857-6872.

(S8) Blanco, V.; Leigh, D. A.; Marcos, V.; Morales-Serna, J. A.; Nussbaumer, A. L., A Switchable [2]Rotaxane Asymmetric Organocatalyst That Utilizes an Acyclic Chiral Secondary Amine. *J. Am. Chem. Soc.* **2014**, *136*, 4905-4908.

(S9) Buter, J.; Heijnen, D.; Vila, C.; Hornillos, V.; Otten, E.; Giannerini, M.; Minnaard, A. J.; Feringa, B. L., Palladium-Catalyzed, *tert*-Butyllithium-Mediated Dimerization of Aryl Halides and Its Application in the Atropselective Total Synthesis of Mastigophorene A. *Angew. Chem. Int. Ed.* **2016**, *55*, 3620-3624.

(S10) Ogoshi, T.; Yamafuji, D.; Aoki,T.; Yamagishi, T.-a., Thermally responsive shuttling behavior of a pillar[6]arene-based [2]rotaxane. *Chem. Commun.* **2012**, *48*, 6842-6844.

(S11) Chen, S.; Wang, Y.; Nie, T.; Bao, C.; Wang, C.; Xu, T.; Lin, Q.; Qu, D.-H.; Gong, X.; Yang, Y.; Zhu, L.; Tian, H., An Artificial Molecular Shuttle Operates in Lipid Bilayers for Ion Transport. *J. Am. Chem. Soc.* **2018**, *140*, 17992-17998.

(S12) Melhuish, W. H., Quantum Efficiencies of Fluorescence of Organic Substances: Effect of Solvent and Concentration of the Fluorescent Solute. *J. Phys. Chem.* **1961**, *65*, 229-235.

(S13) Valeur, B.; Berberan-Santos, M. N., *Molecular Fluorescence. Principles and Applications, 2nd ed*. Wiley-VCH: Weinheim, 2012.

(S14) Lakowicz, J., *Principles of Fluorescence Spectroscopy, 3rd Ed*. Springer-Verlag: New York, 2006.

(S15) Sheldrick, G. M., SHELXT – Integrated space-group and crystal-structure determination. *Acta Cryst.* **2015**, *A71*, 3-8.

(S16) (a) Sheldrick, G. M., A short history of SHELX. *Acta Cryst.* **2008**, *A64*, 112-122; *(b)* Sheldrick, G. M., Crystal structure refinement with SHELXL. *Acta Cryst.* **2015**, *C71*, 3-8.

(S17) Farrugia, L. J., WinGX and ORTEP for Windows: an update. *J. Appl. Cryst.* **2012**, *45*, 849-854.

(S18) Spek, A. L., PLATON SQUEEZE: a tool for the calculation of the disordered solvent contribution to the calculated structure factors. *Acta Cryst.* **2015**, *C71*, 9-18.

(S19) Spek, A. L., Structure validation in chemical crystallography. *Acta Cryst.* **2009**, *D65*, 148-155.

(S20) The ellipsoid image was generated with the OLEX2 software package: Dolomanov, O. V.; Bourhis, L. J.; Gildea, R. J.; Howard, J. A. K.; Puschmann, H., OLEX2: a complete structure solution, refinement and analysis program. *J. Appl. Cryst.* **2009**, *42*, 339-341.